Proteomische Identifizierung und Charakterisierung Tumor-spezifischer Biomarker

Habilitationsschrift

vorgelegt am

der Medizinischen Fakultät
der Friedrich-Schiller-Universität Jena

von

Dr. rer. nat. Christian Melle

aus Jena

Gutachter

1. Prof. Dr. Aria Baniahmad
2. Prof. Dr. Stefan Diekmann
3. Prof. Dr. Anja Katrin Bosserhoff (Regensburg)

Erteilung der Lehrbefähigung am

Für Simone, Jacob und Lilith

Inhaltsverzeichnis

I Zusammenfassende Darstellung

1 Einleitung

Tumor-spezifische Biomarker können in Verbindung mit ihren Kooperationspartnern nicht nur medizinisch zur Früherkennung bei Krebserkrankungen genutzt werden, sondern auch zum besseren Verständnis der Tumorentstehung und Progression beitragen. In diesem medizinisch-biologischen Umfeld ist die vorliegende Arbeit einzuordnen.
In der folgenden Einleitung werden Probleme bei der Diagnose von Tumorerkrankungen mittels bekannter Biomarker benannt und Strategien für ein erfolgreiches Auffinden von potentiellen Tumormarker-Kandidaten aufgezeigt. Am Beispiel der Familie der S100-Proteine, deren Mitglieder diskriminierend in spezifischen Tumorentitäten auftreten, werden potentielle Tumormarker-Kandidaten vorgestellt und diese durch die Identifizierung von Interaktionspartnern biologisch charakterisiert.

1.1 Probleme in der Diagnostik von Tumorerkrankungen

Trotz der Anwendungen neuester Erkenntnisse und Methoden aus Genomik, Proteomik und molekularer Medizin zeigen die Mortalitätsraten der häufigsten Tumorentitäten im Moment keine signifikante Reduzierung (Jemal et al. 2005). Somit ist der „Kampf gegen Krebs“ gegenwärtig nur bedingt erfolgreich. Eine der zurzeit besten Strategien in diesem Kampf ist eine frühe Diagnose und die Gewährleistung einer effektiven Behandlung. Ein weiterer Ansatz hierbei ist die Überwachung von Krebspatienten nach einer initialen, gewöhnlich chirurgischen Behandlung, um ein Rezidiv frühzeitig zu erkennen und eine zusätzliche Therapie festzulegen. Einen dritten wertvollen Ansatz in diesem Kampf stellt die Stratifizierung von Patienten hinsichtlich ihres Ansprechens auf unterschiedliche Behandlungsprozeduren dar, welche zu einer differenzierten, individuell orientierten Tumortherapie führen soll (Etzioni et al. 2003). Neben dem zunehmenden und teilweise erfolgreichen Einsatz von molekularbiologischen Erkenntnissen als Therapieansatz wie beispielsweise der Blockierung des BCR-ABL-Signalweges durch Imatinib (Druker et al. 1996; Sawyers et al. 2002) können auch Biomarker aus Körperflüssigkeiten wie Serum, Plasma, Urin und/oder Mamilla-Aspirat sowie aus Gewebe hierbei wertvolle Instrumente sein. Gegenwärtig sind Biomarker aus Serum aber noch nicht ausreichend sensitiv und/oder spezifisch, um Krebserkrankungen frühzeitig zu diagnostizieren (Diamandis, van der Merwe 2005). Die im Moment zur Verfügung stehenden Tumor-Biomarker wie beispielsweise PSA

(*prostate serum antigen*) zur Detektion von Prostatakarzinomen, CEA (*carcinoembryonic antigen*) bei der Detektion von Kolon-, Mamma-, Lungen-, Pankreaskarzinomen und *cancer antigen*s (CA) wie CA125 beim Ovarialkarzinom, CA15.3 beim Mammakarzinom oder CA19.9 beim gastrointestinalem Karzinom werden zwar routinemäßig für eine frühe Diagnose sowie für Vorsorgeuntersuchungen benutzt, besitzen aber auf Grund geringer Sensitivität und/oder Spezifität keine ausreichendes Vorhersage-Potential (Diamandis 2004). Die geringe Spezifität dieser Biomarker führt nicht selten zu falsch-positiven Resultaten.
Das biologische Verständnis der Tumorentstehung gilt es also zu verbessern, das im Zusammenhang mit der Entwicklung möglichst sensitiver und spezifischer Biomarker steht.

1.2 Strategien für das Auffinden neuer Biomarker

Viele Biomarker wurden in biologischen Flüssigkeiten von Tumorpatienten mit erhöhter Konzentration im Vergleich zu Kontrollpersonen gefunden. Daraus wurde die Hypothese abgeleitet, dass die wertvollsten Biomarker wahrscheinlich sekretorische Proteine, die ca. 20-25 % aller humanen Proteine entsprechen, sein werden (Welsh et al. 2003). Es wird angenommen, dass eine Vielzahl an momentan noch nicht identifizierten bzw. ungenutzten Peptiden/Proteinen im Blut existiert, die potentielle diagnostische Biomarker darstellen (Liotta et al. 2003).
Die Massenspektrometrie (MS) stellt derzeit die wichtigste analytisch-proteomische Methode in der Biologie dar (Aebersold, Mann 2003). Mittels dieser Methode können multiparametrische Analysen von komplexen biologischen Proben durchgeführt werden und dabei spezifische Proteinprofile detektiert sowie Proteine und Peptide identifiziert werden. Die Massenspektrometrie kann in der Tumor-Diagnostik zur Suche nach neuen Markern eingesetzt werden, indem beispielsweise biologische Flüssigkeiten wie Serum, Plasma etc. mit Hilfe chromatographischer oder elektrophoretischer Techniken fraktioniert und anschließend mittels MS analysiert werden, um neue Proteinmarker zu identifizieren. Eine Vielzahl an Studien von biologischen Flüssigkeiten wurden mit unterschiedlichen massenspektrometrischen Systemen wie MALDI-TOF (*matrix assisted laser desorption/ionization – time of flight*) oder SELDI-TOF (*surface-enhanced laser desorption/ionization-time of flight*) durchgeführt und hierbei erfolgreich potentielle Biomarker in unterschiedlichen Tumorentitäten identifiziert (Vlahou et al. 2001; Alexander et al. 2004; Zhang et al. 2004; Kooman 2005; Malik 2005; Chen et al. 2007). Es stellte sich dabei aber heraus, dass die Detektion und Identifizierung von Proteinmarkern aus biologischen Flüssigkeiten auf Grund der Komplexität dieser Proben limitiert ist (Kooman et

al. 2005). Plasma umfasst beispielsweise eine dynamische Breite an unterschiedlichen Proteinen von zehn Magnituden und ist mit einer einzelnen analytischen Technik ohne Fraktionierung, Protein-Konzentrierung oder -Depletion nicht bearbeitbar (Anderson and Anderson 2002); Serum beinhaltet Proteine, die einen Konzentrationsbereich von wenigen pmol/L bis zu hohen µmol/L (z.B. Albumin, 0,6 mmol/L) aufweisen (Service 2003). Es wird angenommen, dass massenspektrometrische Ansätze nicht sensitiv genug sind, um die in den Blutstrom abgegebenen potenziellen Proteinmarker, die mit Konzentrationen von weniger als einem Nanogramm pro Milliliter vorliegen, zu identifizieren (Diamandis, van der Merwe 2005). So ist es auch nicht verwunderlich, dass viele der im Serum bzw. Plasma identifizierten Proteinmarker sogenannte *high-abundance* Proteine sind, die wenigstens teilweise Akute-Phase-Proteine repräsentieren (Zhang et al. 2003; Ye et al. 2003; Hlavaty et al. 2003; Cho et al. 2004). Diese Akute-Phase-Moleküle werden von der Leber und anderen Organen in die Blutzirkulation abgegeben und stellen keine spezifischen Tumor-Biomarker dar (Diamandis 2004).

Es wird spekuliert, dass ein potentieller Proteinmarker-Kandidat an dem Ort, in dem der Krankheitsprozess ursprünglich stattfindet, in einer höheren Konzentration vorliegt als nach Verdünnung im peripheren Blut. Daher müsste ein Konzept zur Aufdeckung onkologischer Marker Gewebe-basierend sein (Zolg 2006). Eine detaillierte histopathologische Beurteilung der zu untersuchenden Gewebe ist entscheidend für erfolgreiche Proteinmarker-Identifizierung in der anschließenden proteomischen Analyse. Durch die vor allem Tumorgewebe auszeichnende Heterogenität ist eine genaue Separierung einzelner, histologisch unterschiedlicher Gewebeareale essentiell, um einheitliche, von ungewünschten Gewebekomponenten befreite Proben zu erhalten, was durch den Einsatz Laser-basierender Mikrodissektion gewährleistet wird (von Eggeling et al. 2007). Auch wenn die Kompatibilität von Gewebe-Mikrodissektion und Massenspektrometrie in einer Reihe von Studien gezeigt wurde (Xu et al. 2002; Cheung et al. 2004; Zhang et al. 2005; Mustafa et al. 2007), wird diese Technik bei der proteomischen Untersuchung von Gewebe nicht routinemäßig angewandt. Dieser Fakt kann begründet sein durch (I) die Erfordernis von pathohistologischer Kompetenz bei der Beurteilung der Gewebe, (II) den zeitlichen Aufwand, den die Durchführung von Mikrodissektion erfordert sowie (III) die Kosten, die durch Anschaffung und Erhalt der Mikrodissektionstechnik entstehen.

Ein massenspektrometrisches Verfahren, dessen Kompatibilität mit Mikrodissektion schon gezeigt wurde, ist die SELDI-MS (Abb. 1; Melle et al. 2003; Cheung et al. 2004; Krieg et al. 2004; Guedj et al. 2006).

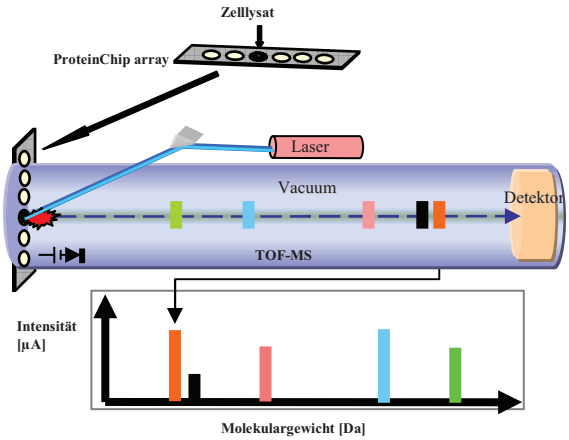

Abb. 1. Schematische Darstellung der Arbeitsweise der surface-enhanced laser desorption/ionization (SELDI) Massenspektrometrie (MS). Die Proteine aus einem Zelllysat binden entsprechend ihrer physikochemischen Eigenschaften auf den chromatographischen Spots eines *ProteinChip array*. Nach Waschen und Einbettung in eine Energie-absorbierende Matrix werden die Proteine mittels eines Laser-Impulses ionisiert und im MS mittels *time-of-flight* (TOF) vermessen. Hierbei werden niedermolekulare Proteine nach Durchquerung der elektromagnetischen Flugröhre früher am Detektor aufgezeichnet als höhermolekulare.

Diese MS-Technik erfordert nur geringe Probenmengen und macht sie daher ideal zur Bearbeitung von mikrosezierten Präparaten. Die SELDI-Massenspektrometrie basiert auf sogenannten *ProteinChip arrays*, die unterschiedliche chromatographische Oberflächen besitzen (Hutchens, Yip 1993). Diese Oberflächen binden Proteine aus Zell-Rohextrakten entsprechend deren physikochemischen Eigenschaften, die anschließend direkt mittels Massenspektrometrie analysiert werden. Proteine, die so auf den Affinitäts-Oberflächen der *ProteinChip arrays* zurückgehalten werden, können leicht von Kontaminanten wie Salzen oder Detergensien, die aus entsprechenden Lysis- bzw. Lade-/Wasch-Puffern stammen, gereinigt werden und müssen im Vergleich zu anderen massenspektrometrischen Techniken nicht vorgereinigt werden.

1.3 Die Familie der S100 Ca^{2+}-bindenden Proteine und ihr Auftreten in Tumoren

Die S100-Proteinfamilie umfasst mindestens 26 Mitglieder, deren Gene größtenteils im sogenannten *epidermal differentiation complex* auf Chromosom 1q21 lokalisiert sind. Die S100-Familie ist die Mitglieder-stärkste Untergruppe der Kalzium-bindenden Proteine mit EF-Hand-Domäne (Schäfer et al. 1995; Heizmann et al. 2002). Ihr Name leitet sich von ihrer Eigenschaft ab, bei neutralem pH in 100 % Ammoniumsulfat löslich zu sein (Moore 1965). Trotz ihrer hohen Sequenz-Homologie erscheint ihr Expressionmuster Zell-, Gewebe- sowie Kontext-spezifisch (Dowen, Crnogorac-Jurcevic 2006). Die S100 sind niedrig-molekulare, saure Proteine, die Homo- und Heterodimere bilden. Nach Ca^{2+}-Bindung kommt es zu Konformationsänderungen, in deren Folge eine hydrophobe Region exponiert wird, die mit spezifischen Proteinen interagieren kann (Heizmann et al. 2002).

S100-Proteine wurden mit unterschiedlichen zellulären Prozessen in Verbindung gebracht, inklusive Zellzyklus-Regulation, Zellwachstum und -differenzierung, Transkription sowie Zellbewegung und Invasivität (Heizmann, Cox 1998). Die funktionelle Komplexität der S100-Proteine wird durch verschiedene Charakteristika bestimmt. Neben der Zell- und Gewebe-spezifischen Expression lokalisieren S100-Proteine im Zytosol wie auch im Nukleus. Außerdem bindet S100-Protein Kalzium und andere zweiwertige Kationen mit verschiedener Affinität, was in unterschiedlichen Konformationsänderungen und dadurch unterschiedlichen Protein-Interaktionspartnern resultiert.

Die Rolle der S100-Proteine in der Tumorgenese wird extensiv untersucht (Salama et al. 2007). Differentielle Expressionen verschiedener S100-Proteine wurden in unterschiedlichen Tumortypen beschrieben und es scheint, dass diese Proteine in Abhängigkeit der untersuchten Tumoren onkogenetisches wie auch tumorsuppressives Potential besitzen (Dowen, Crnogorac-Jurcevic 2006). Dieses Phänomen spiegelt sich auch in ihrem Verhalten gegenüber Interaktionspartnern wider. So wurden unter anderen Proteininteraktionen zwischen Jab1, Cox-1 und den Tumorsuppressorproteinen BRCA1 sowie p53 und einer Reihe von S100-Proteinen gezeigt (Donato 2003; Emberley et al. 2003; Kennedy et al. 2005; Tsai et al. 2006). Beispielsweise hemmen S100A4 wie auch S100B die Phosphorylierung von p53 was zur Inhibition der transkriptionellen Aktivität und dadurch zur Einschränkung der tumorsuppressiven Aktivität von p53 führt (Grigorian et al. 2001). Im Gegensatz dazu unterstützt S100A2 die transkriptionelle Aktivität von p53 (Mueller et al. 2005). Eine Vielzahl der S100-Proteine spielt eine Rolle bei der Zytoskelett-Dynamik und zeigt direkte Interaktionen mit Tubulin, Intermediär-Filamenten, Actin und Myosin (Santamaria-Kisiel et al. 2006). Einige dieser Prozesse scheinen bei der Metastasierung beteiligt zu sein (Davies et al. 1996; Kriajevska et al. 1998). Außerdem können Mitglieder der S100-Familie die Zellproliferation regulieren. So zeigt S100A1 eine Hemmung der Proliferation (Donato 2001). Interessanterweise besitzt S100A11 dahingehend eine duale Funktion, indem es die Zellproliferation von Keratinozyten einerseits intrazellulär inhibieren und andererseits autokrin stimulieren kann (Sakaguchi et al. 2005; Sakaguchi et al. 2008). Andere extrazellulär vorliegende S100-Mitglieder können als Leukozyten-Chemoattraktante sowie Makrophagen-Aktivatoren wirken (Devery et al. 1994; Lau et al. 1995; Hiratsuka et al. 2006).

Es scheint, dass jedes S100-Protein individuelle Rollen bei Tumorgenese und Metastasierung spielen kann. Die Expression der S100-Proteine ist nicht einheitlich und scheint in Abhängigkeit zu den untersuchten Tumortypen zu stehen. So zeigt S100B eine erhöhte Konzentration im Serum von Patienten mit Melanomen, die Tumorgrad-abhängig und mit

Metastasierung assoziiert ist (Bonfrer et al. 1998; Schlagenhauff et al. 2000). Eine Überexpression verschiedener S100-Proteine wie S100A4, S100A8, S100A9, S100A6 und S100A7 in unterschiedlichen Tumorentitäten, z.B. Kolorektal-, Prostata-, Magen- und Brustkarzinomen, die häufig mit einem erhöhten Metastasierungspotential korreliert, wurde beobachtet (Stulik et al. 1999; Komatsu et al. 2000; Nikitenko et al. 2000; Gongoll et al. 2002; Cho et al. 2003; Emberley et al. 2003; Hermani et al. 2006; Rafii, Lyden 2006; Saleem et al. 2006; Yong, Moon 2007). Im Gegensatz dazu ist die Expression von S100A2 bei einigen Tumoren (z. B. Bronchialkarzinom) herunterreguliert, jedoch in papillären Karzinomen und im NSCLC (*non-small cell lung carcinoma*) überexprimiert (Feng et al. 2001; Smith et al. 2004; Ito et al. 2005). S100A11 zeigt unterschiedliche, vom Tumortyp abhängige Wirkungen. Im Blasenkarzinom scheint die S100A11-Proteinexpression mit Tumorsuppression zu korrespondieren, wodurch hier eine verminderte Expression mit verschlechterter Prognose und einer verringerten Überlebensrate assoziiert ist (Memon et al. 2005). Konträr dazu scheint S100A11 in Prostata-Tumoren eine Tumor-unterstützende Wirkung zu besitzen und die Expression in dieser Tumorentität geht mit einem höheren pathologischen Tumorgrad einher (Rehman et al. 2004).

2 Zielstellung der Arbeit

Ziel der vorliegenden Arbeit war es, diskriminierende Proteinmarker, die möglichst Tumorentitäts-spezifisch auftreten, zu identifizieren und bioinformatisch zu validieren und dadurch zu entwickeln sowie mittels proteomischer, immunologischer und zellbiologischer Techniken zu charakterisieren. Dafür wurden vier Schwerpunkte bearbeitet.

Der **erste Schwerpunkt** stellte die Charakterisierung verschiedener Tumorentitäten mittels proteomischer und immunologischer Analysen dar. Hierfür wurde eine methodische Prozedur entwickelt, die die Identifizierung und Beurteilung von Biomarkern erlaubt. Dabei wurden die mittels ProteinChip-basierender SELDI (*surface-enhanced laser desorption/ionisation*) Massenspektrometrie erzeugten Proteinprofile von epithelialen Tumorzellen aus Hals-Kopf-Tumoren sowie kolorektalen Karzinomen nach exakter Mikrodissektion mit den Proteinprofilen von entsprechenden, ebenfalls mikrosezierten Tumor-distanten normalen Pharynx- und Kolon-Epithelien verglichen. Die für Tumor- und Normalgewebe jeweils spezifischen Signale wurden identifiziert und ihre räumliche Verteilung im Tumor durch Immunhistochemie (IHC) dargestellt.
Der **zweiter Schwerpunkt** dieser Arbeit bestand darin, die zuerst im Gewebe identifizierten Proteinmarker hinsichtlich ihres Auftretens in Patientenseren zu untersuchen. Dafür erfolgten massenspektrometrisch Untersuchungen wie auch ELISA-Analysen.
Die Untersuchung unterschiedlicher Tumorentitäten hinsichtlich ihrer proteomischen Ähnlichkeit/Übereinstimmung einerseits, sowie die Identifizierung von Proteinen, die andererseits zur Diskriminierung von unterschiedlichen Tumorentitäten geeignet sind, wurden als **dritter Schwerpunkt** dieser Arbeit formuliert.
Als **vierter Schwerpunkt** erfolgte eine biologische und funktionelle Charakterisierung der in den Proteinprofiling-Experimenten gefundenen Biomarkern. Hierfür wurde ein Ansatz, der massenspektrometrische und immunologische Techniken vereinigte, entwickelt, um endogene Interaktionspartner der gefundenen Biomarker zu identifizieren. Diese Proteinkomplexe wurden anschließend hinsichtlich ihrer biologischen Funktion in Abhängigkeit spezifischer physiologischer Bedingungen wie der Einführung von DNA-Schäden oder der Depletion eines Interaktionspartners mittels RNA Interferenz verifiziert.

3 Ergebnisse

3.1 Identifizierung und Charakterisierung von Biomarkern mittels der technischen Triade

Im **ersten Schwerpunkt** wurden die methodischen Voraussetzungen für die proteomische Analyse von Tumorproben geschaffen (**Melle et al., Cancer Res. 2004; 64: 4099-4104 – siehe Anhang 1.1**). Bedingt durch die Komplexität von Serum wie auch Plasma hinsichtlich der Proteinzusammensetzung und der Dynamik in der Konzentration unterschiedlicher Proteine fokusierten wir unsere Untersuchungen auf Tumorgewebe. Da Tumorgewebe sich auf Grund seiner Zusammensetzung aus Tumorzellarealen, Tumorstroma und Tumornekrosen durch eine innewohnende Heterogenität auszeichnet, analysierten wir ausschliesslich Proben von mikroseziertem Gewebe. Hierfür wurde das Laser-Mikrodissektionssystem von P.A.L.M. benutzt. Dadurch konnten wir sicherstellen, dass das untersuchte Gewebematerial weitestgehend frei von Kontaminationen und ungewünschten Gewebekomponenten war, was außerordentlich wichtig für das Auffinden von zuverlässigen Biomarkern für die Krebsdiagnose ist (Craven and Banks 2001). Im Fall der in dieser Arbeit untersuchten epithelialen Tumoren der Pharynx wurden die epithelialen Tumorzellen von benachbarten Gewebekomponenten separiert. Im Gegensatz zu normalem Epithel ist die Abgrenzung der epithelialen Tumorzellkomplexe zum Tumorstroma und anderen Gewebeabschnitten unregelmäßig. Durch den Einsatz der Laser-basierenden Mikrodissektion konnten wir jedoch nahezu kontaminationsfreies Material gewinnen, welches ca. 3000-5000 Zellen pro Probe umfasste. Ähnliche Mengen an mikrosezierten Zellen wurden ebenfalls durch andere Arbeitsgruppen zur Darstellung von aussagekräftigen Proteinprofilen benutzt (Cazares et al. 2002; Cheung et al. 2004).

Die Proteinprofile der 101 mikrosezierten Gewebeproben (57 epitheliale Tumorgewebe und 44 normale, Tumor-distante Pharynxepithel-Gewebe) wurden durch den Einsatz von *ProteinChip arrays* mit Anionenaustauscher- bzw. Kationenaustauscher-Oberfläche und der Analyse mittels SELDI-MS erzeugt. Die Cluster-Analyse der detektierten Signale und die Ermittlung der *P*-Werte für die Proben aus normalem und Tumorgewebe erfolgten mittels des Biomarker Wizzard Program (version 3.0). Für die *P*-Wert Kalkulation wurden die Spektren mit dem Mann-Whitney *U* test für nicht-parametrische Datensätze analysiert. Damit konnten wir 96 Proteinsignal-Cluster nach Normalisierung im Messbereich zwischen 2 und 20 Kilo-Dalton (kD) detektieren. Hierbei wurden 15 Signale gefunden, mit denen Tumor- und normales Gewebe signifikant unterschieden werden können. Da ein diskriminierendes Signal

nur als nutzbarer Proteinmarker betrachtet werden kann, wenn es identifiziert ist (Diamandis 2006), wurden die beiden Signalmassen mit den besten *P*-Werten für eine weitere Identifizierung ausgewählt. Diese zwei interessanten Signale, 10,84 kD ($P = 3{,}34 \times 10^{-5}$) und 13,23 kD ($P = 4{,}6 \times 10^{-5}$), lagen im epithelialen Tumorgewebe im Vergleich zu normalem Pharynxgewebe mit herunterregulierter Proteinexpression vor. Als Kontrolle zur Beurteilung der angewandten Methoden wurde ein Signal (11,87 kD) mit nicht-signifikantem *P*-Wert ($P = 0{,}379$) ebenfalls identifiziert.

Zur Identifizierung wurden Proteinlysate von histologisch beurteilten Tumorgeweben und Biopsien von normalen, Tumor-distanten Pharynxepithelien mittels zwei-dimensionaler Gelelektrophorese (2DE) aufgetrennt. Mehrere Proteinspots mit differentieller Expression konnten in den mit Coomassie gefärbten Gelen visuell detektiert werden. Auf Grund der Bindung der drei zu identifizierenden Proteine an *ProteinChip arrays* mit Anionenaustauscher-Oberfläche in den vorangegangenen Proteinprofiling-Experimenten konnten wir einen isoelektrischen Punkt der Proteinkandidaten von < 7,5 erwarten. Aus diesem Grund konzentrierten wir uns in den 2DE-Gelen auf Proteinspots mit einem molekularen Gewicht im Bereich von 5 – 20 kD und einem isoelektrischen Punkt im Bereich von 3 – 7,5. Proteinspots, die diese Kriterien erfüllten, wurden aus dem Gel geschnitten und einem tryptischen Verdau unterzogen. Die beim Verdau entstandenen Fragmente wurden mittels SELDI-MS analysiert und die so gewonnenen *peptide mass fingerprints* (PMF) zur Suche in Protein-Datenbanken benutzen. Der erfolgreiche Einsatz dieser Technik hinsichtlich der Generierung von PMF konnte schon in einer früheren Arbeit gezeigt werden (Melle et al. 2003). Die Suche in einer Datenbank deckte S100A8 (Calgranulin A), S100A9 (Calgranulin B) bzw. S100A11 (Calgizzarin) als die besten Kandidaten auf. Diese Ergebnisse konnten mittels Tandem-MS-Analyse bestätigt werden. S100A8, S100A9 und S100A11 gehören zur Familie der S100 Ca^{2+}-binde Proteine (Donato 2001). Zur Überprüfung, dass S100A8, S100A9 bzw. S100A11 mit den in der Proteinprofil-Analyse gefundenen Signale von 10,84 kD, 13,23 kD bzw. 11,87 kD übereinstimmen, wurden Immundepletions-Experimente mit spezifischen Antikörpern gegen S100A8, S100A9 bzw. S100A11 und Proteinlysaten von mikrosezierten Pharynxepithelium, die als Ausgangsmaterial dienten, durchgeführt. Hierbei zeigte sich in der Analyse mittels SELDI-MS, dass die Signale, die zu den drei identifizierten Proteinen korrespondieren, signifikant reduziert wurden. Zur weiteren Bestätigung der Identität und zur Lokalisierung dieser Proteine im Phayrnxgewebe führten wir immunhistochemische Untersuchungen durch. Hierbei zeigte sich eine identische Immun-Reaktivität von S100A8 und S100A9 im normalen, Tumor-distanten Epithel. Im Vergleich

dazu konnten im Tumorgewebe keine Signale, die zu S100A8 bzw. S100A9 korrespondieren, detektiert werden. Dieses identische Verhalten von S100A8 und S100A9 ist nicht verwunderlich, da beide Proteine unter physiologischen Bedingungen ein ähnliches Proteinexpression-Niveau zeigen sowie Heterodimere bilden können (Thorey et al. 2001; Dell´Angelica et al. 1996). S100A11, das als Kontrolle diente, zeigte in Tumor wie auch in normalen epithelialen Geweben positive Immunreaktionen. Als weitere Überprüfung, dass S100A8, S100A9 und S100A11 identisch zu den in der Proteinprofil-Analyse gefundenen Signalen sind, wurden IHC-positive bzw. –negative Zellareale mittels Mikrodissektion separiert und entsprechende Proteinlysate hinsichtlich der drei identifizierten Signale massenspektrometrisch untersucht. Hierbei konnten in Lysaten aus positiven Arealen Signale detektiert werden, die den in der initialen Proteinprofil-Analyse gefundenen Signalen entsprechen. Keine entsprechenden Signale wurden in Lysaten aus IHC-negativen Zellfraktionen gefunden.

Das in dieser Untersuchung gezeigte Ergebnis einer verminderten Proteinexpression von S100A8 und S100A9 steht im Kontrast zu früher publizierten Studien, die eine erhöhte Expression der beiden Proteine hinsichtlich ihres Gen-Niveaus wie auch ihres Protein-Niveaus in Tumoren im Vergleich zu korrespondierenden normalen Geweben zeigten (Stulik et al. 1999; Chaurand et al. 2001; Mueller et al. 2003). Diese Diskrepanz kann erklärt werden durch den Fakt, dass (I) unsere Analyse auf einer anderen Tumorentität basiert, (II) dass das mRNA-Niveau auf Grund translationaler Kontrollmechanismen nicht notwendigerweise mit dem Niveau der Proteinexpression korrelieren muss und (III) dass wir im Gegensatz zu den oben erwähnten Studien mikroseziertes Material benutzten und unsere Ergebnisse mit IHC bestätigten. Interessanterweise ist zu erwähnen, dass in einer Genexpressions-Studie zu Hals-Kopf-Tumoren eine verringerte Expression von *S100A9* mittels IHC bestätigt wurde (Gonzalez et al. 2003).

Durch den Einsatz der hier aufgezeigten „technischen Triade“, die sich aus Gewebemikrodissektion zur Gewinnung von definiertem Probenmaterial, Analyse dieses Materials zur Identifizierung spezifischer Proteinmarker mittels SELDI-MS, 2DE sowie Tandem-MS und Untersuchung dieser Marker mittels IHC zusammensetzt, ist es möglich, Tumormarker zu ermitteln und zu charakterisieren (Abb. 2; **Melle et al., Cancer Res. 2004; 64: 4099-4104 – siehe Anhang 1.1**).

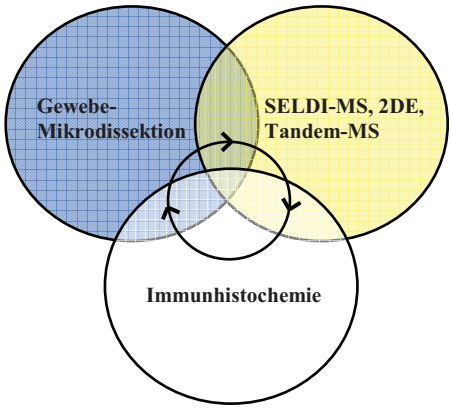

Abb. 2. „Technische Triade“ zur proteomischen Identifizierung und Charakterisierung von Tumormarkern. Beginnend mit der Mikrodissektion wird Probenmaterial gewonnen, das mittels SELDI-MS analysiert wird. Proteinmarker werden mittels 2DE, Tandem-MS und Immundepletion identifiziert und anschliessend durch IHC charakterisiert. Mikrodissektion von immunhistochemisch behandelten Gewebearealen und Re-Analyse dieser mittels ProteinChip arrays und SELDI-MS schließen den Kreis. (modifiziert nach Melle et al. 2004)

Diese „technische Triade“ wurde von uns in zahlreichen weiteren Untersuchungen verschiedener Tumorentitäten erfolgreich validiert (Melle et al. 2005b; Melle et al. 2006b; Melle et al. 2007a; Melle et al. 2007b). In einer dieser Untersuchungen wurden jeweils mikrosezierte Gewebeproben aus epithelialen Tumorzellen von kolorektalen Karzinomen (CRC) (n = 13) bzw. Adenomen (n = 30) und normalen, Tumor-distanten Kolongewebe (n = 19) miteinander verglichen (**Melle et al., Int. J. Oncol. 2006; 28: 195-200 – siehe Anhang 1.2**). In dieser Studie detektierten wir nach Normalisierung 158 Proteinsignal-Cluster im Messbereich zwischen 2,5 – 200 kD. Unter den 18 signifikant differentiell exprimierten Signalen konnte S100A11 (S100C; Calgizzarin) im kolorektalen Karzinom mit einer signifikant erhöhten Proteinexpression im Vergleich zu kolorektalem Adenom bzw. normalem Kolonepithelium identifiziert werden. Auffällig ist, dass hier S100A11 im Vergleich zur oben erwähnten Studie zu Hals-Kopf-Tumoren (Melle et al. 2004), in der S100A11 nicht-differentiell exprimiert gefunden wurde, zwischen kolorektalem Karzinom, kolorektalem Adenom und normalem Kolongewebe diskriminieren kann.

3.2 Validierung von Proteinmarkern aus Tumorgewebe im Serum

Eine Detektion früher Tumorstadien ist durch die Analyse nicht-invasiv gewonnenen Materials wie Serum vorstellbar. Auch wenn Serum breit verfügbar und einfach zu sammeln und zu asservieren ist, könnte die Konzentration an Tumor-spezifischen Proteinen, vor allem in frühen Phasen, zu gering sein. Im Gegensatz dazu können im Gewebe geringste, Tumor-relevante Veränderungen im Proteinprofil detektiert werden. Aus diesem Grund fokusierten wir im **zweiten Schwerpunkt** auf die Verbindung der Vorteile von Serum- und Gewebe-

Analyse, indem wir in mikroseziertem Gewebe differentiell exprimierte Proteine aufdeckten und nach diesen anschließend in Seren mittels Antikörper-basierenden Tests suchten (**Melle et al., Gastroenterology 2005; 129: 66-73 – siehe Anhang 1.3**). Hierzu wurde zu Beginn das Proteinprofil von 39 kolorektalen Karzinomen (CRC) und 40 normalen, Tumor-distanten Kolonepithelgeweben mittels ProteinChip array-basierender SELDI-Massenspektrometrie ermittelt. Nach Normalisierung und bioinformatorischer Bearbeitung mittels des Biomarker Wizzard Program ergaben sich hierfür im Messbereich von 2 – 20 kD 126 Proteinsignal-Cluster, die 13 Signale enthielten, die zwischen epithelialen Tumorzellen aus kolorektalen Karzinomen und normalen Kolonepithelien diskriminieren konnten. Drei Signale mit bemerkenswert geringen *P*-Werten [3,37 kD ($P = 4{,}39\text{x}10^{-5}$); 3,44 kD ($P = 1{,}88\text{x}10^{-5}$); 3,49 kD ($P = 9{,}91\text{x}10^{-5}$)], die in kolorektalen Karzinomproben überexprimiert vorlagen, ähnelten in ihrem Proteinmuster und ihrem Molekulargewicht den zur Familie der Defensine zählenden α-Defensine 1-3 (HNP1-3, human neutrophil protein 1-3), die in früheren Arbeiten mittels SELDI oder Tandem-MS beschrieben bzw. identifiziert wurden (Vlahou et al. 2001; Diamond et al., 2001; Zhang et al. 2002). Die Identität dieser drei Signale als HNP1-3 konnte von uns mittels Immundepletions- und immuno capturing-Experimenten bestätigt werden. HNP1-3 sind kleine Peptide, die zu den Defensinen gehören und in intestinalen Epithelzellen unter verschiedensten Bedingungen exprimiert werden. Neuere Studien zeigen die Expression von HNP1-3 in epithelialen Zellen des Ileum und des Kolon bei entzündlichen Erkrankungen, ohne diese im normalen intestinalen Gewebe detektieren zu können (Ogawa et al. 2000; Cunliffe et al. 2002). Da wir in unserer Studie mikroseziertes Material benutzten und hierbei entzündlich infiltrierte Abschnitte, die Neutrophile enthalten können, ausschlossen, konnten wir nachweisen, dass die im kolorektalem Karzinom überexprimiert gefundenen HNP1-3 direkt aus dem Tumorgewebe stammen, da die mikrosezierten Tumorgewebeproben nicht mehr Neutrophile beinhalteten als das parallel analysierte und ebenfalls mikrosezierte normale Kolongewebe.

Immunohistochemische Analysen mit einem Antikörper gegen HNP1-3 zeigten im Vergleich zu normalen Kolongeweben starke Reaktionen in kolorektalen Tumorgeweben und in invasiv wachsenden Karzinomen und in der Re-Analyse dieser IHC-positiven Zellareale konnten im Gegensatz zur Re-Analyse der IHC-negativen Gewebeareale Signale detektiert werden, die zu HNP1-3 korrespondieren. Zur Suche nach HNP1-3 in Seren von Patienten mit kolorektalen Tumoren und normalen Kontrollen benutzten wir zwei Proben-Gruppen (n = 48; n = 42), in denen unabhängig die HNP1-3 – Konzentration mittels ELISA quantifiziert wurden. In der ersten Probengruppe konnte eine signifikant höhere Konzentration von HNP1-3 in Seren von

Tumorpatienten im Vergleich zu normalen Kontrollen ermittelt werden ($P = 2{,}14 \times 10^{-5}$). Der Median für die Kontrollen lag bei 8,1 ng/ml; der Median für Patienten mit Kolonkarzinom lag bei 29,4 ng/ml. Die entsprechende ROC (engl.; receiver operating curve) zeigte eine Sensitivität von 100% und eine Spezifität von 69%. Der cut-off lag bei 14,8 ng/ml. Die unabhängige Validierung der zweiten Probengruppe zeigte die gleiche Verteilung wie die erste Probengruppe und resultierte in einem *P*-Wert von $5{,}60 \times 10^{-3}$. Hierbei lag der Median für die Kontrollen bei 5,6 ng/ml und der für Patienten bei 14,99 ng/ml. Die ROC resultierte in einer Sensitivität von 100% und einer Spezifität von 65,2%. Der cut-off lag hier bei 12,3 ng/ml. HNP1-3 konnten bei einer Analyse der Seren mittels SELDI-MS nicht diskriminierend detektiert werden (unveröffentlichte Resultate). Mit dieser Studie zeigten wir erstmals die Effizienz von Gewebe-basierenden ProteinChip-Analysen zur Detektion und Identifizierung von Proteinmarkern aus Seren.

In weiteren Untersuchungen konnten wir diskriminierende Proteinmarker, die in Geweben von Pankreaskarzinomen bzw. in normalen Epithelien der Pharynx mittels SELDI-MS gefunden wurden, ebenfalls in entsprechenden Seren nachweisen (Melle et al. 2007b; unveröffentlichte Resultate). So konnten wir S100A8, das in epithelialen Tumorzellen des Pharynx herunterreguliert gefunden wurde (Melle et al. 2004), in Kontrollseren mit erhöhter Konzentration im Vergleich zu Seren von Patienten mit Hals-Kopf-Tumoren detektieren (Abb. 3; unveröffentlichte Resultate).

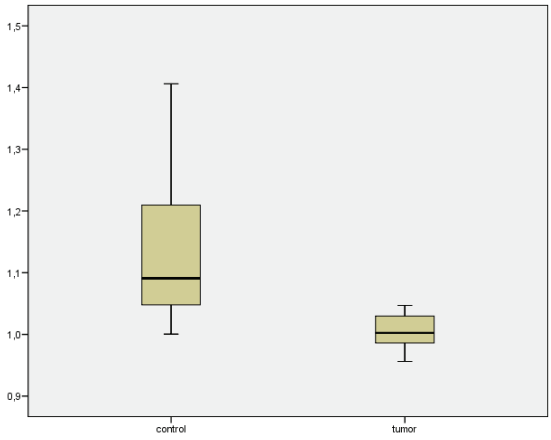

Abb. 3. Box plot der Serumkonzentration von S100A8 für Kontrollen (n = 31) und Patienten (n = 31) mit Hals-Kopf-Tumoren. Die y-Achse stellt die Konzentration in ng/ml dar.

3.3 Proteomischer Vergleich verschiedener Tumorentitäten

Um einzelne Tumorentitäten zu charakterisieren und dabei mittels dem oben vorgestellten proteomischem Ansatz möglichst Entitäts-spezifische Proteinmarker zu detektieren, wurden im **dritten Schwerpunkt** der vorliegenden Arbeit Proteinprofile von epithelialen

Tumorzellen aus kolorektalen Karzinomen (CRC) mit denen aus hepatozellulären Karzinomen (HCC) und/oder denen aus Leber-Metastasen von kolorektalem Karzinom (MTS) verglichen (**Melle et al., PLoS ONE 2008; 3: e3767 – siehe Anhang 1.4**). Die Analyse der mittels SELDI-basierender Massenspektrometrie erzeugten Proteinprofile der mikrosezierten MTS (n = 17) mit den bereits publizierten Proteinprofilen von mikrosezierten kolorektalen Karzinomen (n = 14) (Melle et al. 2006a) und hepatozellulären Karzinomen (n = 46) (Melle et al. 2007a) zeigte 372 Proteinsignal-Cluster nach Normalisierung im Messbereich zwischen 2,5 – 200 kD. Nach der Evaluierung mit dem CiphergenExpress Progamm detektierten wir für CRC, HCC und MTS eine Vielzahl von signifikant unterschiedlichen Signalen (n = 49). Zwei Signale mit bemerkenswert niedrigen *P*-Werten (*P* = $3{,}00 \times 10^{-9}$ bzw. *P* = $1{,}82 \times 10^{-6}$), die in MTS wie auch CRC eine im Vergleich zu HCC signifikant erhöhte Proteinexpression zeigten, wurden als S100A6 bzw. S100A11 identifiziert. Beide Proteine können CRC gegen HCC sowie im Fall von S100A6 MTS gegen HCC sehr gut diskriminieren. Diese Ergebnisse konnten wir in immunhistochemischen Experimenten bestätigen. Mit diesen Untersuchungen konnten wir frühere Studien bestätigen, die S100A6 wie auch S100A11 mit verschiedenen epithelialen Tumoren und mit Metastasierung in Verbindung bringen (Maelandsmo et al. 1997; Komatsu et al. 2000; Yao et al. 2007). Eine Unterscheidung von CRC und MTS war mit keinem der beiden Proteinen möglich, was sich auch in der Ähnlichkeit der Proteinprofile der primären kolorektalen Karzinome und der davon abstammenden Leber-Metastasen widerspiegelt. Die Analyse der Proteinprofile von Metastasen aus unterschiedlichen Typen metastasierender Tumore könnte zu einem für viele Metastasisgewebe allgemeinen „metastatischen Proteinprofil“ führen. Mit S100A6 liegt ein vielversprechender Kandidat zur Unterscheidung von primären HCC und CRC-MTS vor, da die Diskriminierung zwischen primärem hepatozellulären Karzinom und in der Leber lokalisierten Metastasen kompliziert und fehlerbehaftet ist (Helmberger et al. 2002).
In einer weiteren dem **dritten Schwerpunkt** zu zuordnenden, systembiologischen Studie wurden im Gegensatz zu den oben aufgeführten Untersuchungen nach Signalen in den Proteinprofilen verschiedener Tumorentitäten gesucht, die zur Konvergenz dieser proteomischen Muster beitragen (**Müller et al.; Bioinformatics 2006; 22: 1293-1296 – siehe Anhang 1.5**). Dafür wurden die in früheren Arbeiten ermittelten Proteinprofile epithelialer Tumorzellen aus Hals-Kopf-Tumoren der Pharynx und aus kolorektalen Karzinomen sowie die der entsprechenden, Tumor-distanten normalen Epithelgewebe mittels einer Vielzahl an statistischen und bioinformatorischen Programmen analysiert (Melle et al. 2003; Melle et al. 2004; Melle et al. 2005a). Hierbei konnte gezeigt werden, dass epitheliale Tumore aus

Pharynx und Kolon hinsichtlich ihres proteomischen Musters größere Ähnlichkeiten zueinander aufweisen als gegenüber ihren ursprünglichen Geweben. Dabei wurden die Proteinprofile in die folgenden acht Probengruppen eingeteilt: NCOL (normales Kolonepithel-Gewebe, n = 18), TuCOL (kolorektales Karzinom-Gewebe, n = 29), NHN (normales pharyngeales Epithel, n = 28), TuNH (Hals-Kopf-Tumorgewebe, n = 31), NALL (normals Kolonepitel und Pharynxepithel-Gewebe, n = 46), TuALL (kolorektales Karzinom- und Hals-Kopf-Tumorgewebe, n = 60), COLALL (normales Kolonepithel- und kolorektales Karzinom-Gewebe, n = 47) und HNALL (normales pharyngeales Epithel und Hals-Kopf-Tumorgewebe, n = 59). In diesen Gruppen wurden mittels *t*-test, decision trees (engl.), random forest classification (engl.) und support vector machines (engl.) nach charakteristischen Merkmalen gesucht indem die Probengruppen wie folgt verglichen wurden: NALL versus TuALL, NCOL versus TuCOL, NHN versus TuHN, COLALL versus HNALL, NCOL versus NHN und TuCOL versus TuHN. Beim Vergleich von NCOL verus NHN wurde der klarste decision tree aller durchgeführten sechs Vergleiche gefunden. Um diese beiden Gruppen exakt voneinander zu trennen, war nur ein sogenannter split point ausreichend, der zum Signal bei 10848,5 Da korrespondierte. Dieses Signal wurde von uns in einer frühere Studie als S100A8 identifiziert (Melle et al. 2004). Für die anderen fünf Vergleiche wurden komplexere decision trees für eine Trennung zweier Gruppen gefunden, was eine geringere Unterscheidung dieser Paare impliziert. Mit allen vier Gewebetypen (NHN, NCOL, TuHN, TuCOL), hier als Klassen bezeichnet, führten wir eine random forest (RF) classification durch, bei der ohne Ausnahme alle „Normal“-Proben ihrem entsprechenden Gewebetyp korrekt zugeordnet wurden. Abweichend davon wurden jeweils zwei Proben zwischen TuCOL-Gruppe und TuHN-Gruppe falsch zugeordnet. Häufig auftretende Verwechslungen traten zwischen „Normal“- und „Tumor“-Proben innerhalb des selbem Gewebes auf. Aus dieser Klassifizierung wurde die Wichtigkeit der Merkmale (entspricht den Proteinsignalen), die den random forest aufbauen, abgeleitet. Diese Kalkulation setzte sich aus 50 Merkmalen, die für spezifische Signale in den Proteinprofilen stehen, zusammen. Die beiden herausragendsten Merkmale, die bedeutender als die übrigen Merkmale sind, korrespondieren zu Signalen mit einem Molekulargewicht von 13245,3 Da bzw. 10848,5 Da. Das letztbenannte Merkmal von 10848,5 Da spielte hierbei eine wichtige Rolle in der Identifizierung von jeder der vier Klassen. Die RF-Analysen für jeweils zwei Klassen zeigten eine perfekte Klassifizierung für die Proben der „Normal“-Gewebe (NHN versus NCOL). Im Gegensatz dazu kam es bei allen anderen Fällen aber zu Falscheinteilungen der Proben. Mittels Analysen mit support vector machines (SVM)

ermittelten wir die maximale Exaktheit einer Vorhersage zur Verteilung von Proben in spezifische Gruppen. Hierbei wurden 50 Paare von Proteinen ermittelt, deren Expressionssignale die Proben aus NCOL versus NHN mit 100 %iger Genauigkeit vorhersagen. Die Vorhersage-Exaktheit für die Tumorproben (TuCOL versus TuHN) betrug 93,3 %. Die Genauigkeit der Vorhersage zu TuCOL versus NCOL betrug 87,2 %, die zu TuHN versus NHN 84,8 %; die Vorhersage-Exaktheit zu Tumor- versus „Normal"-Gewebe betrug 78,3 %.

Das in der RF-Klassifizierung ermittelte, bedeutende Merkmal, das Signal mit 10848,5 Da, stand für die höchsten Distanzen zwischen NCOL und NHN (39 *mean square distance* [msd] und zwischen TuHN und NHN (25 msd). Die höchsten Konvergenzen zeigten NCOL und TuCOL (1 msd) sowie TuCOL und TuHN (8 msd) hinsichtlich dieses Signals.

3.4 Biologische Charakterisierung diskriminierender Proteinmarker

Neben der Detektion und Identifizierung von Proteinmarkern, die zwischen Tumor- und Normalgewebe diskriminieren können, ist es ebenfalls von herausragender Bedeutung, diese Proteine hinsichtlich ihrer biologischen Funktion zu untersuchen. Eine Möglichkeit, Proteine zu charakterisieren und dadurch Einblicke in ihre physiologische Rolle zu erhalten, ist die Identifizierung von Interaktionspartnern (Coulombe et al. 2004). Die Aufklärung der Zusammensetzung molekularer Maschinen kann dabei zum Verständnis zellulärer Mechanismen beitragen und war Inhalt des **vierten Schwerpunkts** der vorliegenden Arbeit. Zu diesem Zweck entwickelten wir einen sogenannten „Protein-Protein-Interaktionstest" (PPIT), der auf massenspektrometrischer Analyse mittels SELDI-MS und immunologischen Techniken basiert (Abb. 4; **Lehmann et al., J. Proteome Res. 2005; 4: 1717-1721 – siehe Anhang 1.6**). Um die Tendenz der Detektion von falsch-positiven Proteininteraktionen zu vermeiden, wurden ausschließlich endogen exprimierte Proteine analysiert. Hierbei untersuchten wir als Modellsystem mit S100A8 ein Mitglied der S100 Ca^{2+}-binde Familie hinsichtlich möglicher interagierender Proteinpartner. S100A8 wurde in einer früheren Studie als differentiell unterschiedlich exprimiert in Hals-Kopf-Tumoren beschrieben (Melle et al. 2004). Neben einem Signal, das zum Molekulargewicht (MW) von S100A8 korrespondiert, wurden in der SELDI-basierenden massenspektrometrischen Analyse der mittels eines spezifischen anti-S100A8 Antikörpers aus HaCaT-Keratinozyten-Lysat präzipitierten Proteine weitere spezifische Signale detektiert. Diese Signale wurden nicht in einem Kontroll-Experiment mit einem unspezifischen Antikörper gefunden.

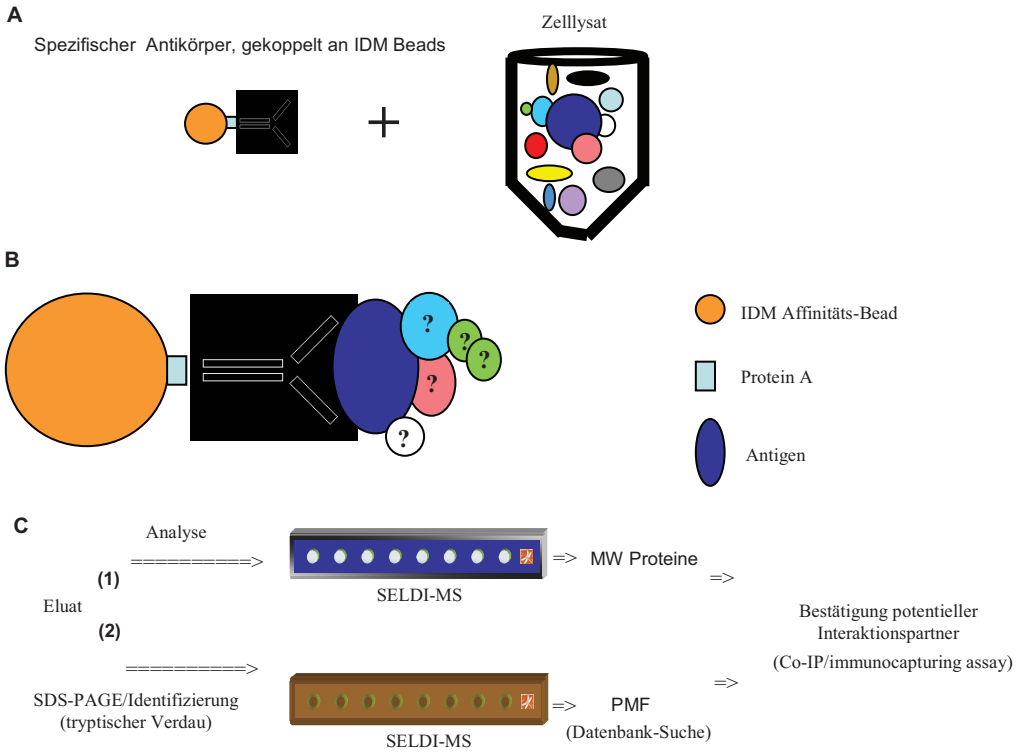

Abb. 4. Schematische Darstellung des Protein-Protein-Interaktionstests (PPIT). Dieser Test setzt sich aus drei experimentellen Schritten zusammen: Präzipitation, Elution und Analyse der potentiellen Interaktionspartner. (*A*) Mittels eines spezifischen Antikörpers, der an *Interaction Discovery Mapping* (IDM) Beads gekoppelt wurde, wurde das Antigen zusammen mit endogen exprimierten, interagierenden Partnern aus einem Zelllysat gefällt. (*B*) Der/Die präzipitierte(n) Proteinkomplex(e) wurde(n) von den Beads eluiert. Dabei wurden die Bindungen zwischen interagierenden Proteinen, inklusive der Bindung zwischen Antikörper und Antigen aufgebrochen. (*C*) Das Eluat wurde anschließend parallel mittels zwei Verfahren bearbeitet. (1) Ein Teil des Eluats wurde benutzt, um die Molekulargewichte (MW) der Bestandteile der(s) präzipitierten Proteinkomplexe(s) mittels SELDI-MS zu ermitteln. (2) Der andere Teil des Eluats wurde, z.T. nach vorangegangener Auftrennung im SDS-Polyacrylamid-Gel sowie anschließender Detektion und Bearbeitung spezifischer Proteinbanden, tryptisch verdaut und die dabei entstandenen Fragmente im SELDI-Massenspektrometer vermessen. Die so ermittelten *peptide mass fingerprints* (PMF) wurden zur Suche in Datenbanken benutzt. Mit Antikörper-basierenden Experimenten wie Coimmunpräzipitation (Co-IP) und/oder *immunocapturing assays* wurde der bei dieser Suche gefundene Kandidat als potentieller Interaktionspartner bestätigt oder ausgeschlossen.

Ein spezifisches Signal bei 13,22 kD korrespondierte sehr gut zum MW von S100A9, einem bekannten Interaktionspartner von S100A8 (Dell´Angelica et al. 1996). Ein weiteres spezifisches Signal bei 11.065 kD wurde mittels PPIT als S100A10 identifiziert. Bei der anschließenden Suche nach Interaktionspartnern von S100A10 mit einem entsprechenden spezifischen Antikörper wurde in einem PPIT S100A7 als interagierendes Protein von S100A10 aufgedeckt. Mittels dieser „proof of principle“ Studie konnte wir erstmals zeigen, dass mit Hilfe von SELDI-MS, eingebunden in einen sogenannten „Protein-Protein-Interaktionstest“, Proteininteraktionen detektiert und mittels immunologischer Verfahren die daran beteiligten Faktoren identifiziert werden können. Eine Reihe weiterer Protein-Protein-

Interaktionen konnte durch den Einsatz dieses Verfahrens erstmals beschrieben werden (Arndt et al. 2007; Escher et al. 2007; Fegers et al. 2007; Kob et al. 2007; Marx et al. 2007).
Bei der Suche nach Interaktionspartnern von S100A11, das in kolorektalen Karzinomen überexprimiert vorliegt (Melle et al. 2006a), wurden weitere Proteininteraktionen detektiert. In dieser Studie konnten wir mittels eines PPIT feststellen, dass Rad54B spezifisch mit S100A11 interagiert (**Murzik et al.; Mol. Biol Cell 2008; 19: 2926-2935 – siehe Anhang 1.7**). Neben dieser Proteininteraktion konnte eine schon beschriebene Interaktion zwischen S100A11 und Aktin detektiert werden (Xhao et al. 2000). Um eine biologische Funktion dieses Komplexes zu ermitteln, wurden Immunfluoreszenz-basierende Untersuchungen mit anschließender konfokaler Laser-scanning Mikroskopie durchgeführt, da beide Proteine im Zellkern lokalisiert sein können (Broome et al. 1999; Wesoly et al. 2006). Hierbei konnten wir feststellen, dass beide Proteine in einem Foci-ähnlichen Muster im Zellkern von HaCaT-Keratinocyten kolokalisieren. Rad54B ist eine DNA-abhängige ATPase, die an der homologen Rekombinations-Reparatur von DNA beteiligt ist (Miyagawa et al. 2002; Wesoly et al. 2006). Homologe Rekombination (HR) ist ein Haupt-Reparaturweg von Doppelstrang-Brüchen (DSB) in der DNA (Wolner et al. 2003). Die Induktion von DNA-Schäden mittels Bleomycin (BLM) verursachte schon 30 min nach Schadensinduktion eine sichtbare Zunahme der Kolokalisierung zwischen S100A11 und Rad54B an Stellen der DNA-DSB-Reparatur. Diese Reparaturstellen wurden durch Immunfluoreszenz gegen γH2AX-Foci detektiert. Die Phosphorylierung von H2AX und die Bildung von γH2AX-Foci an DSB ist eine der ersten zellulären Antworten nach Induktion von DNA-Schäden (Rogakou et al. 1998). Die S100A11 – Rad54B-Kolokalisierung erreichte drei Stunden nach BLM-Behandlung ihr höchstes Niveau und verringerte sich danach wieder auf das Niveau vor der DNA-Schadensinduktion, welches nach ungefähr 24 Stunden erreicht wurde. Der Komplex aus S100A11 und Rad54B kolokalisiert direkt mit DNA-Schadensstellen wie wir in einem Immunfluoreszenz-basierenden Experiment zeigten, das gleichzeitig S100A11, Rad54B und γH2AX detektierte. Hierbei kolokalisierten S100A11, Rad54B und γH2AX in Foci im Nukleoplasma von HaCaT-Zellen. Der Einfluss von S100A11 hinsichtlich der Erkennung von DNA-Schadensstellen durch Rad54B wurde mittels RNA-Interferenz-Experimenten geklärt. Dafür wurde S100A11 mittels einer spezifischen siRNA depletiert und die Foci-Formierung in mit BLM behandelten HaCaT-Keratinozyten untersucht. Eine signifikante Reduktion des S100A11 Proteinniveaus wurde 72 Stunden nach der Transfektion mit der spezifischen S100A11 siRNA in Immunblot-Untersuchungen gefunden. Im Gegensatz zu mit BLM behandelten HaCaT-Zellen, die mit einer unspezifischen, so genannten non-silencing siRNA transfiziert wurden und in denen

Rad54B in Foci erschien, zeigten die mit der spezifischen S100A11 siRNA transfizierten Zellen eine diffuse nukleoplasmatische Lokalisierung von Rad54B. In den HaCaT-Zellen, die mit der unspezifischen siRNA transfiziert wurden, konnte weiterhin eine Kolokalisierung des S100A11/Rad54-Komplexes mit γH2AX in Foci an DNA-Schadens-Reparaturstellen gefunden werden. Daraus lässt sich schließen, dass das Auftreten von Rad54B-Foci an DNA-Schadensstellen vom Protein-Status von S100A11 abhängt und nicht von der Induktion von DNA-Schäden mittels BLM.

Zusätzlich konnten wir eine erhöhte Proteinexpression von p21 nach Induktion von DNA-Schäden mittels BLM in HaCaT-Zellen finden. Überraschenderweise wurde das p21-Proteinniveau signifikant reduziert, wenn S100A11 mittels einer spezifischen siRNA herunterreguliert wurde. Diese Daten können in Einklang mit einer kürzlich erschienen Studie gebracht werden, die eine Induktion von p21 nach dem Transfer von S100A11 in den Zellkern zeigte (Sakaguchi et al. 2003). Gleichzeitig verschlechterte sich die Proliferationskapazität der HaCaT-Zellen mit durch RNA-Interferenz herunterregulierten S100A11. Der Anteil der apoptotischen Zellfraktion von S100A11 *knock-down* Zellen erhöhte sich signifikant im Vergleich zu Kontrollzellen. Hierbei scheint die Funktion von p21 als Inhibitor der Apoptose, eingeschränkt zu sein (Gartel, Tyner 2002). Es scheint, dass S100A11 einerseits Verantwortung für die Akkumulation von Rad54B an Orten der DNA-DSB-Reparatur trägt und andererseits eine Rolle bei der p21-vermittelten Zellzyklus-Regulation spielt.

4 Zusammenfassung und Ausblick

Trotz des enormen Aufwandes, der mittels des Einsatzes der neuesten Ergebnisse und Ansätze aus Genomik, Proteomik und molekularer Medizin unternommen wird, zeigen sich bei früher Diagnose und adäquater Behandlung der häufigsten Tumorentitäten nur hinter den Erwartungen zurückliegende Erfolge. Die momentan benutzten Tumormarker, die vor allem bei Analysen von Serum und anderen Körperflüssigkeiten gefunden wurden, besitzen hinsichtlich ihrer Eignung zur Früherkennung oder Prognose spezifischer Tumorentitäten nur eingeschränktes Potential.

Der **erster Schwerpunkt** der vorliegenden Arbeit war es, einen technischen Ansatz zu entwickeln, mit dem differentiell exprimierte Proteine aus Gewebe identifiziert werden, die zwischen Tumorgewebe und Tumor-distanten Gewebe diskriminieren können. Hierfür wurde als zentrale proteomische Technik die SELDI (engl.; surface-enhanced laser desorption/ionization) Massenspektrometrie (MS) benutzt. Diese Technik wird als „cancer biomarker discovery tool“ angesehen (Diamandis 2004), die bei der Detektion Tumor-spezifischer Proteinmuster und Identifizierung von Tumormarkern aus Körperflüssigkeiten schon zum Einsatz kam. Hierbei zeigte sich aber, dass die mit SELDI-MS in Serum detektierten diskriminierenden Signale Proteinen entsprachen, die in Konzentrationsbereichen vorlagen, die nicht mit den erwarteten Konzentrationen eines vom Primärtumor in den Blutstrom abgegebenen Proteins in Einklang zu bringen waren und wahrscheinlich sekundären Krankheitserscheinungen, die nicht direkt mit Tumorgenese in Verbindung stehen, zu zuordnen sind. Da momentan noch keine massenspektrometrische Technik beschrieben wurde, um solch niedrig konzentrierten Proteine in Körperflüssigkeiten ausreichend sicher detektieren zu können, wurde mit Tumorgewebe die unmittelbare Quelle potentieller Tumormarker als Untersuchungsmaterial ausgewählt. Um Kontaminationen mit ungewünschten Gewebearealen zu vermeiden und einzuschränken, wurden die zu untersuchenden Gewebeproben mittels Laser-Mikrodissektion gewonnen. Nach der SELDI-MS - Analyse dieser Probe ergab sich ein Gewebe-spezifisches Proteinmuster, das sich aus differentiell exprimierten Proteinen zusammensetzte. Zur Identifizierung solcher diskriminierenden Signale wurden die Proteinlysate mittels zwei-dimensionaler Gelelektrophorese aufgetrennt, die „petide mass fingerprints“ (PMF) einzelner, tryptisch verdauter Proteinspots aus dem Gel mittels SELDI-MS ermittelt und zur Suche in einer Protein-Datenbank benutzt. Die hierbei erhaltenen Kandidaten wurden mittels immunologischen Techniken und SELDI-Analyse bestätigt oder verworfen. Um die so

gefundenen potentiellen Tumormarker-Kandidaten weiter zu charakterisieren, wurden immunhistochemische Untersuchungen durchgeführt. Dabei konnte die Lokalität dieser Proteine im Gewebe aufgeklärt werden, die Rückschlüsse auf mögliche physiologische Funktionen erlauben.

Die in dieser Arbeit entwickelte technische Triade, bestehend aus Gewebe-Mikrodissektion, SELDI-MS-Analyse und Immunhistochemie (IHC), wurde zur Identifizierung und Charakterisierung differentiell exprimierter Proteine aus unterschiedlichen Tumorentitäten benutzt. Mittels dieser technischen Triade wurden die Ca^{2+}-bindenden Proteine S100A8 und S100A9 als diskriminierende Proteine bei einer Untersuchung von Hals-Kopf-Tumoren identifiziert. Es wurde gezeigt, dass mittels oben benannter Proteine Tumor-distantes, normales Pharynxepithel von epithelialen Tumorzellen der Pharynx genau unterschieden werden kann. S100A8 wie auch S100A9 wurden bisher mit einer signifikant erhöhten Proteinexpression in verschiedenen Tumorentitäten (z. B. Kolon-, Prostata-, Magenkarzinom) beschrieben. In der hier vorliegenden Arbeit konnte das erste Mal eine verminderte S100A8- bzw. S100A9-Proteinexpression mit einer Tumorentität in Verbindung gebracht werden. Mit S100A2 und S100A11 gibt es zwei weitere Mitglieder der S100-Proteinfamilie, die ein ähnliches Charakteristikum zeigen, indem sie in spezifischen Tumorentitäten überexprimiert und in anderen spezifischen Tumorentitäten mit zum entsprechenden Normalgewebe verringerter Proteinexpression vorliegen. Das Expressionsverhalten von S100A8 bzw. S100A9 in weiteren Tumorentitäten muss Gegenstand zukünftiger Untersuchungen sein.

Der **zweiter Schwerpunkt** der vorliegenden Arbeit war die Validierung der im Gewebe mittels technischer Triade gefundenen potentiellen Proteinmarker im Serum. Hierbei konnten die α-Defensine 1-3 (HNP1-3), die im Kolonkarzinom im Vergleich zu Tumor-distanten, normalen Kolonepithel differentiell überexprimiert gefunden wurden, ebenfalls in ELISA-Tests mit Seren von Kolonkarzinom-Patienten mit signifikant erhöhter Konzentration im Vergleich zu Kontrollseren detektiert werden. Hierbei ist anzumerken, dass Signale, die zu HNP1-3 korrespondieren, auf Grund ihrer geringen Proteinkonzentration in Seren mittels SELDI-MS nicht detektiert werden konnten und somit die Identifizierung der HNP1-3 als potentieller Tumormarker-Kandidat für Kolonkarzinome ausschließlich durch die initiale Untersuchung am Gewebe erfolgreich war. Momentan ist unsere Arbeitsgruppe in ein durch das BMBF gefördertes Projekt maßgeblich involviert, das in Zusammenarbeit mit universitären und Industrie-Partnern die Entwicklung und Validierung von Antikörper-Chips zur Detektion von Kolonkarzinomen, die unter anderem auf der Vermessung der HNP1-3 - Konzentration basieren, beinhaltet.

Kürzlich wurde als Kongressbeitrag ebenfalls das geplante Konzept einer anderen Arbeitsgruppe zur Validierung von Tumormarkern aus Serum, die in vorangehenden Analysen in Gewebe detektiert werden sollen, vorgestellt (Meyer, Stühler 2007; Cottingham 2007).

In dieser Arbeit wurde des Weiteren die Proteinkonzentration von S100A8, das wie oben erwähnt als diskriminierendes Protein in Pharynxkarzinomen gefunden wurde, in Seren von Patienten mit Hals-Kopf-Tumoren und Kontrollen validiert. Hierbei wurden die Ergebnisse der vorangegangenen Untersuchungen in Pharynxgewebe bestätigt, indem gezeigt wurde, dass die S100A8-Proteinkonzentration in Normalseren gegenüber Patientenseren signifikant erhöht vorliegt. Zukünftige Studien mit einer größeren Anzahl an Seren, die in spezifische Gruppen hinsichtlich Tumorgrad, Normalkontrollen ohne Befund, Tumor-negative Kontrollen mit Befund etc. eingeteilt sind, müssen zeigen, ob S100A8, ähnlich S100B für Melanome (Salama et al. 2007), als potentieller, diagnostischer und/oder prognostischer Tumormarker-Kandidat dienen kann.

In der vorliegenden Arbeit wurden im **dritten Schwerpunkt** außerdem die Proteinprofile verschiedener Tumorentitäten miteinander verglichen. Hierbei wurde gezeigt, dass Karzinome des Kolon und Pharynx hinsichtlich ihres Proteinprofiles eine größere Ähnlichkeit besitzen als zum entsprechenden Tumor-distanten Normalgewebe. Gleichzeitig wurden in dieser Arbeit mit S100A6 und S100A11 zwei Proteinmarker ermittelt, mit denen zwei unterschiedliche Tumorentitäten, hepatozelluläres Karzinom (HCC) und kolorektales Karzinom (CRC), unterschieden werden können. Es scheint, dass mit S100A6 zusätzlich ein potentieller Proteinmarker-Kandidat existiert, mit dem Leber-Metastasen aus kolorektalem Karzinom (MTS) und HCC diskriminiert werden können. Zukünftige Arbeiten hierzu sollen einerseits zu einem einheitlichen Tumor-Proteinprofil und andererseits zu einem spezifischen, vom jeweiligen Primärtumor unabhängigen Metastasen-Proteinprofil führen. Außerdem sollen proteomische Ähnlichkeiten zwischen Metastase und jeweiligen Primärtumor erarbeitet werden. Dadurch erwarten wir zweierlei: (I) die Unterscheidung der Metastasen von einem möglicherweise parallel dazu auftretenden primären Tumor im selben Gewebe und (II) Rückschlüsse auf die Identität des metastasierenden Primärtumors.

Ein Weg, um die in „protein profiling“-Experimenten identifizierten Proteinmarker-Kandidaten zu charakterisieren und einen Einblick hinsichtlich ihrer biologischen Funktion zu erhalten, ist die Identifizierung von mit diesen Proteinmarkern interagierenden Proteinen. Hierzu wurde im **vierten Schwerpunkt** dieser Arbeit ein sogenannter „Protein-Protein-Interaktionstest“ (PPIT) etabliert. Mit diesem wurden ausschließlich in vivo existierende

Protein-Interaktionen aufgedeckt. Hierbei wurden in einer „proof of principle“-Studie Interaktionspartner von S100-Proteinen identifiziert. In dieser Arbeit wurde des Weiteren Rad54B, eine DNA-abhängige ATPase, die an der homologen Rekombinationsreparatur beteiligt ist, als Interaktionspartner von S100A11 identifiziert und diese Proteininteraktion charakterisiert. Dabei konnte gezeigt werden, dass Rad54B mit S100A11 an DNA-Doppelstrang-Brüchen kolokalisiert. In Zellkulturen, in denen S100A11 mittels RNA-Interferenz depletiert wurde, konnte Rad54B Orte mit Doppelstrang-Brüchen nicht erkennen, was scheinbar zu einer Verminderung der DNA-Schadensreparatur führte, da das Potential dieser Zellen Kolonien zu bilden im Vergleich zu Kontrollen signifikant eingeschränkt war. Gleichzeitig war in den S100A11 depletierten Zellen eine Abnahme der p21-Proteinexpression zu verzeichnen, die sich auch in einer erhöhten Anzahl an apoptotischen Zellen und in einer reduzierten Proliferationskapazität widerspiegelte. Zukünftige Experimente müssen zeigen, ob und wenn ja, welche Rolle S100A11 bei der Regulation des Zellzykluses spielt.

Die in der vorliegenden Arbeit dargestellten Experimente haben potentielle Tumormarker-Kandidaten aufgedeckt. Umfassende Studien mit einer erweiterten Probenzahl inklusive Proben von Patienten ohne entsprechende Tumorentität sollen eine mögliche Spezifität dieser Tumormarker-Kandidaten validieren sowie Untersuchungen zum Inhalt haben, ob diese Marker neben Gewebe zusätzlich auch in nicht-invasiv zu entnehmenden Material wie Serum auftreten und hier ebenfalls diskriminierend sind, wie die in dieser Arbeit aufgeführten ersten Ergebnisse vermuten lassen. Des Weiteren sollen in zukünftigen Experimenten weitere Interaktionspartner von in vorangegangenen Proteinprofil-Untersuchungen detektierten Markern sowie von weiteren Mitgliedern der S100-Proteinfamilie identifiziert und diese Proteinkomplexe zell- und molekularbiologisch charakterisiert werden, um so Rückschlüsse auf ihre biologischen Funktionen zu gewinnen.

5 Literatur

Aebersold R, Mann M. Mass spectrometry-based proteomics. Nature 2003; 422: 198-207.

Alexander H, Stegner AL, Wagner-Mann C, et al. Proteomic analysis to identify breast cancer biomarkers in nipple aspirate fluid. Clin. Cancer Res. 2004; 10: 7500-7510.

Anderson NL, Anderson NG. The human plasma proteome: history, character, and diagnostic prospects. Mol. Cell. Proteomics 2002; 1: 845-867.

Arndt S, Melle C, Mondal K, et al. Interactions of TANGO and leukocyte integrin CD11c/CD18 regulate the migration of human monocytes. J. Leukoc. Biol. 2007; 82: 1466-1472.

Bonfrer JM, Korse CM, Nieweg OE, et al. The luminescence immunoassay S-100: a sensitive test to measure circulating S-100B: ist prognostic value in malignant melanoma. Br. J. Cancer 1998; 77: 2210-2214.

Broome AM, Ryan D, Eckert RL. S100 protein subcellular localization during epidermal differentiation and psoriasis. J. Histochem. Cyctochem. 2003; 51: 675-685.

Cazares LH, Adam BL, Nasim S, et al. Normal, benign, preneoplastic, and malignant prostate cells have distinct protein expression profiles resolved by surface enhanced laser desorption/ionization mass spectrometry. Clin. Cancer Res. 2002; 8: 2541-2552.

Chaurand P, DaGue BB, Pearsall RS; et al. Profiling proteins from azoxymethane-induced colon tumors as the molecular levels by matrix-assisted laser desorption/ionization mass spectrometry. Proteomics 2001; 1: 269-279.

Chen CD, Wang CS, Huang YH, et al. Overexpression of CLIC1 in human gastric carcinoma and its clinicopathological significance. Proteomics 2007; 7: 155-167.

Cheung PK, Woolcock B, Adomat H, et al. Protein profiling of microdissected prostate tissue links growth differentiation factor 15 to prostate carcinogenesis. Cancer Res. 2004; 64: 5929-5933.

Cho YG, Nam SW, Kim TY, et al. Overexpression of S100A4 is closely related to the aggressiveness of gastric cancer. APMIS 2003; 111: 539-545.

Cho WSC, Yip TTC, Yip C, et al. Identification of serum amyloid A protein as a potentially useful biomarker to monitor relapse of nasopharyngeal cancer by serum proteomic profiling. Clin. Cancer Res. 2004; 10: 43-52.

Cottingham K. Meeting news: discovering biomarkers with high-performance proteomics. J. Proteome Res. 2007; 6: 4546.

Coulombe B, Jeronimo C, Langelier MF, et al. Interaction networks of the molecular machines that decode, replicate, and maintain the integrity of the human genome. Mol. Cell. Proteomics 2004; 3: 851-856.

Craven RA, Banks RE. Laser capture microdissection and proteomics: possibilities and liminations. Proteomics 2001; 1: 1200-1204.

Cunliffe RN, Kamal M, Rose FR, et al. Expression of antimicrobial neutrophil defensins in epithelial cells of active inflammatory bowel disease mucosa. J. Clin. Pathol. 2002; 55: 298-304.

Davies MP, Rudland PS, Robertson L, et al. Expression of the calcium-binding protein S100A4 (p9Ka) in MMTV-neu transgenic mice induces metastasis of mammary tumours. Oncogene 1996; 13: 1631-1637.

Dell´Angelica EC, Schleicher CH, Simpson RJ, et al. Complex assembly of calgranulins A and B, two S100-like calcium-binding proteins from pig granulocytes. Int. J. Biochem. Cell Biol. 1996; 28: 53-62.

Devery JM, King NJ, Geczy CL, et al. Acute inflammatory activity of the S100 protein CP-10: activation of neutrophils in vivo and in vitro. J. Immunol. 1994; 152: 1888-1897.

Diamandis EP. Mass spectrometry as a diagnostic and a cancer biomarker discovery tool. Mol. Cell. Proteomics 2004; 3: 367-378.

Diamandis EP. Serum proteomic profiling by matrix-assisted laser desorption-ionization time-of-flight mass spectrometry for cancer diagnosis: next steps. Cancer Res. 2006; 66: 5540-5541.

Diamandis EP, van der Merwe DA. Plasma protein profiling by mass spectrometry for cancer diagnosis: oportunities and liminations. Clin. Cancer Res. 2005; 11: 963-965.

Diamond DL, Kimball JR, Krisanaprakornkit S, et al. Detection of β-defensins secreted by human oral epithelial cells. J. Immunol. Methods 2001; 256: 65-76.

Donato R. S100: a multigenic family of calcium-modulated proteins of the EF-hand type with intracellular and extracellular functional roles. Int. J. Biochem. Cell Biol. 2001; 33: 637-668.

Donato R. Intracellular and extracellular roles of S100 proteins. Microsc. Res. Technol. 2003; 60: 540-551.

Dowen SE, Crnogorac-Jurcevic T. S100 proteins in cancer. Calcium Binding Proteins 2006; 1: 143-149.

Druker BJ, Tamura S, Buchdunger E, et al. Effects of a selective inhibitor of the Abl tyrosine kinase on the growth of Bcr-Abl positive cells. Nat. Med. 1996; 2: 561-566.

Emberley ED, Niu Y, Leygue E, et al. Psoriasin interacts with Jab1 and influences breast cancer progression. Cancer Res. 2003; 63: 1954-1961.

Escher N, Kob R, Tenbaum SP, et al. Various members of the E2F transcription factor family interact in vivo with the corepressor Alien. J. Proteome Res. 2007; 6: 1158-1164.

Etzioni R, Urban N, Ramsey S, et al. The case for early detection. Nature Rev. Cancer 2003; 3: 243-252.

Fegers I, Kob R, Eckey M, et al. The tumor suppressor p33ING1 and p33ING2 interact with Alien in vivo and enhance Alien-mediated gene silencing. J. Proteome Res. 2007; 6: 4182-4188.

Feng G, Xu X, Youssef EM, et al. Diminished expression of S100A2, a putative tumor suppressor, at early stage of human lung carcinogenesis. Cancer Res. 2001; 61: 7999-8004.

Gartel AL, Tyner AL. The role of the cyclin-dependent kinase inhibitor p21 in apoptosis. Mol. Cancer Ther. 2002; 1: 639-649.

Gongoll S, Peters G, Mengel M, et al. Prognostic significance of calcium-binding protein S100A4 in colorectal cancer. Gastroenterology 2002; 123: 1478-1484.

Gonzalez HE, Gujrati M, Frederick M, et al. Identification of 9 genes differentially expressed in head and neck squamous cell carcinoma. Arch. Otolaryngol. Head Neck Surg. 2003; 129: 754-759.

Grigorian M, Andresen S, Tulchinsky E, et al. Tumor suppressor p53 protein is a new target for the metastatis-associated Mts/S100A4 protein: functional consequences of their interaction. J. Biol. Chem. 2001; 276: 22699-22708.

Guedj N, Dargere D, Degos F, et al. Global proteomic analysis of microdissected cirrhotic nodules reveals significant biomarkers assoziated with clonal expansion. Lab. Invest. 2006; 86: 951-958.

Heizmann CW, Cox JA. New perspectives on S100 proteins: a multi-functional Ca^{2+}-, ZN^{2+}- and Cu^{2+}-binding protein family. Biometals 1998; 11: 383-397.

Heizmann CW, Fritz G, Schafer BW. S100 proteins: structure, functions and pathology. Front. Biosci. 2002; 7: d1356-1368.

Helmberger TK, Laubenberger J, Rummeny E, et al. MRI characteristics in focal hepatic disease before and after administration of MnDPDP: discriminant analysis as a diagnostic tool. Eur. Radiol. 2002; 12: 62-70.

Hermani A, De Servi B, Medunjanin S, et al. S100A8 and S100A9 activate MAP kinase and NF-kappaB signaling pathways and trigger translocation of RAGE in human prostate cancer cells. Exp. Cell Res. 2006; 312: 184-197.

Hiratsuka S, Watanabe A, Aburatani H, et al. Tumour-mediated upregulation of chemoattractants and recruitment of myeloid cells predetemines lung metastasis. Nat. Cell Biol. 2006; 8: 1369-1375.

Hlavaty JJ, Partin AW, Shue MJ, et al. Identification and preliminary clinical evaluation of a 50.8 kDa serum marker for prostate cancer. Urology 2003; 61: 1261-1265.

Hutchens TW, Yip TT. New desorption strategies for the mass spectrometric analysis of macromolecules. Rapid Commun. Mass Spektrom. 1993; 7: 576-580.

Ito Y, Yoshida H, Tomoda C, et al. Expression of S100A2 and S100A6 in thyroid carcinomas. Histopathology 2005; 46: 569-575.

Jemal A, Murray T, Ward E, et al. Cancer statistics, 2005. CA Cancer J. Clin. 2005; 55: 10-30.

Kennedy RD, Gorski JJ, Quinn JE, et al. BRCA1 and c-Myc associate to transcriptionally repress psoriasin, a DNA damage-inducible gene. Cancer Res. 2005; 65: 11326-11334.

Kob R, Baniahmad A, Escher N, et al. Detection and identification of transcription factors as interaction partners of Alien in vivo. Cell Cycle 2007; 6: 393-396.

Komatsu K, Andoh A, Ishiguro S, et al. Increased expression of S100A6 (Calcyclin), a calcium-binding protein of the S100 family, in human colorectal adenocarcinoma. Clin. Cancer Res. 2000; 6: 172-177.

Kooman JM, Shih LN, Coombes KR, et al. Plasma protein profiling for diagnosis of pancreatic cancer reveals the presence of host response proteins. Clin. Cancer Res. 2005; 11: 1110-1118.

Kooman JM, Li D, Xiao LC, et al. Direct tandem mass spetrometry reveals limitations in protein profiling experiments for plasma biomarker discovery. J. Proteome Res. 2005; 4: 972-981.

Kriajevska M, Tarabykina S, Bronstein I, et al. Metastasis-associated Mts1 (S100A4) protein modulates protein kinase C phosphorylation of the heavy chain of nonmuscle myosin. J. Biol Chem. 1998; 273: 9852-9856.

Krieg RC, Fogt F, Braunschweig T, et al. ProteinChip Array analysis of microdissected colorectal carcinoma and associated tumor stroma shows specific protein bands in the 3.4 to 3.6 kDa range. Anticancer Res. 2004; 24: 1791-1796.

Lau W, Devery JM, Geczy CL. A chemotactic S100 peptide enhances scavenger receptor and Mac-1 expression and cholesteryl ester accumulation in murine peritoneal macrophages in vivo. J. Clin. Invest. 1995; 95: 1957-1965.

Lehmann R, Melle C, Escher N, et al. Detection and identification of protein interactiosn of S100 proteins by ProteinChip technology. J. Proteome Res. 2005b; 4: 1717-1721.

Liotta LA, Ferrari M, Petricoin E. Written in blood. Nature 2003; 425: 905.

Maelandsmo GM, Florenes VA, Mellingsaeter T, et al. Differential expression patterns of S100A2, S100A4 and S100A6 during progression of human malignant melanoma. Int. J. Cancer 1997; 74: 464-469.

Malik G, Ward MD, Gupka SK, et al. Serum levels of an isoform of apolipoprotein A-II as a potential marker for prostate cancer. Clin. Cancer Res. 2005; 11: 1073-1085.

Marx FP, Soehn AS, Berg D, et al. The proteosomal subunit S6 ATPase is a novel synphilin-1 interacting protein – implications for Parkinson´s disease. FASEB J. 2007; 21: 1759-1767.

Melle C, Ernst G, Schimmel B, et al. Biomarker discovery and identification in laser microdissected head and neck squamous cell carcinoma with ProteinChip technology, two-dimensional gel electrophoresis, tandem mass spectrometry, and immunohistochemistry. Mol. Cell. Proteomics 2003; 2: 443-452.

Melle C, Ernst F, Schimmel B, et al. A technical triade for proteomic identification and characterization of cancer biomarkers. Cancer Res. 2004; 64: 4099-4104.

Melle C, Ernst G, Schimmel B, et al. Discovery and identification of α-defensins as low abundant, tumor-derived serum markers in colorectal cancers. Gastroenterology 2005a; 129: 66-73.

Melle C, Ernst G, Schimmel B, et al. Characterization of pepsinogen C as potential biomarker for gastric cancer using a histo-proteomic approach. J. Proteome Res. 2005b; 4: 1799-1804.

Melle C, Ernst G, Schimmel B, et al. Different expression of calgizzarin (S100A11) in normal colonic epithelium, adenoma and colorectal carcinoma. Int. J. Oncol. 2006a; 28: 195-200.

Melle C, Bogumil R, Ernst G, et al. Detection and identification of heat shock protein 10 as a biomarker in colorectal cancer by protein profiling. Proteomics 2006b; 6: 2600-2608.

Melle C**,** Ernst G, Scheibner O, et al. Identification of specific protein markers in microdissected HCC. J. Proteome Res. 2007a; 6: 306-315.

Melle C, Ernst G, Escher N, et al. Protein profiling of microdissected pancreas carcinoma and identification of HSP27 as a potential serum marker. Clin. Chem. 2007b; 53: 629-635.

Melle C, Ernst G, Schimmel B, et al. Colon-derived liver metastasis, colorectal carcinoma, and hepatocellular carcinoma can be discriminated by Ca^{2+}-binding proteins S100A6 and S100A11. PLoS ONE 2008; 3: e3767.

Memon AA, Sorensen BS, Meldgaard P, et al. Down-regulation of S100C is associated with bladder cancer progression and poor survival. Clin. Cancer Res. 2005; 11: 606-611.

Meyer HE, Stühler K. High-performance proteomics as a tool in biomarker discovery. Proteomics 2007; 7 Suppl. 1: 18-26.

Miyagawa K, Tsuruga T, Kinomura A, et al. A role for RAD54B in homologous recombination in human cells. EMBO J. 2002; 21, 175-180.

Moore BW. A soluble protein characteristic of nervous system. Biochem. Biophys. Res. Commun. 1965; 19: 739-744.

Mueller A, O`Rourke J, Grimm J, et al. Distinct gene expression profiles characterize the histopathological stages of disease in Helicobacter-induced mucosa-associated lymphiod tissue lymphoma. Proc. Natl. Acad. Sci. USA 2003; 100: 1292-1297.

Mueller A, Schafer BW, Ferrari S, et al. The calcium-binding protein S100A2 interacts with p53 and modulates its transcriptional ctivity. J. Biol. Chem. 2005; 280: 29186-29193.

Müller U, Ernst G, Melle C, et al. Convergence of the proteomic pattern in cancer. Bioinformatics 2006; 22: 1293-1296.

Murzik U, Hemmerich P, Weidtkamp-Peters S, et al. Rad54B targeting to DNA double-strand break sites requires complex formation with S100A11. Mol. Biol. Cell 2008; 19: 2926-2935.

Mustafa DA, Burgers PC, Dekker LJ, et al. Identification of glioma neovascularization-related proteins by using MALDI-FTMS and nano-LC fractionation to microdissected tumor vessels. Mol. Cell. Proteomics 2007; 6: 1147-1157.

Nikitenko LL, Lloyd BH, Rudland PS, et al. Localisation oby in situ hybridisation of S100A4 (p9Ka) mRNA in primary human breast tumour specimens. Int. J. Cancer 2000; 86: 219-228.

Ogawa H, Fukushima K, Sasaki I, et al. Identification of genes involved in mucosal defense and inflammation associated with normal enteric bacteria. Am. J. Physiol. Gastrointest. Liver Physiol. 2000; 279: G492-G499.

Rafii S, Lyden D. S100 chemokines mediate bookmarking of premetastatic niches. Nat. Cell Biol. 2006; 8: 1321-1323.

Rehman I, Azzouzi AR, Cross SS, et al. Dysregulated expression of S100A11 (calgizzarin) in prostate cancer and precursor lesions. Hum. Pathol. 2004; 35: 1385-1391.

Rogakou EP, Pilch DR, Orr OH, et al. DNA double-strand breaks induce histone H2AX phosphorylation on serine 139. J. Biol. Chem. 1998; 273: 5858-5868.

Sakaguchi M, Miyazaki M, Takaishi M, et al. S100C/A11 is a key mediator of Ca^{2+} -induced growth inhibition of human epidermal keratinocytes. J. Cell Biol. 2003; 163, 825-835.

Sakaguchi M, Sonegawa H, Nukui T, et al. Bifurcated converging pathways for high Ca2+- and TGFbeta-induced inhibition of growth of normal human keratinocytes. Proc. Natl. Acad. Sci. USA 2005; 102: 13921-13926.

Sakaguchi M, Sonegawa H, Murata H, et al. S100A11, an dual mediator for growth regulation of human keratinocytes. Mol. Biol. Cell 2008; 19: 78-85.

Salama I, Malone PS, Mihaimeed F, et al. A review of the S100 proteins in cancer. Eur. J. Surg. Oncol. 2008; 34: 357-364.

Saleem M, Kweon MH, Johnson JJ, et al. S100A4 accelerates tumorigenesis and invasion of human prostate cancer through the transcriptional regulation of matrix metalloproteinase 9. Proc. Natl. Acad. Sci. USA 2006; 103: 14825-14830.

Santamaria-Kisiel L, Rintala-Dempsey AC, Shaw GS. Calcium-dependent and –independent interactions of the S100 protein family. Biochem. J. 2006; 396: 201-214.

Sawyers CL, Hochhaus A, Feldman E, et al. Imatinib induces hematologic and cytogenetic responses in patients with chronic myelogenous leukemia in myeloid blast crisis: results of a phase II study. Blood 2002; 99: 3530-3539.

Schäfer BW, Wicki R, Engelkamp D. et al. Isolation of YAC clone covering a cluster of nine S100 genes on human chromosome 1q21: rationale for a new nomenclature of the S100 calcium-binding protein family. Genomics 1995; 25: 638-643.

Schlagenhauff B, Schittek B, Ellwanger U, et al. Significance of serum protein S100 levels in screening for melanoma metastasis: does protein S100 enable early detection of melanoma recurrence? Melanoma Res. 2000; 10: 451-459.

Service RF. Public projects gear up to chart the protein landscape. Science 2003; 302: 1316-1318.

Smith SL, Gugger M, Hoban P, et al. S100A2 is strongly expressed in airway basal cells, preneoplastic bronchial lesions and primary non-small cell lung carcinomas. Br. J. Cancer 2004; 91: 1515-1524.

Stulik J, Osterreicher J, Koupilova K, et al. The analysis of S100A8 and S100A9 in matched sets of macroscopically normal colon mucosa and colorectal carcinoma: the S100A8 and S100A9 positive cells underlie and invade tumor mass. Electrophoresis 1999; 20: 1047-1054.

Thorey IS, Roth J, Regenbogen J, et al. The Ca2+-binding proteins S100A8 and S100A9 are encoded by novel injury-regulated genes. J. Biol. Chem. 2001; 276: 35818-35825.

Tsai WC, Tsai ST, Jin YT, et al. Cyclooxygenase-2 is involved in S100A2-mediated tumor suppression in squamous cell carcinoma. Mol. Cancer Res. 2006; 4: 539-547.

Vlahou A, Schellhammer PF, Mendrinos S, et al. Development of a novel proteomic approach for the detection of transitional cell carcinoma of the bladder in urine. Am. J. Pathol. 2001; 158: 1491-1502.

von Eggeling F, Melle C, Ernst G. Microdissecting the proteome. Proteomics 2007; 7: 2729-2737.

Welsh JB, Sapinoso LM, Kern SG, et al. Large-scale delineation of secreted protein biomarkers overexpressed in cancer tissue and serum. Proc. Natl. Acad. Sci. USA 2003; 100: 3410-3415.

Wesoly J, Agarwal S, Sigurdsson S, et al. Different contributions of mammalian Rad54 paralogs to recombination, DNA damage repair, and meiosis. Mol. Cell. Biol. 2006; 26, 976-989.

Wolner B, van Komen S, Sung P, et al. Recruitment of the recombinational repair machinery at DNA double-strand break in yeast. Mol. Cell 2003; 12; 221-232.

Xhao XQ, Naka M, Muneyuki M, et al. Ca(2+)-dependent inhibition of actin-activated myosinATPase activity by S100C (S100A11), a novel member of the S100 protein family. Biochem. Biophys. Res. Commun. 2000; 267: 77-79.

Xu BJ, Caprioli RM, Sanders ME, et al. Direct analysis of laser capture microdissected cells by MALDI mass spectrometry. J. Am. Soc. Mass Spectrom. 2002; 13 :1292-1297.

Yao R, Davidson DD, Lopez-Beltran A, et al. The S100 proteins for screening and prognostic grading of bladder cancer. Histol. Histopathol. 2007; 22: 1025-1032.

Ye B, Cramer DW, Skates SJ, et al. Haptoglobin-alpha subunit as potential serum biomarker in ovarian cancer: identification and characterization using protein profiling and mass spectrometry. Clin. Cancer Res. 2003; 9: 2904-2911.

Yong HY, Moon A. Roles of calcium-binding proteins, S100A8 and S100A9, in invasive phenotype of human gastric cancer cells. Arch. Pharm. Res. 2007; 30: 75-81.

Zhang Z, Bast RC Jr, Yu Y, et al. Three biomarkers identified from serum proteomic analysis for detection of early stage ovarian cancer. Cancer Res. 2004; 64: 5882-5890.

Zhang D, Tai LK, Wong LL, et al. Proteomic study reveals that proteins involved in metabolic and detoxification pathways are highly expressed in HER-2/neu-positive breast cancer. Mol. Cell. Proteomics 2005; 4: 1686-1696.

Zhang L, Yu W, He T, et al. Contribution of human α-defensin 1, 2, 3 to the anti-HIV-1 activity of CD8 antiviral factor. Science 2002; 298: 995-1000.

Zolg W. The proteomic search for diagnostic biomarker. Mol. Cell. Proteomics 2006; 5: 1720-1726.

6 Danksagung

Die in der vorliegenden Habilitationsschrift zusammengefassten Arbeiten zur proteomischen Charakterisierung Tumor-spezifischer Biomarker wurden am Institut für Humangenetik und Anthropologie der Friedrich-Schiller-Universität Jena durchgeführt.

Mein Dank gilt an erster Stelle Herrn Prof. Dr. Uwe Claussen für eine stetige Förderung, verbunden mit seiner Diskussionsbereitschaft, die mir Probleme bewusst gemacht und Lösungen aufgezeigt hat.

Mein ganz besonderer Dank gilt Herrn PD Dr. Ferdinand von Eggeling für sein stetiges Interesse an der vorliegenden Arbeit und die immerwährende kollegial-kameradschaftliche Zusammenarbeit.

Herrn OA Dr. Günther Ernst danke ich sehr für seine Einführung in die medizinische Sichtweise hinsichtlich Tumorentstehung und -progression.

Ein ganz herzlicher Dank gebührt Ulrike Murzik, Niko Escher und Roland Lehmann, die an entscheidenden Teilaspekten dieser Arbeit mitgewirkt haben.

Mein Dank gilt des Weiteren Annett Bleul und Bettina Schimmel sowie den Mitarbeitern der Core Unit Chip Application (CUCA) Juliane Förste, Juliane Kelm, Robert Kob, Ute Müller, Julia Rosenhahn, Heike Thieme und Liane Wehder.

Schliesslich möchte ich mich herzlich bei den Kooperationspartnern bedanken, insbesondere Dr. R. Kaufmann, Dr. H. Mothes und Prof. Dr. U. Settmacher, Klinik für Allgemeinchirurgie des Universitätsklinikums Jena; Prof. Dr. K. H. Halbhuber, Institut für Anatomie 2 des Universitätsklinikums Jena; PD Dr. S. Koscielny, Klinik für HNO des Universitätsklinium Jena; PD Dr. R. Guthke, HKI Jena; PD Dr. P. Hemmerich, FLI Jena; Dr. D. Osterloh, Sirslab GmbH Jena; sowie Dr. R. Bogumil und Dr. A. Wiesner, Ciphergen GmbH.

II Einzelarbeiten

Veröffentlichungen, die dieser Arbeit zugrunde liegen

1.1 **Melle C**, Ernst G, Schimmel B, Bleul A, Koscielny S, Wiesner A, Bogumil R, Möller U, Osterloh D, Halbhuber KH, von Eggeling F. A technical triade for proteomic identification and characterization of cancer biomarkers. *Cancer Res.* **2004**; 64: 4099-4104.

1.2 **Melle C**, Ernst G, Schimmel B, Bleul A, Mothes H, Kaufmann R, Settmacher U, von Eggeling F. Differential expression of calgizzarin (S100A11) in normal colonic epithelium, adenoma and colorectal carcinoma. *Int. J. Oncol.* **2006**; 28: 195-200.

1.3 **Melle C**, Ernst G, Schimmel B, Bleul A, Thieme H, Kaufmann R, Mothes H, Settmacher U, Claussen U, Halbhuber KH, von Eggeling F. Discovery and identification of α-defensins as low abundant, tumor-derived serum markers in colorectal cancer. *Gastroenterology* **2005**; 129: 66-73.

1.4 **Melle C**, Ernst G, Schimmel B, Bleul A, von Eggeling F. Discrimination of colon-derived liver metastasis, primary colorectal carcinoma, and primary hepatocellular carcinoma by Ca^{2+}-binding proteins S100A6 and S100A11. *PLoS ONE* **2008**; 3: e3767.

1.5 Müller U, Ernst G, **Melle C**, Guthke R, von Eggeling F. Convergence of the proteomic pattern in cancer. *Bioinformatics* **2006**; 22: 1293-1296.

1.6 Lehmann R[*], **Melle C**[*#], Escher N, von Eggeling F. Detection and identification of protein interactions of S100 proteins by ProteinChip technology. *J. Proteome Res.* **2005**; 4: 1717-1721. ([*]beide Autoren fungieren als Erstautor; [#]korrespondierender Autor)

1.7 Murzik U, Hemmerich P, Weidtkamp-Peters S, Ulbricht T, Bussen W, Rosenhahn J, von Eggeling F, **Melle C**. Rad54B targeting to DNA double-strand break repair sites requires complex formation with S100A11. *Mol. Biol. Cell* **2008**; 19: 2926-2935.

Ehrenwörtliche Erklärung

Ich erkläre hiermit, dass mir die Habilitationsordnung der Friedrich-Schiller-Universität Jena vom 07. Januar 1997 bekannt ist.

Ferner erkläre ich, dass ich die vorliegende Arbeit ohne unzulässige Hilfe Dritter und ohne Benutzung anderer als der angegebenen Hilfsmittel angefertigt habe. Die aus anderen Quellen direkt oder indirekt übernommenen Daten und Konzepte sind unter Angabe der Quelle gekennzeichnet.

Keine zusätzlichen Personen waren an der inhaltlich-materiellen Erstellung der Arbeit beteiligt. Insbesondere habe ich hierfür nicht die entgeltliche Hilfe von Vermittlungs- bzw. Beratungsdiensten in Anspruch genommen. Niemand hat von mir unmittelbar oder mittelbar geldwerte Leistungen für Arbeiten erhalten, die im Zusammenhang mit dem Inhalt der vorliegenden Arbeit stehen.

Die Arbeit wurde bisher weder im In- noch Ausland in gleicher oder ähnlicher Form einer anderen Prüfungsbehörde vorgelegt.

Ich versichere, dass ich nach bestem Wissen die reine Wahrheit gesagt und nichts verschwiegen habe.

Jena, den 15.04.2008

Lebenslauf

Christian Melle

Persönliche Daten

Geburtsdatum:	06. April 1968
Geburtsort:	Jena
Familienstand:	verheiratet mit Simone Melle, geb. Czerwensky; zwei Kinder: Jacob (geb. 2001), Lilith (geb. 2005)
Nationalität:	deutsch
Wohnort:	Lutherstr. 155, 07743 Jena; Tel. 06341/446202

Schulbildung

1974 – 1984	Allgemeinbildende Oberschule Kahla
1984 – 1986	Erweiterte Oberschule Jena
1986	Abitur

Militärdienst

1986 – 1989	Militärdienst

Studium

1989 – 1990	Studiengang Agrarwissenschaften/Tierproduktion, Humboldt Universität zu Berlin
1990	Abbruch Studiengang Agrarwissenschaften/Tierproduktion
1990 – 1996	Studiengang Biologie/Dipl., Justus-Liebig-Universität Giessen
1993	Vordiplom
1995	Mündliche Prüfungen Diplom (Hauptfächer: Biochemie, Botanik; Nebenfächer: Pflanzenphysiologie, Zellbiologie)
1995 – 1996	Diplomarbeit am Fraunhofer-Institut für atmosphärische Umweltforschung, Garmisch-Partenkirchen; Thema: Charakterisierung von Monoterpenzyklasen aus Kiefer
1996	Erlangung des akademischen Grades „Diplom-Biologe“

Promotion

1996 – 1999	Doktorarbeit am Institut für Molekulare Biotechnologie Jena, Abt. Biochemie (Leitung Prof. Dr. F. Grosse); Thema: Komplexbildung zwischen der DNA-Polymerase α-Primase und dem Tumorsuppressorprotein p53
2000	Erlangung Dr. rer. nat.

Weitere wissenschaftliche Beruftätigkeit

2000	Postdoc; Div. of Biochemistry/Molecular Biology, IBLS, Univ. of Glasgow, UK; Labor Prof. Dr. N.B. La Thangue; Studien zur HAT-Aktivität von p300 und dem Kofaktor JMY
2001	wissenschaftlicher Mitarbeiter Biolitec AG Jena; Studien zur photodynamischen Therapie
2002	wissenschaftlicher Mitarbeiter am Institut für Humangenetik und Anthropologie, Universitätsklinikum Jena

[CANCER RESEARCH 64, 4099–4104, June 15, 2004]

A Technical Triade for Proteomic Identification and Characterization of Cancer Biomarkers

Christian Melle,[1] Günther Ernst,[1] Bettina Schimmel,[1] Annett Bleul,[1] Sven Koscielny,[2] Andreas Wiesner,[4] Ralf Bogumil,[4] Ursula Möller,[3] Dirk Osterloh,[5] Karl-Jürgen Halbhuber,[3] and Ferdinand von Eggeling[1]

[1]Core Unit Chip Application, Institute of Human Genetics and Anthropology, [2]Clinic of ENT Diseases, and [3]Institute of Anatomy II, Friedrich-Schiller-University, Jena; [4]Ciphergen Biosystems GmbH, Göttingen; and [5]SIRS-Lab GmbH, Jena, Germany

ABSTRACT

Biomarkers are needed to elucidate the biological background and to improve the detection of cancer. Therefore, we have analyzed laser-microdissected cryostat sections from head and neck tumors and adjacent mucosa on ProteinChip arrays. Two differentially expressed proteins ($P = 3.34 \times 10^{-5}$ and 4.6×10^{-5}) were isolated by two-dimensional gel electrophoresis and identified as S100A8 (calgranulin A) and S100A9 (calgranulin B) by in-gel proteolytic digestion, peptide mapping, tandem mass spectrometry analysis, and immunodepletion assay. The relevance of these single marker proteins was evaluated by immunohistochemistry. Positive tissue areas were reanalyzed on ProteinChip arrays to confirm the identity of these proteins. As a control, a peak with low *P* was identified as calgizzarin (S100A11) and characterized in the same way. This technical triade of tissue microdissection, ProteinChip technology, and immunohistochemistry opens up the possibility to find, identify, and characterize tumor relevant biomarkers, which will allow the movement toward the clonal heterogeneity of malignant tumors. Taking this approach, proteins were identified that might be responsible for invasion and metastasis.

INTRODUCTION

Despite enormous efforts, in only a few tumor diseases have relevant markers been established that can be used for early diagnosis or improved therapy in cancer (1, 2). This remains the case, although many new parallel genomic and proteomic techniques have been introduced in the last 5 years. The strategy of how to search for biomarkers therefore has to be reconsidered. One point might be that the *in situ* situation in tumors is neglected because results from starting material such as serum and nonmicrodissected tissue cannot be traced back to the biological properties or the heterogeneity of the tumor itself. Hence, microdissection, proteomic techniques, and immunohistochemistry (IHC) for the characterization have to be combined in a technical triade.

In this study, the proteomic technique surface-enhanced laser desorption/ionization-mass spectrometry (MS)-based ProteinChip technology has been used (3–5). First described by Hutchens and Yip (6), the technology makes use of affinity surfaces to retain proteins based on their physicochemical characteristics, followed by direct analysis by time of flight-MS. Proteins being retained on chromatographic surfaces can be easily purified from contaminants such as buffer salts or detergents, thus eliminating the need for preseparation techniques, as required with other MS techniques. Furthermore, the low sample requirements of this technique are ideal for small biopsies or microdissected tissue, which are required to produce the homogeneous tissue samples typically used in cancer research (7–10). Microdissected tissue material, free of contaminating and unwanted tissue components, is extremely important for finding reliable biomarkers in cancer diagnosis (11) and in elucidating clonal heterogeneity of tumors. In the case of epithelial tumors, the epithelial cells are separated from all surrounding tissue constituents. In normal tissue, the lining epithelium consists of only one or a few cell rows, whereas in tumor tissues, the boundaries to normal pharyngeal tissue are irregular and therefore can only be isolated with an extremely precise technique such as laser-based microdissection. The compatibility of laser-based microdissection with ProteinChip technology has been shown in a number of small studies (4, 8, 9, 12), but until now, only very few studies with a statistically relevant number of cases have been performed (10, 13).

When specific changes between the protein profile of microdissected tumor and normal pharyngeal epithelium tissue are found by ProteinChip technology, single peaks can be isolated and identified. Isolation and identification can be performed by either two-dimensional electrophoresis (14) or ProteinChip technology (15), where the isolated protein is digested by proteolytic enzyme cleavage, and the mass values of the fragments generated are used for peptide mapping to identify the protein of interest by a database search. Furthermore, for confirmatory identification, selected peptides can be sequenced by collision-induced dissociation using a ProteinChip Interface coupled to a tandem mass spectrometer (16, 17). Although successful identifications of surface-enhanced laser desorption/ionization-detected protein markers are frequently reported for other biological samples (18–21), those from microdissected materials are very rare (10). After identification, IHC with a specific antibody opens up the possibility to determine tissue distribution and localization of the identified proteins. By locating expression to specific tissue areas, insight into clonal heterogeneity and functional differentiation of the tumor can be obtained.

In the study presented here, pure microdissected populations of normal pharyngeal epithelium and tumor squamous epithelial cells were analyzed using ProteinChip arrays. The two differentially expressed peaks with the best *P* values, along with a control peak showing a low *P*, were identified using two-dimensional electrophoresis and in-gel digestion, peptide mapping, and tandem MS. The assumption that these proteins are identical to the differentially expressed peaks found by ProteinChip analysis was confirmed with an immunodepletion assay. The localization of these proteins in tissue was subsequently verified on cryostat sections of the squamous cell carcinomas of the head and neck (HNSCC) by IHC, using the corresponding monoclonal antibodies or antiserum, respectively. Positive tissue areas were microdissected in corresponding serial unstained tissue sections and reanalyzed using ProteinChip arrays to show that these proteins are matching to the differentially expressed peaks found in the prior analysis. Thereby, the relevance of statistically significant proteins could be traced back to the *in situ* situation in the tumor.

MATERIALS AND METHODS

Laser Microdissection of Tissue Sections. All 57 head and neck tumor samples and matched normal mucosa ($n = 44$) were obtained after surgical

Received 12/5/03; revised 2/19/04; accepted 4/8/04.

Grant support: German Federal Ministry of Education and Research (Bundesministerium für Bildung und Forschung) and the Interdisciplinary Center for Clinical Research, Jena.

The costs of publication of this article were defrayed in part by the payment of page charges. This article must therefore be hereby marked *advertisement* in accordance with 18 U.S.C. Section 1734 solely to indicate this fact.

Requests for reprints: Ferdinand von Eggeling, Institut für Humangenetik und Anthropologie, Core Unit Chip Application, 07740 Jena, Germany. Phone: 0049-0-3641-935526; Fax: 0049-0-3641-935518; E-mail: fegg@mti.uni-jena.de.

resection at the ENT Department of the Friedrich-Schiller-University (Jena, Germany); these were collected fresh, snap-frozen in liquid nitrogen, and stored at −80°C. Tumor specimens were categorized according their Union International Contre Cancer-Tumor-Node-Metastasis classification. All were classified as squamous cell carcinoma G_2, M_0.

Laser microdissection was performed with a laser microdissection and pressure-catapulting microscope (Palm, Bernried, Germany) as described elsewhere (10). In brief, we microdissected on native air-dried cryostat tissue sections ~3000–5000 cells each in a maximum of 20–30 min. Proteins were extracted by a lysis buffer [100 mM sodium phosphate (pH 7.5), 5 mM EDTA, 2 mM $MgCl_2$, 3 mM 2-β-mercaptoethanol, 0.1% 3-[(3-cholamidopropyl)dimethylammonio]-1 -propanesulfonic acid, 500 μM leupeptin, and 0.1 mM phenylmethylsulfonyl fluoride] for 30 min on ice. After centrifugation (15 min; 15,000 rpm), the supernatant was immediately analyzed or frozen in liquid nitrogen for a maximum of 1 day.

Profiling of Microdissected Normal Pharyngeal Epithelium and Tumor Tissue. The protein lysates from both microdissected tissues were analyzed on a strong anion exchange array (SAX2; Ciphergen Biosystems, Inc., Fremont, CA) as described elsewhere (10). In brief, array spots were preincubated by a washing/loading buffer containing 100 mM Tris-buffer (pH 8.5), with 0.05% Triton X-100 followed by an application of 2 μl of sample extract on ProteinChip arrays, which were incubated at room temperature for 90 min in a humidity chamber. After washing twice and application of 2× 0.5 μl sinapinic acid (saturated solution in 0.5% trifluoroacetic acid/50% acetonitrile), mass analysis was performed in a ProteinChip Reader (model PBS II; Ciphergen Biosystems, Inc.) according to an automated data collection protocol. Cluster analysis of the detected signals and the determination of the respective *P* values for normal and tumor tissue were carried out with the Biomarker Wizard Program (Version 3.0; Ciphergen Biosystems, Inc.). For *P* calculation, spectra with at least 10 signals in the range between 2 and 20 kDa exhibiting a signal-to-noise ratio of at least 5 were selected and analyzed with the Mann-Whitney *U* test for nonparametric data sets.

Identification of Differential-Expressed Protein Peaks. Samples for two-dimensional electrophoresis were prepared directly from surgical material of ProteinChip System-analyzed HNSCC and corresponding normal tissue. Proteins were isolated and two-dimensional electrophoresis was performed as described elsewhere (10). In brief, isoelectric focusing was carried out on a PROTEAN IEF Cell (Bio-Rad) using 17-cm immobilized pH gradient strips. Vertical SDS-PAGE was performed in a cooled PROTEAN II Multi Cell (Bio-Rad) using linear gradient gels with total acrylamide concentrations ranging from 7 to 20%. Analytical gels were silver stained using the Vorum protocol (22), and semipreparative gels were stained with Coomassie brilliant blue G-250.

Protein patterns of the two-dimensional gels from normal pharyngeal epithelium and tumor tissue were compared, and consistent differentially expressed proteins with a size of ~5–20 kDa were excised. In-gel digestion of proteins was performed as described elsewhere (10). In brief, excised gel pieces were destained and dried. After rehydration and digestion with 10 μl of a trypsin solution (0.04 μg/μl; Roche) at 37°C for 7 h, supernatants were applied directly on a ProteinChip array with a hydrophobic surface (H4; Ciphergen Biosystems, Inc.). After addition of the matrix (CHCA; Ciphergen Biosystems, Inc.), peptide fragment masses were analyzed using the PBS II instrument. The spectra for the peptide mapping experiments were internally calibrated using three common trypsin autolysis products. Proteins were identified using the fragment masses generated through trypsin digestion by searching in a publicly available database.[6]

The criteria for positive identification of proteins were as follows: (*a*) probability index should be 1.0e +000; (*b*) Z score for the protein should be >2; and (*c*) molecular weight and isoelectric point of identified proteins should match estimated values obtained from two-dimensional gel electrophoresis.

Tandem MS data were acquired on a Micromass QTOF II (Manchester, United Kingdom) tandem quadrupole-time of flight mass spectrometer equipped with a Ciphergen PCI 1000 ProteinChip Interface. The system was externally calibrated in tandem MS mode using the parent ion and selected fragments of adrenocorticorticotropic hormone human fragment 18–39 (m/z = 2465.1983). Tandem MS spectra were used for database searches with MASCOT,[7] using National Center for Biotechnology Information and SwissProt databases.

For immunodepletion, 2 μl (40 ng) of antihuman monoclonal antibody for calgranulin A(S100A8) (S13.67; BMA Biomedicals; Augst, Switzerland), calgranulin B (S100A9) (S36.48; BMA Biomedicals), or an anti-calgizzarin (S100A11) serum (gift of Dr. Jean-Christophe Deloulme), respectively, were incubated with 10 μl of protein A-agarose (Sigma) for 15 min on ice. A pellet was generated by centrifugation, and the supernatant was discarded. The pellet was washed twice with a buffer containing 20 mM HEPES (pH 7.8), 25 mM KCl, 5 mM $MgCl_2$, 0.1 mM EDTA, and 0.05% NP40. Afterward, 5 μl of a lysate from a laser-dissected tumor or normal tissue were incubated with this pellet for 45 min on ice. As a negative control, 5 μl of the lysate were incubated with protein A-agarose without antibody for 45 min on ice. After incubation, samples were cleared by centrifugation, and 3 μl of each supernatant were analyzed by ProteinChip arrays with a hydrophobic surface.

Characterization of Proteins by IHC. Eight-μm cryostat sections of frozen head and neck cancer tissue containing both normal and pharyngeal epithelium and HNSCC were placed on charged slides, dried for ~60 min at 20°C, and fixed as described by Melle *et al.* (10). After fixation, slides were treated with 10% methanol in Tris-buffered saline containing 1% H_2O_2 to inhibit endogenous peroxidatic activity. Subsequently, they were rinsed twice with Tris-buffered saline and incubated with the corresponding monoclonal antibody against calgranulin A (S100A8; clone S13.67; BMA Biomedicals), calgranulin B (S100A9; clone S36.48; BMA Biomedicals), or with an anti-calgizzarin (S100A11) serum, respectively. A Jenchrom pxbl-kit (MoBiTec, Göttingen, Germany) was used according to manufacturer's instructions to visualize the location of the antibody. Negative controls were incubated only with the labeled secondary antibody. Sections cut in parallel to the IHC-treated sections were stained by H&E for better identification of different tissue areas. IHC staining was evaluated by a pathologist and an anatomist.

The laser scanning microscopy was performed with a LSM 310 (Carl Zeiss, Oberkochen-Jena, Germany) in the transmission mode using an Argon-ion laser. In most cases, Zeiss objective NEOFLUAR 40×/1.30 oil was used in combination with pinhole 20 at a scanning time of 60 s (23, 24).

RESULTS

Profiling of Microdissected Normal Pharyngeal Epithelium and Tumor Tissue. For this study, areas corresponding to ~3000–5000 cells/tissue probe were excised, and 101 tissue sections (57 tumor and 44 normal pharyngeal epithelium tissues) were successfully dissected by a pathologist. All protein lysates from the microdissected tissues were applied to SAX2 arrays and analyzed on a PBS II instrument. In the low range (2–20 kDa), up to 96 peaks were detected with normalized intensities.

After evaluation with Biomarker Wizard Program, the peak masses with the two best *P* values and down-regulated in epithelial tumor tissue, 10.84 kDa ($P = 3.34 \times 10^{-5}$) and 13.23 kDa ($P = 4.6 \times 10^{-5}$), were selected for additional characterization and identification. As a control, one peak (11.78 kDa) with no significant *P* ($P = 0.379$) was investigated in parallel. First, we used the TagIdent tool from ExPASy[8] by entering the mass of these unknown proteins. This tool searches for proteins similar in size and in isoelectric point in the SWISS-Prot and TrEMBL Translation of EMBL (European Molecular Biology Laboratory) databases, which can give some indication about possible candidates. The latter identified calgranulin A (accession number P05109), calgranulin B (accession number P06702), and calgizzarin (accession number P31949) were among the proteins listed.

Identification of Differential-Expressed Protein Peaks. Histologically assessed tumor pieces and biopsies from normal tissue were subjected to two-dimensional electrophoresis to identify the detected peaks at 10.84, 13.23, and 11.78 kDa. Numerous protein spots show-

[6] Internet address: http://129.85.19.192/profound_bin/WebProFound.exe.

[7] Internet address: http://www.matrixscience.com.

[8] Internet address: http://www.expasy.ch/tools/tagident.

Table 1 *Identified proteins by two-dimensional electrophoresis and SELDI-MS[a] (mass accuracy better than 200 ppm)*

Protein	Swissprot	Z-score	Molecular mass (kDa)	Isoelectric point	Sequence coverage (%)	Masses matched (Da)
Calgranulin A (S100A8)	P05109	2.34	10.89	6.5	62	963.0; 1111.1; 1421.6; 1549.8; 1563.7; 1877.17; 2391.3
Calgranulin B (S100A9)	P06702	2.37	13.30	5.7	84	971.3; 1455.6; 1614.6; 1630.7; 1807.1; 2193.2; 2613.2
Calgizzarin	P31949	2.31	11.86	6.6	48	771.4; 1142.0; 1480.1; 1850.4; 1866.3; 2892.3; 2907.8

[a] SELDI-MS, surface-enhanced laser desorption/ionization-mass spectrometry.

Table 2 *Results obtained from the CID-MS/MS analysis of selected peptides derived from calgranulin A, calgranulin B, and calgizzarin, respectively*

Peptide (*m/z*)	Sequence	Residues
Calgranulin A		
963.50	GNFHAVYR	24–31
1421.69	LLETECPQYIR	37–47
Calgranulin B		
1455.69	LGHPDTLNQGEFK	26–38
Calgizzarin		
1141.60	NQKDPGVLDR	53–62

ing differential expression in both specimens were observed. Because of the binding of the unknown protein species to a strong anion exchange surface at pH 8.5 in our ProteinChip analysis, we expected the isoelectric point of this protein candidate to be <8.5. We therefore decided to concentrate on 19 spots in range of 5–20 kDa exhibiting an isoelectric point in the range of 4.5–7 in our two-dimensional electrophoresis. Selected spots were cut out from the second dimension gels and subsequently subjected to in-gel digestion with trypsin and protein identification. An empty gel piece underwent the same treatment as a control. The digest solution was spotted on a hydrophobic H4 array and the masses of the fragments determined by the PBS II instrument. Database searches revealed calgranulin A, calgranulin B, and calgizzarin with high Z-score (2.34, 2.37, and 2.31, respectively) and good sequence coverage (Profound)[6] as the best candidates (Table 1).

These results were further confirmed by tandem MS analysis. The H4 array with the tryptic digests was transferred to a tandem MS equipped with a surface-enhanced laser desorption/ionization ProteinChip Interface. The peptides generated were selected and fragmented into smaller ions by collision-induced dissociation. Sequences of the peptides are given in Table 2. These results confirmed the identification of the proteins as calgranulin A, calgranulin B, and calgizzarin.

To confirm that calgranulin A, calgranulin B, and calgizzarin are matching to the differentially expressed peaks at 10.84, 13.23, and 11.78 kDa found by ProteinChip analysis, an immunodepletion assay was performed with microdissected tumor and normal pharyngeal epithelium tissue. Analysis of the supernatant of the immunodepletion assay by ProteinChip arrays showed that the peaks corresponding to calgranulin A, calgranulin B, and calgizzarin were significantly reduced. In the negative control (immunodepletion process with no antibody), the corresponding peaks were clearly detectable (Fig. 1).

Characteriziation of Proteins by IHC. To further confirm identification and to localize calgranulin A, calgranulin B, and calgizzarin in tissue sections, we examined their expression in five head and neck cancer tissue sections, using both IHC and ProteinChip technology. Negative controls without the primary or with no antibody all demonstrated negative results.

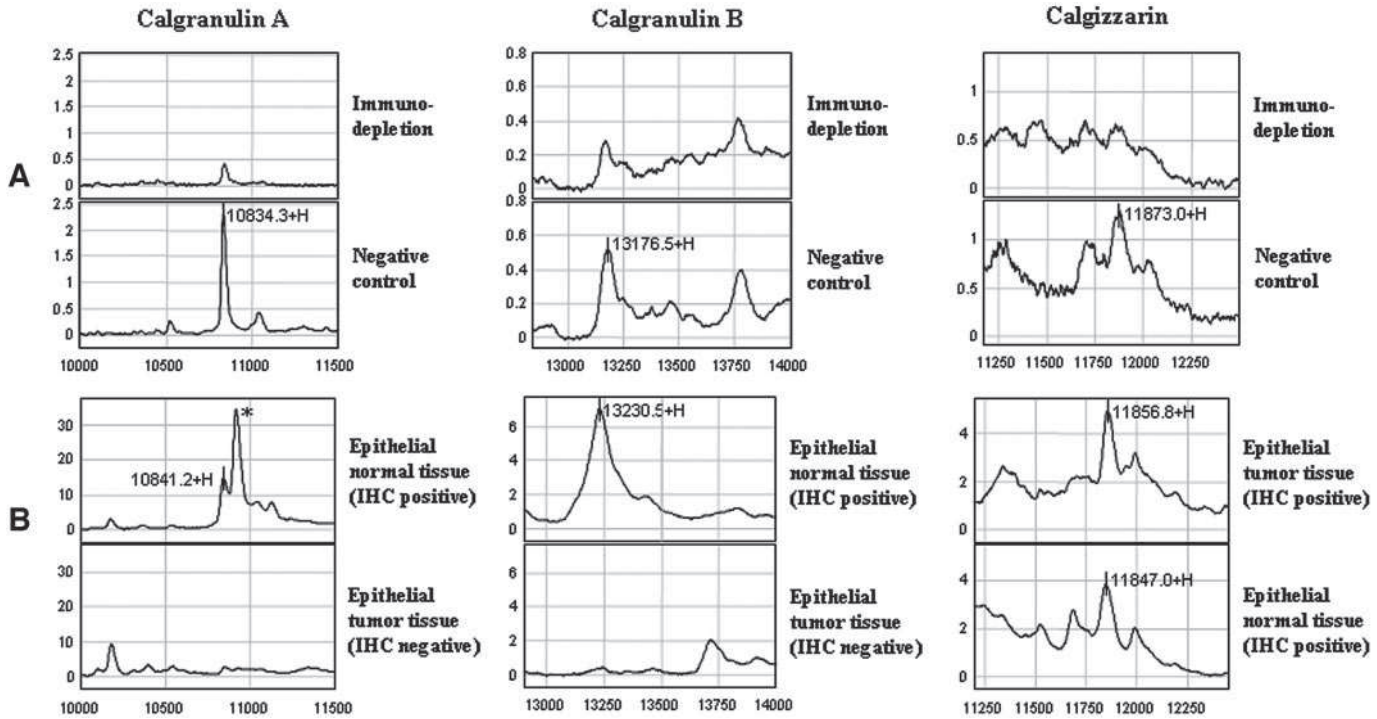

Fig. 1. *A*, normalized ProteinChip array profiles of the immunodepletion assay of head and neck cancer tissue with calgranulin A, calgranulin B, and calgizzarin and corresponding negative controls. The peaks at 10.83, 13.18, and 11.87 kDa representing calgranulin A, calgranulin B, and calgizzarin were detectable in the negative control but not in the corresponding depleted probe. *B*, normalized ProteinChip array profiles of microdissected immunohistochemical positive and negative tissue areas. The signals with a molecular mass of 10.84 and 13.23 kDa representing calgranulin A and calgranulin B were detectable in protein lysates from positive areas and were absent in the negative areas. The peak right of calgranulin A might be a phosphorylated form (*). In case of calgizzarin (11.87 kDa), both normal and tumor epithelial tissues were positive in immunohistochemistry (IHC; Fig. 2).

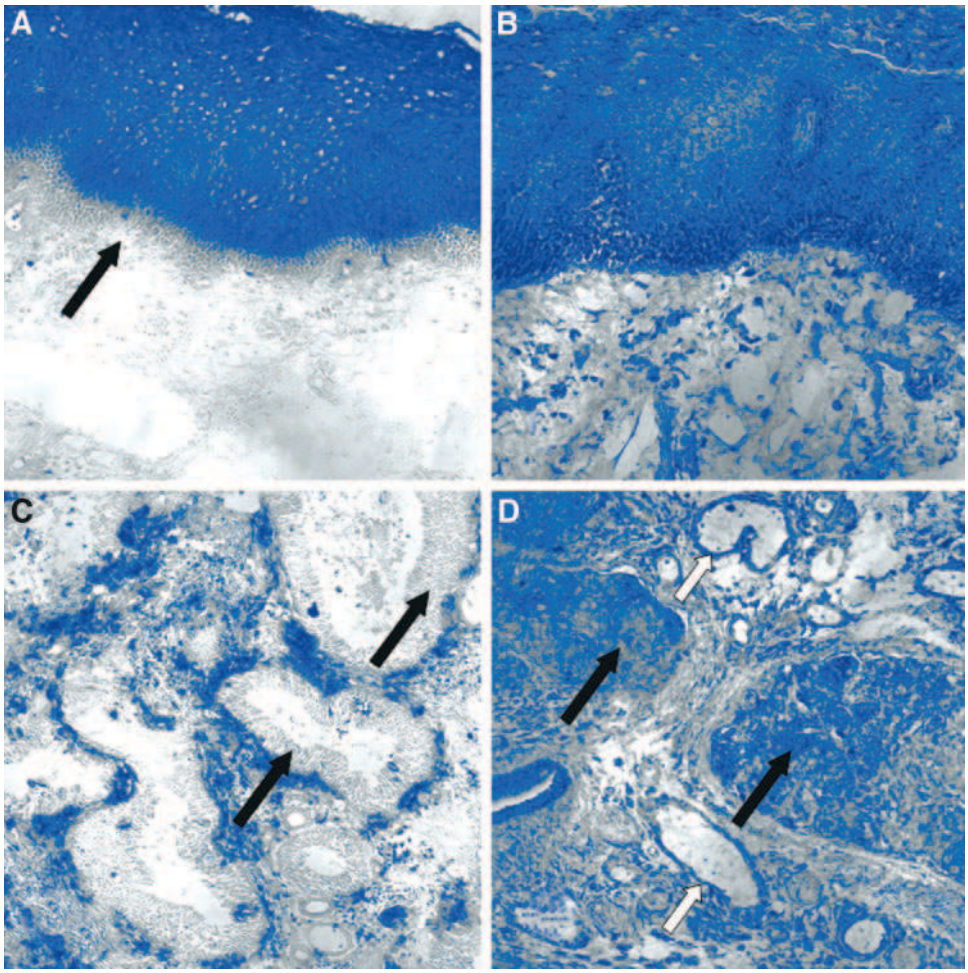

Fig. 2. Immunohistochemistry (IHC) of calgranulin A/B and calgizzarin visualized by laser scanning microscopy. Positive reaction is depicted in *blue* with a magnification of ×180. *A* and *C*, IHC of calgranulin A; *B* and *D*, IHC of calgizzarin. *A*, normal pharyngeal epithelium with expression of calgranulin A in epithelial cells, except in basal and parabasal cells (*arrow*). All connective tissue constituents were negative. *B*, expression of calgizzarin in all normal epithelial cells and stromal cells (fibrocytes). *C*, pharyngeal tumor tissue with no expression of calgranulin A in epithelial tumor cells (*arrows*). Positive expression could be found in connective tissue cells, fibrocytes, macrophages, and as deposition on collagenic fibers. *D*, pharyngeal tumor tissue with expression of calgizzarin in epithelial tumor cells (*black arrow*), in constituents of connective tissue and in glandular ducts (*white arrows*).

Calgranulin A and calgranulin B showed an identical reactivity in tissue, with a strong immune reactivity in the normal epithelium, except in the basal and parabasal cells. In tumor tissue, no expression could be detected for either protein (Fig. 2, *A* and *C*). Normal and tumor tissue components such as collagenic fibers, fibrocytes, fibroblasts, and macrophages were positive, whereas glandular ductal cells and endothelial cells were negative for calgranulin A/B. Calgizzarin showed a positive immune reaction with all layers of normal and tumor epithelium (Fig. 2, *B* and *D*). In contrast to calgranulin A/B, endothelial cells and glandular ductal cells were positive. Table 3 summarizes all immunohistological results for calgranulin A/B and calgizzarin.

To ensure that the localized calgranulin A, calgranulin B, and calgizzarin are identical to the peaks found by ProteinChip analysis, IHC-positive and -negative cell areas were obtained by tissue laser microdissection. In protein lysates from the positive fraction, a signal identical in mass to the peak obtained with the initial ProteinChip analysis was detected. In the protein lysate from the negative fraction, this peak was not visible (Fig. 1).

DISCUSSION

New biomarkers or biomarker patterns found by genomic or proteomic high-throughput techniques will enable scientists and medical staff to make a more reliable early diagnosis of certain human diseases, especially malignant tumors, and facilitate the prediction of their progression. In this way, biomarkers may contribute to a more differentiated, individually orientated tumor therapy. Despite enormous efforts, until now only in a few tumor disease relevant markers have been established (1).

One of the most promising proteomic tools for the detection of new proteomic cancer biomarkers is Ciphergen's ProteinChip technology (for examples, see Refs. 25, 26). Until now, this technique has been predominantly used for body fluid analyses because they are fast and easy to analyze by direct application onto ProteinChip arrays. Nevertheless, it is known that inter- and intraindividual changes in serum depending on sex, hormone level, nutrition state, or inflammation are high and can change the protein profile drastically. Hence, biomarkers involved in the genesis and progression of cancer must be present at a high level to be observed above normal changes. Despite these concerns, a large number of studies using body fluids as starting material have been published [serum (25, 27); urine (28); nipple

Table 3 *Protein expression of calgranulin A, calgranulin B, and calgizzarin in different normal and tumor tissue components*

	Calgranulin A, B	Calgizzarin
Normal epithelium		
Basal layer	−	+
Parabasal layers	−	+
Superficial layer	+	+
Epithelial tumor cells	−	+
Other tissue or hematological components		
Collagenic fibers	+	+
Fibrocytes/fibroblasts	+	+
Glandular ductal cells	−	+
Macrophages	+	+
Leukocytes	+	+
Endothelial cells	−	+

aspirate fluid (29); and pancreatic juice (26)]. However, if after bioinformatic processing markers can be found, they would be ideal for screening high-risk individuals or even individuals without elevated risk, which is discussed by the latest study on ovarian cancer (30) or others (18, 19, 21).

In contrast to serum, the analysis of tissues is more time consuming because here microdissection is necessary to separate tumorous from healthy cells, although the chance to find a reliable tumor marker might be higher than in serum. There is certainly a higher chance of obtaining more information about the biological mechanisms leading to the genesis and progression of cancer. Studies using tissue as a starting material have been underrepresented until now, and in most cases, a low number of samples were analyzed, which might be because even laser-based microdissection is tedious and has to be done by an experienced pathologist. To date, prostate cancer (4, 12, 31), melanomas (8, 32), lung tumors (13), renal cell carcinomas (9, 32), and HNSCC (10) have been assessed in this way.

After a significant protein has been detected by profiling experiments with ProteinChip arrays, two questions have to be addressed: first, how the protein can be enriched and identified, and second, whether this identified protein can be found and localized in the starting tissue. Localization may give insight to the heterogeneity of tissue and the tumor itself.

In our study, we addressed the first question by detecting differentially expressed proteins in microdissected tissue using ProteinChip technology and subsequent enrichment and identification of the proteins of interest by two-dimensional electrophoresis, in-gel digestion, peptide mapping, tandem MS, and immunodepletion assay. After profiling, the obtained masses of proteins were used for database searches, which gave some indication about possible candidates. Two-dimensional electrophoresis offers the opportunity to enrich and isolate putative candidates and to digest them with trypsin. The generated peptides could then be analyzed on the PBS II ProteinChip Reader and database searches pointed with a high probability to calgranulin A, calgranulin B and calgizzarin. To confirm that the isolated and digested proteins are identical to the differentially expressed peaks found with ProteinChip arrays, we performed an immunodepletion assay with the same starting material and corresponding antibodies. The respective peaks were absent in the analyzed supernatant and must therefore be depleted by the antibody. The identification was further confirmed by tandem MS analysis of selected peptides from the digest. The second question about the localization of calgranulin A, calgranulin B, and calgizzarin in tissue was then addressed by IHC. These proteins could be found in different normal and tumor tissue components. The reanalysis of calgranulin A-, calgranulin B-, and calgizzarin-positive and -negative tissue areas by microdissection and profiling confirms moreover their identities to the differentially expressed peaks. This process enabled the tissue heterogeneity of samples to be partly solved by laser microdissection, dividing epithelial tissue from connective tissue. The clonal heterogeneity of the tumor itself concerning the transcriptome and the proteome is morphologically hard to recognize and therefore cannot be completely solved by microdissection, unless by repeated cycles of microdissection, protein profiling, and immunohistochemical analyses with different antibodies.

In contrast to publications that show the protein profiles of specific tissues exclusively without an identification and characterization (12, 25, 30), we were able to identify significant signals in protein profiles from microdissected tissues. Calgranulin A, calgranulin B, and calgizzarin belong to the group of S100 proteins involved in the Ca^{2+} signaling network and regulate intracellular activities such as cell growth and motility, cell cycle progression, transcription, and cell differentiation (33, 34). This group of proteins has received increased

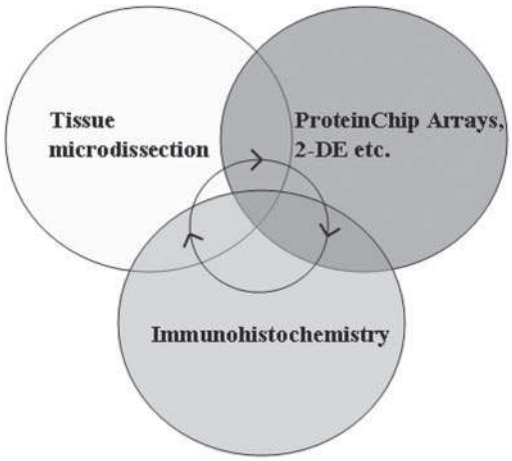

Fig. 3. Technical triade for proteomic identification and characterization of cancer biomarkers. Starting point is the tissue microdissection, where probes for ProteinChip arrays are gained. After profiling the biomarkers identified by two-dimensional electrophoresis (2-DE), immunodepletion, and other techniques, they were characterized by immunohistochemistry. Microdissection of immunohistologically positive areas and reanalyzes on ProteinChip arrays close this *circle*.

attention because of their involvement in several human diseases such as rheumatoid arthritis, acute inflammatory lesions, cardiomyophathy, Alzheimer's disease, and cancer (35–38). It is unique that the individual members of S100 proteins are located in specific cellular compartments from which they are able to relocate upon Ca^{2+} activation, transducing the Ca^{2+} signal in a temporal and spatial manner by interacting with different targets specific for each S100 protein (39). Another important aspect exclusive to the S100 protein family is that most genes of the members are located in a gene cluster on human chromosomal region 1q21 (40).

This region is characterized by several rearrangements that occurred during tumor development (41). This circumstance might be linked to the deregulation of some S100 gene expression in various tumor types and might be associated with tumor development and metastasis (33).

The proteins identified here have been described earlier in gene expression studies, *e.g.,* in breast carcinoma (42), in murine epithelial skin tumors (43), and in a mouse model of a gastric B-cell mucosa-associated lymphoid tissue lymphoma (44) with increased gene expression of *S100A8* (*MRP8*; *calgranulin A*), *S100A9* (*MRP14*; *calgranulin B*), and *S100A11* (*S100C*; *calgizzarin*), respectively. Also, protein expression studies have detected an increased level of these S100 proteins in different tumor tissues compared with their corresponding abundance in normal tissues (45–47). These observations are only consistent with our nonsignificant results concerning S100A11, calgizzarin. In our study, we detected signals of S100A11 by IHC that were distributed in both tissue types with a slightly stronger signal in HNSCC than in normal tissues.

On the other hand, our findings concerning the expression of the S100A8 and S100A9 proteins are contrary to the previously published studies. We estimate that a reason for the discrepancy to the other studies might be the fact that (*a*) our analysis is based on different tumor entities, (*b*) the level of mRNA does not necessarily correlate with protein expression level because of translational control mechanisms, and (*c*) we used microdissection and reanalysis of the found proteins by IHC to confirm our data. Only one recently published gene expression study on head and neck tumor used IHC for the confirmation of the results. Interestingly, these authors also found a decrease of the expression of the *S100A9* gene (48).

In conclusion, it can be stated that a better estimation of the biological importance of certain cell populations and tumor clonal

heterogeneity in regard to the progression from preneoplastic tissue alterations to malignant tumors and the prediction of the metastasis forming potential of a given cell population by biomarkers will be necessary prerequisites for providing a more detailed insight and understanding of tumor progression. The paradigmatic triade of microdissection, surface-enhanced laser desorption/ionization-based ProteinChip technology, and IHC (Fig. 3) opens up this possibility while reducing the complexity of the proteome by using a defined cell population.

ACKNOWLEDGMENTS

We thank Dr. Jean-Christophe Deloulme (INSERM 0104, DRDC-TS, CEA de Grenoble) for providing S100A11 (calgizzarin) antibody.

REFERENCES

1. van't Veer LJ, Dai HY, van de Vijver MJ, et al. Gene expression profiling predicts clinical outcome of breast cancer. Nature (Lond.) 2002;415:530–6.
2. Pritzker KPH. Cancer biomarkers: easier said than done. Clin Chem 2002;48: 1147–50.
3. Davies H, Lomas L, Austen B. Profiling of amyloid beta peptide variants using SELDI ProteinChip (R) arrays. Biotechniques 1999;27:1258–61.
4. Wright GL, Cazares LH, Leung SM, et al. Proteinchip((R)) surface enhanced laser desorption/ionization (SELDI) mass spectrometry: a novel protein biochip technology for detection of prostate cancer biomarkers in complex protein mixtures. Prostate Cancer Prostatic Dis 1999;2:264–76.
5. Merchant M, Weinberger SR. Recent advancements in surface-enhanced laser desorption/ionization-time of flight-mass spectrometry. Electrophoresis 2000;21: 1164–77.
6. Hutchens TW, Yip TT. New desorption strategies for the mass spectrometric analysis of macromolecules. Rapid Commun Mass Spectrom 1993;7:576–80.
7. Schütze K, Lahr G. Identification of expressed genes by laser-mediated manipulation of single cells [see comments]. Nat Biotechnol 1998;16:737–42.
8. von Eggeling F, Davies H, Lomas L, et al. Tissue-specific microdissection coupled with ProteinChip array technologies: applications in cancer research. Biotechniques 2000; 29:1066–70.
9. von Eggeling F, Junker K, Fiedler W, et al. Mass spectrometry meets chip technology: a new proteomic tool in cancer research? Electrophoresis 2001;22:2898–902.
10. Melle C, Ernst G, Schimmel B, et al. Biomarker discovery and identification in laser microdissected head and neck squamous cell carcinoma with ProteinChip(R) technology, two-dimensional gel electrophoresis, tandem mass spectrometry and immunohistochemistry. Mol Cell Proteomics 2003;2:443–52.
11. Craven RA, Banks RE. Laser capture microdissection and proteomics: possibilities and limitation. Proteomics 2001;1:1200–4.
12. Cazares LH, Adam BL, Ward MD, et al. Normal, benign, preneoplastic, and malignant prostate cells have distinct protein expression profiles resolved by surface enhanced laser desorption/ionization mass spectrometry. Clin Cancer Res 2002;8: 2541–52.
13. Zhukov TA, Johanson RA, Cantor AB, Clark RA, Tockman MS. Discovery of distinct protein profiles specific for lung tumors and premalignant lung lesions by SELDI mass spectrometry. Lung Cancer 2003;40:267–9.
14. Klose J. Protein mapping by combined isoelectric focusing and electrophoresis of mouse tissues. A novel approach to testing for induced point mutations in mammals. Humangenetik 1975;26:231–43.
15. Weinberger SR, Boschetti E, Santambien P, Brenac V. Surface-enhanced laser desorption-ionization retentate chromatography (TM) mass spectrometry (SELDI-RC-MS): a new method for rapid development of process chromatography conditions. J Chromatogr B Analyt Technol Biomed Life Sci 2002;782:307–16.
16. Reid G, Gan BS, She YM, Ens W, Weinberger S, Howard JC. Rapid identification of probiotic lactobacillus biosurfactant proteins by ProteinChip tandem mass spectrometry tryptic peptide sequencing. Appl Environ Microbiol 2002;68:977–80.
17. Zhang L, Yu W, He T, et al. Contribution of human alpha defensin-1, -2 and -3 to the anti-HIV-1 activity of CD8 antiviral factor. Science (Wash. DC) 2002;298:995–1000.
18. Shiwa M, Nishimura Y, Wakatabe R, et al. Rapid discovery and identification of a tissue-specific tumor biomarker from 39 human cancer cell lines using the SELDI ProteinChip platform. Biochem Biophys Res Commun 2003;309:18–25.
19. Ye B, Cramer DW, Skates SJ, et al. Haptoglobin-alpha subunit as potential serum biomarker in ovarian cancer: identification and characterization using proteomic profiling and mass spectrometry. Clin Cancer Res 2003;9:2904–11.
20. Thulasiraman V, McCutchen-Maloney SL, Motin VL, Garcia E. Detection and identification of virulence factors in Yersinia pestis using SELDI ProteinChip system. Biotechniques 2001;30:428–32.
21. Uchida T, Fukawa A, Uchida M, Fujita K, Saito K. Application of a novel protein biochip technology for detection and identification of rheumatoid arthritis biomarkers in synovial fluid. J Proteome Res 2002;1:495–9.
22. Mortz E, Krogh TN, Vorum H, Gorg A. Improved silver staining protocols for high sensitivity protein identification using matrix-assisted laser desorption/ionization-time of flight analysis. Proteomics 2001;1:1359–63.
23. Halbhuber KJ, Krieg R, Konig K. Laser scanning microscopy in enzyme histochemistry. Visualization of cerium-based and dab-based primary reaction products of phosphatases, oxidases and peroxidases by reflectance and transmission laser scanning microscopy. Cell Mol Biol (Noisy-le-grand) 1998;44:807–26.
24. Halbhuber KJ, Konig K. Modern laser scanning microscopy in biology, biotechnology and medicine. Ann Anat 2003;185:1–20.
25. Petricoin EF, Ardekani AM, Hitt BA, et al. Use of proteomic patterns in serum to identify ovarian cancer. Lancet 2002;359:572–7.
26. Rosty C, Christa L, Kuzdzal S, et al. Identification of hepatocarcinoma-intestine-pancreas/pancreatitis-associated protein I as a biomarker for pancreatic ductal adenocarcinoma by protein biochip technology. Cancer Res 2002;62:1868–75.
27. Petricoin EF, Mills GB, Kohn EC, Liotta LA. Proteomic patterns in serum and identification of ovarian cancer [reply]. Lancet 2002;360:170–1.
28. Vlahou A, Schellhammer PF, Mendrinos S, et al. Development of a novel proteomic approach for the detection of transitional cell carcinoma of the bladder in urine. Am J Pathol 2001;158:1491–502.
29. Paweletz CP, Trock B, Pennanen M, et al. Proteomic patterns of nipple aspirate fluids obtained by SELDI-TOF: potential for new biomarkers to aid in the diagnosis of breast cancer. Dis Markers 2001;17:301–7.
30. Kozak KR, Amneus MW, Pusey SM, et al. Identification of biomarkers for ovarian cancer using strong anion-exchange ProteinChips: potential use in diagnosis and prognosis. Proc Natl Acad Sci USA 2003;100:12343–8.
31. Wellmann A, Wollscheid V, Lu H, et al. Analysis of microdissected prostate tissue with ProteinChip (R) arrays: a way to new insights into carcinogenesis and to diagnostic tools. Int J Mol Med 2002;9:341–7.
32. Fetsch PA, Simone NL, Bryant-Greenwood PK, et al. Proteomic evaluation of archival cytologic material using SELDI affinity mass spectrometry: potential for diagnostic applications. Am J Clin Pathol 2002;118:870–6.
33. Schafer BW, Heizmann CW. The S100 family of EF-hand calcium-binding proteins: functions and pathology. Trends Biochem Sci 1996;21:134–40.
34. Heizmann CW, Fritz G, Schafer BW. S100 proteins: structure, functions and pathology. Front Biosci 2002;7:d1356–68.
35. Van Eldik LJ, Griffin WS. S100 beta expression in Alzheimer's disease: relation to neuropathology in brain regions. Biochim Biophys Acta 1994;1223:398–403.
36. Kerkhoff C, Klempt M, Sorg C. Novel insights into structure and function of MRP8 (S100A8) and MRP14 (S100A9). Biochim Biophys Acta 1998;1448:200–11.
37. Barraclough R. Calcium-binding protein S100A4 in health and disease. Biochim Biophys Acta 1998;1448:190–9.
38. Donato R. S100: a multigenic family of calcium-modulated proteins of the EF-hand type with intracellular and extracellular functional roles. Int J Biochem Cell Biol 2001;33:637–68.
39. Mandinova A, Atar D, Schafer BW, Spiess M, Aebi U, Heizmann CW. Distinct subcellular localization of calcium binding S100 proteins in human smooth muscle cells and their relocation in response to rises in intracellular calcium. J Cell Sci 1998;111(Pt. 14):2043–54.
40. Marenholz I, Zirra M, Fischer DF, Backendorf C, Ziegler A, Mischke D. Identification of human epidermal differentiation complex (EDC)-encoded genes by subtractive hybridization of entire YACs to a gridded keratinocyte cDNA library. Genome Res 2001;11:341–55.
41. Schutte BC, Carpten JD, Forus A, Gregory SG, Horii A, White PS. Report and abstracts of the sixth international workshop on human chromosome 1 mapping 2000. Iowa City, Iowa USA. 30 September–3 October 2000. Cytogenet Cell Genet 2001; 92:23–41.
42. Moog-Lutz C, Bouillet P, Regnier CH, et al. Comparative expression of the psoriasin (S100A7) and S100C genes in breast carcinoma and co-localization to human chromosome 1q21–q22. Int J Cancer 1995;63:297–303.
43. Gebhardt C, Breitenbach U, Tuckermann JP, Dittrich BT, Richter KH, Angel P. Calgranulins S100A8 and S100A9 are negatively regulated by glucocorticoids in a c-Fos-dependent manner and overexpressed throughout skin carcinogenesis. Oncogene 2002;21:4266–76.
44. Mueller A, O'Rourke J, Grimm J, et al. Distinct gene expression profiles characterize the histopathological stages of disease in Helicobacter-induced mucosa-associated lymphoid tissue lymphoma. Proc Natl Acad Sci USA 2003;100:1292–7.
45. Stulik J, Osterreicher J, Koupilova K, et al. The analysis of S100A9 and S100A8 expression in matched sets of macroscopically normal colon mucosa and colorectal carcinoma: the S100A9 and S100A8 positive cells underlie and invade tumor mass. Electrophoresis 1999;20:1047–54.
46. Chaurand P, DaGue BB, Pearsall RS, Threadgill DW, Caprioli RM. Profiling proteins from azoxymethane-induced colon tumors at the molecular level by matrix-assisted laser desorption/ionization mass spectrometry. Proteomics, 1: 1320–6, 2001.
47. Celis JE, Celis P, Palsdottir H, et al. Proteomic strategies to reveal tumor heterogeneity among urothelial papillomas. Mol Cell Proteomics 2002;1:269–79.
48. Gonzalez HE, Gujrati M, Frederick M, et al. Identification of 9 genes differentially expressed in head and neck squamous cell carcinoma. Arch Otolaryngol Head Neck Surg 2003;129:754–9.

Different expression of calgizzarin (S100A11) in normal colonic epithelium, adenoma and colorectal carcinoma

CHRISTIAN MELLE[1], GÜNTHER ERNST[1], BETTINA SCHIMMEL[1], ANNETT BLEUL[1], HENNING MOTHES[2], ROLAND KAUFMANN[3], UTZ SETTMACHER[3] and FERDINAND VON EGGELING[1]

[1]Core Unit Chip Application (CUCA), Institute of Human Genetics and Anthropology; Departments of [2]Traumatology, and [3]General and Visceral Surgery, University Hospital, Friedrich-Schiller-University, 07740 Jena, Germany

Received July 8, 2005; Accepted August 18, 2005

Abstract. The aim of the study was to detect proteomic markers usable to distinguish colorectal carcinoma from colon adenoma for a better understanding of the molecular mechanisms in the process of tumourigenesis. Therefore, we microdissected colon carcinoma tissue, epithelial colon adenoma tissue as well as normal adjacent colon epithelium and determined protein profiles by SELDI-TOF MS. A multitude of significantly different signals was detected. For their identification colon biopsis were lysed and subjected to a two-dimensional gel electrophoresis for separation. Subsequently, we identified nearly 100 proteins by tryptic digestion, peptide fingerprint mapping and database search. Calgizzarin (S100A11; S100C) identified by peptide fingerprint mapping correlated very well with a significantly differentially expressed signal found in prior protein profiling. Using an immunodepletion assay we confirmed the identity of this signal as calgizzarin. To localise calgizzarin in tissues we performed immunohistochemistry. For further confirmation of the identity of calgizzarin we re-analysed IHC-positive as well as IHC-negative tissue sections on ProteinChip arrays. This work demonstrates that biomarkers in colorectal cancer can be detected, identified and assessed by a proteomic approach comprising tissue-microdissection, protein profiling and immunological techniques.

Introduction

Colorectal cancer is ranked the third most common form of cancer worldwide in terms of incidence (estimated to result in 945000 new cases, 9.4% of the world total population) and mortality (492000 deaths, 7.9% of the total) in 2000 (1). The majority of colorectal cancers are non-hereditary and sporadic, which makes early detection even more important. Tumourigenesis in sporadic colorectal cancer (CRC) has been extensively studied and can be seen as a multistep process, with each step representing specific gene mutations or epigenetic changes (2). The progression from adenoma to sporadic CRC results from the accumulation of genetic and epigenetic alterations involving activation of oncogenes and inactivation of tumour suppressor genes (3). Several other molecular mechanisms were also shown to be involved in tumour development, but tend to occur infrequently. Despite the dominant role of the adenoma-carcinoma sequence these changes are thought to be responsible for the different biological nature and clinical behaviour of CRC. In addition epidemiological studies revealed a strong impact of environmental and dietary factors.

Regardless of the enormous efforts and introduction of new parallel genomic and proteomic techniques in recent years, relevant markers that can be used for early diagnosis or improved therapy in cancer have only been established in a few tumour diseases (4). One point might be that the *in situ* situation in tumours is neglected, because results from starting material like serum and non-microdissected tissue cannot be traced back to the biological properties or the heterogeneity of the tumour itself. Hence, microdissection, proteomic techniques and immunohistochemistry have been combined in a technical triade (5).

The proteomic technique, SELDI-MS (surface enhanced laser desorption/ionization-mass spectrometry), uses chromatographic surfaces able to retain proteins depending on their physico-chemical properties followed by direct analysis via time of flight mass spectrometry (TOF-MS) (6). This technique does not require large amounts of samples making it ideal for small biopsies or microdissected tissue which are required to produce the homogeneous tissue samples indispensable in cancer research (7-9). Microdissected tissue material, free of contaminating and unwanted tissue components, is extremely important for producing clean data for biomarker identification in cancer diagnostics and in elucidating clonal heterogeneity of tumours. In the present study, the epithelial tumour cells respectively adenoma cells had to be separated from all surrounding tissue constituents. This separation was done with an extremely precise technique such as laser based microdissection. This technique has previously been combined

Correspondence to: Dr Ferdinand von Eggeling, Institut für Humangenetik und Anthropologie, CUCA, 07740 Jena, Germany
E-mail: fegg@mti.uni-jena.de

Key words: colorectal cancer, proteomics, biomarker, microdissection, SELDI-TOF MS, ProteinChip technology, two-dimensional gel electrophoresis, immunohistochemistry

with ProteinChip technology to identify protein markers in other cancers (10-12).

We analysed pure microdissected populations of cells from colorectal carcinoma tissue, colon adenoma epithelium as well as normal colon epithelium using SELDI-MS ProteinChip technology.

The protein patterns derived by this analysis showed a multitude of significant differences. To identify this differentially expressed proteins crude extracts of biopsis were separated by 2D gel electrophoresis followed by tryptic digestion and peptide fingerprint mapping. Among nearly 100 identified proteins calgizzarin (S100A11; S100C) correlated very well to a significantly different marker which was overexpressed in CRC found in prior protein profiling. The identity of this protein was also confirmed as calgizzarin by immunological techniques.

Materials and methods

Laser microdissection of tissue sections. All 13 CRC samples and matched normal mucosa (n=19) as well as 30 adenoma tissue samples were obtained after surgical resection at the Department of General and Visceral Surgery of the Friedrich-Schiller-University Jena; these were collected fresh, snap-frozen in liquid nitrogen, and stored at -80˚C. Tumour specimens were categorized according to their WHO classification. Most of the tumours were classified as pT2 and pT3.

Laser microdissection was performed with a laser microdissection and pressure catapulting microscope (LMPC; Palm, Bernried, Germany) as described elsewhere (10). Briefly, we microdissected on native air-dried cryostat tissue sections ~3000-5000 cells each in a maximum of 20-30 min. Proteins were extracted by 10 μl lysis buffer (100 mM Na-phosphate (pH 7.5), 5 mM EDTA, 2 mM $MgCl_2$, 3 mM 2-ß-mercaptoethanol, 0.1% CHAPS, 500 μM leupeptin, and 0.1 mM PMSF) for 30 min on ice. After centrifugation (15 min; 15000 rpm) the supernatant was immediately analyzed or frozen in liquid nitrogen for a maximum of one day.

Profiling of microdissected normal colon epithelium, adenoma tissue and epithelial carcinoma tissue. The protein lysates from microdissected tissues (carcinoma, adenoma and normal) were analysed on strong anion exchange arrays (Q10; Ciphergen Biosystems Inc., Fremont, CA) as described elsewhere (10). In brief, array spots were preincubated by a washing/loading buffer containing 100 mM Tris-buffer, pH 8.5 with 0.02% Triton X-100 followed by application of 2 μl of sample extract on ProteinChip arrays, which were incubated at room temperature for 90 min in a humidity chamber. After washing three times with the same buffers and two final washing steps with water, 2x0.5 μl sinapinic acid (saturated solution in 0.5% TFA/50% acetonitrile) was applied. Mass analysis was performed in a ProteinChip Reader (Series 4000, Ciphergen Biosystems Inc.) according to an automated data collection protocol. Spectra were normalised with total ion current and cluster analysis of the detected signals and the determination of respective P-values for normal, adenoma and carcinoma tissue was carried out with the CiphergenExpress Program (Version 3.0; Ciphergen Biosystems Inc.). For P-value calculation, normalised spectra with signals in the range between 2.5 and 200 kDa exhibiting a signal-to-noise ratio (S/N) of at least 10 were selected and analysed with the Mann-Whitney U test for non-parametric data sets.

Two-dimensional gel electrophoresis. Samples for two-dimensional gel electrophoresis (2-DE) were prepared directly from surgical material of colon tumour and corresponding normal colon epithelium tissue assessed by a pathologist. Proteins were isolated and 2-DE was performed as described elsewhere (10). In brief, isoelectric focusing (IEF) was carried out on a Multiphor II (Amersham) using 7 cm IPG strips. Vertical SDS-PAGE was performed in a cooled Protean II xi Cell (Bio-Rad) using 4-12% Bis-Tris Zoom™ gel (Invitrogen). The gels were stained with Simply Blue Safe Stain (Enhanced Coomassie, Invitrogen).

In-gel digestion. Protein patterns of the 2-DE gels from normal colon epithelium and tumour tissue were comparatively analysed and protein spots with a molecular mass of nearly 10-50 kDa were excised. In-gel digestion of proteins was performed as described elsewhere (10). In brief, excised gel pieces were destained and dried. After rehydration and digestion with 10 μl of a trypsin solution (0.02 μg/μl; Roche) at 37˚C for 7 h supernatants were applied directly on a NP20 Protein Chip array (Ciphergen Biosystems Inc.). An empty gel piece underwent the same treatment as a control. After addition of the matrix (CHCA; Ciphergen Biosystems Inc.), peptide fragment masses were analysed using the ProteinChip Reader. The spectra for the peptide mapping experiments were externally calibrated using five standard proteins including Arg8-vasopressin (1082.2 Da), somatostatin (1637.9 Da), dynorphin (2147.5 Da), ACTH (2933.5 Da) and insulin ß-chain (3495.94 Da). Proteins were identified using the fragment masses generated through trypsin digestion by searching in a publicly available database (http://129.85.19.192/profound_bin/WebProFound.exe).

Immunodepletion assay. Anti-calgizzarin serum (2 μl) (gift of Dr Jean-Christophe Deloulme) were incubated with 10 μl protein A-agarose (Sigma) for 15 min on ice. A pellet was generated by centrifugation and the supernatant was discarded. The pellet was washed two times with a buffer containing 20 mM Hepes (pH 7.8), 25 mM KCl, 5 mM $MgCl_2$, 0.1 mM EDTA and 0.05% NP-40. Afterwards, 5 μl of a lysate from laser-dissected CRC were incubated with this pellet for 45 min on ice. As a negative control 5 μl of the lysate were incubated with protein A-agarose without the specific antibody for 45 min on ice. After incubation samples were cleared by centrifugation and 3 μl of each supernatant were analysed by ProteinChip arrays.

Immunohistochemistry. Cryostat sections (8-μm) of colon cancer tissue and colon adenoma tissue were placed on slides, air dried for approximately 60 min at 20˚C and fixed in paraformaldehyde as described (10). After fixation, slides were treated in the microwave at 80 watts (3x3 min) in 10 mM citric acid pH 6.0 to inhibit endogenous peroxidatic activity. Subsequently, they were rinsed twice with TBS pH 7.4, and incubated overnight at 4˚C in humidity chamber with the corresponding primary anti-calgizzarin serum. Slides were

Table I. Significantly different signals which separate CRC, adenoma and normal tissue samples detected on Q10 ProteinChip arrays. The signal representing the subsequently identified calgizzarin is displayed bold.

MW (kD)	P-value
4.968	$1.04x10^{-2}$
5.087	$3.83x10^{-5}$
8.212	$1.24x10^{-2}$
8.406	$2.91x10^{-3}$
9.757	$3.24x10^{-2}$
10.179	$2.42x10^{-5}$
10.357	$9.38x10^{-5}$
10.396	$9.83x10^{-6}$
10.532	$7.77x10^{-6}$
12.001	$9.64x10^{-3}$
12.189	$6.18x10^{-3}$
16.810	$6.01x10^{-3}$
16.937	$8.93x10^{-3}$
18.480	$5.5x10^{-3}$
23.826	$2.61x10^{-4}$
24.785	$2.08x10^{-3}$
27.973	$3.18x10^{-4}$
46.581	$4.09x10^{-4}$

rinsed 3x10 min in TBS and the Vectastain Elite ABC kit (Vector Laboratories, Burlingame, CA) and the Jenchrom pxbl-kit (MoBiTec, Göttingen, Germany) were used according to the manufacturer's instructions to visualize the localization of the antibody. Negative controls were incubated with the labeled secondary antibody only. Sections cut in parallel to the IHC-treated sections were stained by HE for better identification of different tissue areas. IHC staining was evaluated by a pathologist.

Results

Protein profiling of microdissected CRC, colon adenoma and normal colonic epithelium. Areas corresponding to about 3000-5000 cells per tissue probe were excised, and 62 tissue sections in total (13 carcinoma, 30 adenoma and 19 normal colonic epithelium tissues) were successfully dissected by a pathologist. All protein lysates from the microdissected tissues were applied to Q10 arrays and analysed on a ProteinChip Reader Series 4000 instrument. In the range between 2.5-200 kDa, up to 158 peaks were detected with normalised intensities. After evaluation with the CiphergenExpress Program, a multitude of significantly different signals were detectable for CRC, adenoma and normal tissue samples (Table I).

Identification of a differentially expressed signal. For identification of signals histologically checked pieces of different colon tissues were lysed and subjected to 2-DE for separation. Numerous protein spots in the range of about 10-50 kDa were excised from the gels and peptide finger-prints of the tryptic digested spots were determined using SELDI-TOF MS. In this way we were able to identify nearly 100 proteins by database search (profound; http://129.85.19.192/profound_bin/WebProFound.exe). One of these proteins, calgizzarin, correlated very well with a significantly different signal found in prior protein profiling. This signal of ~12 kDa showed an increased expression in samples derived from colorectal carcinoma and discriminated significantly between CRC and adenoma tissue and normal colon tissue ($P=9.64x10^{-3}$) as well as between CRC and adenoma or normal colon epithelium, respectively ($P=2.35x10^{-3}$ or $3.01x10^{-3}$, respectively). The distribution of the intensities for the different tissues is given in Fig. 1. Representative examples of SELDI-MS spectra from CRC, colon adenoma and normal colon epithelium are shown in Fig. 2 in the range from 10.5 to 14 kDa. The identification of further significant signals is in progress.

The reassurance that calgizzarin matches to the differentially expressed peak at 12 kDa found by ProteinChip analysis was done with an immunodepletion assay using

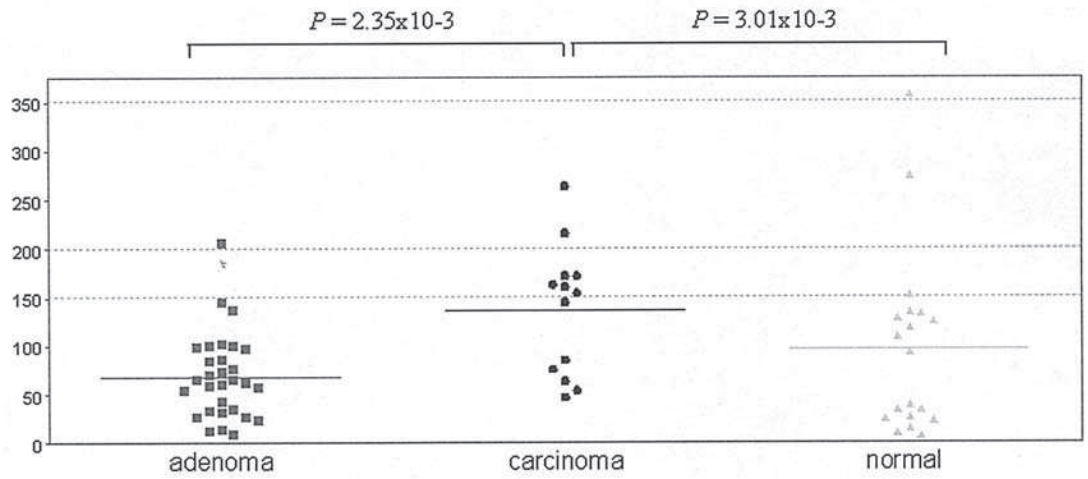

Figure 1. The distribution of the intensities of 12 kDa peak in colon adenoma samples (adenoma), CRC samples (carcinoma) and normal colon epithelium samples (TZ LCM). The spectra were obtained using Q10 arrays. X-axis indicate the sample groups, Y-axis the intensity (μA).

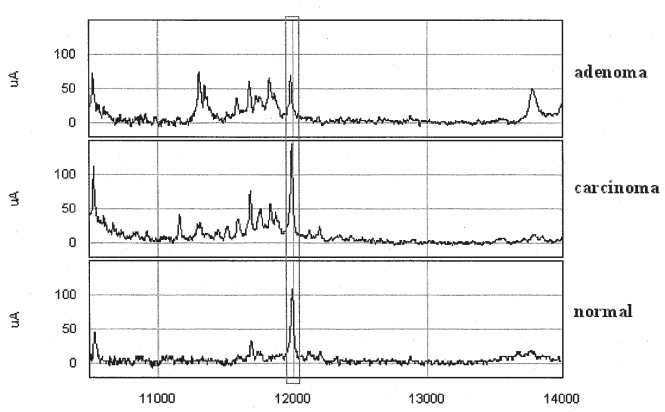

Figure 2. Representative examples of SELDI-TOF MS spectra of colon adenoma, CRC and normal colon epithelium. Data are obtained using Q10 array. The peak of interest at 12 kDa is marked with a frame.

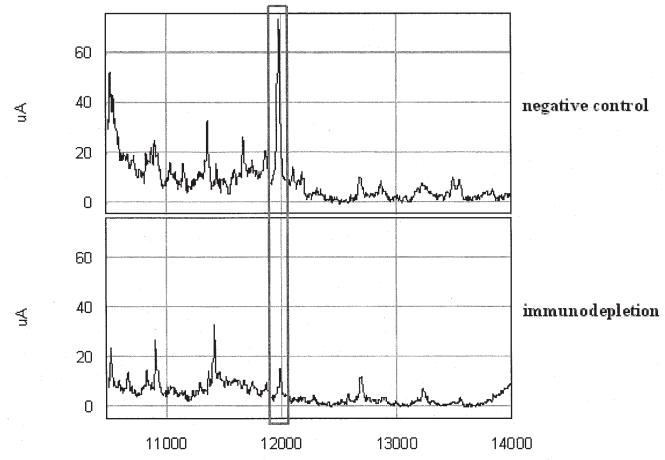

Figure 3. Immunodepletion assay of CRC. A peak (marked with a frame) representing calgizzarin was detectable in the negative control and clearly decreased in the corresponding depleted probe.

microdissected colorectal cancer tissue as starting material. Analysis of the supernatant of the immunodepletion assay by ProteinChip arrays showed that the peak corresponding to calgizzarin was significantly reduced. In the negative control without the specific antibody the peak at 12 kDa was clearly detectable (Fig. 3).

Characterisation of calgizzarin by immunohistochemistry. To characterise the identified marker and to localise calgizzarin in tissue sections, we examined their expression in several colon epithelium tissue samples by immunohistochemistry using a specific anti-calgizzarin serum. Negative controls without the primary antibody or without antibody at all demonstrated negative results. Adenoma cells, normal colon epithelial cells as well as CRC cells demonstrated cytoplasmic signals for calgizzarin in all tissue samples examined. The CRC cells showed an unequivocally increased signal compared to the signal detected in normal epithelial cells or epithelial adenoma cells, respectively (Fig. 4). Quantitative differences between the expression of calgizzarin in normal epithelial colon cells, adenoma cells and colorectal carcinoma cells are as clearly noticeable as in ProteinChip array results.

To further confirm that the localised calgizzarin is identical to the peak found by ProteinChip areas of similar size from carcinoma and adenoma tissue that were prior positively analysed in IHC were obtained by tissue laser microdissection. In protein lysate from carcinoma tissue a signal identical in mass to the peak obtained with the initial SELDI-MS analysis was detected on a Q10 array. In the protein lysate derived from colon adenoma this peak was significantly reduced (Fig. 5).

Discussion

Genomic and proteomic techniques are used for profiling studies of colon tumours (13-15). Besides these studies, protein profiling experiments were carried out using the proteomic technique surface-enhanced laser desorption/

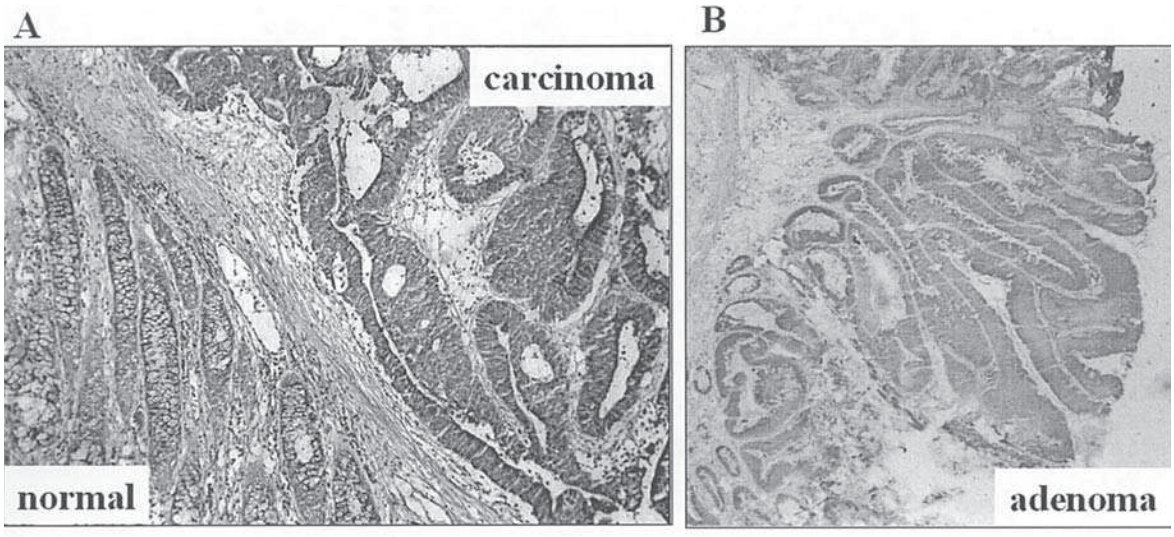

Figure 4. Immunohistochemistry of calgizzarin. (A) CRC (carcinoma) and normal colon epithelium (normal) and (B) colon adenoma (adenoma) with a magnification of x100.

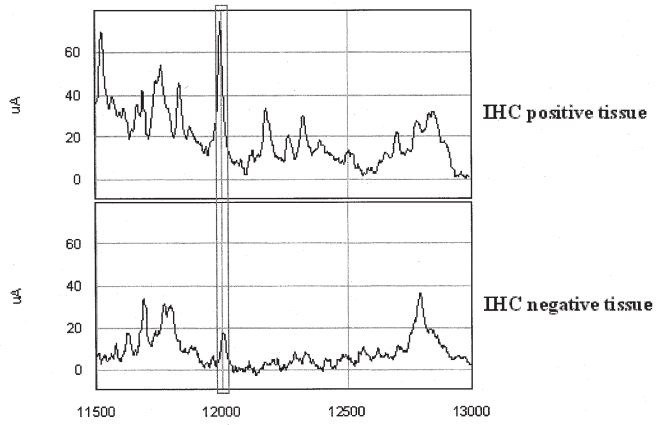

Figure 5. IHC-positive areas of similar size of tumorous and adenoma tissue were microdissected and analysed on ProteinChip arrays. A signal (marked with a frame) with a molecular mass of 12 kDa representing calgizzarin was detectable in protein lysate derived from CRC. In the protein lysate from the colon adenoma fraction this signal is significantly decreased.

ionisation time-of-flight mass spectrometry (SELDI-TOF MS) (ProteinChip technology) (16-18). In the present study, we analysed 62 microdissected samples all derived from CRC, colon adenoma and normal colon epithelium by ProteinChip technology to find significantly differences between CRC and colon adenoma for better understanding of the molecular mechanisms behind the process of tumourigenesis. Among a multitude of various signals which significantly differ between CRC and adenoma and normal epithelium one signal corresponded very well to the molecular mass of calgizzarin (also named S100A11 or S100C, respectively). This signal was up-regulated in colorectal cancer and distinguished significantly between colorectal carcinoma and colon adenoma. We were able to confirm the identity of this signal as calgizzarin by an immunodepletion assay. An elevated calgizzarin expression in CRC compared to normal colon epithelium is described on cDNA level as well as on protein level (19,20). In the present study we confirmed this up-regulation in CRC compared to normal colon epithelium by ProteinChip technology as shown recently by 2D gel electrophoresis (21). Beside this we determined also the protein pattern of samples derived from epithelial colon adenoma tissue and compared, to our knowledge for the first time, the expression ratio between CRC and adenoma on protein level. In a recent study, the transcriptional profiles of intestinal tumours in mice were analysed by cDNA microarrays and here as well as in human colorectal cancer cell lines an up-regulation of the *calgizzarin* gene derived from adenocarcinomas compared to adenoma was described (22). Calgizzarin belongs to the group of S100 proteins involved in the Ca^{2+} signaling network, and regulates intracellular activities such as cell growth and motility, cell cycle progression, transcription, and cell differentiation (23,24). It is a nuclear phosphoprotein linked to suppression of DNA synthesis in normal confluent human fibroblasts, although in neoplastic cells such as HeLa and Saos-2 cells loss of nuclear calgizzarin localisation has been observed (25). In a study using also mass spectrometry a specific induction of calgizzarin protein expression in response to the treatment with transforming growth factor-ß (1) was measured in fibroblasts (26).

IHC demonstrates the heterogeneous distribution of calgizzarin in all tissue samples examined underlining the importance of tissue microdissection prior to all analyses. Microdissection enabled exact separation of the epithelial and mesenchymal tissue components and the separation of benign and malignant cell complexes. Only in this way it is possible to detect and to quantify the different levels of expression of calgizzarin in biological different colon tissues. The clonal heterogeneity of the tumour itself concerning the transcriptome and the proteome is morphologically hard to recognise and therefore cannot be completely solved by microdissection, unless repeated cycles of microdissection, protein profiling and immunohistochemical analysis with specific antibodies is employed.

In this case the differential expression of calgizzarin could be visualised so clearly by IHC as it could be done with ProteinChip analysis. Re-analysis of IHC positive areas of CRC, colon adenoma and normal colon epithelium by microdissection and ProteinChip analysis display again a clear difference in expression level.

In conclusion, through protein profiling, we were able to detect, identify and characterise calgizzarin as a marker differentially expressed in CRC and colon adenoma. The combination of tissue microdissection with SELDI-MS and IHC in a proteomic triade opens up the possibility for a more detailed insight and understanding of tumour progression by reducing the complexity of the proteome using a defined cell population.

Acknowledgements

This study was supported by a grant of the German Federal Ministry of Education and Research (BMBF) and the Interdisciplinary Center for Clinical Research (ICCR), Jena. The S100A11 (calgizzarin) antibody was a gift of Dr Jean-Christophe Deloulme (INSERM 0104, DRDC-TS, CEA de Grenoble).

References

1. Parkin DM: Global cancer statistics in the year 2000. Lancet Oncol 2: 533-543, 2001.
2. Kondo Y and Issa JP: Epigenetic changes in colorectal cancer. Cancer Metastasis Rev 23: 29-39, 2004.
3. Cahill DP, Lengauer C, Yu J, Riggins GJ, Willson JK, Markowitz SD, Kinzler KW and Vogelstein B: Mutations of mitotic checkpoint genes in human cancers. Nature 392: 300-303, 1998.
4. Pritzker KPH: Cancer biomarkers: easier said than done. Clinical Chemistry 48: 1147-1150, 2002.
5. Melle C, Ernst G, Schimmel B, Bleul A, Koscielny S, Wiesner A, Bogumil R, Moller U, Osterloh D, Halbhuber KJ and von Eggeling F: A technical triade for proteomic identification and characterization of cancer biomarkers. Cancer Res 64: 4099-4104, 2004.
6. Tang N, Tornatore P and Weinberger SR: Current developments in SELDI affinity technology. Mass Spec Rev 23: 34-44, 2004.
7. Von Eggeling F, Davies H, Lomas L, Fiedler W, Junker K, Claussen U and Ernst G: Tissue-specific microdissection coupled with ProteinChip array technologies: applications in cancer research. Biotechniques 29: 1066-1070, 2000.
8. Craven RA and Banks RE: Laser capture microdissection and proteomics: possibilities and limitation. Proteomics 1: 1200-1204, 2001.
9. Cheung PK, Woolcock B, Adomat H, Sutcliffe M, Bainbridge TC, Jones EC, Webber D, Kinahan T, Sadar M, Gleave ME and Vielkind J: Protein profiling of microdissected prostate tissue links growth differentiation factor 15 to prostate carcinogenesis. Cancer Res 64: 5929-5933, 2004.

10. Melle C, Ernst G, Schimmel B, Bleul A, Koscielny S, Wiesner A, Bogumil R, Moller U, Osterloh D, Halbhuber KJ and von Eggeling F: Biomarker discovery and identification in laser microdissected head and neck squamous cell carcinoma with ProteinChip® technology, two-dimensional gel electrophoresis, tandem mass spectrometry and immunohistochemistry. Mol Cell Proteomics 2: 443-452, 2003.
11. Melle C, Kaufmann R, Hommann M, Bleul A, Driesch D, Ernst G and von Eggeling F: Proteomic profiling in microdissected hepatocellular carcinoma tissue using ProteinChip technology. Int J Oncol 24: 885-891, 2004.
12. Kwapiszewska G, Meyer M, Bogumil R, Bohle RM, Seeger W, Weissmann N and Fink L: Identification of proteins in laser-microdissected small cell numbers by SELDI-TOF and Tandem MS. BMC Biotechnol 4: 30, 2004.
13. Chaurand P, Da Gue BB, Pearsall RS, Threadgill DW and Caprioli RM: Profiling proteins from azoxymethane-induced colon tumors at the molecular level by matrix-assisted laser desorption/ionization mass spectrometry. Proteomics 1: 1320-1306, 2001.
14. Nishizuka S, Chen ST, Gwadry FG, Alexander J, Major SM, Scherf U, Reinhold WC, Waltham M, Charboneau L, Young L, Bussey KJ, Kim S, Lababidi S, Lee JK, Pittaluga S, Scudiero DA, Sausville EA, Munson PJ, Petricoin EF III, Liotta LA, Hewitt SM, Raffeld M and Weinstein JN: Diagnostic markers that distinguish colon and ovarian adenocarcinomas: identification by genomic, proteomic and tissue array profiling. Cancer Res 63: 5243-5250, 2003.
15. Ushigome M, Ubagai T, Fukuda H, Tsuchiya N, Sugimura T, Takatsuka J and Nakagama H: Up-regulation of hnRNP A1 gene in sporadic human colorectal cancers. Int J Oncol 26: 635-640, 2005.
16. Krieg RC, Fogt F, Braunschweig T, Herrmann PC, Wollscheidt V and Wellmann A: ProteinChip array analysis of microdissected colorectal carcinoma and associated tumor stroma shows specific protein bands in the 3.4-3.6 kDa range. Anticancer Res 24: 1791-1796, 2004.
17. Albrethsen J, Bogebo R, Gammeltoft S, Olsen J, Winther B and Raskov H: Up-regulated expression of human neutrophil peptides 1, 2 and 3 (HNP 1-3) in colon cancer serum and tumours: a biomarker study. BMC Cancer 5: 8, 2005.
18. Melle C, Ernst G, Schimmel B, Bleul A, Thieme H, Kaufmann R, Mothes H, Settmacher U, Claussen U, Halbhuber KJ and von Eggeling F: Discovery and identification of α-defensins as low abundant, tumor-derived serum markers in colorectal cancer. Gastroenterology 129: 66-73, 2005.
19. Tanaka M, Adzuma K, Iwami M, Yoshimoto K, Monden Y and Itakura M: Human calgizzarin; one colorectal cancer-related gene selected by a large scale random cDNA sequencing and nothern blot analysis. Cancer Lett 89: 195-200, 1995.
20. Strulik J, Koupilova K, Osterreicher J, Knizek J, Macela A, Bures J, Jandik P, Langr F, Dedic K and Jungblut PR: Protein abundance alterations in matched sets of macroscopically normal colon mucosa and colorectal carcinoma. Electrophoresis 20: 3638-3646, 1999.
21. Melle C, Osterloh D, Ernst G, Schimmel B, Bleul A and von Eggeling F: Identification of proteins from colorectal cancer tissue by two-dimensional gel elctrophoresis and SELDI mass spectrometry. Int J Mol Med 16: 11-17, 2005.
22. Reichling T, Gross KH, Carson DJ, Holdcraft RW, Ley-Ebert C, Witte D, Aronow BJ and Groden J: Transcriptional profiles of intestinal tumors in Apc(Min) mice are unique from those of embryonic intestine and identify novel gene targets dysregulated in human colrectal tumors. Cancer Res 65: 166-176, 2005.
23. Schafer BW and Heizmann CW: The S100 family of EF-hand calcium-binding proteins: functions and pathology. Trends Biochem Sci 21: 134-140, 1996.
24. Heizmann CW, Fritz G and Schafer BW: S100 proteins: structure, functions and pathology. Front Biosci 7: D1356-D1368, 2002.
25. Sakaguchi M, Miyazaki M, Inoue Y, Tsuji T, Kouchi H, Tanaka T, Yamada H and Namba M: Relationship between contact inhibition and intranuclear S100C of normal human fibroblasts. J Cell Biol 149: 1193-1206, 2000.
26. Malmstrom J, Lindberg H, Lindberg C, Bratt C, Wieslander E, Delander EL, Sarnstrand B, Burns JS, Mose-Larsen P, Fey S and Marko-Varga G: Transforming growth factor-beta 1 specifically induce proteins involved in the myofibroblast contractile apparatus. Mol Cell Proteomics 3: 466-477, 2004.

Discovery and Identification of α-Defensins as Low Abundant, Tumor-Derived Serum Markers in Colorectal Cancer

CHRISTIAN MELLE,* GÜNTHER ERNST,* BETTINA SCHIMMEL,* ANNETT BLEUL,* HEIKE THIEME,* ROLAND KAUFMANN,† HENNING MOTHES,§ UTZ SETTMACHER,† UWE CLAUSSEN,* KARL–JÜRGEN HALBHUBER,‖ and FERDINAND VON EGGELING*

*Core Unit Chip Application (CUCA), Institute of Human Genetics and Anthropology, †University Hospital, Department of General and Visceral Surgery, §University Hospital, Department of Traumatology, and ‖Institute of Anatomy II, Friedrich-Schiller-University, Jena, Germany

Background & Aims: **Although colorectal cancer is one of the best characterized tumors with regard to the multistep genetic progression, it remains one of the most frequent and deadly neoplasms in Western countries. This is mainly due to the fact that, up to now, no clinically relevant serum markers could be established in an early routine diagnostic procedure.** ***Methods:*** **We comparatively analyzed microdissected normal and tumorous colonic epithelium by ProteinChip technology to detect proteins specific for the tumor directly in the tissue. Immunohistochemistry (IHC) was used for the in situ localization of the discovered proteins, and an ELISA was performed to quantify these proteins in serum.** ***Results:*** **By this approach, we found and identified α-defensins 1–3 (HNP1–3) to be more highly expressed in the tumor than in normal epithelium. These findings could be confirmed by IHC. Detection of these peptides in the corresponding serum samples was subsequently performed with ELISA, resulting in an average sensitivity of 69% and specificity of 100% for the recognition of colorectal cancer when using the HNP1–3 level in the serum of the patients.** ***Conclusions:*** **The direct analysis of microdissected tissue for the discovery of tumor-specific markers followed by the specific detection of these markers in serum by antibody-based methods proved to be a successful strategy in this study. Therefore, we can conclude that these promising markers would not have been found in serum without the information gained through the analysis of microdissected tissue by ProteinChip technology.**

Tumorigenesis in sporadic colorectal cancer (CRC) has been extensively studied and can be seen as a multistep process, each step representing specific gene mutations or epigenetic changes.[1,2] DNA of CRC cells usually shows mutations of the APC, K-ras, p53, and DCC genes. The progression from adenoma to sporadic CRC results from the accumulation of genetic and epigenetic alterations involving activation of oncogenes and inactivation of tumor suppressor genes.[3] Several other molecular mechanisms were also shown to be involved in tumor development but tend to occur infrequently. Despite the dominant role of the adenoma-carcinoma sequence, these changes are thought to be responsible for the different biologic nature and clinical behavior of CRC. In addition, epidemiologic studies revealed a strong impact of environmental and dietary factors.

Regardless of this knowledge and enormous efforts for CRC, up to now, no relevant serum markers have been established that can be used for early diagnosis or improved therapy in cancer. This remains the case, although many new parallel genomic and proteomic techniques have been introduced in the last 5 years. The strategy of how to search for biomarkers, therefore, has to be reconsidered. Therefore, as a main part of our study, the proteomic technique, surface-enhanced laser desorption/ionization-mass spectrometry (MS)-based ProteinChip (Ciphergen Biosystems Inc, Fremont, CA) technology has been used.[4–6] First described by Hutchens and Yip,[7] the technology makes use of affinity surfaces to retain proteins based on their physicochemical characteristics, followed by direct analysis by time of flight MS. Proteins being retained on chromatographic surfaces can be easily purified from contaminants such as buffer salts or detergents, thus eliminating the need for preseparation techniques, as required with other MS techniques. Furthermore, the low sample requirements of this technique are ideal for small biopsies or microdissected tissue.[8–10] Microdissected tissue material, free of contaminating and unwanted tissue components, is extremely important for finding reliable biomarkers in cancer diagnosis[11] and in elucidating clonal heterogeneity of tumors. The compatibility of laser-based microdissection with ProteinChip

Abbreviations used in this paper: CRC, colorectal cancer; IDM, interaction discovery mapping; IHC, immunohistochemistry; LMPC, laser microdissection and pressure catapulting microscope.

0016-5085/05/$30.00
doi:10.1053/j.gastro.2005.05.014

technology has been shown in a number of small studies,[5,12–15] but, mainly, studies using serum from patients and normal controls have been published.[16–21] The advantage of serum is its availability and its easy way of being processed, but the concentration of tumor-specific proteins might be too low for detection, especially in early stages. The advantage of tissue is that also minute but tumor-specific changes in the protein pattern can be detected. Therefore, it seems reasonable to combine the advantages of serum and tissue analysis. This can be done by first analyzing the microdissected tissue and identifying differentially expressed proteins and then screening for these markers in serum with antibody-based tests for their presence and value for diagnosis.

Using the ProteinChip arrays,[6,10] we analyzed protein expression profiles of microdissected CRC tissue and normal colonic epithelium. Three of the differentially expressed peaks were identified as α-defensins 1–3 (HNP1–3) by immunocapturing and depletion assays. The up-regulation of HNP1–3 in tumor tissue was confirmed by the corresponding immunohistochemical analysis. Positive tissue areas were microdissected in corresponding serial unstained tissue sections and reanalyzed using ProteinChip arrays to show that these proteins are matched to the differentially expressed peaks found in the prior analysis. The up-regulation of HNP1–3 could also be proven in serum by an ELISA-based assay. Thus, it could be shown for the first time that markers, originally discovered by the ProteinChip technology used directly in microdissected tissues, can be redetected and quantified by an ELISA in serum.

Materials and Methods

Laser Microdissection of Tissue Sections

All 39 colon tumor samples and adjacent normal mucosa (n = 40) were obtained after surgical resection at the Department of General and Visceral Surgery of the Friedrich-Schiller-University Jena; these were collected fresh, snap frozen in liquid nitrogen, and stored at −80°C. Tumor specimens were categorized according to their WHO classification. Most of the tumors were classified as pT2 und pT3.

Laser microdissection was performed with a laser microdissection and pressure catapulting microscope (LMPC; Palm, Bernried, Germany) as described elsewhere.[10] In brief, we microdissected approximately 3000 to 5000 cells from native air-dried cryostat tissue sections—avoiding inflammatory infiltrated areas in tumor—each in a maximum of 20–30 minutes. Proteins were extracted by a lysis buffer (100 mmol/L Na-phosphate (pH 7.5), 5 mmol/L EDTA, 2 mmol/L $MgCl_2$, 3 mmol/L 2-β-mercaptoethanol, 0.1% CHAPS, 500 μmol/L leupeptin, and 0.1 mmol/L PMSF) for 30 minutes on ice. After centrifugation (15 minutes; 15,000 rpm), the supernatant was immediately analyzed or frozen in liquid nitrogen for a maximum of 1 day.

Profiling of Microdissected Normal Colon Epithelium and Epithelial Tumor Tissue

The protein lysates from microdissected tissues (tumor and normal) were analyzed on both strong anion exchange arrays (SAX2) and weak cation exchange arrays (WCX2; Ciphergen Biosystems Inc, Fremont, CA) as described elsewhere.[10] In brief, array spots were preincubated by a washing/loading buffer containing 100 mmol/L Tris-buffer, pH 8.5, with 0.02% Triton X-100 for SAX arrays and 100 mmol/L Tris-buffer, pH 4.5, with 0.02% Triton X-100 for WCX arrays followed by application of 2 μL sample extract on ProteinChip arrays, which were incubated at room temperature for 90 minutes in a humidity chamber. After washing 3 times with the same buffers and 2 final washing steps with water, 2 × 0.5 μL sinapinic acid (saturated solution in 0.5% TFA/50% acetonitrile) was applied. Mass analysis was performed in a ProteinChip Reader (model PBS II; Ciphergen Biosystems Inc) according to an automated data collection protocol.[10] Cluster analysis of the detected signals and the determination of respective *P* values for normal and tumor tissue were carried out with the Biomarker Wizard Program (version 3.0; Ciphergen Biosystems Inc). For *P* value calculation, spectra with at least 10 signals in the range between 2 and 20 kilodaltons exhibiting a signal-to-noise (S/N) ratio of at least 5 were selected and analyzed with the Mann–Whitney *U* test for nonparametric data sets.

Identification of Differentially Expressed Protein Peaks

For immunodepletion, 2 μL (40 ng) antihuman monoclonal antibody for α-defensins 1–3 (HNP1–3; T-1034; BMA Biomedicals; Augst, Switzerland) were incubated with 10 μL Protein A-agarose (Sigma Chemical Co, St. Louis, MO) for 15 minutes on ice. A pellet was generated by centrifugation, and the supernatant was discarded. The pellet was washed 2 times with a buffer containing 20 mmol/L Hepes (pH 7.8), 25 mmol/L KCl, 5 mmol/L $MgCl_2$, 0.1 mmol/L EDTA, and 0.05% NP-40. Afterward, 5 μL lysate from laser-dissected tumor was incubated with this pellet for 45 minutes on ice. As a negative control, 5 μL lysate was incubated with Protein A-agarose without a specific antibody for 45 minutes on ice. After incubation, samples were cleared by centrifugation, and 3 μL of each supernatant was analyzed on hydrophobic ProteinChip arrays.

For immunocapturing of specific target proteins, Protein A was directly coupled to Interaction Discovery Mapping (IDM) affinity beads (Ciphergen Biosystems Inc); 10 μL beads were washed extensively 5 times with 1.0 mL aqua bidest before 5 μL Protein A in acetate buffer, pH 5.0, was added and incubated overnight at 4°C in an end-over-end mixer. After incubation, the supernatant was removed, and the beads were washed twice with acetate buffer, pH 5.0. Residual reactive groups were subsequently blocked with 0.5 mol/L Tris-HCl,

pH 9.0, 0.1% Triton X-100 for 2 hours at room temperature with shaking. The beads were washed 3 times with 1 mL PBS. Afterwards, 4 μg HNP1–3-specific monoclonal antibody (0.1 μg/mL; BMA) in 50 mmol/L sodium acetate, pH 5.0, was applied to the beads and allowed to bind at room temperature for 1 hour in an end-over-end mixer. Unbound antibody was removed by washing in 0.5 mL PBS and 0.1% Triton X-100 and twice in 0.5 mL PBS. Twenty microliters cell extract derived by laser microdissection was diluted in 100 μL PBS and applied to the IDM beads for incubation overnight at 4°C in an end-over-end mixer. The unbound proteins were washed away by sequential washes in PBS, 0.5 mmol/L sodium chloride, 0.05% Triton X-100, 1 mol/L urea in PBS, PBS, and aqua bidest. Bound proteins were eluted from the IDM beads by 10 μL 50% acetonitrile/0.5% trifluoroacetic acid and gently centrifuged for 5 minutes. Five microliters of the eluted samples were applied to the activated, hydrophobic surface of an H4 ProteinChip Array (Ciphergen Biosystems Inc) and dried in air. The protein chip was analyzed in a PBS II reader.

Characterization of Proteins by Immunohistochemistry

Eight-micrometer cryostat sections of colon cancer tissue and normal colon epithelium were placed on slides, air dried for ~60 minutes at 20°C, and fixed in paraformaldehyde as described.[10] After fixation, slides were treated in the microwave at 80 watts (3 × 3 minutes) in 10 mmol/L citric acid, pH 6.0, to inhibit endogenous peroxidatic activity. Subsequently, they were rinsed twice with TBS, pH 7.4, and incubated overnight at 4°C in a humidity chamber with the corresponding primary monoclonal antibody against α-defensins 1–3 (T-1034; BMA Biomedicals; Augst, Switzerland). Slides were rinsed 3 × 10 minutes in TBS and incubated at room temperature for 40 minutes with the secondary biotinylated monoclonal antibody (Santa Cruz Biotechnology, Santa Cruz, CA). Slides were rinsed 3 × 10 minutes in TBS and the Vectastain Elite ABC kit (Vector Laboratories, Burlingame, CA) and the Jenchrom pxbl-kit (MoBiTec, Göttingen, Germany) were used according to the manufacturer's instructions to visualize antibody localization. Negative controls were incubated with the labeled secondary antibody only. Sections cut in parallel to the IHC-treated sections were stained by H&E for better identification of different tissue areas. IHC staining was evaluated by a pathologist and an anatomist.

The 1-photon laser-scanning microscopy was performed with a LSM 310 (Carl Zeiss, Oberkochen-Jena, Germany) in the transmission mode using an Argon-ion laser at a wavelength of 480 nm. In most cases, Zeiss objective NEOFLUAR 40X/1.30 oil was used at a scanning time of 60 seconds.[22,23]

Quantification of HNP1–3 in Serum of Colon Cancer Patients and Normal Controls

In addition to the investigated tissue samples, we took serum probes (n = 26) from the same patients. These probes were taken before surgery and immediately aliquoted and frozen at −80°C. Serum samples from healthy donors (n = 22) were taken with the same protocol.

Serum HNP1–3 concentrations were determined using an appropriate ELISA kit (HNP1–3; HyCult Biotechnology, The Netherlands) in duplicate, according to the manufacturer's instructions. ELISA plates were measured on a microtiter plate reader (MRX II; Dynex Technology, Chantilly, VA) at 450 nm. Concentration of the respective protein in serum was calculated according to a standard curve. *P* values were calculated by 1-sided *t* test. Receiver operating characteristic (ROC) curves were constructed for HNP1–3 serum concentration by plotting sensitivity vs 1-specificity, and the areas under the ROC curves (AUC) were calculated. To validate the results, a second totally independent set of serum probes including 19 samples of healthy donors and 23 patient samples was analyzed.

Results

Profiling of Microdissected Normal Colonic Epithelium and Tumor Tissue

For this study, areas corresponding to approximately 3000 to 5000 cells per tissue probe were excised, and 79 tissue sections (39 tumor and 40 normal colonic epithelium tissues) were successfully dissected by a pathologist. All protein lysates from the microdissected tissues were applied to SAX2 and WCX arrays and analyzed on a PBS II instrument. In the low range (2–20 kilodaltons), up to 126 peaks were detected with normalized intensities.

After evaluation with the Biomarker Wizard Program (Ciphergen Biosystems Inc), peak masses that possessed remarkably low *P* values were selected for further characterization and identification. These signals of 3.37 ($P = 4.39 \times 10^{-5}$), 3.44 ($P = 1.88 \times 10^{-5}$), and 3.49 kilodaltons ($P = 9.91 \times 10^{-5}$) were up-regulated in colon tumor tissue. The distribution of the intensities for normal and tumor tissue is shown in Figure 1.

Identification of Differential Expressed Protein Peaks

To confirm that HNP1–3 were matching to the differentially expressed peaks at 3.37, 3.44, and 3.49 kilodaltons found by ProteinChip analysis, an immunodepletion assay was performed with microdissected tumor and normal colonic epithelium tissue. Analysis of the supernatant of the immunodepletion assay by ProteinChip arrays showed that the peaks corresponding to HNP1–3 were significantly reduced. In the negative control (immunodepletion process with no specific antibody), the corresponding peaks were clearly detectable (Figure 2*A*). Furthermore, the pattern and sizes of HNP1–3 were described or identified by Tandem MS

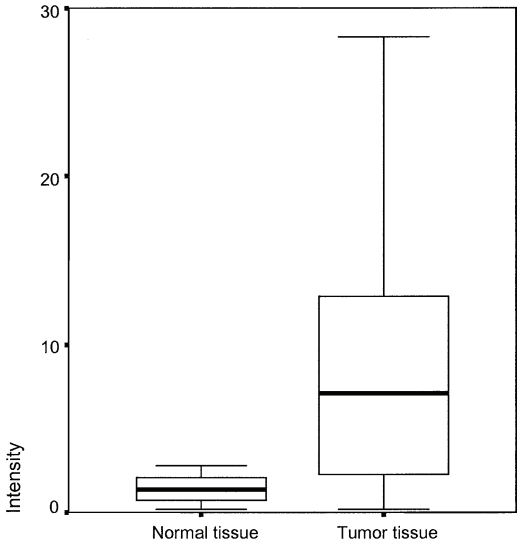

Figure 1. Box plot of concentration of HNP1–3 in normal and tumor tissue found by ProteinChip arrays (SAX2).

elsewhere.[24–26] The sequence of the processed peptides is shown in Figure 3. The identification of additionally found differentially expressed proteins is in progress.

For further confirmation of the identity of the differentially expressed HNP1–3, an immunoassay was performed using a monoclonal antibody against HNP1–3. A specific anti-HNP1–3 antibody bound on IDM beads captured α-defensins 1–3 from a cell extract derived from laser microdissected colon carcinoma tissue. The captured proteins were eluted from the beads and applied to an H4 ProteinChip for analysis by SELDI-MS. The spectra of the analysis showed peaks corresponding to HNP1–3. In a control assay using IDM beads without a specific antibody, no proteins specific for HNP1–3 were captured (Figure 2*B*).

```
HNP-1     ACYCR IPACI AGERR YGTCI YQGRL WAFCC
HNP-2      CYCR IPACI AGERR YGTCI YQGRL WAFCC
HNP-3     DCYCR IPACI AGERR YGTCI YQGRL WAFCC
```

Figure 3. Structure of mature human HNP1–3. Amino acid sequence is shown in *single letter code*, differences in *bold letters*.

Localization of HNP1–3 by Immunohistochemistry

Further to confirm identification and, above all, to localize HNP1–3 in tissue sections, we examined their expression in 5 different colon cancer tissues and adjacent normal tissue sections using immunohistochemistry. Normal colonic epithelium showed a weak positive reaction (Figure 4*A*), tumor tissue an explicit strong reaction (Figure 4*A* and 4*B*). Negative controls without the primary or with no antibody at all demonstrated negative results. A positive stain for HNP1–3 could also be found in fibroblasts and macrophages of the mucous membrane.

To ensure that the localized HNP1–3 are identical to the peaks found by ProteinChip analysis, IHC-positive and -negative cell areas were obtained by tissue laser microdissection. In protein lysates from the positive fraction, signals identical in mass to the peaks obtained with the initial ProteinChip analysis was detected. In the protein lysate from the negative fraction, these peaks were not visible (Figure 2*C*).

Analyses of HNP1–3 in Serum

Two serum sample sets from patients with colon cancer and normal controls (n = 48; n = 42, respec-

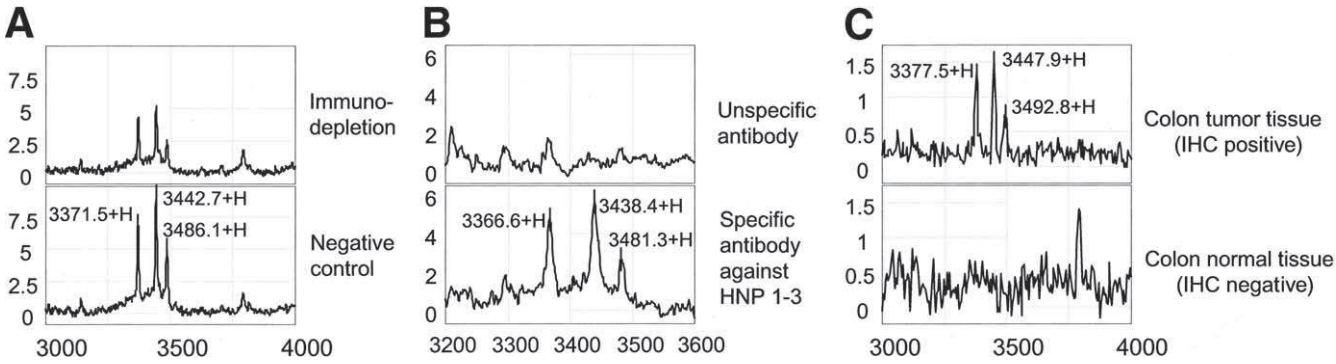

Figure 2. Identification of HNP1–3: (*A*) Normalized ProteinChip arrays profiles of the immunodepletion assays of microdissected colonic tissue. For HNP1–3 identification, colon cancer tissue was used as starting material for immunodepletion assays by the corresponding monoclonal antibody. The negative control was performed without a specific antibody. The peaks at 3.37, 3.44, and 3.49 kilodaltons representing HNP1–3 were detectable in a higher amount in the negative control. (*B*) Normalized ProteinChip arrays spectra of the immunocapturing assay of microdissected colon carcinoma tissue. HNP1–3 were captured from microdissected colon carcinoma tissue by the corresponding monoclonal antibody bound on IDM beads. The peaks at 3.37, 3.44, and 3.48 kilodaltons representing HNP1–3 were clearly detectable in samples eluted from the IDM beads. In control assays without the specific antibody, no HNP1–3 were captured. (*C*) Areas with positive and negative reaction in IHC were microdissected and analyzed on ProteinChip arrays. Signals with a molecular mass of 3.37, 3.44, and 3.49 kilodaltons representing HNP1–3 were detectable in protein lysates from positive areas and were absent in the negative areas.

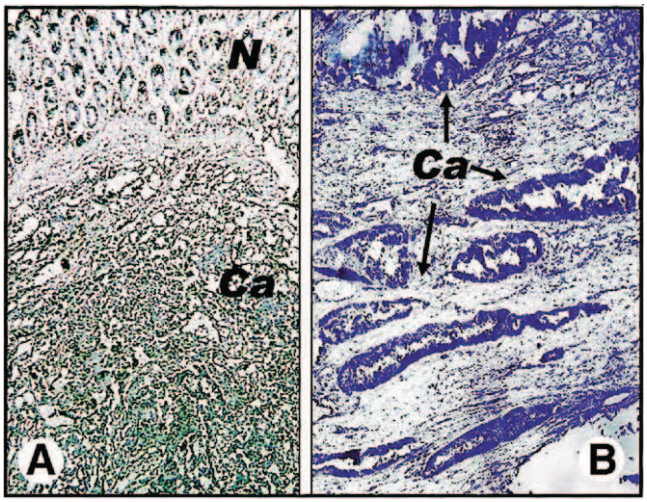

Figure 4. Immunohistochemistry (IHC) of HNP1–3 visualized by normal and laser scanning microscopy (LSM; positive reaction is depicted in *blue*). (*A* and *B*) IHC of HNP1–3 on colon carcinoma. (*A*) Increased signal intensity in carcinoma (Ca) structures (overview with ×25 magnification; N, normal epithelium). (*B*) Strong positive reaction of invasive growing carcinoma complexes (Ca; magnification of ×120).

tively) were independently analyzed by ELISA for quantification of HNP1–3. In the first set, the concentration of HNP1–3 in serum from tumor patients was significantly higher than in serum from normal controls ($P = 2.14 \times 10^{-5}$). The median for normal control was 8.1 ng/mL; for patients with colon carcinoma it was 29.4 ng/mL (Figure 5). ROC curves were constructed for HNP1–3 serum concentration, resulting in a sensitivity of 100% at a specificity of 69% and a cut-off of 14.8 ng/mL. The AUC was calculated as 0.77 (Figure 6). The independent analysis of the validation set showed an equal distribution like the first set and resulted in a *P* value of .0056. The median for normal controls was 5.60 ng/mL and 14.99 ng/mL for patients (Figure 5). The ROC resulted in a sensitivity of 100% at a specificity of 65.2% and a cut-off of 12.3 ng/mL. The AUC was calculated as 0.840 (Figure 6).

Discussion

New molecular biomarkers or biomarker patterns found by genomic or proteomic high-throughput techniques will enable a more reliable early diagnosis of malignant tumors and facilitate the prediction of their progression. In this way, biomarkers may contribute to a more differentiated, individually orientated tumor therapy. Despite enormous efforts, until now, only in a few tumor diseases, have relevant markers useful for screening been established.[27,28]

Besides 2-dimensional gel electrophoresis (2-DE), the ProteinChip technology (for examples, see Petricoin et al[16] and Rosty et al[29]) is a promising proteomic tool for the detection of new proteomic cancer biomarkers. Until now, this technique has been predominantly used for body fluid analyses because they are fast and easy to analyze by direct application onto ProteinChip arrays. Nevertheless, it is known that inter- and intraindividual changes in serum depending on sex, hormone level, nutrition state, or inflammation are high and can change the protein profile drastically. Hence, it is possible that biomarkers present in low level in serum could not be found or statistically differentiated with 2-DE or ProteinChip technology. Despite these concerns, a large number of studies using body fluids as starting material have been published (serum,[16,30] urine,[24] nipple aspirate fluid,[31] and pancreatic juice[29]). However, if markers can be found, they would be ideal for screening high-risk individuals or even individuals without elevated risk, discussed by the latest study on ovarian cancer[32] or others.[17,19,33,34]

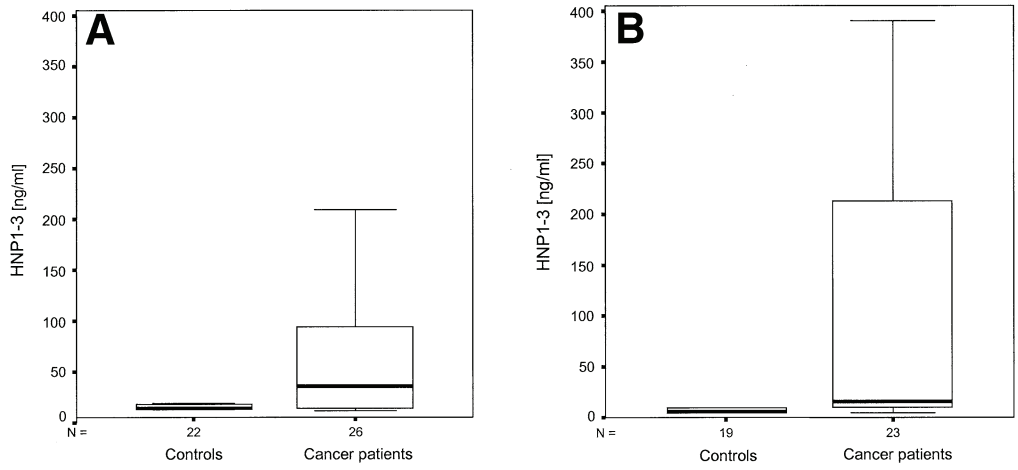

Figure 5. Box plot of serum concentration of HNP1–3 for controls and patients with colon carcinoma for both independently analyzed sample sets (*A* and *B*).

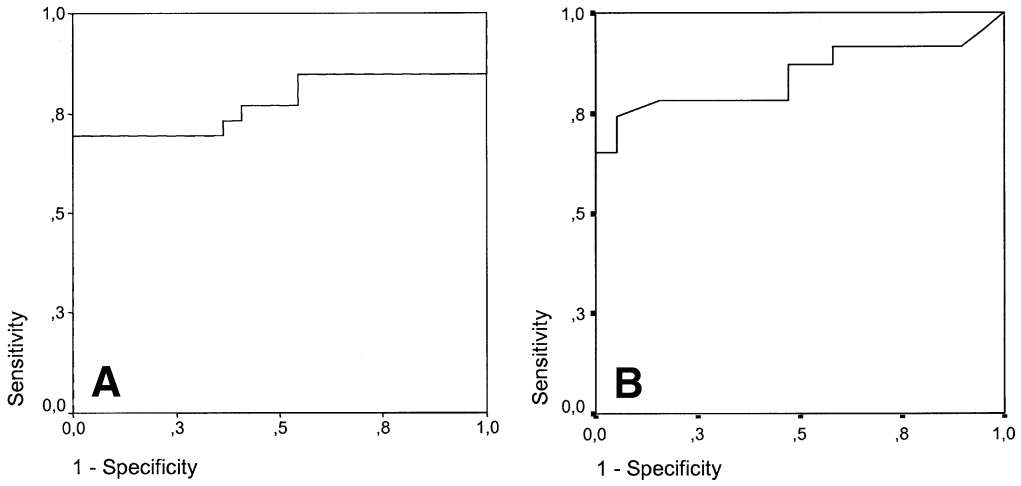

Figure 6. ROC curve for HNP1–3 serum concentration of colon cancer patients and normal controls. The AUC was calculated as 0.77: The sensitivity of 100% is corresponding to a specificity of 69% (*A*). The independent analysis of the validation set (*B*) resulted in a *P* value of .0056. The median for normal controls was 5.60 ng/mL and 14.99 ng/mL for patients. The ROC resulted in a sensitivity of 100% at a specificity of 65.2% and a cut-off of 12.3 ng/mL. The AUC was calculated as 0.840.

In contrast to serum, the analysis of tissues is more time consuming because here microdissection is necessary to separate tumorous from healthy cells, although the chance to find reliable tumor markers might be higher than in serum. However, these markers could not be used per se for an early diagnosis, but there is certainly a higher chance of obtaining more information about the biologic mechanisms leading to the genesis and progression of cancer. Studies using tissue as a starting material have been underrepresented until now, and, in most cases, a low number of samples was analyzed, which might be due to the fact that even laser-based microdissection is tedious and has to be done by an experienced pathologist. To date, prostate cancer,[5,13,35] melanoma,[9,36] lung tumors,[14] renal cell carcinoma (RCC),[12,36] and head and neck squamous cell carcinoma (HNSCC)[10,11] have been assessed in this way.

In the present work, we combined the advantages of biomarker search in microdissected tumor tissue and in serum. First, we looked for significant markers by comparing tumor and normal tissue. Subsequently, we analyzed these identified proteins specifically in serum by a corresponding ELISA. Three peaks were identified as HNP1–3 (up-regulated in tumor) by size and characteristic pattern published elsewhere[25,26] and further confirmed by immunodepletion and capturing assays using the same starting material. In situ localization of these proteins in tissue was performed using IHC, and the results were concurrent with those found by ProteinChip technology. Positive tissue areas were microdissected and reanalyzed using ProteinChip arrays to show that these proteins are matching to HNP1–3. Furthermore, the ELISA assay on serum revealed exactly the same results for HNP1–3. Consequently, this study confirmed the consistency of ProteinChip arrays, IHC, and ELISA results for HNP1–3 and therefore demonstrates for, to our knowledge, the first time the efficiency of tissue-based ProteinChip studies for the detection of serum markers. In addition, HNP1–3 might be, at least in combination with other screening methods, a potential serum marker for colon cancer screening. In principle, ProteinChip arrays could also be used for the specific and more sensitive capturing of defensins by using antibody-coupled arrays. Such assays have already been established for the detection of defensins in urine.[24] With this technology, the limit of detection for synthetic defensin peptides is reported to be in the lower femtomolar range.[26]

Defensins are small peptides that contain 6 cystein residues, which form 3 disulfide bonds. On the basis of the position of these residues, they can be divided into α- and β-defensins. So far, only 2 enteric α-defensins (human defensins 5 and 6; HD-5 and -6) have been identified in humans,[37] but many more probably exist.[38] The known human enteric HD-5 and HD-6 are predominantly expressed in Paneth cells and rarely present in intermediate cells of the small intestine.[39–41] Their expression seems to be constitutive and in contrast to β-defensin 2 (HBD-2)[42–44] bacterial stimuli are not required for their production. The 5′-flanking region of the HD-5 gene contains consensus binding sites for a nuclear transcription factor, nuclear factor interleukin-6 (NF-IL-6), which may provide a mechanism whereby this up-regulation could occur in response to inflammatory stimuli.[45] Expression of HD-5 (and HD-6) has also been demonstrated in the colonic epithelium in Crohn's disease and ulcerative colitis.[46] In addition to the human

enteric defensins 5 and 6, neutrophil defensins (HNP-1, -2, -3) may also be expressed in intestinal epithelial cells in certain conditions. In a recent study, expression of HNP1–3 was observed in epithelial cells of the ileum and colon in cases of inflammatory diseases but not in normal intestinal tissue.[47,48] Whether this reflects induction of gene expression or uptake by epithelial cells of peptides released by neutrophils in the vicinity remains to be determined.[41] In different cancer entities such as RCC[49] or oral squamous cell carcinoma (OSCC),[50] HNP1–3 were also found up-regulated. Now, it can be assessed that α-defensins expressed in the colon also include HNP1–3. This has been demonstrated in our study by ProteinChip technology and IHC. Nevertheless, this expression might come from neutrophils, but neutrophils could be well visualized in H&E-stained sections with the appropriate magnification. We avoided in our study microdissecting areas with neutrophils, not because of the neutrophils, but because these regions are normally inflamed. Therefore, it could be stated that the microdissected tumor tissue does not contain more neutrophils than the normal tissue. So far, this is the first study demonstrating the presence of human α-defensins 1–3 in the colonic mucosa. These findings strengthen the hypothesis that the increased value in serum of patients with colon cancer is derived from tumor cells.

In conclusion, we were able to show that, for biomarker detection, it is an efficient approach to compare first pure and defined normal and tumor cells to detect and identify the up-regulation of tumor relevant proteins and then to detect and quantify them specifically in serum. Additionally, with this approach, we could show for the first time the up-regulation of HNP1–3 in colon cancer and its potential use as serum marker with high sensitivity and specificity. If the present results can be confirmed further with higher sample numbers and additionally in adenoma tissue or early tumor stages, HNP1–3 could be used in combination with other markers for an early and better diagnosis of colon cancer.

References

1. Fearon ER, Vogelstein B. A genetic model for colorectal tumorigenesis. Cell 1990;61:759–767.
2. Kondo Y, Issa JP. Epigenetic changes in colorectal cancer. Cancer Metastasis Rev 2004;23:29–39.
3. Cahill DP, Lengauer C, Yu J, Riggins GJ, Willson JK, Markowitz SD, Kinzler KW, Vogelstein B. Mutations of mitotic checkpoint genes in human cancers. Nature 1998;392:300–303.
4. Davies H, Lomas L, Austen B. Profiling of amyloid β peptide variants using SELDI ProteinChip (R) arrays. Biotechniques 1999; 27:1258–1261.
5. Wright GL, Cazares LH, Leung SM, Nasim S, Adam BL, Yip TT, Schellhammer PF, Gong L, Vlahou A. Proteinchip(R) surface enhanced laser desorption/ionization (SELDI) mass spectrometry: a novel protein biochip technology for detection of prostate cancer biomarkers in complex protein mixtures. Prostate Cancer Prostatic Dis 1999;2:264–276.
6. Merchant M, Weinberger SR. Recent advancements in surface-enhanced laser desorption/ionization-time of flight-mass spectrometry. Electrophoresis 2000;21:1164–1177.
7. Hutchens TW, Yip TT. New desorption strategies for the mass spectrometric analysis of macromolecules. Rapid Commun Mass Spectrom 1993;7:576–580.
8. Schütze K, Lahr G. Identification of expressed genes by laser-mediated manipulation of single cells (see comments). Nat Biotechnol 1998;16:737–742.
9. von Eggeling F, Davies H, Lomas L, Fiedler W, Junker K, Claussen U, Ernst G. Tissue-specific microdissection coupled with ProteinChip array technologies: applications in cancer research. Biotechniques 2000;1066–1070.
10. Melle C, Ernst G, Schimmel B, Bleul A, Koscielny S, Wiesner A, Bogumil R, Moller U, Osterloh D, Halbhuber KJ, von Eggeling F. Biomarker discovery and identification in laser microdissected head and neck squamous cell carcinoma with ProteinChip(R) technology, two-dimensional gel electrophoresis, tandem mass spectrometry, and immunohistochemistry. Mol Cell Proteomics 2003;2:443–452.
11. Melle C, Ernst G, Schimmel B, Bleul A, Koscielny S, Wiesner A, Bogumil R, Moller U, Osterloh D, Halbhuber KJ, von Eggeling F. A technical triade for proteomic identification and characterization of cancer biomarkers. Cancer Res 2004;64:4099–4104.
12. von Eggeling F, Junker K, Fiedler W, Wollscheid V, Durst M, Claussen U, Ernst G. Mass spectrometry meets chip technology: a new proteomic tool in cancer research? Electrophoresis 2001; 22:2898–2902.
13. Cazares LH, Adam BL, Ward MD, Nasim S, Schellhammer PF, Semmes OJ, Wright GL. Normal, benign, preneoplastic, and malignant prostate cells have distinct protein expression profiles resolved by surface enhanced laser desorption/ionization mass spectrometry. Clin Cancer Res 2002;8:2541–2552.
14. Zhukov TA, Johanson RA, Cantor AB, Clark RA, Tockman MS. Discovery of distinct protein profiles specific for lung tumors and pre-malignant lung lesions by SELDI mass spectrometry. Lung Cancer 2003;40:267–279.
15. Melle C, Kaufmann R, Hommann M, Bleul A, Driesch D, Ernst G, von Eggeling F. Proteomic profiling in microdissected hepatocellular carcinoma tissue using ProteinChip technology. Int J Oncol 2004;24:885–891.
16. Petricoin EF, Ardekani AM, Hitt BA, Levine PJ, Fusaro VA, Steinberg SM, Mills GB, Simone C, Fishman DA, Kohn EC, Liotta LA. Use of proteomic patterns in serum to identify ovarian cancer. Lancet 2002;359:572–577.
17. Ye B, Cramer DW, Skates SJ, Gygi SP, Pratomo V, Fu L, Horick NK, Licklider LJ, Schorge JO, Berkowitz RS, Mok SC. Haptoglobin-α subunit as potential serum biomarker in ovarian cancer: identification and characterization using proteomic profiling and mass spectrometry. Clin Cancer Res 2003;9:2904–2911.
18. Thulasiraman V, McCutchen-Maloney SL, Motin VL, Garcia E. Detection and identification of virulence factors in Yersinia pestis using SELDI ProteinChip system. Biotechniques 2001;30:428–432.
19. Uchida T, Fukawa A, Uchida M, Fujita K, Saito K. Application of a novel protein biochip technology for detection and identification of rheumatoid arthritis biomarkers in synovial fluid. J Proteome Res 2002;1:495–499.
20. Li J, White N, Zhang Z, Rosenzweig J, Mangold LA, Partin AW, Chan DW. Detection of prostate cancer using serum proteomics pattern in a histologically confirmed population. J Urol 2004;171: 1782–1787.
21. Tolson J, Bogumil R, Brunst E, Beck H, Elsner R, Humeny A, Kratzin H, Deeg M, Kuczyk M, Mueller GA, Mueller CA, Flad T. Serum protein profiling by SELDI mass spectrometry: detection of

multiple variants of serum amyloid alpha in renal cancer patients. Lab Invest 2004;84:845–856.
22. Halbhuber KJ, Krieg R, Konig K. Laser scanning microscopy in enzyme histochemistry. Visualization of cerium-based and dab-based primary reaction products of phosphatases, oxidases and peroxidases by reflectance and transmission laser scanning microscopy. Cell Mol Biol (Noisy-le-grand) 1998;44:807–826.
23. Halbhuber KJ, Konig K. Modern laser scanning microscopy in biology, biotechnology and medicine. Ann Anat 2003;185:1–20.
24. Vlahou A, Schellhammer PF, Mendrinos S, Patel K, Kondylis FI, Gong L, Nasim S, Wright G-LJ Jr. Development of a novel proteomic approach for the detection of transitional cell carcinoma of the bladder in urine. Am J Pathol 2001;158:1491–1502.
25. Zhang L, Yu W, He T, Yu J, Caffrey RE, Dalmasso EA, Fu S, Pham T, Mei J, Ho JJ, Zhang W, Lopez P, Ho DD. Contribution of human α-defensin 1, 2, and 3 to the anti-HIV-1 activity of CD8 antiviral factor. Science 2002;298:995–1000.
26. Diamond DL, Kimball JR, Krisanaprakornkit S, Ganz T, Dale BA. Detection of β-defensins secreted by human oral epithelial cells. J Immunol Methods 2001;256:65–76.
27. van't Veer LJ, Dai HY, van de Vijver MJ, He YDD, Hart AAM, Mao M, Peterse HL, van der Kooy K, Marton MJ, Witteveen AT, Schreiber GJ, Kerkhoven RM, Roberts C, Linsley PS, Bernards R, Friend SH. Gene expression profiling predicts clinical outcome of breast cancer. Nature 2002;415:530–536.
28. Sidransky D. Emerging molecular markers of cancer. Nat Rev Cancer 2002;2:210–219.
29. Rosty C, Christa L, Kuzdzal S, Baldwin WM, Zahurak ML, Carnot F, Chan DW, Canto M, Lillemoe KD, Cameron JL, Yeo CJ, Hruban RH, Goggins M. Identification of hepatocarcinoma-intestine-pancreas/pancreatitis-associated protein I as a biomarker for pancreatic ductal adenocarcinoma by protein biochip technology. Cancer Res 2002;62:1868–1875.
30. Petricoin EF, Mills GB, Kohn EC, Liotta LA. Proteomic patterns in serum and identification of ovarian cancer (reply). Lancet 2002; 360:170–171.
31. Paweletz CP, Trock B, Pennanen M, Tsangaris T, Magnant C, Liotta LA, Petricoin EF. Proteomic patterns of nipple aspirate fluids obtained by SELDI-TOF: potential for new biomarkers to aid in the diagnosis of breast cancer. Dis Markers 2001;17:301–307.
32. Kozak KR, Amneus MW, Pusey SM, Su F, Luong MN, Luong SA, Reddy ST, Farias-Eisner R. Identification of biomarkers for ovarian cancer using strong anion-exchange ProteinChips: potential use in diagnosis and prognosis. Proc Natl Acad Sci U S A 2003;100: 12343–12348.
33. Shiwa M, Nishimura Y, Wakatabe R, Fukawa A, Arikuni H, Ota H, Kato Y, Yamori T. Rapid discovery and identification of a tissue-specific tumor biomarker from 39 human cancer cell lines using the SELDI ProteinChip platform. Biochem Biophys Res Commun 2003;309:18–25.
34. Rogers MA, Clarke P, Noble J, Munro NP, Paul A, Selby PJ, Banks RE. Proteomic profiling of urinary proteins in renal cancer by surface enhanced laser desorption ionization and neural-network analysis: identification of key issues affecting potential clinical utility. Cancer Res 2003;63:6971–6983.
35. Wellmann A, Wollscheid V, Lu H, Ma ZL, Albers P, Schutze K, Rohde V, Behrens P, Dreschers S, Ko Y, Wernert N. Analysis of microdissected prostate tissue with ProteinChip(R) arrays—a way to new insights into carcinogenesis and to diagnostic tools. Int J Mol Med 2002;9:341–347.
36. Fetsch PA, Simone NL, Bryant-Greenwood PK, Marincola FM, Filie AC, Petricoin EF, Liotta LA, Abati A. Proteomic evaluation of archival cytologic material using SELDI affinity mass spectrometry: potential for diagnostic applications. Am J Clin Pathol 2002; 118:870–876.
37. Jones DE, Bevins CL. Paneth cells of the human small intestine express an antimicrobial peptide gene. J Biol Chem 1992;267: 23216–23225.
38. Rodriguez-Jimenez FJ, Krause A, Schulz S, Forssmann WG, Conejo-Garcia JR, Schreeb R, Motzkus D. Distribution of new human β-defensin genes clustered on chromosome 20 in functionally different segments of epididymis. Genomics 2003;81: 175–183.
39. Kamal M, Wakelin D, Ouellette AJ, Smith A, Podolsky DK, Mahida YR. Mucosal T cells regulate Paneth and intermediate cell numbers in the small intestine of *T. spiralis*-infected mice. Clin Exp Immunol 2001;126:117–125.
40. Cunliffe RN, Rose FR, Keyte J, Abberley L, Chan WC, Mahida YR. Human defensin 5 is stored in precursor form in normal Paneth cells and is expressed by some villous epithelial cells and by metaplastic Paneth cells in the colon in inflammatory bowel disease. Gut 2001;48:176–185.
41. Cunliffe RN, Mahida YR. Expression and regulation of antimicrobial peptides in the gastrointestinal tract. J Leukoc Biol 2004; 75:49–58.
42. Wehkamp J, Harder J, Weichenthal M, Mueller O, Herrlinger KR, Fellermann K, Schroeder JM, Stange EF. Inducible and constitutive β-defensins are differentially expressed in Crohn's disease and ulcerative colitis. Inflamm Bowel Dis 2003;9:215–223.
43. Yoshimoto T, Yamaai T, Mizukawa N, Sawaki K, Nakano M, Yamachika E, Sugahara T. Different expression patterns of β-defensins in human squamous cell carcinomas. Anticancer Res 2003;23:4629–4633.
44. Donald CD, Sun CQ, Lim SD, Macoska J, Cohen C, Amin MB, Young AN, Ganz TA, Marshall FF, Petros JA. Cancer-specific loss of β-defensin 1 in renal and prostatic carcinomas. Lab Invest 2003;83:501–505.
45. Mallow EB, Harris A, Salzman N, Russell JP, DeBerardinis RJ, Ruchelli E, Bevins CL. Human enteric defensins. Gene structure and developmental expression. J Biol Chem 1996;271:4038–4045.
46. Fahlgren A, Hammarstrom S, Danielsson A, Hammarstrom ML. Increased expression of antimicrobial peptides and lysozyme in colonic epithelial cells of patients with ulcerative colitis. Clin Exp Immunol 2003;131:90–101.
47. Ogawa H, Fukushima K, Sasaki I, Matsuno S. Identification of genes involved in mucosal defense and inflammation associated with normal enteric bacteria. Am J Physiol Gastrointest Liver Physiol 2000;279:G492–G499.
48. Cunliffe RN, Kamal M, Rose FR, James PD, Mahida YR. Expression of antimicrobial neutrophil defensins in epithelial cells of active inflammatory bowel disease mucosa. J Clin Pathol 2002; 55:298–304.
49. Muller CA, Markovic-Lipkovski J, Klatt T, Gamper J, Schwarz G, Beck H, Deeg M, Kalbacher H, Widmann S, Wessels JT, Becker V, Muller GA, Flad T. Human α-defensins HNPs-1, -2, and -3 in renal cell carcinoma: influences on tumor cell proliferation. Am J Pathol 2002;160:1311–1324.
50. Lundy FT, Orr DF, Gallagher JR, Maxwell P, Shaw C, Napier SS, Gerald CC, Lamey PJ, Marley JJ. Identification and overexpression of human neutrophil α-defensins (human neutrophil peptides 1, 2 and 3) in squamous cell carcinomas of the human tongue. Oral Oncol 2004;40:139–144.

Received November 3, 2004. Accepted March 30, 2005.

Address requests for reprints to: Ferdinand von Eggeling, PhD, Institut für Humangenetik und Anthropologie, CUCA, 07740 Jena, Germany. e-mail: fegg@mti.uni-jena.de; fax: (49) 03641-935518.

Supported by a grant of the German Federal Ministry of Education and Research (BMBF) and the Interdisciplinary Center for Clinical Research (ICCR), Jena, Germany.

OPEN ACCESS Freely available online

PLoS one

Colon-Derived Liver Metastasis, Colorectal Carcinoma, and Hepatocellular Carcinoma Can Be Discriminated by the Ca2+-Binding Proteins S100A6 and S100A11

Christian Melle, Günther Ernst, Bettina Schimmel, Annett Bleul, Ferdinand von Eggeling*

Core Unit Chip Application, Institute of Human Genetics and Anthropology, Medical Faculty at the Friedrich Schiller University, Jena, Germany

Abstract

Background: It is unknown, on the proteomic level, whether the protein patterns of tumors change during metastasis or whether markers are present that allow metastases to be allocated to a specific tumor entity. The latter is of clinical interest if the primary tumor is not known.

Methodology/Principal Findings: In this study, tissue from colon-derived liver metastases (n = 17) were classified, laser-microdissected, and analysed by ProteinChip arrays (SELDI). The resulting spectra were compared with data for primary colorectal (CRC) and hepatocellular carcinomas (HCC) from our former studies. Of 49 signals differentially expressed in primary HCC, primary CRC, and liver metastases, two were identified by immunodepletion as S100A6 and S100A11. Both proteins were precisely localized immunohistochemically in cells. S100A6 and S100A11 can discriminate significantly between the two primary tumor entities, CRC and HCC, whereas S100A6 allows the discrimination of metastases and HCC.

Conclusions: Both identified proteins can be used to discriminate different tumor entities. Specific markers or proteomic patterns for the metastases of different primary cancers will allow us to determine the biological characteristics of metastasis in general. It is unknown how the protein patterns of tumors change during metastasis or whether markers are present that allow metastases to be allocated to a specific tumor entity. The latter is of clinical interest if the primary tumor is not known.

Citation: Melle C, Ernst G, Schimmel B, Bleul A, von Eggeling F (2008) Colon-Derived Liver Metastasis, Colorectal Carcinoma, and Hepatocellular Carcinoma Can Be Discriminated by the Ca2+-Binding Proteins S100A6 and S100A11. PLoS ONE 3(12): e3767. doi:10.1371/journal.pone.0003767

Editor: Joseph Alan Bauer, Cleveland Clinic, United States of America

Received September 3, 2008; **Accepted** October 30, 2008; **Published** December 2, 2008

Funding: This work was supported by a grant from the German Federal Ministry of Education and Research (BMBF) and the Interdisciplinary Center for Clinical Research (ICCR), Jena. The funders had no role in study design, data collection and analysis, decision to publish, or preparation of the manuscript.

Competing Interests: The authors have declared that no competing interests exist.

* E-mail: fegg@mti.uni-jena.de

Introduction

Distant metastases are the principal causes of death in patients with colorectal carcinoma (CRC). A common site of metastases derived from CRC is the liver.[1] The underlying mechanisms of liver metastasis of CRC are not fully understood, but metastases are at least involved in tumor initiation and promotion, uncontrolled proliferation, angiogenesis, invasion, intra- and extravasation, and colony formation at the liver site.[2,3] The analysis of the expression of a single protein is not practical because these processes seem to be induced by the altered expression of several different proteins. Proteomic approaches are practical in the global analysis of altered protein patterns, in which diverse mass spectrometry (MS)-based methods are used for these kinds of high-throughput analyses.[4,5] In this context, surface-enhanced laser desorption/ionization (SELDI) is a proteomic high-throughput technique that uses chromatographic surfaces that are able to retain proteins depending on their physico-chemical properties, followed by direct analysis via time-of-flight mass spectrometry (TOF-MS).[6] A multitude of studies using ProteinChip technology have been carried out to establish the protein profiles of biological fluids, especially serum samples.[7–9] Because this technique demands only a small amount of sample, it can be used for small biopsies or microdissected tissues, which produce the homogeneous tissue samples typically used in cancer research. The separation of functional tissue areas can be achieved by laser-based microdissection (for review see [10]). When laser microdissection was first introduced as a novel preparation technique in 1998, the challenge was to prove that reliable results could be achieved by selecting defined small amounts of isolated cells from complex tissue sections.[11] Since then numerous applications has been published in different fields and has proven its necessity.[12] Microdissected tissue material free from contaminating and unwanted tissue components is extremely important for the production of clean data for biomarker identification in cancer diagnostics and in determining the clonal heterogeneity of tumors. We have shown in a previous study that the detection of differentially expressed proteins was only possible in pure microdissected samples.[13] Laser-based microdissection has previously been combined with ProteinChip technology to identify protein markers in several cancer types.[14–16]

The aim of this study was to analyse the protein patterns of liver metastases derived from CRC (MTS) and detect biologically and diagnostically relevant signals. We wanted to analyze whether it is possible to draw conclusions from the proteome of the MTS on the origin/localization of the primary tumor.

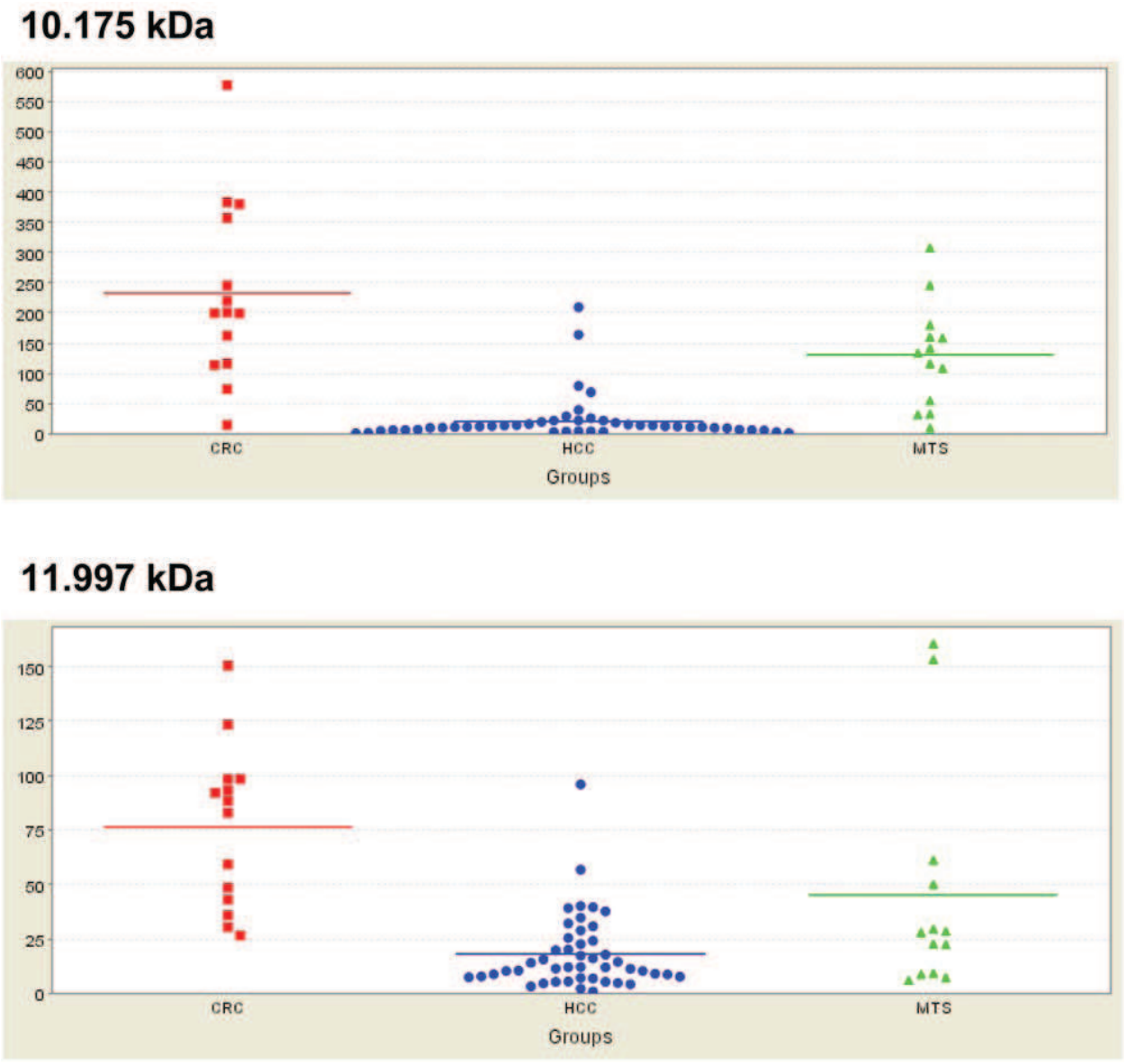

Figure 1. Distribution of the intensities of peaks expressed significantly differently in liver metastases derived from colorectal carcinoma (MTS), colorectal carcinoma tumor (CRC), and hepatocellular carcinoma (HCC) tumor margins. *Upper panel*: Distribution of the intensities of the 10.175 kDa signal. *Bottom panel*: Distribution of the intensities of the 11.997 kDa signal. The spectra were obtained using Q10 arrays. X-axis indicates the sample groups, Y-axis the intensity (μA).
doi:10.1371/journal.pone.0003767.g001

Materials and Methods

Laser microdissection of tissue sections

All 17 human samples from liver metastases derived from CRC (MTS) were obtained after surgical resection at the Department of General and Visceral Surgery of the Friedrich Schiller University, Jena. They were collected fresh, snap frozen in liquid nitrogen, and stored at −80°C. Primary tumor specimens were categorized according to the WHO classification. Most of these tumors were classified as pT2 and pT3.

Laser microdissection was performed with a laser microdissection and pressure catapulting microscope (LMPC; Palm, Bernried, Germany) as previously described.[17] Briefly, we microdissected native air-dried cryostat tissue sections of approximately 3000–5000 cells, each in a maximum of 20–30 min. Proteins were extracted in 10 μL lysis buffer (100 mM Na-phosphate [pH 7.5], 5 mM EDTA, 2 mM $MgCl_2$, 3 mM 2-β-mercaptoethanol, 0.1% CHAPS, 500 μM leupeptin, and 0.1 mM PMSF) for 30 min on ice. After centrifugation (15 min; 15,000 rpm) the supernatant was immediately analysed or frozen in liquid nitrogen for a maximum of one day.

Profiling microdissected liver-localized metastases

The protein lysates from microdissected metastatic tissues were analysed on strong anion exchange arrays (Q10) (Bio-Rad), as previously described.[17] In brief, Q10 array spots were pre-incubated in a washing/loading buffer containing 100 mM Tris buffer (pH 8.5) and 0.02% Triton X-100. Then 2 μL sample

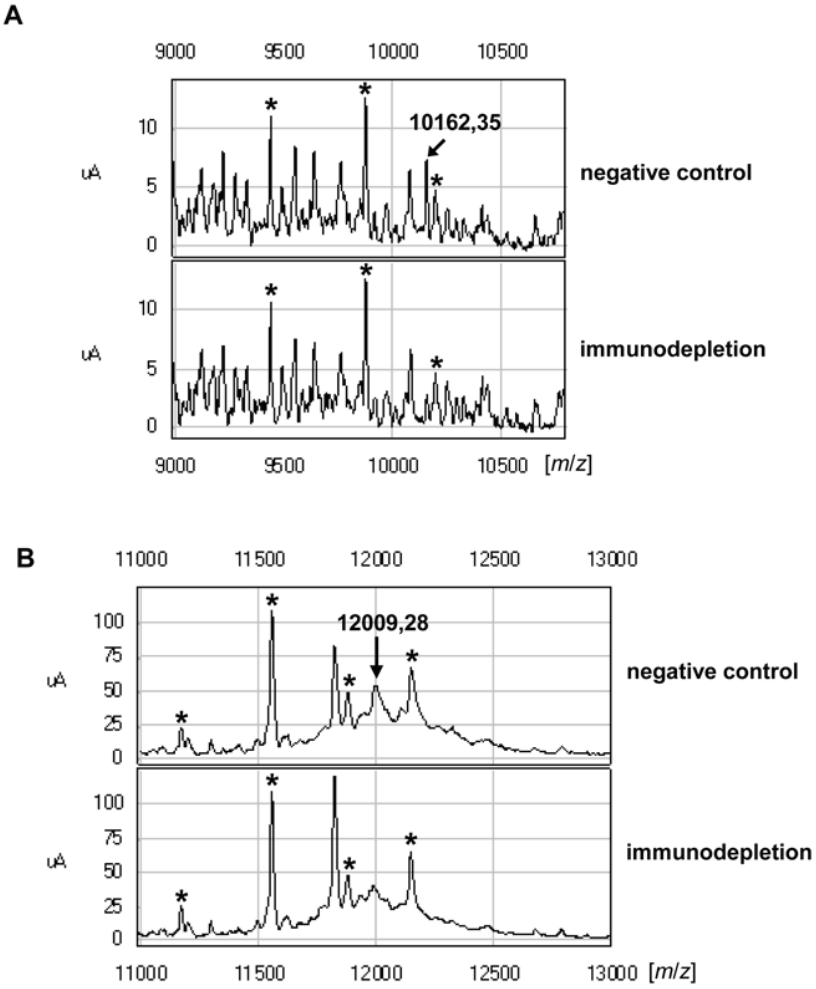

Figure 2. Immunodepletion assays of S100A6 and S100A11. Normalized ProteinChip® array profiles of metastatic tissue show that the peaks representing S100A6 (A, 10.162 kDa) or S100A11 (B, 12.009 kDa) were detectable in the negative controls but only with decreased intensity with the corresponding depleted probes. Reference peaks that were not influenced by immunodepletion are labelled with asterisks.
doi:10.1371/journal.pone.0003767.g002

aliquots were applied to the ProteinChip Arrays, which were incubated at room temperature for 90 min in a humidified chamber. After the samples had been washed three times with the fresh buffer and twice with water, 2×0.5 µL of sinapinic acid (saturated solution in 0.5% TFA/50% acetonitrile) were applied. Mass analysis was performed with a ProteinChip Reader (Series 4000; Ciphergen Biosystems Inc., Fremont, CA), according to an automated data collection protocol.

Immunodepletion assay

Two microlitres of anti-S100A6 antibody (ab 141; Swant, Bellinzona, CH) or a specific antibody directed against S100A11 (rabbit polyclonal; Protein Tech Group, IL) were incubated with 10 µL of protein A–agarose (Sigma, St Louis, MO) for 15 min on ice. A pellet was generated by centrifugation and the supernatant was discarded. The pellet was washed twice with buffer containing 20 mM Hepes (pH 7.8), 25 mM KCl, 5 mM $MgCl_2$, 0.1 mM EDTA, and 0.05% NP-40. Then, lysate (5 µL) from the microdissected tissue was incubated with this pellet for 45 min on ice. As a negative control, 5 µL of the lysate was incubated for 45 min on ice with protein A–agarose without the specific antibody. After incubation, the samples were cleared by centrifugation and 3 µL of each supernatant (immunodepleted sample) was analysed on the ProteinChip Arrays (Q10, BioRad).

Immunohistochemistry

Cryostat sections (8 µm) of MTS-containing tissue (n = 5) or CRC tissue (n = 5) were placed on slides, air-dried for about 60 min at 20°C, and fixed in paraformaldehyde, as described previously.[18] After fixation, the slides were treated in a microwave at 80 watts (3×3 min) in 10 mM citric acid (pH 6.0) to inhibit endogenous peroxidase activity. They were then rinsed twice with Tris-buffered saline (TBS; pH 7.4), and incubated overnight at 4°C in a humidified chamber with the corresponding primary anti-S100A6 antibody or anti-S100A11 antibody. The slides were rinsed three times, for 10 min each, in TBS. The Vectastain Elite ABC kit (Vector Laboratories, Burlingame, CA) and the Jenchrom pxbl-kit (MoBiTec, Göttingen, Germany) were used according to the manufacturers' instructions to visualize the antibodies. Negative controls were incubated with only the labelled secondary antibody. Sections cut in parallel to the immunohistochemically treated sections were stained with haematoxylin–eosin for better identification of the different tissue areas. Immunohistochemical staining was evaluated by a pathologist.

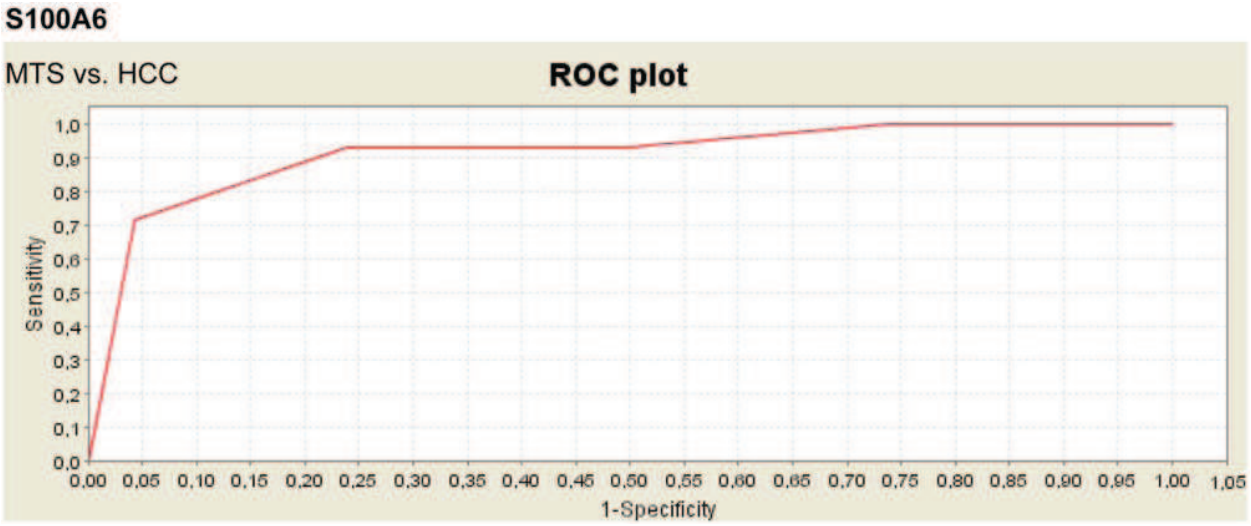

Figure 3. ROC curve of S100A6 in liver metastases derived from colorectal carcinoma (MTS) and in hepatocellular carcinoma (HCC). S100A6 is significantly upregulated in MTS.
doi:10.1371/journal.pone.0003767.g003

Statistical Analyses

Mass spectra from ProteinChip arrays were normalized to a total ion current and cluster analysis of the detected signals was performed. The respective *P* values for MTS, CRC,[19] and HCC [17] were determined with the CiphergenExpress program (version 3.0; Ciphergen Biosystems Inc.). To calculate the *P* values, normalized spectra with signals in the range of 2.5–200 kDa, with a signal-to-noise ratio (S/N) of at least 10, were selected and analysed with the Mann–Whitney U test for non-parametric data sets, and the Kruskal–Wallis test. Receiver operating characteristic (ROC) curves [20] were constructed for S100A6 and S100A11 expression data derived CRC, MTS or HCC, respectively by plotting sensitivity versus 1-specificity (CiphergenExpress 3.0).

Results

Proteomic analysis of microdissected tissues from liver metastases derived from CRC, primary CRC, and HCC by SELDI–MS

For this study, microdissected tissue probes containing about 3000–5000 cells each were successfully dissected from 17 liver metastases derived from colorectal cancer (MTS) by an experienced pathologist. All protein lysates were applied to strong anion exchanger Q10 ProteinChip Arrays and analysed individually by SELDI–MS on a ProteinChip Reader Series 4000 instrument. The spectra generated from the MTS were compared with specific spectra derived from primary CRC (n = 14) and HCC (n = 46), which were generated as described previously [17,19], to detect any distinguishing protein signals. In the range of 2.5–200 kDa, up to 372 peaks were detected with normalized intensities. After evaluation with the CiphergenExpress program, many significantly different signals (n = 49) were detected for MTS, CRC, and HCC (Table S1). Among these, the peak masses with markedly low *P* values were selected for further identification and characterization. The signals at 10.175 kDa ($P = 3.00 \times 10^{-9}$) and 11.997 kDa ($P = 1.82 \times 10^{-6}$) were significantly upregulated in both MTS and CRC compared with samples derived from HCC (Figure 1). The signal with a molecular mass of 10.175 kDa was the most significant single signal capable of discriminating between the two sample groups in this analysis. The 11.997 kDa signal was ranked in 12th position (Table S1). Representative examples of SELDI–MS spectra of MTS, CRC, and HCC are shown in Figure S1.

Identification of differentially expressed protein peaks

The interesting proteins with molecular masses of 10.175 kDa and 11.997 kDa, which corresponded very well to the Ca^{2+}-binding proteins S100A6 (NCBI NP_055439) and S100A11 (NCBI NP_005611), respectively, were also detected by ProteinChip technology, as has been described by ours and other groups [17,19,21]. To confirm that S100A6 and S100A11 match the differentially expressed peaks observed at 10.175 kDa and 11.997 kDa, respectively, in this protein profiling analysis, immunodepletion assays were carried out using microdissected MTS tissue as the starting material. Analysis of the supernatants of the immunodepletion assays by Q10 arrays showed that the peaks corresponding to S100A6 and S100A11 were significantly reduced. In the negative controls without specific antibodies, the peaks were clearly detectable (Figure 2). The identification of other differentially expressed proteins is in progress.

Characterization of the differentially expressed protein signals

To assess the impact of S100A6 and S100A11 as discriminatory signals for different tumorous tissue samples, we compared the spectra derived from different sample groups in individual assays. We found that S100A6 was significantly upregulated in CRC and MTS compared with HCC ($P = 2.81 \times 10^{-6}$) (Figure 3). Hence, S100A again ranked first as the most significant signal (Table S2). An analysis of CRC and HCC showed that S100A6 ($P = 2.62 \times 10^{-7}$) and S100A11 ($P = 5.54 \times 10^{-7}$) were both significantly upregulated in the samples derived from CRC (Figure 4). In this analysis, S100A6 and S100A11 ranked in third place and fourth place, respectively, in the most significant signals (Table S3). Interestingly, neither S100A6 nor S100A11 were significantly differentially expressed in MTS compared with CRC (Table S4).

Localization of S100A6 and S100A11 in tissue

To confirm their identification and in particular to localize S100A6 and S100A11 in tissue sections, we assessed their

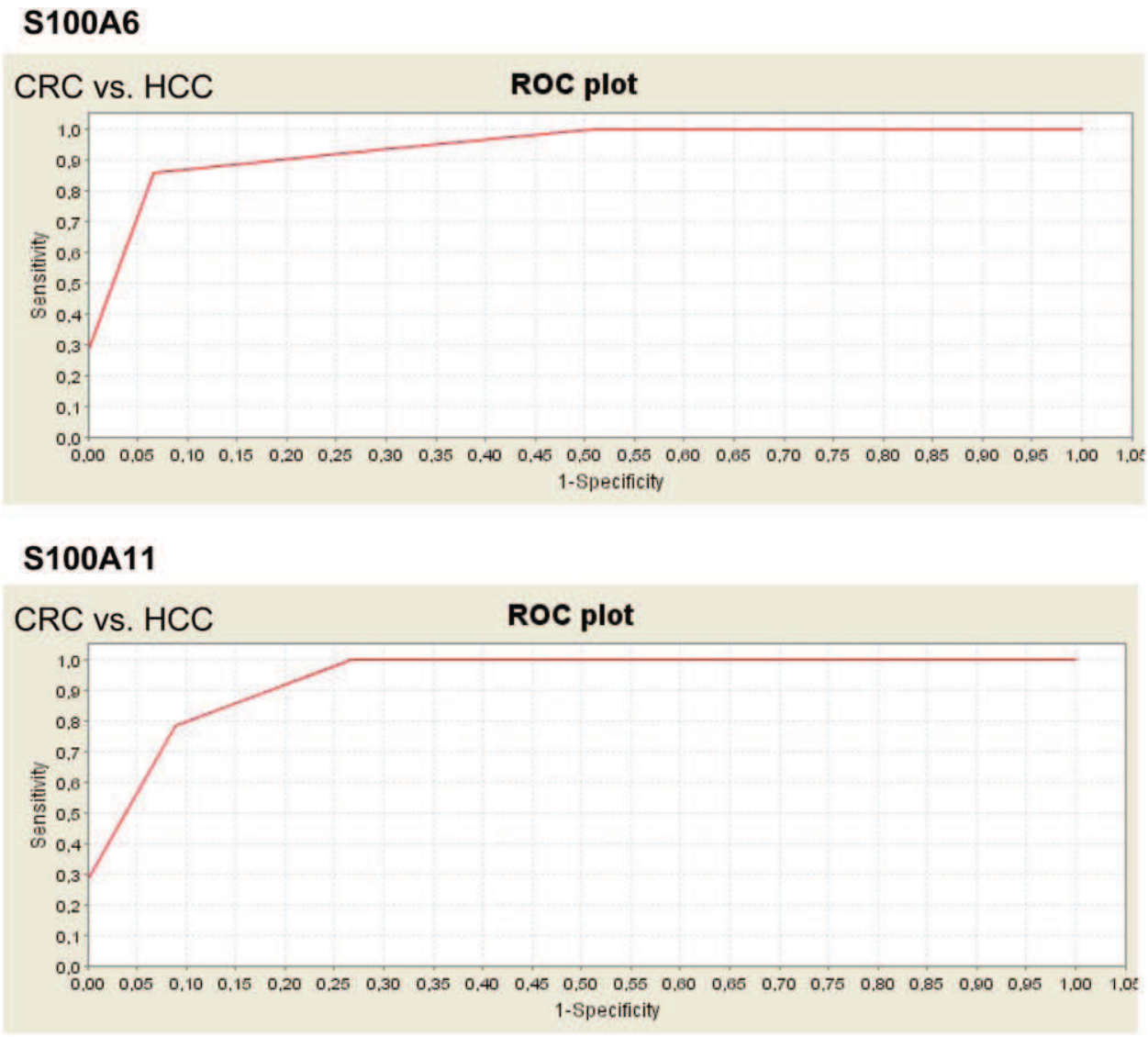

Figure 4. ROC curves of S100A6 and S100A11 in colorectal carcinoma (CRC) and in hepatocellular carcinoma (HCC). Both proteins are significantly upregulated in CRC.
doi:10.1371/journal.pone.0003767.g004

expression in MTS and in primary CRC by immunohistochemistry using specific antibodies. All these tissues showed a positive reaction to the antibodies directed against S100A6 or S100A11 (Figure 5). In contrast to these findings, only very poor signals were detectable in the tissue surrounding the MTS (Figure 5A and D). Interestingly, the immunoreactivity of the tumor cell complexes was stronger at the tumor margin than that in the central tumor area in CRC, when we used the specific antibody directed against S100A6 (Figure 5E). Consistent with the SELDI analysis of HCC, neither signal was detectable by immunohistochemistry (data not shown).

Discussion

Liver metastasis of CRC is a major reason for the poor prognosis of patients. An improved understanding of the molecular and cellular mechanisms underlying metastasis would contribute greatly to its early detection and treatment. The initiation of MTS affects the expression of multiple proteins.[22–24] The identification of proteins that are characteristic of metastasis might allow the discrimination of different tumor entities. To address this challenge, specific proteomic approaches have been used that focus on the complex analysis of protein levels in metastases using cell lines.[2527] Such altered expression patterns have been detected for cytokeratin 18, tissue transglutaminase, Rho GDP-dissociation inhibitor 1, fibroblast-type tropomyosin, interleukin-18, annexin I, disulfide isomerase, heat shock protein 60, peroxiredoxin 1, chlorine intracellular channel protein 1, and creatine kinase B chain, as well as for some ribosomal proteins. Since the early 1990s, a number of studies have investigated, with genomic approaches, tissues derived directly from both primary tumors and organs involved in metastasis.[28–31] This is, to the best of our knowledge, the first study to use a proteomic approach in a comparative investigation of tissues derived from different metastasising primary tumors and in the identification of proteins that can discriminate between these

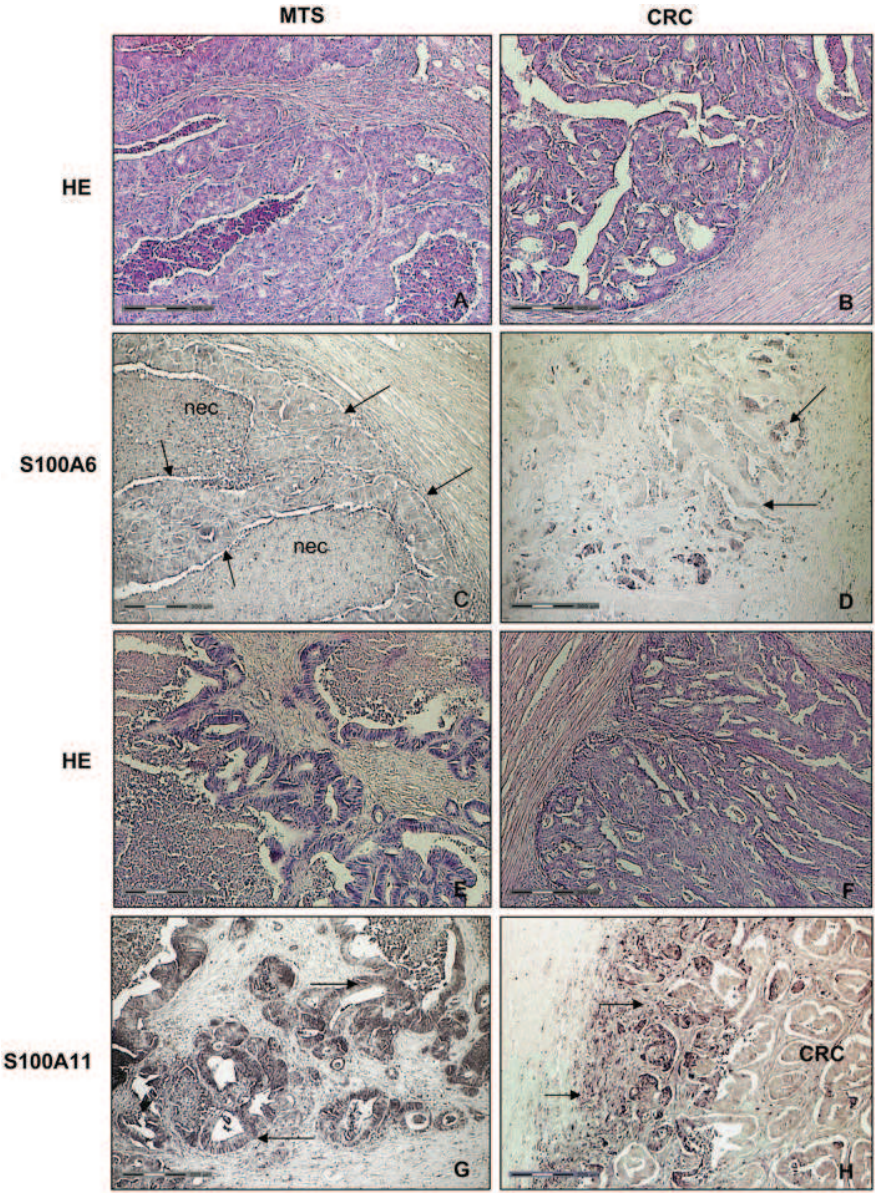

Figure 5. Immunohistochemical analysis of S100A6 and S100A11 and corresponding H&E sections. (A) and (B) H&E section from liver metastases derived from colorectal carcinoma (MTS) and colorectal carcinoma (CRC). (C) Corresponding section to (A) immunostained for S100A6 using a specific antibody. A positive immunohistochemical reaction was detectable in the MTS (labeled with arrows) and in adjacent necrotic tissue (nec). The surrounding liver tissue was negative. (D) Corresponding section to (B). Scattered immunoreactive tumor cell complexes (labeled with arrows) at the tumor periphery of a colorectal carcinoma (CRC) detected with anti-S100A6 antibody. (E) and (F) H&E section from liver metastases derived from colorectal carcinoma (MTS) and colorectal carcinoma (CRC). (G) Corresponding section to (E). S100A11-positive tumor cell complex (labeled with an arrow) in MTS. (H) Corresponding section to (F). Strong S100A11 immunoreactivity in CRC tumor cell complexes (labeled with arrows). Immunoreactivity against S100A11 was stronger in the tumor margin compared to central tumor area.
doi:10.1371/journal.pone.0003767.g005

tumor types and between tumors and metastases. In contrast to the majority of SELDI–MS-based studies, we identified significantly differentially expressed proteins. The Ca^{2+}-binding proteins identified here, S100A6 and S100A11, can distinguish very clearly between MTS, primary CRC, and primary HCC, as well as between CRC and HCC. A number of additional signals were detected that discriminate between MTS and CRC, but S100A6 and S100A11 do not. The identification of specific signals that can distinguish between metastases and the primary tumor is in progress. Until now, only two small studies have comparatively assessed the expression of S100A6 in human colorectal mucosa, primary colorectal adenocarcinomas, and liver metastases using a specific western blot analysis [32,33]. In contrast, we analysed an extended number of samples using a hypothesis-free proteomic approach and thereby detected and identified S100A6 as a factor with the potential to discriminate between primary HCC and MTS. S100A6 and S100A11 belong to the group of S100 proteins involved in the Ca^{2+} signalling network, and regulate intracellular activities such as cell growth and motility, cell-cycle progression, transcription, and cell differentiation.[34,35] Both S100A6 and

S100A11 have been observed in several epithelial tumors and are linked to metastasis.[19,32,36,37]

In this study, we have demonstrated the potential of SELDI–MS in characterizing metastasis in terms of protein profiles and in discriminating between different tumor entities. In future, it would be very interesting to assess and compare the protein profiles of metastases derived from different types of metastasising tumors. We might expect to find a panel of protein signals or a "metastatic protein profile" that is common to all metastatic tissues. This panel will presumably contain proteins involved in the coordination of metastatic processes. Although neither S100A6 nor S100A11 can discriminate between MTS and the corresponding primary CRC, they can discriminate between primary CRC and primary HCC. Perhaps more importantly, S100A6 is a potential candidate to discriminate between MTS and primary HCC. The discrimination of primary HCC and its metastases located in the liver is presently complicated and afflicted with difficulties.[38] Therefore, S100A6 might provide some resolution of this problem.

Supporting Information

Figure S1 Representative examples of SELDI-TOF MS spectra of liver metastases derived from colorectal carcinoma (MTS), colorectal carcinoma (CRC), and hepatocellular carcinoma (HCC). Data are obtained using Q10 arrays. The peaks of interest at 10.175 kDa and 11.997 kDa are marked with frames.
Found at: doi:10.1371/journal.pone.0003767.s001 (0.18 MB DOC)

Table S1
Found at: doi:10.1371/journal.pone.0003767.s002 (0.07 MB DOC)

Table S2
Found at: doi:10.1371/journal.pone.0003767.s003 (0.05 MB DOC)

Table S3
Found at: doi:10.1371/journal.pone.0003767.s004 (0.06 MB DOC)

Table S4
Found at: doi:10.1371/journal.pone.0003767.s005 (0.04 MB DOC)

Acknowledgments

We would like to thank Roland Kaufmann, Henning Mothes, Utz Settmacher (Department of General and Visceral Surgery, Jena), Arndt Hartmann (Institute of Pathology, Erlangen), and Alexander Berndt (Institute of Pathology, Jena) for providing the tissue samples and S. Michel for critical reading of the manuscript.

Author Contributions

Conceived and designed the experiments: CM GE FvE. Performed the experiments: CM GE BS AB. Analyzed the data: CM GE FvE. Wrote the paper: CM FvE.

References

1. Nakamura S, Suzuki S, Baba S (1997) Resection of liver metastases of colorectal carcinoma. World J Surg 21: 741–747.
2. Weiss L (2000) Metastasis of cancer: a conceptual history from antiquity to the 1990s. Cancer Metastasis Rev 19: I-383.
3. Ridley A (2000) Molecular switches in metastasis. Nature 406: 466–467.
4. Pan S, Zhang H, Rush J, Eng J, Zhang N, et al. (2005) High throughput proteome screening for biomarker detection. Mol Cell Proteomics 4: 182–190.
5. Drake RR, Schwegler EE, Malik G, Diaz J, Block T, et al. (2006) Lectin capture strategies combined with mass spectrometry for the discovery of serum glycoprotein biomarkers. Mol Cell Proteomics 5: 1957–1967.
6. Tang N, Tornatore P, Weinberger SR (2004) Current developments in SELDI affinity technology. Mass Spectrom Rev 23: 34–44.
7. Paradis V, Degos F, Dargere D, Pham N, Belghiti J, et al. (2005) Identification of a new marker of hepatocellular carcinoma by serum protein profiling of patients with chronic liver diseases. Hepatology 41: 40–47.
8. Li Y, Dang TA, Shen J, Perlaky L, Hicks J, et al. (2006) Identification of a plasma proteomic signature to distinguish pediatric osteosarcoma from benign osteochondroma. Proteomics 6: 3426–3435.
9. Ward DG, Suggett N, Cheng Y, Wei W, Johnson H, et al. (2006) Identification of serum biomarkers for colon cancer by proteomic analysis. Br J Cancer 94: 1898–1905.
10. von Eggeling F, Melle C, Ernst G (2007) Microdissecting the proteome. Proteomics 7: 2729–2737.
11. Schütze K, Lahr G (1998) Identification of expressed genes by laser-mediated manipulation of single cells. Nat Biotechnol 16: 737–742.
12. Schütze K, Niyaz Y, Stich M, Buchstaller A (2007) Noncontact laser microdissection and catapulting for pure sample capture. Methods Cell Biol 82: 649–673.
13. Melle C, Ernst G, Schimmel B, Bleul A, Thieme H, et al. (2005) Discovery and identification of alpha-defensins as low abundant, tumor-derived serum markers in colorectal cancer. Gastroenterology 129: 66–73.
14. Cheung PK, Woolcock B, Adomat H, Sutcliffe M, Bainbridge TC, et al. (2004) Protein profiling of microdissected prostate tissue links growth differentiation factor 15 to prostate carcinogenesis. Cancer Res 64: 5929–5933.
15. Melle C, Ernst G, Schimmel B, Bleul A, Koscielny S, et al. (2003) Biomarker Discovery and Identification in Laser Microdissected Head and Neck Squamous Cell Carcinoma with ProteinChip(R) Technology, Two-dimensional Gel Electrophoresis, Tandem Mass Spectrometry, and Immunohistochemistry. Mol Cell Proteomics 2: 443–452.
16. Guedj N, Dargere D, Degos F, Janneau JL, Vidaud D, et al. (2006) Global proteomic analysis of microdissected cirrhotic nodules reveals significant biomarkers associated with clonal expansion. Lab Invest 86: 951–958.
17. Melle C, Ernst G, Scheibner O, Kaufmann R, Schimmel B, et al. (2007) Identification of Specific Protein Markers in Microdissected Hepatocellular Carcinoma. J Proteome Res 6: 306–315.
18. Melle C, Ernst G, Schimmel B, Bleul A, Thieme H, et al. (2005) Discovery and identification of alpha-defensins as low abundant, tumor-derived serum markers in colorectal cancer. Gastroenterology 129: 66–73.
19. Melle C, Ernst G, Schimmel B, Bleul A, Mothes H, et al. (2006) Different expression of calgizzarin (S100A11) in normal colonic epithelium, adenoma and colorectal carcinoma. International Journal of Oncology 28: 195–200.
20. Raslich MA, Markert RJ, Stutes SA (2007) Selecting and interpreting diagnostic tests. Biochemia Medica 17: 151–161.
21. Melle C, Ernst G, Schimmel B, Bleul A, Koscielny S, et al. (2004) A Technical Triade for Proteomic Identification and Characterization of Cancer Biomarkers. Cancer Res 64: 4099–4104.
22. Mc DS, Chaudhry V, Mansilla-Soto J, Zeng ZS, Shu WP, et al. (1999) Metastatic and non-metastatic colorectal cancer (CRC) cells induce host metalloproteinase production in vivo. Clin Exp Metastasis 17: 341–349.
23. Tzimas GN, Chevet E, Jenna S, Nguyen DT, Khatib AM, et al. (2005) Abnormal expression and processing of the proprotein convertases PC1 and PC2 in human colorectal liver metastases. BMC Cancer 5: 149.
24. Ueda J, Semba S, Chiba H, Sawada N, Seo Y, et al. (2007) Heterogeneous expression of claudin-4 in human colorectal cancer: decreased claudin-4 expression at the invasive front correlates cancer invasion and metastasis. Pathobiology 74: 32–41.
25. Jiang D, Ying W, Lu Y, Wan J, Zhai Y, et al. (2003) Identification of metastasis-associated proteins by proteomic analysis and functional exploration of interleukin-18 in metastasis. Proteomics 3: 724–737.
26. Cai Z, Chiu JF, He QY (2004) Application of proteomics in the study of tumor metastasis. Genomics Proteomics Bioinformatics 2: 152–166.
27. Kreunin P, Yoo C, Urquidi V, Lubman DM, Goodison S (2007) Differential expression of ribosomal proteins in a human metastasis model identified by coupling 2-D liquid chromatography and mass spectrometry. Cancer Genomics Proteomics 4: 329–339.
28. Finkelstein SD, Sayegh R, Christensen S, Swalsky PA (1993) Genotypic classification of colorectal adenocarcinoma. Biologic behavior correlates with K-ras-2 mutation type. Cancer 71: 3827–3838.
29. Sanchez-Cespedes M, Esteller M, Hibi K, Cope FO, Westra WH, et al. (1999) Molecular detection of neoplastic cells in lymph nodes of metastatic colorectal cancer patients predicts recurrence. Clin Cancer Res 5: 2450–2454.
30. Khan ZA, Jonas SK, Le-Marer N, Patel H, Wharton RQ, et al. (2000) P53 mutations in primary and metastatic tumors and circulating tumor cells from colorectal carcinoma patients. Clin Cancer Res 6: 3499–3504.

31. Conzelmann M, Linnemann U, Berger MR (2005) Molecular detection of clinical colorectal cancer metastasis: how should multiple markers be put to use? Int J Colorectal Dis 20: 137–146.
32. Komatsu K, Kobune-Fujiwara Y, Andoh A, Ishiguro S, Hunai H, et al. (2000) Increased expression of S100A6 at the invading fronts of the primary lesion and liver metastasis in patients with colorectal adenocarcinoma. Br J Cancer 83: 769–774.
33. Komatsu K, Murata K, Kameyama M, Ayaki M, Mukai M, et al. (2002) Expression of S100A6 and S100A4 in matched samples of human colorectal mucosa, primary colorectal adenocarcinomas and liver metastases. Oncology 63: 192–200.
34. Schafer BW, Heizmann CW (1996) The S100 family of EF-hand calcium-binding proteins: functions and pathology. Trends Biochem Sci 21: 134–140.
35. Donato R (2001) S100: a multigenic family of calcium-modulated proteins of the EF-hand type with intracellular and extracellular functional roles. Int J Biochem Cell Biol 33: 637–668.
36. Maelandsmo GM, Florenes VA, Mellingsaeter T, Hovig E, Kerbel RS, et al. (1997) Differential expression patterns of S100A2, S100A4 and S100A6 during progression of human malignant melanoma. Int J Cancer 74: 464–469.
37. Yao R, Davidson DD, Lopez-Beltran A, MacLennan GT, Montironi R, et al. (2007) The S100 proteins for screening and prognostic grading of bladder cancer. Histol Histopathol 22: 1025–1032.
38. Helmberger TK, Laubenberger J, Rummeny E, Jung G, Sievers K, et al. (2002) MRI characteristics in focal hepatic disease before and after administration of MnDPDP: discriminant analysis as a diagnostic tool. Eur Radiol 12: 62–70.

Table S1. Significantly different signals that distinguish tissues from liver metastases derived from colorectal carcinoma (MTS), colorectal carcinoma (CRC), and hepatocellular carcinoma (HCC), detected on Q10 arrays. The signals representing the subsequently identified S100A6 and S100A11 are shown in bold.

Signal in	MW (kD)	P-value
MTS	3.483	3.23x10-2
CRC	4.968	8.66x10-4
CRC	5.077	5.35x10-7
HCC	5.362	1.82x10-7
MTS	5.658	2.09x10-3
CRC	5.943	4.12x10-2
HCC	6.648	1.09x10-3
HCC	6.736	8.35x10-4
HCC	7.571	1.75x10-5
HCC	7.667	1.07x10-4
HCC	7.943	2.87x10-3
CRC	8.225	6.54x10-6
CRC	8.411	3.66x10-2
HCC	9.163	1.02x10-4
HCC	9.613	1.16x10-7
HCC	9.976	4.07x10-6
CRC	**10.175**	3.00x10-9
CRC	10.358	2.80x10-7
CRC	10.394	6.30x10-8
MTS	11.315	1.35x10-2
MTS	11.357	1.23x10-2
CRC	11.683	4.49x10-2
CRC	**11.997**	1.82x10-6
HCC	13.546	1.39x10-3
MTS	13.783	7.62x10-3
MTS	14.018	1.48x10-2
HCC	14.975	1.68x10-7
HCC	15.138	5.14x10-6
HCC	15.351	1.34x10-3
HCC	15.882	8.32x10-5
HCC	19.944	3.00x10-9
HCC	20.845	1.40x10-8
HCC	21.285	1.52x10-6
HCC	22.271	3.20x10-5
CRC	23.162	7.85x10-3
CRC	23.807	3.50x10-6
CRC	24.807	2.79x10-5
MTS	28.117	1.59x10-3
CRC	32.045	1.32x10-4
HCC	41.762	4.20x10-8
HCC	44.215	4.31x10-5
HCC	46.497	1.65x10-2
HCC	51.508	1.15x10-3
MTS	53.673	2.16x10-2
HCC	54.428	3.34x10-7

HCC	55.435	3.00x10-9
CRC	68.187	5.45x10-3
MTS	78.225	2.46x10-5
CRC	118.336	2.50x10-2

Table S1. Significantly different signals that distinguish tissues from liver metastases derived from colorectal carcinoma (MTS), colorectal carcinoma (CRC), and hepatocellular carcinoma (HCC), detected on Q10 arrays. The signals representing the subsequently identified S100A6 and S100A11 are shown in bold.

Signal in	MW (kD)	P-value
MTS	3.483	3.23x10-2
CRC	4.968	8.66x10-4
CRC	5.077	5.35x10-7
HCC	5.362	1.82x10-7
MTS	5.658	2.09x10-3
CRC	5.943	4.12x10-2
HCC	6.648	1.09x10-3
HCC	6.736	8.35x10-4
HCC	7.571	1.75x10-5
HCC	7.667	1.07x10-4
HCC	7.943	2.87x10-3
CRC	8.225	6.54x10-6
CRC	8.411	3.66x10-2
HCC	9.163	1.02x10-4
HCC	9.613	1.16x10-7
HCC	9.976	4.07x10-6
CRC	**10.175**	3.00x10-9
CRC	10.358	2.80x10-7
CRC	10.394	6.30x10-8
MTS	11.315	1.35x10-2
MTS	11.357	1.23x10-2
CRC	11.683	4.49x10-2
CRC	**11.997**	1.82x10-6
HCC	13.546	1.39x10-3
MTS	13.783	7.62x10-3
MTS	14.018	1.48x10-2
HCC	14.975	1.68x10-7
HCC	15.138	5.14x10-6
HCC	15.351	1.34x10-3
HCC	15.882	8.32x10-5
HCC	19.944	3.00x10-9
HCC	20.845	1.40x10-8
HCC	21.285	1.52x10-6
HCC	22.271	3.20x10-5
CRC	23.162	7.85x10-3
CRC	23.807	3.50x10-6
CRC	24.807	2.79x10-5
MTS	28.117	1.59x10-3
CRC	32.045	1.32x10-4
HCC	41.762	4.20x10-8
HCC	44.215	4.31x10-5
HCC	46.497	1.65x10-2
HCC	51.508	1.15x10-3
MTS	53.673	2.16x10-2
HCC	54.428	3.34x10-7

HCC	55.435	3.00x10-9
CRC	68.187	5.45x10-3
MTS	78.225	2.46x10-5
CRC	118.336	2.50x10-2

Table S3. Significantly different signals that distinguish colorectal carcinoma (CRC) and hepatocellular carcinoma (HCC), detected on Q10 arrays. The signals representing S100A6 and S100A11 are shown in bold.

Signal in	MW (kD)	P-value
CRC	4.968	2.98x10-4
CRC	5.079	5.53x10-6
HCC	5.271	3.25x10-2
HCC	5.362	5.08x10-6
HCC	5.658	1.11x10-3
CRC	5.944	1.39x10-2
HCC	6.648	3.28x10-3
HCC	7.571	1.90x10-5
HCC	7.661	2.41x10-5
HCC	7.943	3.09x10-3
CRC	8.226	1.96x10-6
CRC	8.408	1.32x10-2
HCC	9.163	1.27x10-4
HCC	9.613	2.14x10-6
HCC	9.974	7.08x10-5
CRC	**10.182**	2.62x10-7
CRC	10.359	5.54x10-7
CRC	10.541	3.71x10-2
HCC	11.315	2.15x10-2
CRC	**11.997**	5.54x10-7
HCC	13.546	4.36x10-3
HCC	13.787	4.36x10-3
HCC	14.018	8.81x10-3
HCC	14.975	2.16x10-7
HCC	15.138	1.26x10-5
HCC	15.351	2.98x10-4
HCC	15.882	1.47x10-4
HCC	19.951	4.10x10-8
HCC	20.845	1.13x10-5
HCC	21.285	3.30x105-
HCC	22.276	3.88x10-4
CRC	23.166	2.54x10-3
CRC	23.801	8.83x10-6
CRC	24.807	9.09x10-5
HCC	28.003	4.85x10-3
CRC	32.045	4.45x10-4
HCC	41.781	4.05x10-6
HCC	51.559	2.37x10-4
HCC	54.396	1.13x10-5
HCC	55.435	1.98x10-6
CRC	68.188	1.16x10-2
HCC	82.182	3.30x10-5
CRC	118.336	6.08x10-3
CRC	172.524	5.85x10-4

Table S4: Significantly different signals which separate tissues from liver metastases derived from colorectal carcinoma (MTS) and colorectal carcinoma (CRC) detected on Q10 arrays.

Signal in	MW (kD)	P-value
CRC	4.966	3.76x10-2
MTS	5.655	1.26x10-2
CRC	8.208	4.10x10-4
CRC	10.356	2.40x10-3
MTS	10.845	1.82x10-3
MTS	11.308	3.39x10-2
CRC	11.681	2.75x10-2
CRC	11.835	4.60x10-2
MTS	14.024	4.16x10-2
CRC	23.162	6.94x10-3
MTS	47.952	2.51x10-2
MTS	51.431	3.62x10-3
MTS	53.641	6.11x10-3
MTS	94.521	8.90x10-3

BIOINFORMATICS DISCOVERY NOTE Vol. 22 no. 11 2006, pages 1293–1296
doi:10.1093/bioinformatics/btl077

Systems biology

Convergence of the proteomic pattern in cancer

Ute Müller[1,2,†], Günther Ernst[1,†], Christian Melle[1], Reinhard Guthke[3] and Ferdinand von Eggeling[1,*]

[1]Core Unit Chip Application (CUCA), Institute of Human Genetics and Anthropology, Friedrich-Schiller-University, 07740 Jena, Germany, [2]aura optik gmbh, Wildenbruchstrasse 15, 07745 Jena, Germany and [3]Leibniz Institute for Natural Product Research and Infection Biology, Hans Knoell Institute (HKI), 07745 Jena, Germany

Received on January 13, 2006; revised on February 10, 2006; accepted on February 27, 2006
Advance Access publication March 7, 2006
Associate Editor: Jonathan Wren

ABSTRACT

Motivation: On the histological level the differentiation of normal epithelial tissues is well known. The phenomenon of dedifferentiation, which occurs as cells develop towards malignancy is also well described. To identify an epithelial tumor-specific proteomic profile as well as to measure the proximities between we used data from tumor tissue and adjacent normal tissue microdissected from head and neck and colon cancer samples which were analyzed using ProteinChip technology and performed a bioinformatic meta-analysis on the resulting four complex datasets.

Results: All four groups could be identified based on their proteomic signatures and the tumor tissues were found to be more similar to one another than to the normal epithelial tissue from which they progressed. This study shows at the proteomic level that changes in the histological features of tumors as compared to the tissues from which they arise are reflected in the convergence of proteomic pattern during the development to cancer.

Contact: fegg@mti.uni-jena.de

Supplementary information: Supplementary data are available at *Bioinformatics* online.

1 INTRODUCTION

An epithelium is an assembly of polarized cells with defined apical and basolateral domains that lines the inner and outer organ surfaces. There are many types of epithelia specialized to carry out functions, including protection, secretion, nutrient resorption and polarized transport between tissue compartments. The morphological redirection of cellular differentiation during the progression to cancer reflects the functional properties of malignant cells as increased proliferation, invasion and metastasis. However, their way to 'simplicity' was not revealed for the expression of genes and proteins.

The ProteinChip technology (surface-enhanced laser desorption/ionization mass spectrometry; SELDI) which utilizes chromatographic surfaces able to retain proteins depending on their physicochemical properties followed by direct analysis via time of flight mass spectrometry (von Eggeling *et al*., 2001; Hutchens and Yip, 1993) has been predominantly used to analyze bodily fluids including serum (Zhang *et al*., 2004), urine (Vlahou *et al*., 2001), nipple aspirates (Paweletz *et al*., 2001) and pancreatic juice (Rosty *et al*., 2002). We employed microdissected tumor tissue free of adjacent, non-malignant tissue for ProteinChip analysis to improve the chances of identifying reliable biomarkers for cancer diagnostics (Melle *et al*., 2005; Melle *et al*., 2004a). The principal task of studies utilizing ProteinChip technology to date has been tumor marker identification, and not the global analysis of the differences in the tumor and normal tissue proteomes.

From histological prospective, epithelial cells appear to undergo a dedifferentiation process during their progression towards malignant neoplasias. These changes should also be apparent at the biochemical level of the tissue proteome. Bioinformatic analysis methods that are capable of analyzing and comparing the entire proteomes of tumor and normal tissue on a global level should make it possible to identify a potential tumor-specific proteomic signature as well as to show the convergence to a more common protein signature (Fig. 1).

We combined the proteomic profiles generated in previous studies of microdissected tissue areas from head and neck cancers and the adjacent normal pharyngeal epithelium with the proteomic profiles from non-hereditary colorectal cancer and the adjacent normal colonic epithelium in a meta-analysis. We show that these groups can be separated by specific peaks or signatures, and that the two different cancer types are more similar to each other than to the epithelia from which they developed.

2 METHODS

2.1 Tumor specimens and analysis of microdissected tissue by ProteinChip arrays

Tumor samples were obtained after surgical resection in the Department of General and Visceral Surgery and the ENT Department of the Friedrich Schiller University in Jena. Staging and grading information can be found in former studies (Melle *et al*., 2005, 2004a, 2003). Laser microdissection of normal tumor epithelium was performed with a laser microdissection and pressure catapulting microscope (LMPC; Palm, Bernried, Germany) (Melle *et al*., 2005, 2003). Protein lysates were prepared from microdissected tissues, and lysates were analyzed on strong anion exchange arrays (SAX2; Ciphergen Biosystems Inc, Fremont, CA) as described (Melle *et al*., 2003). Mass analysis was performed in a ProteinChip Reader (model PBS IIc, Ciphergen Biosystems Inc, Fremont, CA). Spectra with at least 10 signals in the range between 2 and 20 kDa exhibiting a signal-to-noise ratio (S/N) of at least 5 were selected and exported for further analysis.

*To whom correspondence should be addressed.
†The authors wish it to be known that, in their opinion, the first two authors should be regarded as joint First Authors.

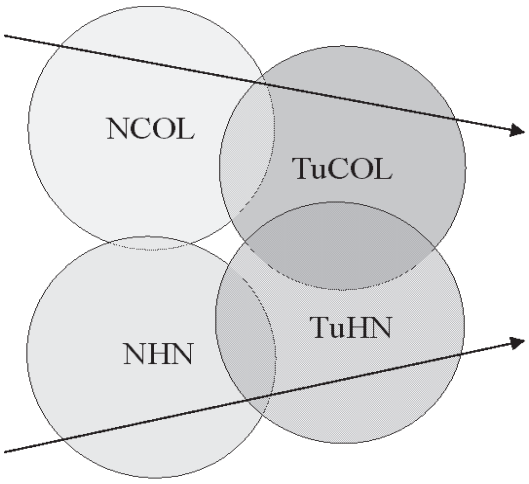

Fig. 1. Convergence of proteomic pattern in cancer (freehand delineation, not to scale).

2.2 Data

The data generated from ProteinChip arrays for 172 ($= m$) protein peaks and 106 samples were averaged over the following groups of samples: NCOL (normal colonic epithelial tissue, $n = 18$), TuCOL (colorectal carcinoma tissue, $n = 29$), NHN (normal pharyngeal epithelial tissue, $n = 28$), TuHN (head and neck tumor tissue, $n = 31$), NALL (normal colonic and pharyngeal epithelial tissues, $n = 46$), TuALL (colorectal carcinoma and head and neck tumor tissue, $n = 60$), COLALL (normal colonic epithelium and colorectal carcinoma, $n = 47$) and HNALL (normal pharyngeal epithelium and head and neck tumors, $n = 59$).

2.3 Statistical and bioinformatic analysis

The following groups were compared using two-sided *t*-tests: NALL versus TuALL, NCOL versus TuCOL, NHN versus TuHN, COLALL versus HNALL, NCOL versus NHN and TuCOL versus TuHN. The probability that two samples were from a normal distribution with unknown but equal variances and had the same mean was analyzed in these *t*-tests and *P*-values were calculated and adjusted according to the Bonferroni method (significance level α, p/m $< \alpha$) (Bonferroni, 1936).

Decision trees were generated to classify the same six pairs of sample subsets that were analyzed using *t*-tests (Breiman *et al*., 1993). The tree-based models were fitted using the MATLAB function, treefit (MathWorks Inc., Natick, MA). Gini's diversity index was applied as the split criterion.

Random forest (RF) is a classification tool based on decision trees. The implementation of RF in R (www.r-project.org) was used in this study. For classification, the program was run in the supervised mode to build 5000 trees using an mtry-parameter of 30. Characteristic features (peaks) were identified and their importance was calculated.

Average group proximities (Breiman, 2004, http://oz.berkeley.edu/users/breiman/Using_random_forests_V3.1.pdf) describing the intrinsic similarity between two sample groups were calculated from the individual proximities from an RF run in the unsupervised mode. Support vector machines (SVMs) (Ma *et al*., 2005, http://www.eleceng.ohio-state.edu/~maj/osu_svm; Vapnik, 1998) were applied to identify profiles that could decide among the six pairs of sample groups listed above in the data description. The classifier was validated using leave-one-out cross-validation. The prediction accuracy was determined as a quotient, *Q*, dividing the number of true predicted observations by the total number of tests (which equals the number, *n*, of samples considered). *Q* characterizes the predictive strength of a parameter pair. Pairs or triples of parameters with the maximum prediction accuracy were selected.

3 RESULTS

3.1 Classification and search for characteristic features

Classification was performed using different methods for six pairs of sample groups which are listed in Supplementary Table 1. As results, the following information was derived: (1) features distinguishing the two groups (classificators), their number as well as their significance and (2) quality of class prediction/error rate.

3.1.1 t-test The number of proteins whose mean expression data averaged over two groups of tissues differ significantly (Supplementary Table 1). Many proteins, i.e. 61 with a significance level of 5% and 33 with a significance of 0.01% of the 172 investigated proteins are differentially expressed in tissues head and neck versus colon. However, the number of proteins which are differentially expressed in normal versus tumor cells are only few. Proteins identified by *t*-test on the significance level 5% are shown in Supplementary Table 2. Supplementary Figure 2 (Supplementary Data) illustrates that the mean values of expression signals for the protein at 9645 Da is different, averaged over normal and tumor samples.

3.1.2 Decision trees Also here all the six comparision were carried out. For the comparision NCOL–NHN, the most clear decision tree was found: there was just one split point corresponding to the peak at 10 848 Da, which was identified in a former study as calgranulin A (Melle *et al*., 2004a). Here intensities smaller than 1 exclusively belong to the group NCOL and such bigger one to NHN. For the other five comparisons more complex trees were found, indicating that these pairs are less different.

3.1.3 Random forest classification The RF for the whole dataset (four classes at once) gave a classification with an error rate close to 20%. This result was attained after parameter optimization. The confusion matrix (Supplementary Table 3) shows for each tissue class the number of samples and the class labels RF assigned to them. The tissue type [colon or head and neck (pharynx)] was almost correctly assigned for both N-groups, except from two cases where TuCOL samples are classified as TuHN. On the contrary, frequent confusion occurred between normal and tumor samples of the same tissue type. From the above classification, the importance of the features making up the forest was derived. These calculations yielded about 50 features which were more important than the background. The 20 most important peaks are listed in Supplementary Table 4 in order of decreasing importance. Among all these classifiers, it is worth noting two outstanding features, the peaks corresponding to and at 13 245.3 Da and 10 848.5 Da are clearly more important than the rest. The importance value of the latter is not so apart from the others, however, this feature has special properties: m/z 10 848.5 was found to play an important role in the identification of each of the four classes. After that, RF for two classes was run. RF performed a perfect classification of normal tissue samples (NCOL versus NHN). In contrast, in all other cases (TuCOL versus TuHN, NHN versus TuHN, NCOL versus TuCOL) misclassification of samples occurred (Supplementary Table 5).

3.1.4 Support vector machines SVM were used to calculate the prediction accuracy as a quotient Q dividing the number of true predicted observations by the total number of tests. A total of 50 pairs of proteins were found whose expression signals predict the samples NCOL versus NHN with the prediction accuracy of 100% (Supplementary Table 6). The expression signals of one of these pairs are shown in Supplementary Figure 3. In opposition to the error free prediction of colon versus head and neck for normal cells (NCOL versus NHN) the prediction accuracy is <94% for tumor cells (TuCOL versus TuHN) (Supplementary Table 6). A total of eight protein pairs were found that allow a prediction accuracy >90% but <94%. The prediction of tumor versus normal tissue is found to be possible only with a reduced accuracy <90%. The pairs of proteins whose expression signals allow an accuracy >85% for the prediction TuCOL versus NCOL are shown in Supplementary Table 7. The prediction accuracy for tumor versus normal head and neck tissue is <85%. A total of 19 pairs of proteins were found whose expression signals allow a prediction accuracy between 80 and 85%, no pair exists with a prediction accuracy >85% (Supplementary Table 6).

3.2 Similarity measures

3.2.1 RF-proximities The average proximities were derived for the same six pairs of sample groups that were compared in the classifications (Supplementary Figure 4). Sorted by magnitude, the proximity values increase almost evenly from 0.06 to 0.16. As a conclusion, it can be stated that there is higher proximity between normal and tumor samples (from one tissue type as well as from both tissue types together) than between samples of different tissue types. It is noted that the lowest proximity is the one between NCOL and NHN, these two classes are the most dissimilar classes.

3.2.2 Mean square distances for classifiers found with random forest For the most important peaks from the RF classification NCOL–NHN, the mean square distances for the six pairs of sample groups were calculated. For the peak at 10 848.5 Da, the result is shown in Figure 2. The mean square distance between colon, head and neck tissue is significantly larger in the normal state than in the tumor state. This should be taken into account because it is not an isolated fact considering 10 of the most important peaks, in 6 cases, the COL–HN distances are larger in the normal state than in the tumor state. The difference between the two values is mainly not so striking as in the above example. However, these data allow to ascertain a tendency. From the overall RF classification, the 20 most important features (listed in Supplementary Table 8) were investigated. For nine among them, mean square distances between COL and HN behave according to the tendency stated in Supplementary Figure 4 (data not shown).

4 DISCUSSION

The combination of different chip-based genomic and proteomic techniques with bioinformatic analysis methods is indispensable for the search of tumor-specific signatures. In addition, the relatedness of different tissues to the tumors arising from these tissues is important to completely understand the biology of cancer. Expression studies have been carried out for many different tumor types. Most of these studies compared homogenates of whole tumor biopsies that contain enough cells of the normal tissue in order to deliver a mixed tumor and normal signature. This provides problems with the analysis, because the tumor signature is not clearly definable.

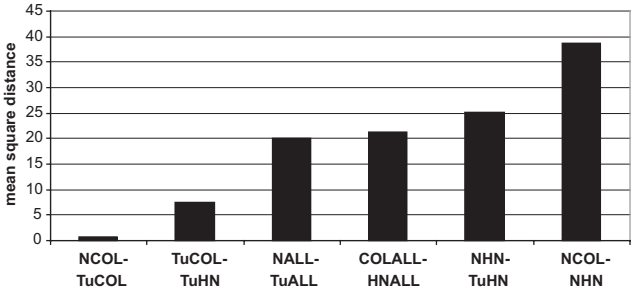

Fig. 2. Mean square distances of the four tissue classes concerning the peak at 10 848.5 Da.

Two basic questions arose during the course of our studies of different microdissected epithelial tumor entities using ProteinChip technology (Melle *et al*., 2005, 2004a,b, 2003; von Eggeling *et al*., 2000). The central question whether it is possible to identify a single or set of individual peaks differentiating between normal and tumor tissues has been affirmatively answered in several studies by our own group as well as others (Melle *et al*., 2005; Zhang *et al*., 2004; Wilson *et al*., 2004; Melle *et al*., 2004a,b). We became curios as to whether a common signature for malignancies arising from various epithelial tissues could be identified. Pathologists have long described that during tumorigenesis a morphological dedifferentiation in comparison with the tissue of tumor origin takes place. However, this process of dedifferentiation has only partly been shown on a molecular level. Proteomic profiling using purely defined tissue material presents an ideal method to show the molecular equivalents of this process as well as to investigate what changes dedifferentiation entails. To approach these questions, we analyzed the data produced from proteomic profiling of microdissected normal and tumor tissues from head and neck and colon cancers using two different bioinformatic approaches.

The different bioinformatic algorithms applied for the meta-analysis of the proteomic profiles of the four tissue groups focused on two different questions. First, to identify characteristic features differentiating between the four tissue groups, and second, to analyze how similar the groups were to one another. Classification of the group using characteristic features was possible using all the bioinformatic methods applied to a certain extent. The comparison NCOL–NHN was the only case where sample classes could be predicted perfectly, whereas in all other comparisons classification errors occurred. We conclude, that these two groups appear to be the most different from one another. Similar features can be found in all the resulting peak lists generated using different methods, indicating that the patterns generated using different methods were quite similar (see Supplementary Tables 2, 4, 7 and 8). That these features were identified by more than one method underlines the significance of these classifiers. The similarity measures calculated in this study agree with the interpretation of the group classification results. Both proximities as well as mean square distances between groups revealed that the tumorous tissues (COL and HN) were more similar than the normal tissues from which they were derived. This is

especially true for the peak at 10 848 Da, which could be identified as a classifier in a former study (Melle *et al*., 2004a).

The results from both bioinformatic approaches concluded that the differences between normal epithelial tissues are larger than between the tumor tissues arising from these epithelial tissues. These results support the hypothesis that epithelial tissues become more similar during their progression towards a tumorous state at the proteomic level (Fig. 1). This conclusion is consistent with the biological features of these tissues. The epithelia from colon and pharynx develop namely from the entoderm, but are functionally reflected in their proteomic distance. The hypo- and mesopharynx is lined by a multi-layered, squamous epithelium that assures a protective function. The colon, however, is lined by a prismatic, single-layered epithelium with predominantly secretory (mucine) und resorptive (water) capabilities in addition to a function for the excretion of heavy metals. In contrast, TuCOL and TuNH display a more closely related common tumor signature that is recognized in bioinformatic analysis through the closer similarity or proximity of these groups. For the tumor, functions such as proliferation, invasion and metastasis become more important for tumor survival than the maintenence of the normal epithelial cell functions. Therefore, structural and functional dedifferentiation from the functionality of the tissue of origin is the result also reflected in the histological appearance of the tumor tissue. Interestingly the dedifferentiation is also known in the histopathological grading which forms the basis for the classification of tumors. Additionally, it could be shown that common signatures are present for the two normal epithelial tissues and for the two tumor tissues. Specific classifiers could be identified using both bioinformics methods employed here to distinguish among all four tissue groups. For the groups with the lowest proximity (NHN versus NCOL) only one peak (10.8 kDa) is necessary, but for groups with a high proximity the classifier becomes more complex. Especially for the classification of clinically relevant groups (e.g. NHN versus TuHN), it becomes clear that a reliable diagnosis can only be achieved using a multi-marker classifier or a specific signature of expressed genes or proteins.

Our analyses support the notion that the identification of a general tumor signature including similarities indicating features, such as malignancy, will be feasible in future. This proteomic signature may further contribute, especially in combination with additional methods, mainly an optimized tissue microdissection and analysis [e.g. Ernst *et al*. (2006)], to reveal the heterogeneity of the tumor and to identify metastasizing clones inside the malignant tissue.

In conclusion, we provide proof-of-principle at the proteomic level that changes in the histological features of tumors as compared with the tissues from which they arise are reflected in the convergence of proteomic pattern during the development to cancer.

ACKNOWLEDGEMENTS

The authors would like to thank Kathy Astrahantseff and Susanne Michel for stimulating discussions and critical reading of the manuscript. This work was supported by the IZKF Jena and the BMBF (NBL3 and FKZ 0313652A).

Conflict of Interest: none declared.

REFERENCES

Bonferroni,C.E. (1936) Theoria statistica classi e calcolo delle probabilità. *Publ. R. Int. Super. Sci. Econ. Comm. Firenze*, **8**, 1–62.

Breiman,L. (2004) Manual On-Setting Up, Using and Understanding Random Forests V3.1. .

Breiman,L. *et al*. (1993) *Classification and Regression Trees*. Chapman and Hall, Boca Raton.

Ernst,G. *et al*. (2006) Proteohistography—direct analysis of tissue with high sensitivity and high spatial resolution using ProteinChip technology. *J. Histochem. Cytochem*., **54**, 13–17.

Hutchens,T.W. and Yip,T.T. (1993) New desorption strategies for the mass spectrometric analysis of macromolecules. *Rapid Commun. Mass Spectrom*., **7**, 576–580.

Ma,J., Zhao,Y. and Ahalt,S. (2005) OSU SVM Classifier Matlab Toolbox (ver 3.00).

Melle,C. *et al*. (2003) Biomarker discovery and identification in laser microdissected head and neck squamous cell carcinoma with ProteinChip(R) technology, two-dimensional gel electrophoresis, tandem mass spectrometry, and immunohistochemistry. *Mol. Cell. Proteomics*., **2**, 443–452.

Melle,C. *et al*. (2004a) A technical triade for proteomic identification and characterization of cancer biomarkers. *Cancer Res*., **64**, 4099–4104.

Melle,C. *et al*. (2004b) Proteomic profiling in microdissected hepatocellular carcinoma tissue using ProteinChip technology. *Int. J. Oncol*., **24**, 885–891.

Melle,C. *et al*. (2005) Discovery and identification of alpha-defensins as low abundant, tumor-derived serum markers in colorectal cancer. *Gastroenterology*, **129**, 66–73.

Paweletz,C.P. *et al*. (2001) Proteomic patterns of nipple aspirate fluids obtained by SELDI-TOF: potential for new biomarkers to aid in the diagnosis of breast cancer. *Dis. Markers*, **17**, 301–307.

Rosty,C. *et al*. (2002) Identification of hepatocarcinoma-intestine-pancreas/pancreatitis-associated protein I as a biomarker for pancreatic ductal adenocarcinoma by protein biochip technology. *Cancer Res*., **62**, 1868–1875.

Vapnik,V. (1998) *Statistical Learning Theory*. Wiley, New York.

Vlahou,A. *et al*. (2001) Development of a novel proteomic approach for the detection of transitional cell carcinoma of the bladder in urine. *Am. J. Pathol*., **158**, 1491–1502.

von Eggeling,F. *et al*. (2000) Tissue-specific microdissection coupled with ProteinChip array technologies: applications in cancer research. *Biotechniques*, **29**, 1066–1070.

von Eggeling,F. *et al*. (2001) Mass spectrometry meets chip technology: a new proteomic tool in cancer research? *Electrophoresis*, **22**, 2898–2902.

Wilson,L.L. *et al*. (2004) Detection of differentially expressed proteins in early-stage melanoma patients using SELDI-TOF mass spectrometry. *Ann. N. Y. Acad. Sci*., **1022**, 317–322.

Zhang,Z. *et al*. (2004) Three biomarkers identified from serum proteomic analysis for the detection of early stage ovarian cancer. *Cancer Res*., **64**, 5882–5890.

Supplementary Data

Tables

Table 1: Number of differentially expressed proteins (t-test, significance level α adjusted according Bonfferoni [1]; *n* – number of samples considered)

Comparison	*n*	Significance level α			
		5 %	1 %	0.1 %	0.01%
NALL vs TuALL	106	5	2	0	0
NCOL vs TuCOL	47	1	1	0	0
NHN vs TuHN	49	15	11	1	0
HNALL vs COLALL	106	61	47	40	33
NHN vs NCOL	46	50	39	25	15
TuHN vs TuCOL	60	21	13	7	3

Table 2: Protein peaks differentially expressed for normal versus tumor tissue (t-test, significance 5% *, 1% **, 0.1 ***)

Peak, Protein [Da]		NALL vs TuALL	NCOL vs TuCOL	NHN vs TuHN
5	3115.18	**		**
63	5519.20			*
90	7353.84			**
110	9087.29			**
113	9334.72			**
115	9645.24		**	***
116	9773.54			**
117	9888.74			**
118	9978.04			*
119	10106.6			**
123	10434.6	*		*
124	10544.2	**		**
125	10640.4	*		**
126	10848.5			*
153	14705.7	*		**

Table 3: Result of the supervised RF classification of the whole dataset in a confusion matrix.

	classified as NCOL	classified as NHN	classified as TuCOL	classified as TuHN
NCOL	13	0	5	0
NHN	0	24	0	4
TuCOL	3	0	24	2
TuHN	0	6	2	23

Table 4: The importance of features (protein peaks) found by RF. The first three were identified in former studies (8;9). Tandem MS data for calgranulin A (10.8 kDa) and calgranulin B (13.2 kDa) are shown in supplemental data (Fig S1 + S2).

Importance	Peak at m/z [Da]
4.63	13245.30
3.85	10848.50
3.83	3471.67
3.68	7353.84
3.58	15823.00
3.56	11056.90
3.34	12490.90
3.30	7910.54
3.27	10544.20
3.23	3798.21
3.21	9645.24
3.17	9087.29
3.13	3400.80
2.86	6145.28
2.83	12347.00
2.82	16238.70
2.81	5519.20
2.76	18355.20
2.59	3515.31
2.56	3115.18

Table 5: Error rates of supervised RF classification dealing with pairs of sample groups

Comparison	*Error rate* [%]
NCOL vs TuCOL	17.0
NHN vs TuHN	18.6
NHN vs NCOL	0.0
TuHN vs TuCOL	3.3

Table 6: Maximum prediction accuracy obtained by SVM together with cross-validation

Comparison	*Qmax* [%]
NALL vs TuALL	78.3
NCOL vs TuCOL	87.2
NHN vs TuHN	84.8
HNALL vs COLALL	94.2
NHN vs NCOL	100.0
TuHN vs TuCOL	93.3

Table 7: Seven pairs of protein peaks whose expression signals allow a prediction of TuCOL versus NCOL with an accuracy greater than 85%

Peak, Protein 1 [Da]		Peak, Protein 2 [Da]		*Q* [%]
17	3697.31	21	3798.21	87.2
12	3471.67	37	4343.47	87.2
21	3798.21	129	11056.9	85.1
20	3763.08	21	3798.21	85.1
17	3697.31	123	10434.6	85.1
12	3471.67	127	10923.8	85.1
12	3471.67	21	3798.21	85.1

Table 8: Mean square distances for the ten most important peaks from the RF classification NCOL vs NHN. For the identification of the first two peaks by Tandem MS see supplemental data figure S1 + S2.

Peak at m/z [Da]	Mean square distance NCOL-NHN	Mean square distance TuCOL-TuHN
10848.50	38.82	7.40
13245.30	3.69	0.74
12490.90	0.25	0.14
10923.60	13.31	3.08
9773.54	0.77	0.70
11056.90	5.77	2.21
5427.23	13.44	5.53
12347.00	0.14	0.17
12278.50	0.13	0.11
10981.50	3.50	1.67

Figure legends

Figure 2: Distribution of samples from normal and tumor tissue from pharynx (left) and colon (right) with respect to the expression signal of the protein at 9645 Da.

Figure 3: Expression signals of the peaks at 13245.3 versus 16238.7 for the samples NCOL (●) and NHN (o)

Figure 4: Average proximities between the sample groups (pairs of groups according to the comparisions in chapter “t-test”).

Figures:

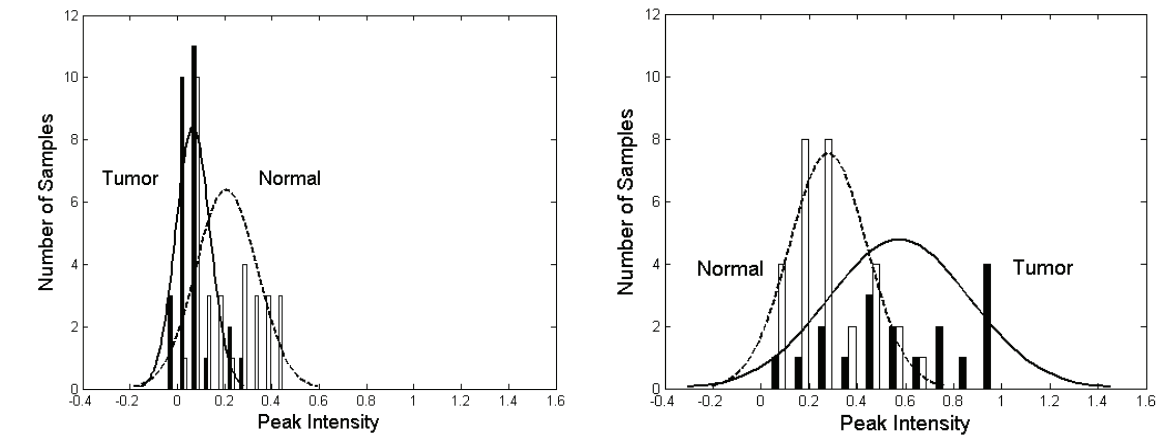

Müller et al., Fig. 2

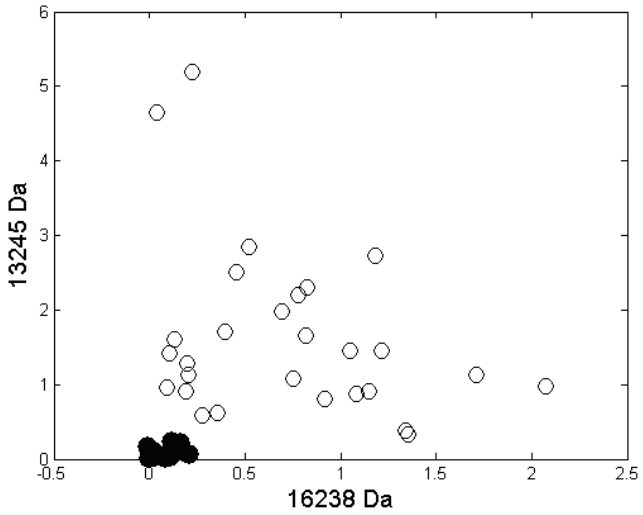

Müller et al., Fig. 3

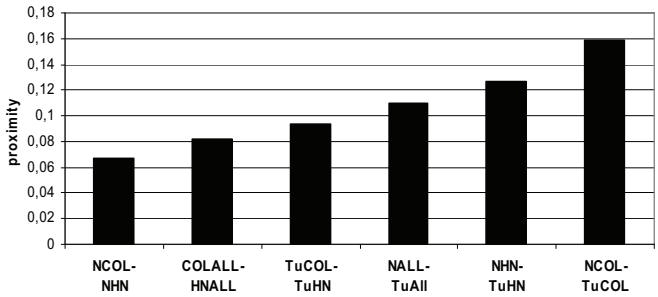

Müller et al., Fig. 4

research articles Journal of proteome research

Detection and Identification of Protein Interactions of S100 Proteins by ProteinChip Technology

Roland Lehmann,† Christian Melle,*,† Niko Escher, and Ferdinand von Eggeling

Core Unit Chip Application (CUCA), Institute of Human Genetics and Anthropology, Friedrich-Schiller-University, 07740 Jena, Germany

Received June 3, 2005

The aim of this work was to establish an approach for identification of protein interactions. This assay used an anti-S100A8 antibody coupled on beads and incubated with cell extract. The bead eluates were analyzed using ProteinChip technology and subsequently subjected to an appropriate digestion. Molecular masses of digestion fragments were determined by SELDI−MS, and database analysis revealed S100A10 as interacting protein. This result was confirmed by co-immunoprecipitation and immunocapturing. Using S100A10 as new bait, a specific interaction with S100A7 was detectable.

Keywords: S100 proteins • protein−protein interaction assay • surface-enhanced laser desorption/ionization−mass spectrometry (SELDI−MS) • immunoprecipitation

Introduction

Functional characterization of the proteome interaction studies are of particular interest, because it is known that most of the proteins are usually interconnected. Interacting proteins are often involved in the same biochemical pathway. The identification of an interacting partner of a protein of unknown function can help to clarify its function. Defining the interaction partners of known proteins is invaluable to detailing its mechanism of action and regulation. The idea of temporal and spatial localization of different proteins at specific sites in the cell suggests that interactions of different components involved in the same cellular processes are required. The clarification of the association of a molecular machine or regulatory factor may help to understand cellular regulatory mechanisms.[1] Recently, many different techniques have been used to define protein−protein interactions.[2] In vitro techniques are recognized as often generating false positives.[3] To avoid this problem, a multitude of in vivo methods have been developed including yeast two hybrid assays.[4] However, yeast two hybrid screens can also generate a fairly high number of both false positives and negatives.[5] Recently, a new technique named SELDI−MS (surface-enhanced laser desorption/ionization mass spectrometry) was developed which comprises ProteinChip arrays and mass spectrometry.[6,7] The ProteinChip array carries spots with different chromatographic surfaces to retain proteins regarding their physicochemical properties. The spots can easily be purified from contaminants such as buffer salts or detergents by washing, thus eliminating the need for prepurification techniques as required with other MS techniques. For this reason, crude biological extracts, such as cell lysis extract, serum ,or other biological fluids can be spotted directly on the ProteinChip arrays for mass spectrometric analysis. One application of SELDI−MS is the analysis of protein patterns of different biological samples mainly derived from cancer and noncancer patients.[8−12] In a former protein profiling study of head and neck squamous cell carcinoma (HNSCC) carried out by SELDI−MS, a decreased expression of S100A8/A9 in microdissected tumor tissue was detected.[13] These proteins are members of the S100 Ca^{2+} binding family and have received increased attention because of their involvement in several human diseases such as rheumatoid arthritis, acute inflammatory lesions, cardiomyopathy, Alzheimer's disease, and cancer.[14,15] The aim of the present study was the proof of principle of a procedure composed of immunoprecipitation techniques and SELDI technology to detect and identify protein−protein interactions from crude cell extracts. On this account, we started to analyze the interaction partners of S100A8/A9. Hereby, we were able to detect specific interactions between different S100 proteins using specific immunoaffinity beads. These interactions were visible by SELDI−MS and the interaction partners were identified as S100A10 (calpactin light chain; p11) and S100A7 (psoriasin), respectively, and further confirmed using co-immunoprecipitation and immunocapturing.

Materials and Methods

Cell Culture. HaCaT cells, a spontaneously immortalized human keratinocyte cell line, were cultured in DMEM supplemented with 10% fetal bovine serum.[16] Cells were grown to 80% confluence and were passaged at a split ratio of 1:4. At 95% confluence, cells were harvested and lysed in a buffer containing 100 mM sodium phosphate pH 7.5, 5 mM EDTA, 2 mM $MgCl_2$, 3 mM 2-β-mercaptoethanol, 0.1% CHAPS, 500 μM leupeptin, and 0.1 mM PMSF. After centrifugation (15 min; 15 000 rpm) the supernatant was used immediately.

Protein−Protein Interaction Assay. A twenty-microliter portion of Interaction Discovery Mapping (IDM) beads (Ciphergen Biosystems Ltd., Fremont, Ca) was incubated with 4 μL protein A (Sigma) overnight at 4 °C. A pellet was generated by centrifugation, and the supernatant was discarded. The pellet was washed twice with a buffer containing 50 mM sodium acetate pH 5.0. Afterward, the beads were incubated in a buffer containing 0.5 M Tris/HCl pH 9.0, 0.1% Triton X-100

* To whom correspondence should be addressed. Tel: +49(0)3641-935529. Fax: +49(0)3641-935518. E-mail: christian.melle@mti.uni-jena.de.
† These authors contributed equally to this work.

10.1021/pr050163s CCC: $30.25

Published on Web 08/24/2005

for 2 h at room temperature for blocking residual reactive groups. The beads were washed three times with 1× PBS. Thereafter, 40 μL of specific antibody (0.2 μg/μL) against human S100A8 (S13.67; BMA Biomedicals; Augst, Switzerland), human S100A9 (S36.48; BMA Biomedicals; Augst, Switzerland), and human S100A10 (H-21; Swant; Bellinzona, Switzerland), respectively, or normal rabbit IgG (Pepro Tech Inc.; Rocky Hill, NJ) as negative control, in 50 mM sodium acetate pH 5.0 were applied to the beads and allowed to bind at room temperature for 1 h in an end-over-end mixer. Unbound antibody was removed by washing in 50 mM sodium acetate. Unspecific binding sites were blocked using a buffer containing 2 mg/mL bovine serum albumin in 0.5 M Tris/HCl pH 9.0, 0.1% Triton X-100 for 2 h at room temperature in an end-over-end mixer. Afterward, the beads were washed in 1× PBS, 0.1% Triton X-100 and in 1× PBS and incubated with 100 μL of crude HaCaT cell extract overnight at 4 °C in an over-end-over mixer. The unbound proteins were washed away by sequential washes in PBS, 0.5 mM sodium chloride, 0.05% Triton X-100, 1 M urea in PBS, PBS, and aqua bidest. Bound proteins were eluated from the IDM beads by 10 μL 50% acetonitrile/0.5% trifluoroacetic acid and gently vortexed for 5 min. Five μL of the eluated samples were applied to the activated, hydrophobic surface of an H50 ProteinChip Array (Ciphergen Biosystem Inc.; Fremont) and dried on air. After washing with 3 μL aqua bidest 0.5 μL sinapinic acid (saturated solution in 0.5% TFA/50% Acetonitrile) was applied twice and the array was analyzed in a PBS II reader (Ciphergen; Fremont) according to an automated data collection protocol.

Tryptic Digestion of IDM Eluates. For the analysis of fragment masses proteins eluated from IDM beads were tryptic digested. Hereby, the volume of the samples was reduced to nearly 5 μL, mixed with 5 μL of a buffer containing 6 M urea, 3 mM 2-β-mercaptoethanol and denaturated for 20 min at 95 °C. Afterward, sample volume was increased until samples contained a maximum of 1 M urea, 15 μL of a tryptic solution (4 ng/μL; in 25 mM ammonium bicarbonate) was added and incubated for 24 h at 35 °C. Samples were sonicated for 5 min, 5 μL of them were applied directly to the activated reverse phase surface of an NP20 array (Ciphergen; Fremont) and dried on air. After addition of the matrix (CHCA), peptide fragment masses were analyzed using the PBS II instrument. A standard protein mix (all-in-1 peptide standard mix; Ciphergen, Fremont), including Arg8-vasopressin (1082.2 Da), somatostatin (1637.9 Da), dynorphin (2147.5 Da), ACTH (2933.5 Da), and insulin beta-chain (3495.94 Da) was used for calibration. Proteins were identified using the fragment masses generated through trypsin digestion by searching in a publicly available database (*http://129.85.19.192/profound_bin/WebProFound.exe)*.

Immunocapturing Assays. For immunocapturing of specific target proteins 2 μL protein A in 2 μL of 50 mM $NaHCO_3$ pH 9.2 was directly coupled to RS100 ProteinChip arrays (Ciphergen; Fremont) overnight at 4 °C in a humidity chamber. After incubation the supernatant was removed and 2 μL BSA (2μg/μL) (Sigma) in 2 μL 1× PBS pH 7.2 was spotted for 2 h at room temperature to block any remaining active sites. Afterward, BSA was removed, spots were washed with 1× PBS pH 7.2 and 2 μL of specific antibody (0.2 μg/μL) against human S100A10 (H-21; Swant; Bellinzona, Switzerland) or human S100A7 (ab13680; Abcam; Cambridge, UK), respectively, or, as negative control, normal rabbit IgG (Pepro Tech Inc.; Rocky Hill, NJ) in 2 μL of 50 mM $NaHCO_3$ pH 9.2 were applied to the arrays for 2 h at room temperature in a humidity chamber. Unbound antibody was removed and spots were washed with 5 μL 1× PBS for 2 min. Afterward, the ProteinChip array was fixed in a Bioprocessor (Ciphergen, Fremont) and 50 μL of crude cell extract diluted in 50 μL of a 0.1% Triton X-100 in 1× PBS pH 7.2 were applied to each spot and incubated for 2 h at room temperature on a shacking platform. The unbound proteins were washed away by sequential washes in 1× PBS, 0.5 mM sodium chloride, 0.05% Triton X-100, 1 M urea in 1× PBS, 1× PBS, and aqua bidest. The array surface was allowed to dry for 5 min, 0.5 saturated sinapinic acid was added twice and the ProteinChip was analyzed in a PBS II reader according to an automated data collection protocol.

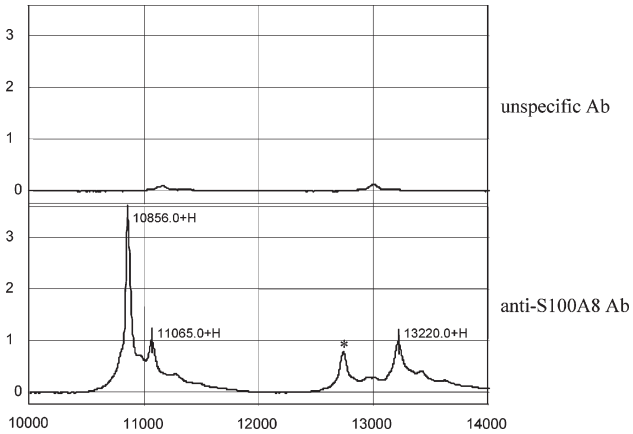

Figure 1. Protein−protein interaction assay using specific anti-S100A8 antibody. An anti-S100A8 antibody was bound on IDM beads, incubated with crude HaCaT cell extract and binding partners were analyzed by SELDI−MS. Among signals of 10.87 kDa and 13.22 kDa that represent S100A8 and S100A9, respectively, a signal of nearly 11.06 kDa was detected. In a negative control using a nonspecific antibody no specific signal was detectable. (Signal labeled by asterisk is still to identify).

Co-immunoprecipitation. Antibodies against human S100A7 (ab13680; Abcam; Cambridge, UK), human S100A8 (S13.67; BMA Biomedicals; Augst, Switzerland), human S100A9 (S36.48; BMA Biomedicals; Augst, Switzerland), and human S100A10 (H-21; Swant; Bellinzona, Switzerland), or, as negative control, normal rabbit IgG (Pepro Tech Inc.; Rocky Hill, NJ) were bound on protein A-agarose beads. Crude extract (250 μL) from human HaCaT cells was incubated with the antibody loaded beads for 1 h at 4 °C. Then the resins were washed three times with Co−IP buffer containing 20 mM HEPES/KOH pH 8.0, 50 mM KCl, 0.1 mM EDTA and 0.05% CHAPS. Bound proteins were subjected to 10% SDS-PAGE and detected by immunoblotting with anti-S100A7, anti-S100A8, anti-S100A9 (S36.48; BMA Biomedicals; Augst, Switzerland), or anti-S10010 antibody, respectively.

Results

Detection of S100A8 Protein Interaction Partners. We first assessed possible interaction partners of S100A8/A9 by SELDI−MS. Hereby, among other peaks we found a specific signal at nearly 11.07 kDa using anti-S100A8 antibody-coupled IDM beads compared to approaches using nonspecific antibody (Figure 1). Beside this mentioned signal, we detected a signal at nearly 13.22 kDa, too. This molecular mass correlates well to the molecular mass of S100A9 that is known as a binding partner of S100A8.

Protein Identification by Tryptic Digestion and Database Search. Proteins eluated from both anti-S100A8 antibody

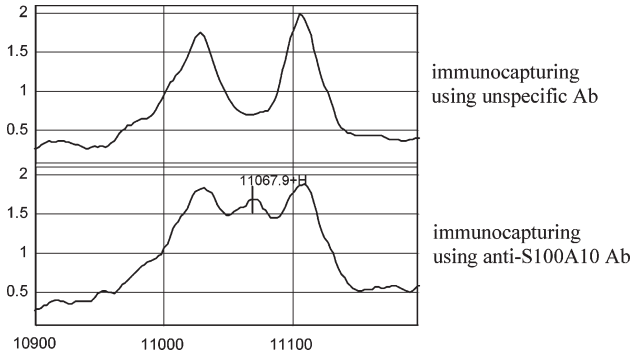

Figure 2. Normalized ProteinChip Arrays spectra of the immunocapturing assay of crude cell extract. S100A10 was captured from HaCat cell extracts by the corresponding monoclonal antibody bound on RS100 ProteinChip arrays. The peak at 11.07 kDa representing S100A10 was clearly detectable. In control assays without the specific antibody no S100A10 signal was captured.

coupled or nonspecific antibody coupled IDM beads were tryptic digested for analysis of fragment masses. The digested solutions were spotted on an NP20 array and the size of the obtained fragments was determined by the PBS II instrument. In parallel, a theoretical tryptic digestion of known proteins of the eluates (e.g., the bait, known interaction partners of the bait, antibody subunits etc.) was carried out using a public database (Expasy findpept tool; http://us.expasy.org/tolls/findpept.html). Afterward, peptide fragments derived from known proteins were eliminated. Database searches (Profound; http://129.85.19.192/profound_bin/WebProFound.exe) using retained peptide fragments revealed S100A10 as a possible candidate. The calculated mass of human S100A10 is 11.072 kDa (www.expasy.ch), and thus slightly higher than the average mass of about 11.065 kDa found in these experiments (Figure 1).

Immunocapturing of S100A10. For confirmation of the identity of the interaction partner of S100A8, an immunoassay was performed using a monoclonal antibody against S100A10. Hereby, a specific antibody bound on RS100 ProteinChip arrays captured S100A10 from HaCaT cell extract. The spectra of the analysis showed a peak corresponding to S100A10. In a control assay using a nonspecific antibody no proteins specific for S100A10 were captured (Figure 2).

Co-immunoprecipitation of S100A8/A9 by an anti-S100A10 Antibody. In a co-immunoprecipitation assay, we were able to precipitate both S100A8 and S100A9 using protein A-agarose beads with a specific antibody against S100A10 from a crude extract of HaCat cells (Figure 3, lane 1 and 3, respectively). In an approach using a nonspecific antibody bound on protein A-agarose neither S100A8 nor S100A9 was detectable (Figure 3, lane 2 and 4, respectively). As a control the specific antibody against S100A10 precipitated its antigene (Figure 3, lane 5).

Detection and Identification of a S100A10 Protein Interaction Partner. In the next step, we assessed S100A10 for possible protein interaction partners. Hereby, we found an interaction partner possessing a molecular mass of nearly 11.29 kDa using anti-S100A10 antibody coupled IDM beads compared to nonspecific antibody coupled IDM beads by SELDI−MS (Figure 4A). Database search (profound) of the tryptic digestion fragments of the eluted proteins revealed S100A7 as a good candidate. For confirmation of this result, an immunocapturing assay using an anti-S100A7 antibody was carried out. Hereby, a signal of nearly 11.37 kDa was detectable. This molecular mass is slightly higher (0.39%) than the calculated mass (expasy). In the control assay, using a nonspecific antibody no signal compared to the molecular mass of S100A7 was detectable (Figure 4B). In a co-immunoprecipitation approach, both an anti-S100A10 and an anti-S100A7 antibody were able to precipitate S100A7 (Figure 4C, lane 1 and 3, respectively). When we used antibodies that recognize S100A8 or S100A9, no clear S100A7 signal was detectable (Figure 4C, lane 2 or data not shown).

Discussion

In the present study, we performed an approach to investigate protein−protein interactions by ProteinChip technology. By the appearance of both false positive and negative results in other in vivo interaction assays we analyzed the endogenous interacting partners in crude cell extract by mass spectrometry.[17] The assay comprises the detection of interaction partners by SELDI−MS and the identification using immunocapturing experiments and coprecipitation, respectively. In our knowledge, it is one of the first studies using SELDI−MS to assess protein interactions.[18,19] As a model system we used members of the S100 Ca^{2+}-binding family. A multitude of protein interactions is known to be performed by S100 proteins.[20] S100 proteins are involved in several human diseases such as

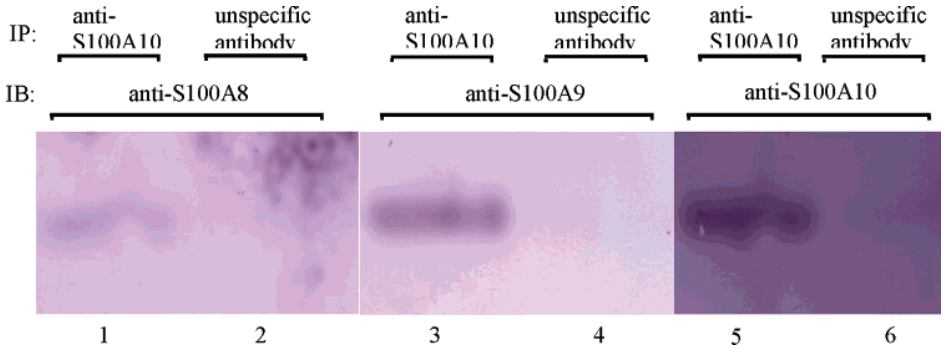

Figure 3. Co-immunoprecipitation of S100A8/A9 and S100A10. Specific anti-S100A10 antibody or, as negative control, nonspecific antibody was coupled to protein A-agarose beads and incubated with HaCaT cell extracts. Beads were washed with Co−IP buffer and bound proteins were subsequently subjected to SDS-PAGE and analyzed by immunoblotting using specific antibodies against S100A8 (lane 1), S100A9 (lane 3), and S100A10 (lane 5), respectively. Co-immunoprecipitation assays using a nonspecific antibody showed no signal (lanes 2, 4, 6).

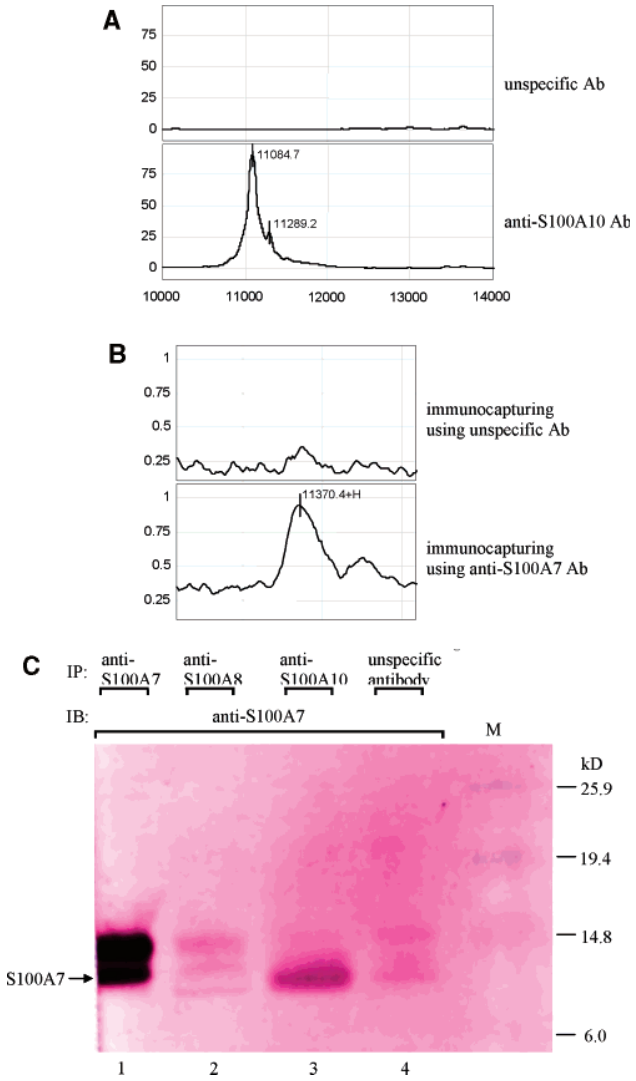

Figure 4. Detection and identification of S100A7 as specific S100A10 interaction partner. (A) Anti-S100A10 antibody was coupled on IDM beads and incubated with HaCaT cell extracts. Bound proteins were analyzed by SELDI−MS. Besides a signal representing S100A10, a signal at nearly 11.29 kDa was detectable that is absent in the assay using nonspecific antibody. (B) In an immunocapturing assay a specific anti-S100A7 antibody was bound on an RS100 ProteinChip array and captured a signal corresponding to S100A7 from crude HaCaT cell extracts. In a control assay without a specific antibody, this signal was not detectable. (C) In a co-immunoprecipitation assay using an S100A10 antibody, S100A7 was detectable subsequently in an immunoblot (lane 3). A similar signal was also detectable using an S100A7 antibody for precipitation (lane 1). No S100A7 signal was detectable using an anti-S100A8 antibody or a nonspecific antibody, respectively (lanes 2 or 4).

rheumatoid arthritis, acute inflammatory lesions, cardiomyopathy, Alzheimer's disease, and cancer.[14,15] Recently, we showed in a study that S100A8/A9 are less expressed in head and neck squamous cell carcinoma compared to normal tissue.[13] S100A8 and S100A9 achieve an interaction together and under physiological conditions, a heterodimer is often existent.[21] Among different protein binding partners S100A8 forms specific interactions to for example cytochrome b558, p67 (phox), and Rac-2 and initiates so the NADPH oxidase activation.[22,23] As we demonstrated, the interaction between S100A8/A9 and S100A10 is detectable under in vivo conditions by mass spectrometry and immunological techniques. It is not clear whether the single components of the S100A8/A9 complex alone are able to bind S100A10 or if this interaction requires a full complex of both. In our knowledge, this study shows for the first time an interaction between S100A8/A9 and S100A10. Further studies will be needed to reveal a potential biological context of this protein interaction. S100A10 forms an interaction with annexin II that results in the formation of a heterotetramer.[24] This interaction can be inhibited by a protein kinase C dependent phosphorylation of a specific serine residue in the annexin II.[25] The S100A10/annexin II complex has been implicated in the structural organization and dynamics of endosomal membranes and cell membrane cytoarchitecture, and is as well involved in the formation of adherent junctions.[26−28] Surprisingly, we only detected the mentioned interaction between S100A10 and annexin II when we used an anti-S100A10 antibody. In the protein−protein interaction assays carried out with the anti-S100A8 antibody, we detected S100A10 but never annexin II (supplementary Figure 1). Until now, we have no explanation for this fact. It might be possible that S100A8 as well as annexin II share a similar binding site to S100A10, because there are no data available about the biological function of S100A10 beyond the complex with annexin II. The interaction between S100A10 and S100A7 detected by several proteomic approaches is described in the present study for the first time. Due to our data, we do assume that S100A8/A9 is not involved in this mentioned interaction as a bridging protein, because no S100A7 signal was detectable using specific anti-S100A8 or anti-S100A9 antibodies in co-immunoprecipitation. The S100A7 Ca^{2+}-binding protein is highly upregulated in psoriatic epidermis as well as in primary human keratinocytes undergoing abnormal differentiation.[29] It is primarily expressed in breast cancer cells and at very low level in normal breast epithelial cells.[30] Also an overexpression in gastric cancer is described.[31] S100A7 interacts with Jab 1 in ductal carcinoma in situ (DCIS) of the breast and because of that it may influence the progression of breast carcinoma.[32] Besides this interaction, an interaction with RanBPM may contribute to breast tumor progression, as well as interactions in keratinocytes with both E-FABP and epidermal fatty acid binding protein are described.[33−35] It seems that several members of the S100 Ca^{2+}-binding protein family form interactions with each other that could be involved in different physiological processes. To assess the biological role of these protein interactions, additional studies are needed. The identification of further interaction partners that is still in process may clarify possible biological functions. In this study, we show a possible proteomic approach composing ProteinChip technology and immunological techniques to detect and identify protein−protein interactions.

Acknowledgment. This work was support by a grant of the German Federal Ministry of Education and Research (BMBF) and the Interdisciplinary Center for Clinical Research (ICCR), Jena.

Supporting Information Available: Supplementary Figure 1. This material is available free of charge at http://pubs.acs.org.

References

(1) Coulombe, B.; Jeronimo, C.; Langelier, M.-F.; Cojocaru, M.; Bergeron, D. *Mol. Cell Proteomics* **2004**, *3*(9), 851−856.

(2) Phizicky, E. M.; Fields, S. *Microbiol. Rev.* **1995**, *59*, 94−123.
(3) Edwards; A. M., Kus, B.; Jansen, R.; Greenbaum, D.; Greenblatt, J.; Gerstein, M. *Trends Genet.* **2004**, *18*, 529−536.
(4) Fields, S.; Song, O. *Nature* **1989**, *340*, 245−246.
(5) Von Mering, C.; Krause, R.; Snel, B.; Cornell, M.; Oliver, S. G.; Fields, S.; Bork, P. *Nature* **2002**, *417*, 399−403.
(6) Hutchens, T. W.; Yip, T. T. *Rapid Commun. Mass Spectrom.* **1993**, *7*, 576−580.
(7) Isaaq, H. J.; Conrads, T. P.; Prieto, D. A.; Tirumalai, R.; Veenstra, T. D. *Anal. Chem.* **2003**, *75*, 148A−155A.
(8) Cazares, L. H.; Adam, B. L.; Ward, M. D.; Nasim, S.; Schellhammer, P. F.; Semmes, O. J.; Wright, G. L. *Clin. Cancer Res.* **2002**, *8*, 2541−2552.
(9) Melle, C.; Ernst, G.; Schimmel, B.; Bleul, A.; Koscielny, S.; Wiesner, A.; Bogumil, R.; Moller, U.; Osterloh, D.; Halbhuber, K. J.; von Eggeling, F. *Mol. Cell. Proteomics* **2003**, *2*, 443−452.
(10) Melle, C.; Kaufmann, R.; Hommann, M.; Bleul, A.; Driesch, D.; Ernst, G.; von Eggeling, F. *Int. J. Oncol.* **2004**, *24*, 885−891.
(11) Ye, B.; Cramer, D. W.; Skates, S. J.; Gygi, S. P.; Pratomo, V.; Fu, L.; Horick, N. K.; Licklider, L. J.; Schorge, J. O.; Berkowitz, R. S.; Mok, S. C. *Clin. Cancer Res.* **2003**, *9*, 2904−2911.
(12) Uchida, T.; Fukawa, A.; Uchida, M.; Fujita, K.; Saito, K. *J. Proteome Res.* **2002**, *1*, 495−499.
(13) Melle, C.; Ernst, G.; Schimmel, B.; Bleul, A.; Koscielny, S.; Wiesner, A.; Bogumil, R.; Moller, U.; Osterloh, D.; Halbhuber, K. J.; von Eggeling, F. *Cancer Res.* **2004**, *64*, 4099−4104.
(14) Kerkhoff, C.; Klempt, M.; Sorg, C. *Biochim. Biophys. Acta* **1998**, *1448*, 200−211.
(15) Heizmann, C. W.; Fritz, G.; Schafer, B. W. *Front. Biosci.* **2002**, *7*, d1356−1368.
(16) Boukamp, P.; Petrussevska, R. T.; Breitkreutz, D.; Hornung, J.; Markham, A.; Fusenig, N. E. *J. Cell Biol.* **1988**, *106*, 761−771.
(17) Jansen, R.; Yu, H.; Greenbaum, D.; Kluger, Y.; Krogan, N. J.; Chung, S.; Emili, A.; Snyder, M.; Greenblatt, J. F.; Gerstein, M. *Science* **2003**, *302*, 449−453.
(18) Oren, D.; Li, Y.; Volovik, Y.; Morris, T. S.; Dharia, C.; Das, K.; Galperina, O.; Gentz, R.; Arnold, E. *Nat. Struct. Biol.* **2002**, *9*, 288−292.
(19) Winer, S.; Tsui, H.; Lau, A.; Song, A.; Li, X.; Cheung, R. K.; Sampson, A.; Afifiyan, F.; Elford, A.; Jackowski, G.; Becker, D. J.; Santamaria, P.; Ohashi, P.; Dosch, H. M. *Nat. Med.* **2003**, *9*(2), 198−205.
(20) Donato, R. *Int. J. Biochem. Cell Biol.* **2001**, *33*(7), 637−668.
(21) Dell'Angelica, E. C.; Schleicher, C. H.; Simpson, R. J.; Santome, J. A. *Int. J. Biochem. Cell Biol.* **1996**, *28*(1), 53−62.
(22) Berthier, S.; Paclet, M. H.; Lerouge, S.; Roux, F.; Vergnaud, S.; Coleman, A. W.; Morel, F. *J. Biol.* Chem. **2003**, *278*(28), 25499−25508.
(23) Kerkhoff, C.; Nacken, W.; Benedyk, M.; Dagher, M. C.; Sopalla, C.; Doussiere, J. *FASEB J.* **2005**, *19*(3), 467−469.
(24) MacLeod, T. J.; Kwon, M.; Filipenko, N. R.; Waisman, D. M. *J. Biol. Chem.* **2003**, *278*(28), 25577−25584.
(25) Jost, M.; Gerke, V. *Biochim. Biophys. Acta.* **1996**, *1313*(3), 283−289.
(26) Zobiack, N.; Rescher, U.; Ludwig, C.; Zeuschner, D.; Gerke, V. *Mol. Biol. Cell* **2003**, *14*(12), 4896−4908.
(27) Benaud, C.; Gentil, B. J.; Assard, N.; Court, M.; Garin, J.; Delphin, C.; Baudier, J. *J. Cell Biol.* **2004**, *164*(1), 133−144.
(28) Yamada, A.; Irie, K.; Hirota, T.; Ooshio, T.; Fukuhara, A.; Takai, Y. *J. Biol. Chem.* **2004**, *280*(7), 6016−6027.
(29) Hoffmann, H. J.; Olsen, E.; Etzerodt, M.; Madsen, P.; Thogersen, H. C.; Kruse, T.; Celis, J. E. *J. Invest. Dermatol.* **1994**, *103*(3), 370−375.
(30) Jiang, W. G.; Watkins, G.; Douglas-Jones, A.; Mansel, R. E. *Int. J. Oncol.* **2004**, *25*(1), 81−85.
(31) El-Rifai, W.; Moskaluk, C. A.; Abdrabbo, M. K.; Harper, J.; Yoshida, C.; Riggins, G. J.; Frierson, H. F., Jr.; Rowell, S. M. *Cancer Res.* **2002**, *62*(23), 6823−6826.
(32) Emberley, E. D.; Niu, Y.; Leygue, E.; Tomes, L.; Gietz, R. D.; Murphy, L. C.; Watson, P. H. *Cancer Res.* **2003**, *63*(8), 1954−1961.
(33) Emberley E. D.; Gietz, R. D.; Campbell, J. D.; HayGlass K. T.; Murphy, L. C.; Watson, P. H. *BMC Cancer* **2002**, *2*(1), 28.
(34) Hagens, G.; Roulin, K.; Hotz, R.; Saurat, J. H.; Hellman, U.; Siegenthaler, G. *Mol. Cell. Biochem.* **1999**, *192*(1−2), 123−128.
(35) Ruse, M.; Broome, A. M.; Eckert, R. L. *J. Invest. Dermatol.* **2003**, *121*(1), 132−141.

PR050163S

Supplementary material

Supplementary figure 1: Protein-protein interaction assay using specific anti-S100A8 antibody or anti-S100A10 antibody. Anti-S100A8 antibody or anti-S100A10 antibody were bound on IDM beads, incubated with crude HaCaT cell extract and binding partners were analysed by SELDI-MS. In the assay using the anti-S100A10 antibody a signal nearly 38,41 kDa was detectable. This signal was neither detectable using anti-S100A8 antibody nor non-specific antibody.

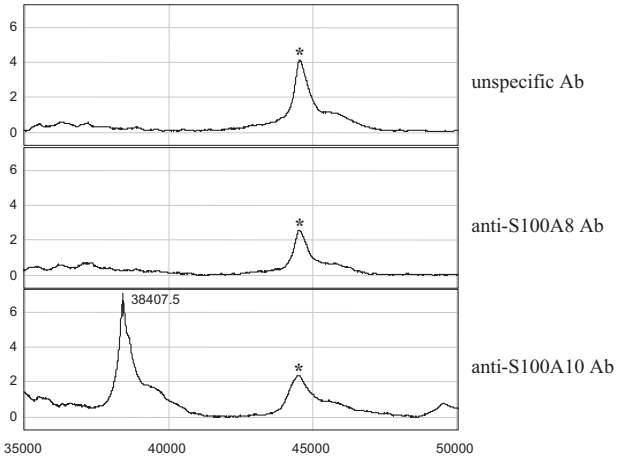

Suppl. Fig. 1

Molecular Biology of the Cell
Vol. 19, 2926–2935, July 2008

Rad54B Targeting to DNA Double-Strand Break Repair Sites Requires Complex Formation with S100A11

Ulrike Murzik,* Peter Hemmerich,† Stefanie Weidtkamp-Peters,†‡ Tobias Ulbricht,† Wendy Bussen,§‖ Julia Hentschel,* Ferdinand von Eggeling,* and Christian Melle*

*Core Unit Chip Application (CUCA), Institute of Human Genetics and Anthropology, Medical Faculty, Friedrich-Schiller-University, 07740 Jena, Germany; †Department of Molecular Biology, Fritz Lipmann Institut (FLI), Leibniz Institute for Age Research, 07708 Jena, Germany; and §Department of Molecular Biophysics and Biochemistry, Yale University School of Medicine, New Haven, CT 06515

Submitted November 20, 2007; Revised March 14, 2008; Accepted April 24, 2008
Monitoring Editor: M. Bishr Omary

S100A11 is involved in a variety of intracellular activities such as growth regulation and differentiation. To gain more insight into the physiological role of endogenously expressed S100A11, we used a proteomic approach to detect and identify interacting proteins in vivo. Hereby, we were able to detect a specific interaction between S100A11 and Rad54B, which could be confirmed under in vivo conditions. Rad54B, a DNA-dependent ATPase, is described to be involved in recombinational repair of DNA damage, including DNA double-strand breaks (DSBs). Treatment with bleomycin, which induces DSBs, revealed an increase in the degree of colocalization between S100A11 and Rad54B. Furthermore, S100A11/Rad54B foci are spatially associated with sites of DNA DSB repair. Furthermore, while the expression of $p21^{WAF1/CIP1}$ was increased in parallel with DNA damage, its protein level was drastically down-regulated in damaged cells after S100A11 knockdown. Down-regulation of S100A11 by RNA interference also abolished Rad54B targeting to DSBs. Additionally, S100A11 down-regulated HaCaT cells showed a restricted proliferation capacity and an increase of the apoptotic cell fraction. These observations suggest that S100A11 targets Rad54B to sites of DNA DSB repair sites and identify a novel function for S100A11 in p21-based regulation of cell cycle.

INTRODUCTION

Proteins may exist in several complexes in a spatial and temporal manner to accomplish distinct functions. Analyses of the interacting partners will provide a strong insight into the physiological role of a particular factor. Therefore, it is essential to identify ideally all interacting partners of proteins in vivo to precisely be able to define their biological function. The investigation of protein complexes of solely endogenously expressed proteins avoid the tendency to detect false positive protein–protein interactions of examinations performed in vitro. A multitude of proteins are involved in both the detection and the repair of DNA damages. It is conceivable that some protein complexes involved in these processes are not yet discovered. A severe form of DNA damage that threaten the integrity of the genome are DNA double-strand breaks (DSBs). DSBs can lead to cell cycle arrest or illegitimate DNA rearrangements that can contribute to cell dysfunction, cell death, or carcinogenesis (Hoeijmakers, 2001). Homologous recombination is a major DNA repair pathway by which DSBs are repaired (Lettier *et al.*, 2006).

For the identification of specific interacting proteins of S100A11 (S100C, calgizzarin) we used in the present study a proteomic approach comprising mass spectrometry and immunological techniques. S100A11 belongs to the group of S100 proteins that are considered as multitasking proteins involved in several biological processes such as the Ca^{2+} signaling network, cell growth and motility, cell cycle progression, transcription, and cell differentiation (Schafer and Heizmann, 1996; Donato, 2001; Eckert *et al.*, 2004). It has been proposed that the S100 proteins are involved in the differentiation of specific tissues including epidermis and that some members of this family are differentially expressed in normal human skin and melanocytic lesions (Boni *et al.*, 1997). In several studies, S100A11 was detected to be up- and down-regulated in different tumors including melanoma (van Ginkel *et al.*, 1998; Chaurand *et al.*, 2001; Melle *et al.*, 2006). S100A11 plays a dual role in growth regulation in human keratinocytes as it is able to mediate a Ca^{2+}-induced growth inhibition as well as it stimulates the growth by enhancement of the level of EGF family proteins (Sakaguchi *et al.*, 2003, 2008). During growth inhibition, S100A11 is specifically phosphorylated by PKCα that is a prerequisite for binding to nucleolin and transfer into the nucleus. In the nucleus, a functional cascade activates the cell cycle modulatory properties of $p21^{WAF1/CIP1}$ (Sakaguchi *et al.*, 2004). The activity of p21 is typically induced by p53 and results in an arrest of the cell cycle in G1 through the

This article was published online ahead of print in *MBC in Press* (http://www.molbiolcell.org/cgi/doi/10.1091/mbc.E07–11–1167) on May 7, 2008.

Present addresses: ‡ Lehrstuhl für Molekulare Physikalische Chemie, Institut für Physikalische Chemie, Heinrich-Heine-Universität Düsseldorf, 40225 Düsseldorf, Germany; ‖ Department of Radiation Oncology, Washington University School of Medicine, St. Louis, MO 63108.

Address correspondence to: Christian Melle (christian.melle@mti.uni-jena.de).

inhibition of CDKs (El-Deiry *et al.*, 1993; Dulic *et al.*, 1994). This allows repair of possible DNA damages before the next replication cycle. In cells containing only a mutated form of p53, alternative induction pathways of the p21 activity occurs, and its expression can be positively regulated through several p53-independent mechanisms (Gartel and Tyner, 1999; Tsuda *et al.*, 2005; Fang *et al.*, 2007). One of these induction mechanisms of p21 seems to be mediated by S100A11 (Sakaguchi *et al.*, 2003). The aim of this study was to identify endogenously expressed interacting partners of S100A11 and to investigate their functional interplay in human cells.

MATERIALS AND METHODS

Cell Culture

The human keratinocyte cell line HaCaT (Boukamp *et al.*, 1988) was cultured in DMEM supplemented with 10% fetal bovine serum.

For protein–protein interaction experiments cells were grown to 80% confluence and were passaged at a split ratio of 1:4. Cells were harvested at 70–90% confluence and lysed in a buffer containing 100 mM sodium phosphate, pH 7.5, 5 mM EDTA, 2 mM $MgCl_2$, 0.1% CHAPS, 500 μM leupeptin, and 0.1 mM PMSF. After centrifugation (15 min; 15,000 rpm) the supernatant was immediately used.

Antibodies

Anti-S100A11 rabbit polyclonal antibody (BC001410; Protein Tech Group, Chicago, IL), anti-Rad54B rabbit polyclonal antibody (Wesoly *et al.*, 2006), anti-Rad54 mouse mAb (ab11055; Abcam, Cambridge, MA), anti-actin rabbit polyclonal antibody (A266; Sigma, St. Louis, MO), and normal rabbit IgG (PeproTech, Rocky Hill, NJ) were used in protein–protein interaction detection assays as well as in coimmunoprecipitation experiments. Anti-S100A11 chicken polyclonal antibody (ab15612; Abcam), anti-Rad54B rabbit polyclonal antibody (Wesoly *et al.*, 2006), anti-SC-35 mouse mAb (S4045; Sigma), anti-Rad54 mouse mAb (ab11055; Abcam), anti-Ku80 mouse mAb (AB-4/N3H10; Labvision, Fremont, CA), anti-PCNA (proliferating cell nuclear antigen) mouse mAb (PC 10; Santa Cruz Biotechnology, Santa Cruz, CA), and anti-γH2AX (Ser139; clone JBW301; Upstate Biotechnology, Lake Placid, NY) were used in two- or three-color immunofluorescence staining as primary antibodies, which were detected with species-specific secondary antibodies linked to fluorescein, Cy3 or Cy5 (Dianova, Rodeo, CA).

Protein–Protein Complex Detection Assay

The protein–protein complex detection assay was described elsewhere (Escher *et al.*, 2007). Briefly, 20 μl of Interaction Discovery Mapping (IDM) beads (Bio-Rad, Richmond, CA) were incubated with 4 μl protein A (Sigma) overnight at 4°C. A pellet was generated by centrifugation, and the supernatant was discarded. The pellet was washed twice with a buffer containing 50 mM sodium acetate, pH 5.0. Afterward, the beads were incubated in a buffer containing 0.5 M Tris/HCl, pH 9.0, 0.1% Triton X-100 for 2 h at room temperature for blocking residual reactive groups. The beads were washed three times with 1× PBS. Thereafter, a specific antibody against human S100A11 or normal rabbit IgG as negative control, in 50 mM sodium acetate, pH 5.0, was applied to the beads and allowed to bind at room temperature for 1 h at 4°C in an end-over-end mixer. Unbound antibody was removed by washing in 50 mM sodium acetate. Afterward, the beads were washed in 1× PBS, 0.1% Triton X-100 and in 1× PBS and incubated with 250 μl of crude HaCaT cell extract for 2 h at 4°C in an end-over-end mixer. The unbound proteins were washed away by sequential washes in PBS, 0.5 M sodium chloride, 0.05% Triton X-100 in PBS, PBS, and aqua bidest. Bound proteins were eluated from the IDM beads by 25 μl 50% acetonitrile/0.5% trifluoroacetic acid and gently vortexed for 30 min. Five microliters of the eluated samples were applied to the activated, hydrophobic surface of an H50 ProteinChip Array (Bio-Rad) and dried on air. After washing with 3 μl aqua bidest, 0.5 μl sinapinic acid (saturated solution in 0.5% TFA/50% acetonitrile) was applied twice and the array was analyzed in a ProteinChip Reader (series 4000; Bio-Rad) according to an automated data collection protocol by SELDI-MS. This includes an average of 265 laser shots to each spot with a laser intensity of 2300 and 3500 nJ, respectively, dependent on the measured region (low = 2.5–20 kDa and high = 20–200 kDa, respectively) and an automatically adapted detector sensitivity.

Peptide Fingerprint Mapping

Peptide fingerprint mapping was carried out as described elsewhere (Escher *et al.*, 2007). In brief, the volume of eluated samples was reduced to a maximum of 10 μl using a speed-vac (ThermoSavant, Fisher Scientific, Pittsburgh, PA) and subjected to SDS-PAGE for separation of containing proteins followed by staining with Simply Blue Safe Stain (Enhanced Coomassie, Invitrogen, Carlsbad, CA). Specific gel bands were excised, destained, and dried, followed by rehydration and digestion with 10 μl of a trypsin solution (0.02 μg/μl; Promega, Madison, WI) at 37°C overnight. The supernatants of the in-gel digestions were applied directly to NP20 arrays (Bio-Rad). After addition of the matrix (CHCA), peptide fragment masses were analyzed using the ProteinChip Reader, series 4000 instrument. A standard protein mix (all-in-1 peptide standard mix; Bio-Rad), including Arg8-vasopressin (1082.2 Da), somatostatin (1637.9 Da), dynorphin (2147.5 Da), ACTH (2933.5 Da), and insulin beta-chain (3495.94 Da) was used for calibration. Proteins were identified using the fragment masses searching in a publicly available database (http://prowl.rockefeller.edu/prowl-cgi/profound.exe).

Coimmunoprecipitation

The coimmunoprecipitation (coIP) assays were carried out as described (Escher *et al.*, 2007). Briefly, specific anti-S100A11 or anti-Rad54B antibody, respectively, or, as negative control, normal rabbit IgG were bound on protein A-agarose beads. Crude extract (100 μl) from HaCaT cells was incubated with the antibody loaded beads for 1 h at 4°C. Then the resins were washed three times with coIP buffer containing 20 mM HEPES/KOH, pH 8.0, 50 mM KCl, 0.1 mM EDTA, and 0.05% CHAPS. Bound proteins were subjected to 10% SDS-PAGE and detected by immunoblotting.

Immunocytochemistry and Confocal Microscopy

Cells grown on coverslips were fixed by treatment with methanol at −20°C for 5 min followed by acetone (prechilled to −20°C) for 2 min or by incubation in 2% paraformaldehyde for 20 min at room temperature followed by acetone treatment (prechilled to −20°C) for 2 min. Immunofluorescence was performed as previously described (von Mikecz *et al.*, 2000). Samples were scanned with a Zeiss LSM 510 laser scanning confocal device attached to an Axioplan 2 microscope using a 63× Plan-Apochromat oil objective (Carl Zeiss, Jena, Germany). Fluorescein, Cy3, or Cy5 dyes were excited by laser light at a 488-, 552-, or 633-nm wavelength, respectively. To avoid bleed-through effects in double- or triple-staining experiments, each dye was scanned independently using the multitracking function of the LSM 510 U. Single optical sections were selected either by eye-scanning the sample in *z*-axis for optimal fluorescence signals or were taken from stack projections. Images were electronically merged using the LSM 510 (Carl Zeiss) software and stored as TIFF files. Figures were assembled from the TIFF files using Adobe Photoshop software (San Jose, CA).

Colocalization Analysis

Colocalization in image pairs was assessed from scatter plots of midnuclear confocal images as described previously (von Mikecz *et al.*, 2000) and quantified using the LSM 510 META software (Carl Zeiss). The colocalization coefficient for two signals was determined according to Manders *et al.* (1993), which provides a value range between 0 and 1 (0, no colocalization; 1, all pixels colocalize). Only signals above a threshold gray value of 100 (of four-bit images, gray value intensity 0–255) were considered for the colocalization analysis.

Induction of DNA Damages by Bleomycin

HaCaT cells were seeded at six-well plates on coverslips for 16 h. DMEM supplemented with 10% fetal calf serum (FCS) was exchanged to fresh DMEM supplemented with 10% FCS, and cells were treated with 12.5 IU/ml bleomycin (BLM). Medium was exchanged after 30 min, and cells were harvested after different time points.

Colony-forming Assay

To assess the survival rate of cells after BLM treatment, 10^4 cells were seeded into 10-cm Petri dishes. After 24 h, the cells were treated with different concentrations of the drug and cultured for another 10 d. In control treatments, single cells had formed colonies of ~30 cells after that time. Colonies were then washed once with PBS, fixed with methanol for 15 min, stained with Giemsa dye, and finally air-dried. The number of colonies formed was then determined.

Small Interfering RNA–mediated Knockdown of S100A11

Small interfering RNA (siRNA) duplex oligonucleotides used in this study are based on the human cDNAs encoding S100A11. S100A11 siRNA as well as a nonsilencing control siRNA were obtained from QIAGEN GmbH (Hilden, Germany). The siRNA sequences applied to target S100A11 were 5′-GAACUAGCUGCCUUCACAAdTdT-3′ (sense) and 5′-UUGUGAAGGCAGCUAGUUCdTdG-3′ (antisense). The siRNA sequences used as negative controls were 5′-UUCUCCGAACGUGUCACGUdTdT-3′ (sense) and 5′-ACGUGACACGUUCGGAGAAdTdT-3′ (antisense). HaCaT (2×10^5) were plated on six-well plates 18 h before transfection and were 50% confluent when siRNA was added. The amount of siRNA duplexes applied was 1.5 μg/well for S100A11. Transfection was performed using the amphiphilic delivery system SAINT-RED (Synvolux Therapeutics B.V., Groningen, The Nether-

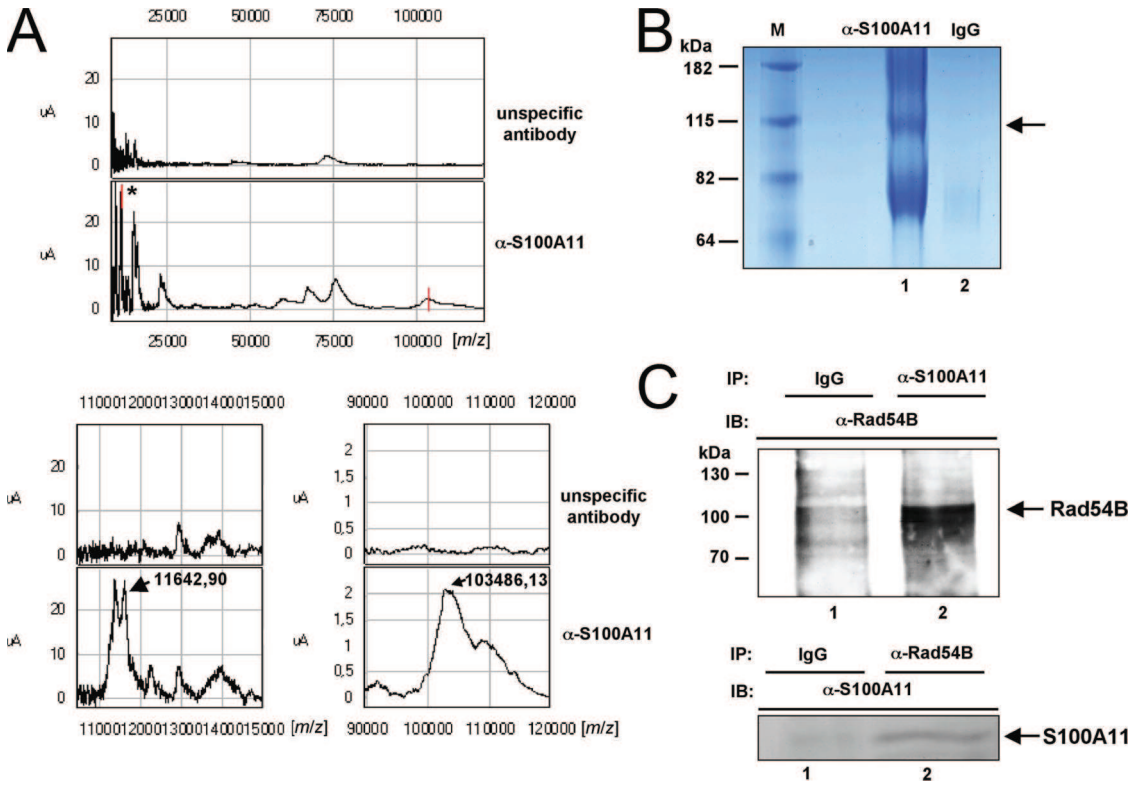

Figure 1. Detection and identification of the DNA-dependent ATPase Rad54B as a specific interacting protein of S100A11 by a protein–protein complex detection assay. (A) An anti-S100A11 antibody was coupled on IDM beads and incubated with HaCaT cell extract. Bound proteins were analyzed by SELDI-MS. Top, spectra of the measured area of m/z 0–120,000; bottom, the enlarged area of m/z 11,000–13,000 or m/z 90,000–120,000, respectively. A number of specific peaks were detectable in the assay using the S100A11 antibody compared with the experiments using an unspecific antibody. Among a signal of approx. 11.7 kDa, which corresponds well to the relative molecular mass of S100A11 (labeled by a peak tic and an asterisk in the top panel), a signal at approx. 103.5 kDa was detectable (labeled by peak tic only in the top panel) using the specific anti-S100A11 antibody. Both signals were absent in the assay using an unspecific antibody. (B) Eluted proteins from IDM beads were subsequently subjected on an SDS-PAGE for separation and a specific band at ~105 kDa (labeled by an arrow) was excised and used for a tryptic in-gel digestion. Peptide mass fingerprints obtain from digestion were analyzed by SELDI-MS and used for a database quest that revealed Rad54B. (C) For an unequivocally confirmation of this result, a coimmunoprecipitation was used. Thereby, a specific anti-S100A11 antibody was capable to precipitate Rad54B from HaCaT cell extract as shown in an immunoblot (lane 2). coIP using an unspecific antibody detected no signal (lane 1). In a reciprocal experiment an anti-Rad54B antibody precipitated S100A11 (lane 2, bottom panel) compared with the negative control (lane 1, bottom panel).

lands) according to the manufacturer's instructions. Briefly, siRNA was complexed with 15 nmol of transfection reagent and added to the cells for 4 h. Subsequently, 2 ml of culture medium was added and incubation proceeded for 72 h.

In colony-forming assays as well as in flow-cytometric experiments, HaCaT cells were retransfected with the specific S100A11 siRNA or a nonsilencing control siRNA after 72 h for a stable down-regulation of S100A11.

RESULTS

Identification of Rad54B as an Interacting Protein of S100A11

S100A11 appears to be involved in a number of cellular processes. Therefore, it is assumed that S100A11 interacts with a number of specific proteins to achieve several functions. It is conceivable that some of these interacting partners are not yet discovered. For this reason, we first performed a protein–protein complex detection assay to identify interacting proteins of endogenously expressed S100A11 in crude extracts of HaCaT cells, an immortalized human keratinocyte line (Boukamp *et al.*, 1988). This assay was used previously for the identification of protein complexes involved in cell cycle regulation as well as of the transcription machinery (Escher *et al.*, 2007; Kob *et al.*, 2007). S100A11-containing protein complexes were captured by a specific antibody against S100A11 coupled to IDM beads followed by elution of the captured proteins and analysis of the complex composition using SELDI-MS (Figure 1A). Hereby, a specific signal possessing an m/z of 11642 was detected that corresponds very well to the relative molecular mass of S100A11. Beside this signal and other specific peaks, we captured an additional specific signal of approx. 103 kDa. Signals derived from S100A11 and at 103 kDa were absent in the negative control using an unspecific antibody. For identification of the 103-kDa signal we subjected the eluted proteins to SDS-PAGE and detected a specific band in the range of approx. 105 kDa. Thus, we confirmed the presence of a specific S100A11-interacting protein. The negative control using rabbit IgG as unspecific antibody did not show a band at that position (Figure 1B). This specific band was excised from the gel and subsequently subjected to an in-gel digestion by trypsin and protein identification. As a control, an empty gel piece underwent the same treatment. The digest yielded solution was spotted on a NP20 array and the peptide mass fingerprints (PMF) were determined by SELDI-MS. Database searches (Profound; http://prowl.rockefeller.edu/prowl-cgi/profound.exe) revealed Rad54B as the best candi-

date with an estimated Z-score of 1.33. Rad54B is a homolog of the DNA repair and recombination protein RAD54 as well as a DNA-dependent ATPase and seems to play an unique role in homologous recombination (Miyagawa *et al.,* 2002; Tanaka *et al.,* 2002). Additionally and as an internal control for the detection of protein–protein interactions in vivo using our approach, we confirmed the well-known protein interaction between S100A11 and actin (Supplemental Figure S1; Xhao *et al.,* 2000). The protein complex between S100A11 and actin occurs temporally and spatially in a manner different from the complex containing S100A11 and Rad54B, because S100A11 interacts with actin exclusively in the cytoplasm.

To confirm the presence of protein complexes containing S100A11 and Rad54B, coIP experiments were carried out with crude extracts of HaCaT cells. In line with the previously determined results, a specific antibody that recognizes S100A11 was able to coprecipitate Rad54B (Figure 1C, top panel). In the negative control using an unspecific antibody, a clear signal corresponding to Rad54B was not detectable. Additionally, we were able to coprecipitate S100A11 by a specific anti-Rad54B antibody in a reciprocal coIP (Figure 1C, bottom panel). Hereby, we detected an, albeit slight, but clearly detectable signal compared with the negative control using the unspecific antibody. A reason for this only slightly coprecipitated signal corresponding to S100A11 might be that solely endogenous proteins were investigated. These results suggest that endogenous S100A11 and endogenous Rad54B exist, at least transiently, in one and the same stable protein complex.

S100A11 and Rad54B Colocalize in the Nucleus of Human Cells

Afterward, we examined the subcellular localization of S100A11 and Rad54B by immunofluorescence experiments on HaCaT cells followed by confocal laser scanning microscopy. S100A11 is described to localize predominantly in the nucleus of gliomablastoma cells and in both, the cytoplasm and the nucleus of normal human epidermis cells (Inada *et al.,* 1999; Broome *et al.,* 2003). Rad54B was described to contribute to homologous recombination-mediated DNA damage repair (Wesoly *et al.,* 2006). On the basis of this function, Rad54B is expected to predominantly localize to the nucleus. Both S100A11 as well as Rad54B were found concentrated at discrete sites throughout the nucleoplasm of human HaCaT cells (Figure 2). The colocalization analysis revealed significant, albeit not complete, overlap between S100A11 and Rad54B in this foci-like pattern. These observations are consistent with the finding that S100A11 and Rad54B reside within the same complexes endogenously (Figure 1) and suggest that these complexes are enriched in a dot-like pattern within the nucleoplasm. No or very little colocalization could be detected between S100A11 or Rad54B, respectively, and the non-snRNP (small nuclear ribonucleoproteins) splicing factor SC-35, which concentrates in a speckle like pattern (Supplemental Figure S2; Bisotto *et al.,* 1995). This result indicates that the regions of overlap between S100A11 and Rad54B are not coincidental (see also Figure 3B). In contrast to these results, a protein–protein interaction or colocalization, respectively, between S100A11 and Rad54 was neither detectable in coIP experiments nor in immunofluorescence experiments (Supplemental Figure S3).

Complex Formation between S100A11 and Rad54B Is Stimulated by DNA Damage

It is supposed that Rad54B plays an unique role in homologous recombination (Miyagawa *et al.,* 2002). Homologous recombination is one of the major repair pathways when DSBs occur as a consequence of application of DNA-damaging agents (Wolner *et al.,* 2003). We therefore determined whether BLM, a DNA-damaging agent, would influence the dynamics of the colocalization between S100A11 and Rad54B in HaCaT cells. First, we determined BLM treatment conditions that induced the formation of DSBs but would not kill the cells (Supplemental Figure 4). H2AX becomes phosphorylated as one of the first cellular responses after DNA damage and forms foci at sites of DSBs (Rogakou *et al.,* 1998). Incubation of U2OS cells with 12.5 IU/ml for 30 min was sufficient to produce 30–40 γH2AX foci 3 h after drug application. After 24 h the number of γH2AX foci dropped to control levels, indicating successful repair of most, if not all, DNA DSBs. A colony-forming assay of cells treated with increasing amounts of BLM confirmed that cells treated with 12.5 IU/ml BLM are viable, proliferate, and had therefore successfully repaired their DSBs. Similar results were obtained with both U2OS and HaCaT cells.

Qualitatively, the induction of DNA DSBs in HaCaT cells by BLM treatment caused an obvious increase of colocalization between S100A11 and Rad54B during the repair process, as indicated by an increase in yellow signals over time (Figure 3A). This up-regulation was accompanied by an increase of coprecipitated Rad54B/S100A11 complexes (Figure 3B). The degree of colocalization in the nucleus was therefore quantitated during the complete repair cycle (Figure 3C). A significant increase in colocalization between nuclear S100A11 and Rad54B foci was already observed 30 min after BLM application. Colocalization persisted at that high level for 3 h, after which it decreased again to pretreatment levels (Figure 3C). Interestingly, the kinetics of colocalization between S100A11 and Rad54B perfectly mirrored the kinetics of the DNA DSB repair based on γH2AX foci formation (compare Figure 3C and Supplemental Figure S4). The colocalization of S100A11 and Rad54B at sites of DNA DSB repair appears to be specific and not coincidental because the degree of colocalization between either S100A11 or Rad54B with foci containing the functionally unrelated splicing factor SC-35 (speckles) was significantly smaller after BLM treatment (Figure 3C).

To assess if this protein complex is specifically linked to DNA damage sites, we next carried out three-color confocal immunostaining to simultaneously detect S100A11, Rad54B,

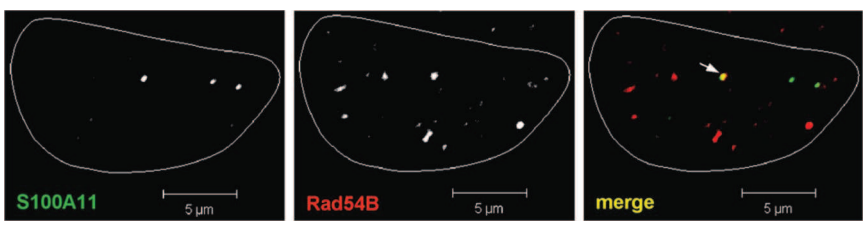

Figure 2. Colocalization of S100A11 and Rad54B in the nucleoplasmic foci. Fixed HaCaT cells were coimmunostained with anti-S100A11 (green) and anti-Rad54B antibody (red). The merged image reveals significant colocalization between S100A11 and Rad54B in a dot-like pattern throughout the nucleoplasm of HaCaT cells. A colocalized S100A11/Rad54B complex is labeled by an arrow.

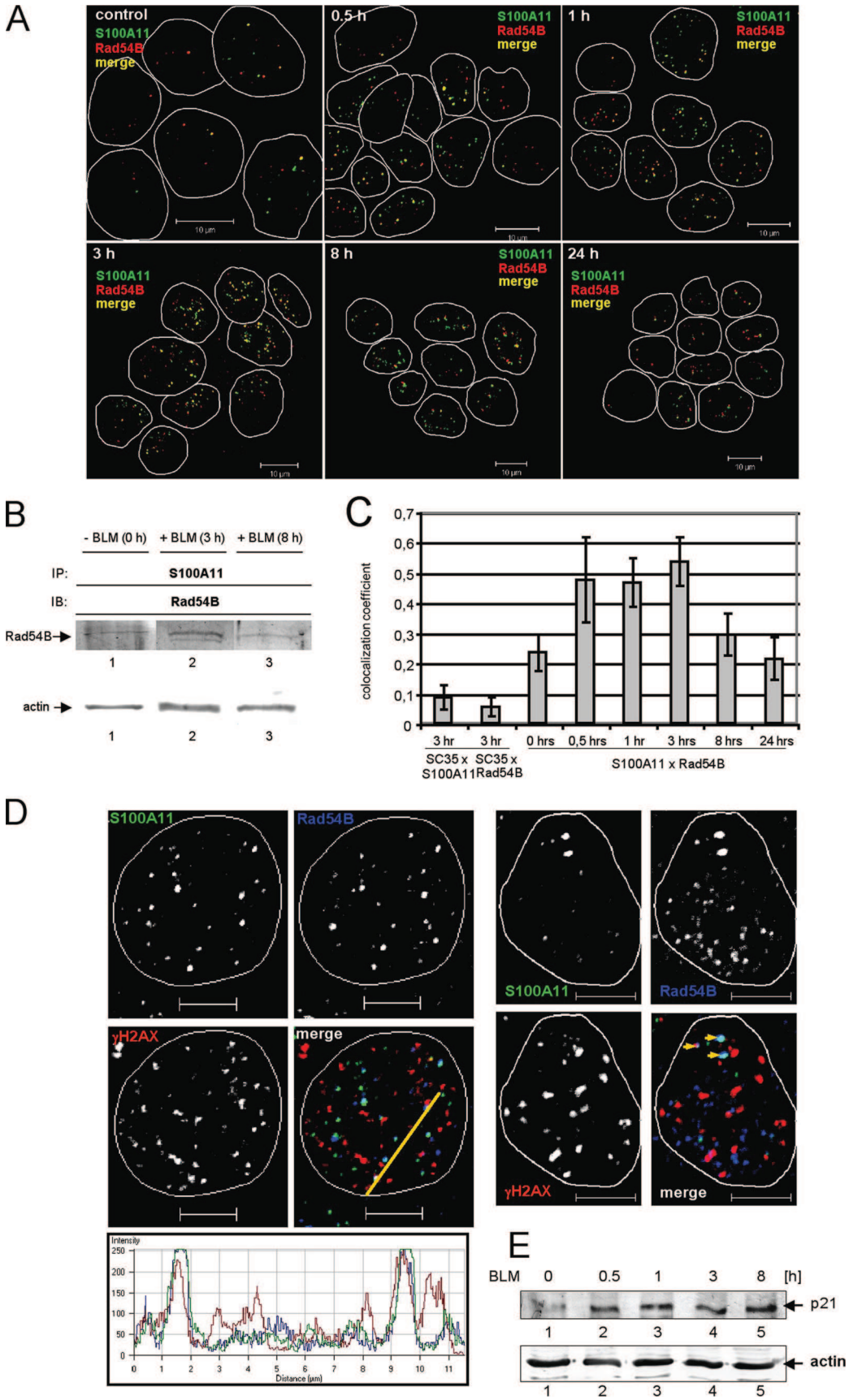

Figure 3. DNA DSBs induce an increase in S100A11/Rad54B foci formation. (A) HaCaT cells were treated with bleomycin (BLM; 12.5 μg ml^{-1}) and analyzed by two-color immunostaining followed by laser scanning microscopy for S100A11 (green) and for Rad54B (red) or

and γH2AX. We detected focal colocalization of S100A11, Rad54B, and γH2AX in the nucleoplasm of HaCaT cells (Figure 3D). This result indicates that a significant subfraction of S100A11 and Rad54B is colocalized directly at sites of DNA damage. Many, but not all γH2AX foci colocalized with S100A11/Rad54B, clearly indicating that at any given time during the DSB repair process only a subpopulation of repair sites is associated with S100A11/Rad54B foci. Recently, an induction of p21 after transfer of S100A11 into the nucleus has been shown (Sakaguchi *et al.,* 2003). Therefore, we also assessed the dynamics of p21 protein expression in HaCaT cells treated with BLM (Figure 3E). Hereby, we were able to detect an increased expression of p21 already 30 min after BLM treatment by immunoblotting.

Additionally, we asked whether the S100A11/Rad54B complex is associated both, with other DNA repair processes such the nonhomologous end joining (NHEJ) or sites of DNA damage induced by stalled replication forks. To this end, we assessed the distribution of S100A11, Rad54B, and Ku80 in HaCaT cells treated with BLM. No or very little colocalization was detectable between S100A11, Rad54B, and Ku80 (Supplemental Figure S5). Interestingly, a colocalization between S100A11 and Rad54B was also detectable here. To assess if the S100A11/Rad54B complex is involved in repair processes triggered by arrested replication, we carried out three-color confocal immunostaining to simultaneously detect S100A11, Rad54B, and PCNA. This allowed investigation of HaCaT cells at different cell cycle phases. Because PCNA redistributes throughout S phase with the same dynamic pattern of endogenous replication factories, its localization pattern discriminates between early, mid- and late replication (Somanathan *et al.,* 2001). Neither in G1 or G2, nor at any stage of S phase did we observe a colocalization between S100A11/Rad54B and PCNA (Supplemental Figure S6). The S100A11/Rad54B complex was again detectable, above all in cells that are in G2 phase.

Figure 3 (cont). merged at different time points as indicated. (B) CoIP of Rad54B by a specific anti-S100A11 antibody from HaCaT cell extracts. HaCaT cells were treated with BLM for 3 h (lane 2) or 8 h (lane 3) or as a control, cells were untreated (lane 1). As a control for equal protein loading corresponding actin levels were shown by immunoblot. (C) Quantification of the increase in colocalization between S100A11 and Rad54B in HaCaT cells after DNA DSB induction. The colocalization coefficient was determined as described in *Materials and Methods* in nuclei of cells treated as described in A. At least 20 nuclei were analyzed per time point. Data are displayed as mean values (±SD). The colocalization coefficient was also determined from SC-35/S100A11 and SC-35/Rad54B colocalization experiments of cells after 3 h of BLM treatment. (D) Examples of fixed HaCaT cells that were analyzed by three-color immunostaining followed by laser scanning microscopy for S100A11 (green), Rad54B (blue), and γH2AX (red) at DNA damage sites 1 h after BLM treatment. The intensities of the immunofluorescences in one cell derived from the Rad54B signal (blue), the γH2AX signal (red) and the S100A11 signal (green) are shown in a linescan (left panel; bottom side of the overlay). In the other example cell (right panel), multiple colocalizations of S100A11/Rad54B complexes with γH2AX foci corresponding to DNA damage sites are labeled by arrows (yellow); Bar, 5 μm. (E) Increased expression of p21 was already detectable after 30 min (lane 2) in HaCaT cells treated by BLM. As a control for equal protein loading corresponding actin levels were shown below. Lane 1, control; lane 2, 0.5 h after BLM treatment; lane 3, 1 h after BLM treatment; lane 4, 3 h after BLM treatment; lane 5, 8 h after BLM treatment.

Appearance of Rad54B Foci Is Dependent on the S100A11 Protein Status

To assess whether S100A11 has an effect on Rad54B targeting to DNA damage sites, we used RNA interference to down-regulate S100A11 protein levels. A significant reduction of the S100A11 protein level was detectable 72 h after transfection. S100A11 down-regulated HaCaT cells that were treated for 1 h with BLM to induce DSBs demonstrated a diffuse nucleoplasmatic localization pattern of Rad54B that was clearly different from the foci-like pattern in untreated cells or cells treated with control siRNA (Figure 4A). In HaCaT cells transfected with control siRNA the colocalization between the S100A11/Rad54B foci at sites of DNA damage repair was indistinguishable from nontreated cells (compare Figures 4A and 3C). Most strikingly, colocalization between Rad54B and γH2AX was abolished in cells with down-regulated S100A11 levels. Thus, the appearance of Rad54B foci at DSB repair sites depends on the S100A11 protein status and not on the induction of DNA damages by BLM. Quantitation of the Rad54B nuclear localization pattern in S100A11 down-regulated versus control-treated cells confirmed the above observations (Figure 4B).

We finally assessed the impact of reduced S100A11 levels on p21 expression in HaCaT cells by Western blotting. Surprisingly, this analysis revealed a significant reduction in p21 protein levels when S100A11 expression was down-regulated by siRNA. This reduction of p21 was independent of BLM treatment of HaCaT cells (Figure 4C). The level of Rad54B persisted unaffected by down-regulation of S100A11. These observations demonstrate that S100A11 is required for both Rad54B accumulation at sites of DNA DSB repair and for maintenance of p21 levels during the DNA damage response.

Depletion of S100A11 Influenced the Proliferation Capacity of HaCaT Cells

To analyze a possible impairment of DNA repair by abolishing the S100A11–Rad54B interaction, we quantified the repair of DNA DSBs by immunofluorescence-based detection of γH2AX foci (Rogakou *et al.,* 1999; Kegel *et al.,* 2007). HaCaT cells were transfected with a specific S100A11 siRNA and γH2AX foci appearance was assessed after 1 or 3 h after BLM treatment. DSB repair by homologous recombination is nearly completed after 3 h (Chai *et al.,* 2005). Only minor or no differences in the number of γH2AX foci were detectable at the different time points in S100A11 down-regulated HaCaT cells compared with cells transfected with a control siRNA (Figure 5A). Because there is a correlation between γH2AX loss and DSB repair activity at low, but not high, cytotoxic doses (Bouquet *et al.,* 2006; Markova *et al.,* 2007), we analyzed the proliferation capacity of S100A11 down-regulated HaCaT cells compared with control cells. First, we assessed HaCaT cells transfected with control or S100A11-specific siRNA in colony-forming assays (Figure 5B). Thereby, we detected a significant decrease of colony formation of S100A11 down-regulated HaCaT cells compared with the control. This decrease of colony formation was even reinforced when HaCaT cells were treated with BLM for 30 min. When S100A11 was down-regulated in HaCaT cells, the proliferation capacity and thus the number of these cells was limited. Hence, we also investigated if the restricted proliferation capacity of S100A11 down-regulated cells is reflected in a change of cell cycle transition or increased apoptosis rate. Flow-cytometric analysis of S100A11 down-regulated HaCaT cells that were treated

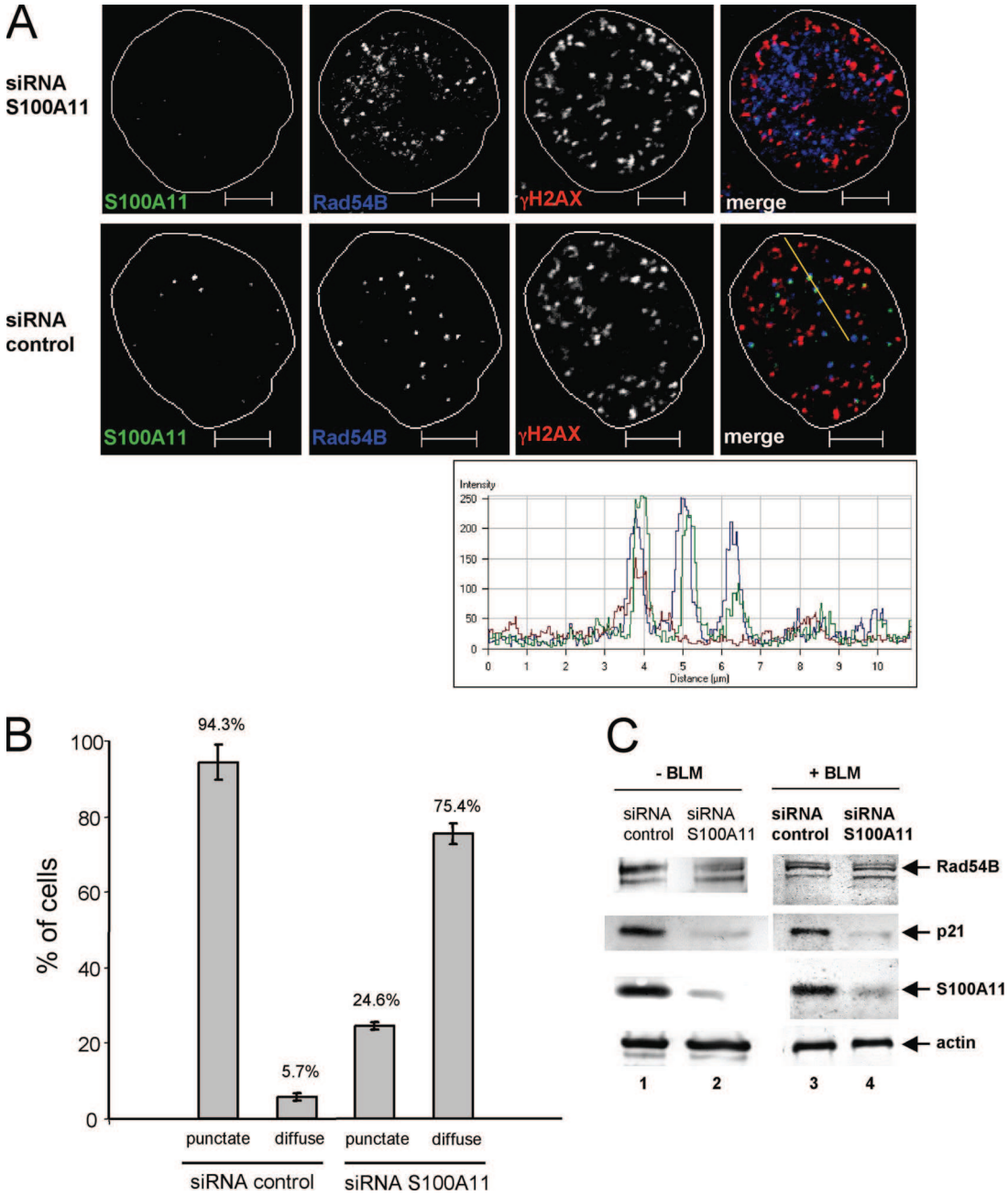

Figure 4. S100A11 is required for Rad54B foci formation. (A) HaCaT cells were transfected with specific siRNA for depletion of S100A11 (siRNA S100A11) or, as a control, nonsilencing siRNA (siRNA control), respectively, and treated by BLM for 1 h followed by immunostaining against S100A11 (green), Rad54B (blue), and γH2AX (red) using specific antibodies. The overlay image (merge) shows that S100A11/Rad54B foci formation significantly overlaps with sites of DNA damage repair in experiments using cells transfected with control siRNA (bottom panel). HaCaT cells transfected with specific S100A11 siRNA oligos show a diffuse nucleoplasmatic localization pattern of Rad54B and no colocalization with γH2AX (top panel). In the image derived from the control experiment, a merged signal with complete overlap between S100A11, Rad54B and γH2AX is indicated in a linescan (bottom panel). Bar, 5 μm. (B) Quantitation of alterations in the Rad54B nuclear distribution pattern after S100A11 knockdown. HaCaT cells were treated as in A and the nuclear distribution pattern of Rad54B was assessed in cells transfected with control siRNA (n = 70) or oligos specific for S100A11 (n = 65). (C) Down-regulation of p21 after knockdown of S100A11. Protein extracts of HaCaT cells transfected with specific S100A11 siRNA (lane 2) or, as a control, nonsilencing siRNA (lane 1), respectively, as well as HaCaT cells treated as in A (lanes 3 and 4) were subjected to immunoblotting against S100A11, p21, and Rad54B using specific antibodies. As a control for equal protein loading corresponding actin levels were shown by immunoblot.

with BLM revealed a significant increase of the sub-G1/apoptotic cell fraction compared with BLM treated control HaCaT cells (Figure 5C). The sub-G1/apoptotic cell fraction of control HaCaT cells was similar to those of wild-type HaCaT cells without BLM treatment. The simultaneous down-regulation of p21 in S100A11 down-regulated HaCaT cells might explain an accelerated transition in the cell cycle from G1 to S phase and thus a smaller G1 cell fraction compared with cells transfected with the control siRNA.

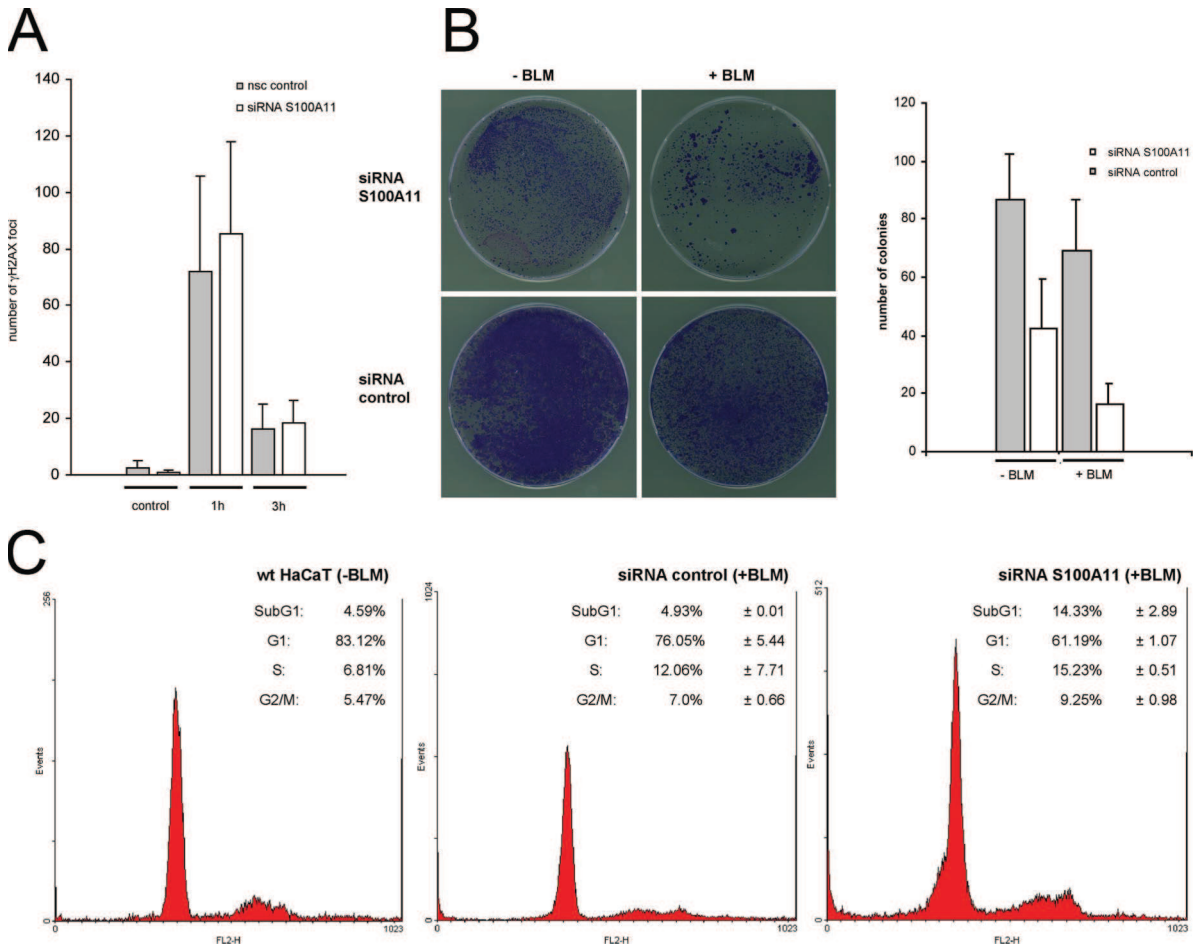

Figure 5. S100A11 down-regulated HaCaT cells possesses a restricted proliferation capacity. (A) Quantification of DNA DSB repair by immunofluorescence-based detection of γH2AX foci in HaCaT cells transfected with a specific S100A11 siRNA (white bars) or, as a control, with a nonsilencing control siRNA (gray bars). Transfected cells were treated with BLM for 30 min and number of γH2AX foci was counted 1 h and 3 h after BLM treatment as well as in untreated cells (control). (B) For analysis of the proliferation capacity of HaCaT cells colony forming assays were carried out. HaCaT cells were transfected as in A, treated by BLM 72 h after transfection and grown for a further 7 d (+BLM). As a control, transfected cells grown without BLM treatment (−BLM). For quantification, the colonies in 10 representative areas (0.5-cm diameter) of Petri dishes with transfected HaCaT cells with (+BLM) or without (−BLM) BLM treatment were counted. □, cells transfected with specific S100A11 siRNA; ▨, cells transfected with a nonsilencing control siRNA. (C) Flow-cytometric analysis of cell cycle phases of HaCaT cells transfected as in A, which were treated by BLM for 30 min. Additionally, the flow-cytometric analysis of wild-type HaCaT keratinocytes (HaCaT control [-BLM]) without BLM treatment is shown as a control. Percentage (±SD) of cells in cell cycle phases is displayed in the diagrams.

DISCUSSION

In this study we used a proteomic approach comprising SELDI mass spectrometry and immunological techniques to identify in vivo interacting partners of S100A11. In this way, we detected a protein complex between endogenously expressed S100A11 and Rad54B in the human keratinocyte cell line HaCaT. A possible functional connection between S100A11 and Rad54B was further characterized by immunofluorescence experiments followed by confocal microscopy. It is believed that this phosphorylation of S100A11 causes dissociation of S100A11 from actin filaments as a prerequisite for its nuclear translocation (Sakaguchi *et al.*, 2000). To simulate physiological conditions, we relinquished at additional Ca^{2+} in our protein–protein interaction detection approach. Previously, we showed that the detection of protein interactions of S100 proteins is not dependent on additional Ca^{2+} (Lehmann *et al.*, 2005). In addition, an increase of the Ca^{2+} concentration may result in an at least transient destabilization of protein complexes containing S100 proteins (Rosenberger *et al.*, 2007). The specific S100A11–Rad54B protein complex formation was further consistent with our two-color immunofluorescence experiments. Hereby, we detected extensive colocalization between S100A11 and Rad54B in small and discrete focal sites throughout the nucleoplasm of several cell lines. Rad54B plays an unique role in homologous recombination-mediated DNA damage repair and appears in complexes after replication arrest resulting from stalled replication forks (Otterlei *et al.*, 2006; Wesoly *et al.*, 2006). Collapsed replication forks can lead to DSBs that are repaired predominantly by homologous recombination (Amaudeau *et al.*, 2001). After induction of DNA damages one of the first cellular responses is phosphorylation of H2AX at the sites of DSB (Rogakou *et al.*, 1998). The subsequent time- and space-regulated accumulation of specific repair factors appears to be essential during DSB repair and signaling (Bekker-Jensen *et al.*, 2006). The accumulation of γH2AX foci has also been found in both apoptotic and senescent human cells

(Rogakou *et al.*, 2000; Sedelnikova *et al.*, 2004). Previously, it was described that γH2AX colocalizes with specific repair factors, for instance Rad51, at nuclear foci after DNA damage (Paull *et al.*, 2000). From our observations we conclude that both, Rad54B and S100A11 share this feature with other DNA repair factors. In this context we propose a novel function for S100A11 in the DNA double-strand process that likely involves DNA repair activity and/or signaling. Rad54B is able to stimulate homologous recombination by interaction with both Dmc1 and Rad51 (Sehorn *et al.*, 2004; Wesoly *et al.*, 2006). We show here that formation of the S100A11–Rad54B protein complex is stimulated by DNA damage and that the kinetics of complex formation appears to be directly correlated with the activity of the DSB repair machinery during successful repair cycles. Moreover, the focal colocalization pattern of S100A11/Rad54B was extensively, albeit not exclusively, spatially associated with sites of DSB repair as detected by γH2AX foci formation. The stimulation of the complex formation between S100A11 and Rad54B is obviously time dependent, with the highest number of S100A11–Rad54B complexes after approx. 3 h. These kinetics are also similar to the temporal stimulation of the Dmc1 recombinase-mediated DNA strand exchange activity by Rad54B (Sarai *et al.*, 2006). As reported, after transfer of S100A11 into the nucleus, an induction of the CDK inhibitor $p21^{WAF1/CIP1}$ is initiated (Sakaguchi *et al.*, 2003). In the present study, we were able to detect elevated p21 protein levels after treatment of HaCaT cells with BLM. The activation of p21 must be p53 independent because HaCaT cells possess only a mutated inactive form of p53 that is not able to induce p21 (Lehman *et al.*, 1993; Yoon and Smart, 2004). A Chk2-induced cellular senescence was associated with p21 expression that was also p53-independent (Chen *et al.*, 2005). The Chk2-induced senescence in HaCaT cells is dependent on a Chk2-mediated up-regulation of p21 (Aliouat-Denis *et al.*, 2005). A functional link between p21-mediated cell cycle regulation and Rad51 is suggested in mammalian cells because Rad51 expression, Rad51 foci formation, and p21 expression are interrelated. Furthermore, increase of p21 levels can be induced by Rad51 overexpression independent of p53 (Raderschall *et al.*, 2002).

As reported here, the S100A11–Rad54B complex occurred in discrete foci in the nucleoplasm of untreated cells as well as in cells treated by BLM where this complex was detectable directly at sites of DNA damages. This specific pattern changed completely when S100A11 was down-regulated by RNA interference. In this case, Rad54B appeared in a more diffuse nucleoplasmatic localization pattern and, most strikingly, Rad54B targeting to DSBs was abolished. An alteration of the Rad54B distribution pattern from a diffuse localization pattern to discrete foci representing stalled replication forks was also observed in HeLa cells treated with mitomycin (Otterlei *et al.*, 2006) at concentrations that induce DNA DSBs at such sites (Mogi and Oh, 2006). Our observations therefore indicate that S100A11 may be required to dynamically relocate Rad54B to or from sites of DSBs. We also demonstrated that elimination of Rad54B from sites of DSB repair after S100A11 depletion caused no significant differences in the number of γH2AX foci in compare to control cells. These data correlate with a report that demonstrated very little sensitivity of Rad54B knockout HCT116 cells to ionizing radiation (IR) and mitomycin C (MMC) compared with wild-type cells (Miyagawa *et al.*, 2002). When Rad54B targeting to DSB is abolished, the homolog protein Rad54 might adopt this task in the repair processes. It was recently shown that Rad54B-deficient mice ES cells possess only slight sensitivity to IR and MMC and a more pronounced phenotype in response to MMC in the additional absence of Rad54 (Wesoly *et al.*, 2006). Interestingly, p21 protein levels were also reduced in repairing cells when S100A11 was down-regulated. This observation suggests that S100A11, besides its Rad54B targeting function, is also involved in the regulation of p21 protein levels. In this context, we report here that S100A11 down-regulation caused a restriction of the proliferation capacity of HaCaT keratinocytes. Concurrently, an increase of the apoptotic cell fraction of S100A11 down-regulated HaCaT cells was detectable. This is not surprising as p21 can act, beside its function in the DNA damage response, as an inhibitor of apoptosis in a number of systems (Gartel and Tyner, 2002). On the basis of these observations we speculate that S100A11 provides a direct link between the repair machinery at DNA DSBs and the signaling machinery that controls cell cycle progression. We currently investigate this possible connection.

ACKNOWLEDGMENTS

We thank Dr. Patrick Sung (Yale University School of Medicine) for critical advice and Ralf Schmidt for technical assistance. This study was supported by a grant from the Wilhelm Sander-Stiftung to C.M.

REFERENCES

Aliouat-Denis, C. M. *et al.* (2005). p53-independent regulation of p21Waf1/Cip1 expression and senescence by Chk2. Mol. Cancer Res. *3*, 627–634.

Amaudeau, C., Lundin, C., and Helleday, T. (2001). DNA double-strand breaks associated with replication forks are predominantly repaired by homologous recombination involving an exchange mechanism in mammalian cells. J. Mol. Biol. *307*, 1235–1245.

Bekker-Jensen, S., Lukas, C., Kitagawa, R., Melander, F., Kastan, M. B., Bartek, J., and Lukas, J. (2006). Spatial organization of the mammalian genome surveillance machinery in response to DNA strand breaks. J. Cell Biol. *173*, 195–206.

Bisotto, S., Lauriault, P., Duval, M., and Vincent, M. (1995). Colocalization of a high molecular mass phosphoprotein of the nuclear matrix (p255) with spliceosomes. J. Cell Sci. *108*, 1873–1882.

Boni, R., Burg, G., Dogouglu, A., Ilg, E. C., Schafer, B. W., Muller, B., and Heizmann, C. W. (1997). Immunohistochemical localization of the Ca^{2+} binding S100 proteins in normal human skin and melanocytic lesions. Br. J. Dermatol. *137*, 39–43.

Boukamp, P., Petrussevska, R. T., Breitkreutz, D., Hornung, J., Markham, A., and Fusenig, N. E. (1988). Normal keratinization in a spontaneously immortalized aneuploid human keratinocyte cell line. J. Cell Biol. *106*, 761–771.

Bouquet, F., Muller, C., and Salles, B. (2006). The loss of gammaH2AX signal is a marker of DNA double strand breaks repair only at low levels of DNA damage. Cell Cycle *5*, 1116–1122.

Broome, A. M., Ryan, D., and Eckert, R. L. (2003). S100 protein subcellular localization during epidermal differentiation and psoriasis. J. Histochem. Cytochem. *51*, 675–685.

Chai, B., Huang, J., Cairns, B. R., and Laurent, B. C. (2005). Distinct roles for the RSC and Swi/Snf ATP-dependent chromatin remodelers in DNA double-strand break repair. Genes Dev. *19*, 1656–1661.

Chaurand, P., DaGue, B. B., Pearsall, R. S., Threadgill, D. W., and Caprioli, R. M. (2001). Strain-based sequence variations and structure analysis of murine prostate specific spermine binding protein using mass spectrometry. Proteomics *1*, 1320–1326.

Chen, C. R., Wang, W., Rogoff, H. A., Li, X., Mang, W., and Li, C. J. (2005). Dual induction of apoptosis and senescence in cancer cells by Chk2 activation: checkpoint activation as a strategy against cancer. Cancer Res. *65*, 6017–6021.

Donato, R. (2001). S100, a multigenic family of calcium-modulated proteins of the EF-hand type with intracellular and extracellular functional roles. Int. J. Biochem. Cell Biol. *33*, 637–668.

Dulic, V., Kaufmann, W. K., Wilson, S. J., Tlsty, T. D., Lees, E., Harper, J. W., Elledge, S. J., and Reed, S. I. (1994). p53-dependent inhibition of cyclin-dependent kinase activities in human fibroblasts during radiation-induced G1 arrest. Cell *76*, 1013–1023.

Eckert, R. L., Broome, A. M., Ruse, M., Robinson, N., Ryan, D., and Lee, K. (2004). S100 proteins in the epidermis. J. Invest. Dermatol. *123*, 23–33.

El-Deiry, W. S., Tokino, T., Velculescu, V. E., Levy, D. P., Parson, R., Trent, J. M., Lin, D., Mercer, W. E., Kinzler, K. W., and Vogelstein, B. (1993). WAF1, a potential mediator of p53. Cell *75*, 817–825.

Escher, N., Kob, R., Tenbaum, S. P., Eisold, M., Baniahmad, A., von Eggeling, F., and Melle, C. (2007). Various members of the E2F transcription factor family interact in vivo with the corepressor Alien. J. Proteome Res. *6*, 1158–1164.

Fang, Z., Fu, Y., Liang, Y., Li, Z., Zhang, W., Jin, J., Yang, Y., and Zha, X. (2007). Increased expression of integrin beta1 subunit enhances p21(WAF1/Cip1) transcription through the Sp1 sites and p300-mediated histone acetylation in human hepatocellular carcinoma cells. J. Cell. Biochem. *101*, 654–664.

Gartel, A. L., and Tyner, A. L. (1999). Transcriptional regulation of the p21(WAF1/CIP1) gene. Exp. Cell Res. *246*, 280–289.

Gartel, A. L., and Tyner, A. L. (2002). The role of the cyclin-dependent kinase inhibitor p21 in apoptosis. Mol. Cancer Ther. *1*, 639–649.

Hoeijmakers, J. H. (2001). Genome maintenance mechanisms for preventing cancer. Nature *411*, 366–374.

Inada, H., Naka, M., Tanaka, T., Davey, G. E., and Heizmann, C. W. (1999). Human S100A11 exhibits differential steady-state RNA levels in various tissues and a distinct subcellular localization. Biochem. Biophys. Res. Commun. *263*, 135–138.

Kegel, P., Riballo, E., Kühne, M., Jeggo, P. A., and Löbrich, M. (2007). X-irradiation of cells on glass slides has a dose doubling impact. DNA Repair *6*, 1692–1697.

Kob, R., Baniahmad, A., Escher, N., von Eggeling, F., and Melle, C. (2007). Detection and identification of transcription factors as interaction partners of Alien in vivo. Cell Cycle *6*, 393–396.

Lehman, T. A. *et al.* (1993). p53 mutations in human immortalized epithelial cell lines. Carcinogenesis *14*, 833–839.

Lehmann, R., Melle, C., Escher, N., and von Eggeling, F. (2005). Detection and identification of protein interactions of S100 proteins by ProteinChip technology. J. Proteome Res. *4*, 1717–1721.

Lettier, G., Feng, Q., de Mayolo, A. A., Erdinez, N., Reid, R. J., Lisby, M., Mortensen, U. H., and Rothstein, R. (2006). The role of DNA double-strand breaks in spontaneous homologous recombination in *S. cerevisiae*. PLoS Genet. *2*, e194.

Manders, E.M.M., Verbeek, F. J., and Aten, J. A. (1993). Measurement of co-localization of objects in dual color confocal images. J. Microscopy *169*, 375–382.

Markova, E., Schultz, N., and Belyaev, I. Y. (2007). Kinetics and dose-response of residual 53BP1/gamma-H2AX foci: xo-localization, relationship with DSB repair and clonogenic survival. Int. J. Radiat. Biol. *83*, 319–329.

Melle, C., Ernst, G., Schimmel, B., Bleul, A., Mothes, H., Settmacher, U., and von Eggeling, F. (2006). Different expression of calgizzarin (S100A11) in normal colonic epithelium, adenoma and colorectal carcinoma. Int. J. Oncol. *28*, 195–200.

Miyagawa, K., Tsuruga, T., Kinomura, A., Usui, K., Katsura, M., Tashiro, S., Mishima, H., and Tanaka, K. (2002). A role for RAD54B in homologous recombination in human cells. EMBO J. *21*, 175–180.

Mogi, S., and Oh, D. H. (2006). gamma-H2AX formation in response to interstrand crosslinks requires XPF in human cells. DNA Repair *5*, 731–740.

Otterlei, M., Bruheim, P., Ahn, B., Bussen, W., Karmakar, P., Bayton, K., and Bohr, V. A. (2006). Werner syndrome protein participates in a complex with RAD51, RAD54, RAD54B and ATR in response to ICL-induced replication arrest. J. Cell Sci. *119*, 5137–5146.

Paull, T. T., Rogakou, E. P., Yamazaki, V., Kirchgessner, C. U., Gellert, M., and Bonner, W. M. (2000). A critical role for histone H2AX in recruitment of repair factors to nuclear foci after DNA damage. Curr. Biol. *10*, 886–895.

Raderschall, E. *et al.* (2002). Formation of higher-order nuclear Rad51 structures is functionally linked to p21 expression and protection from DNA damage-induced apoptosis. J. Cell Sci. *115*, 153–164.

Rogakou, E. P., Pilch, D. R., Orr, O. H., Ivanova, V. S., and Bonner, W. M. (1998). DNA double-stranded breaks induce histone H2AX phosphorylation on serine 139. J. Biol. Chem. *273*, 5858–5868.

Rogakou, E. P., Boon, C., Redon, C., and Bonner, W. M. (1999). Megabase chromatin domains involved in DNA double-strand breaks in vivo. J. Cell Biol. *146*, 905–916.

Rogakou, E. P., Nieves-Neira, W., Boon, C., Pommier, Y., and Bonner, W. M. (2000). Initiation of DNA fragmentation during apoptosis induces phosphorylation of H2AX histone at serine 139. J. Biol. Chem. *275*, 9390–9395.

Rosenberger, S., Thorey, I. S., Werner, S., and Boukamp, P. (2007). A novel regulator of telomerase. S100A8 mediates differentiation-dependent and calcium-induced inhibition of telomerase activity in the human epidermal keratinocyte line HaCaT. J. Biol. Chem. *282*, 6126–6135.

Sakaguchi, M., Miyazaki, M., Inoue, Y., Tsuji, T., Kouchi, H., Tanaka, T., Yamada, H., and Namba, M. (2000). Relationship between contact inhibition and intranuclear S100C of normal human fibroblasts. J. Cell Biol. *149*, 1193–1206.

Sakaguchi, M., Miyazaki, M., Takaishi, M., Sakaguchi, Y., Makino, E., Kataoka, N., Yamada, H., Namba, M., and Huh, N. H. (2003). S100C/A11 is a key mediator of Ca^{2+}-induced growth inhibition of human epidermal keratinocytes. J. Cell Biol. *163*, 825–835.

Sakaguchi, M., Miyazaki, M., Sonegawa, H., Kashiwagi, M., Ohba, M., Kuroki, T., Namba, M., and Huh, N. H. (2004). PKCα mediates TGFβ-induced growth inhibition of human keratinocytes via phosphorylation of S100C/A11. J. Cell Biol. *164*, 979–984.

Sakaguchi, M., Sonegawa, H., Murata, H., Kitazoe, M., Futami, J. I., Kataoka, K., Yamada, H., and Huh, N. H. (2008). S100A11, a dual mediator for growth regulation of human keratinocytes. Mol. Biol. Cell *19*, 78–85.

Sarai, N., Kugawa, W., Kinebuchi, T., Kagawa, A., Tanaka, K., Miyagawa, K., Ikawa, S., Shibata, T., Kurumizaka, H., and Yokoyama, S. (2006). Stimulation of Dmc1-mediated DNA strand exchange by the human Rad54B protein. Nucleic Acids Res. *34*, 4429–4437.

Schafer, B. W., and Heizmann, C. W. (1996). The S100 family of EF-hand calcium-binding proteins: functions and pathology. Trends Biochem. Sci. *21*, 134–140.

Sedelnikova, O. A., Horikawa, I., Zimonjic, D. B., Popescu, N. C., Bonner, W. M., and Barrett, J. C. (2004). Senescing human cells and ageing mice accumulate DNA lesions with unrepairable double-strand breaks. Nat. Cell Biol. *6*, 168–170.

Sehorn, M. G., Sigurdsson, S., Bussen, W., Unger, V. M., and Sung, P. (2004). Human meiotic recombinase DMC1 promotes ATP-dependent homologous DNA strand exchange. Nature *429*, 433–437.

Somanathan, S., Suchyna, T. M., Siegel, A. J., Berezney, R. (2001). Targeting of PCNA to sites of DNA replication in the mammalian cell nucleus. J. Cell. Biochem. *81*, 56–67.

Tanaka, K., Kagawa, W., Kinebuchi, T., Kurumizaka, H., H., and Miyagawa, K. (2002). Human Rad54B is a double-stranded DNA-dependent ATPase and has biochemical properties different from its structural homolog in yeast, Tid1/Rdh54. Nucleic Acids Res. *30*, 1346–1353.

Tsuda, M., Watanabe, T., Seki, T., Kimura, T., Sawa, H., Minami, A., Akagi, T., Isobe, K., Nagashima, K., and Tanaka, S. (2005). Induction of p21(WAF1/CIP1) by human synovial sarcoma-associated chimeric oncoprotein SYT-SSX1. Oncogene *24*, 7984–7990.

van Ginkel, R. P., Gee, R. L., Walker, T. M., Hu, D. N., Weizmann, C. W., and Polans, A. S. (1998). The identification and differential expression of calcium-binding proteins associated with ocular melanoma. Biochim. Biophys. Acta *1448*, 290–297.

von Mikecz, A., Zhang, S., Montminy, M., Tan, E. M., and Hemmerich, P. (2000). CREB-binding protein (CBP)/p300 and RNA polymerase II colocalize in transcriptionally active domains in the nucleus. J. Cell Biol. *150*, 265–273.

Wesoly, J. *et al.* (2006). Different contributions of mammalian Rad54 paralogs to recombination, DNA damage repair, and meiosis. Mol. Cell. Biol. *26*, 976–989.

Wolner, B., van Komen, S., Sung, P., and Peterson, C. L. (2003). Recruitment of the recombinational repair machinery to a DNA double-strand break in yeast. Mol. Cell *12*, 221–232.

Yoon, K., and Smart, R. C. (2004). C/EBPα is a DNA damage-inducible p53-regulated mediator of the G_1 checkpoint in keratinocytes. Mol. Cell. Biol. *24*, 10650–10660.

Xhao, X. O., Naka, M., Muneyuki, M., and Tanaka, T. (2000). Ca(2+)-dependent inhibition of actin-activated myosin ATPase activity by S100C (S100A11), a novel member of the S100 protein family. Biochem. Biophys. Res. Commun. *267*, 77–79.

E07-11-1167 Melle

Supplemental Figure legends

Suppl. Figure S1. The result of the database quest (profound) using PMF derived from actin detected in a protein-protein complex detection assay using an anti-S100A11 antibody as described in Materials and Methods is shown.

Suppl. Figure S2. S100A11 and Rad54B sites do not overlap with SC-35 speckles. Colocalization experiments were performed to detect simultaneously the spilicing factor compartment (SC-35, red), S100A11 (green), and Rad54B (blue), respectively. Bar: 5 μm.

Suppl. Figure S3. S100A11 and Rad54 do neither interact nor colocalize in the nucleus. (A) In coimmunoprecipitation experiments, the specific antibody against S100A11 was not able to precipitate Rad54 (lane 3). The specific anti-Rad54 antibody precipitated his antigen (lane 2) in a positive control. As a negative control (lane 1), rabbit IgG which was used as an unspecific antibody was not able to co-precipitate Rad54 similar to the S100A11 antibody. (B) No colocalization between S100A11 and Rad54 was detectable in a co-immunostaining with anti-S100A11 (green) and anti-Rad54 (red) antibody in fixed HaCaT cells treated with BLM. Bar: 5 μm.

Suppl. Figure S4. Induction of DNA double-strand breaks in U2OS cells by bleomycin treatment. (A) U2OS cells were cultured in the presence of 12.5 IU/ml bleomycin for 30 min on cover slips. After different time intervals, cells were analyzed for the formation of DNA double-strand break repair foci by immunofluorescence detection of γH2AX epitopes. (B) Quantitation of γH2AX formation/nucleus over time in U2OS cells treated for 30 min with

12.5 IU/ml bleomycin. At each time point foci numbers of at least 100 cells were determined. (C) Colony forming assay of U2OS cells treated with increasing concentrations of bleomycin.

Suppl. Figure S5. No to very little colocalzation between the S100A11/Rad54B complex and Ku80. HaCaT cells were treated with bleomycin (BLM) (12.5 μg ml^{-1}) and analyzed by three-colour immunostaining followed by laser scaning microscopy for S100A11 (green), Rad54B (blue), Ku80 (red) or merged as indicated. Bar: 5 μm.

Suppl. Figure S6. No colocalization between the S100A11/Rad54B complex and PCNA in different cell cycle phases. HaCaT cells in G1 (a), early S (b), mid S (c), late S (d), or G2 (e), respectively, were immunostained against S100A11 (green), Rad54B (blue), and PCNA (red) and analyzed by laser scaning microscopy. Bar: 5 μm.

ProFound - Search Result Summary

Version 4.10.5
The Rockefeller University Edition

Protein Candidates for search B796FF1A-03C4-6F18B9E5 [94820 sequences searched]

Rank	Probability	Est'd Z	Protein Information and Sequence Analyse Tools (T)	%	*pI*	kDa	®
+1	9.9e-001	1.17	T gi|15277503|gb|AAH12854.1| ACTB protein [Homo sapiens]	34	5.6	40.63	®

ProFound - Search Result Details

Version 4.10.5
The Rockefeller University Edition

Details for rank 1 candidate in search B796FF1A-03C4-6F18B9E5 </TD< TR>

gi|7441428|pir||JC5818 gamma-actin - human

```
Sample ID :   [Pass:0]
Measured peptides     : 9
Matched peptides      : 5
Min. sequence coverage: 33%
```

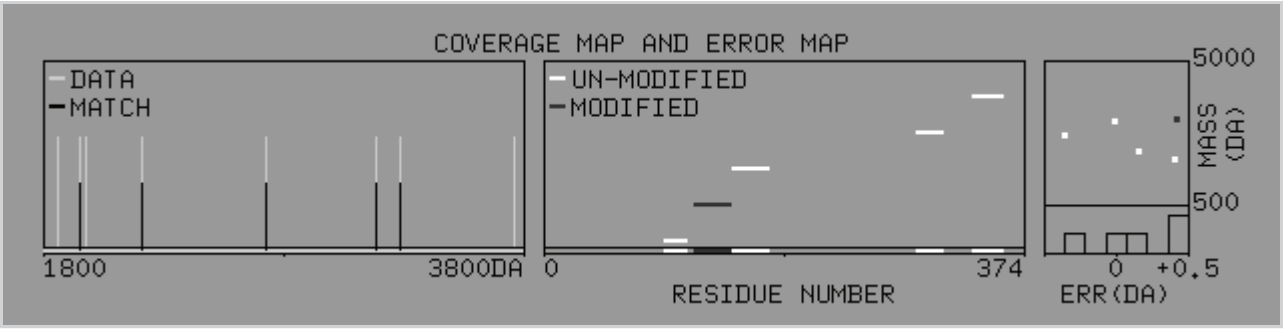

Measured Mass(M)	Avg/ Mono	Computed Mass	Error (Da)	Residues Start	To	Missed Cut	Peptide sequence
1954.652	A	1954.254	0.399	95	112	0	VAPEEHPVLLTEAPLNPK
2215.629	A	2215.469	0.161	291	311	0	DLYANTVLSGGTTMYPGIADR
2730.858	A	2731.211	-0.353	335	358	1	KYSVWIGGSILASLSTFQQMWISK
3184.611	A	3184.620	-0.010	147	176	0	TTGIVMDSGDGVTHTVPIYEGYALPHAILR
3287.254	A	3286.842	0.412	118	146	0	MTQIMFETFNTPAMYVAIQAVLSLYASGR
							(2)+O@M;

Murzik et al. **Supplemental Figure S1**

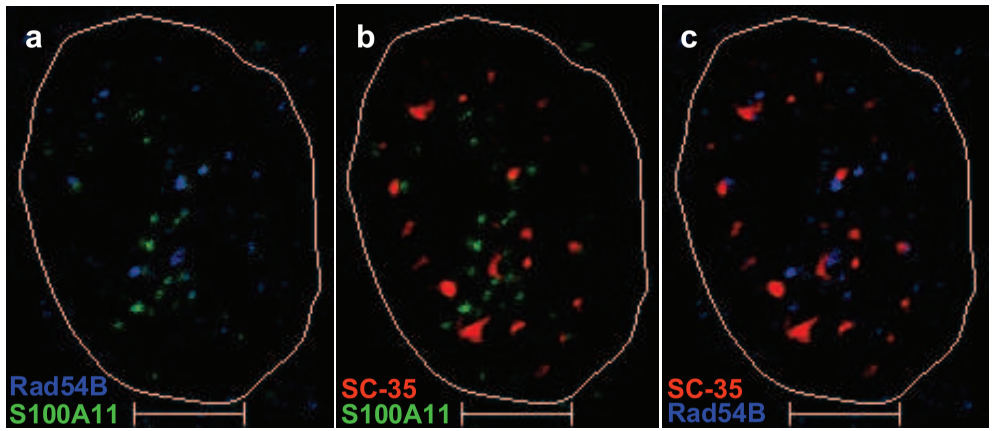

Murzik et al. **Supplemental Figure S2**

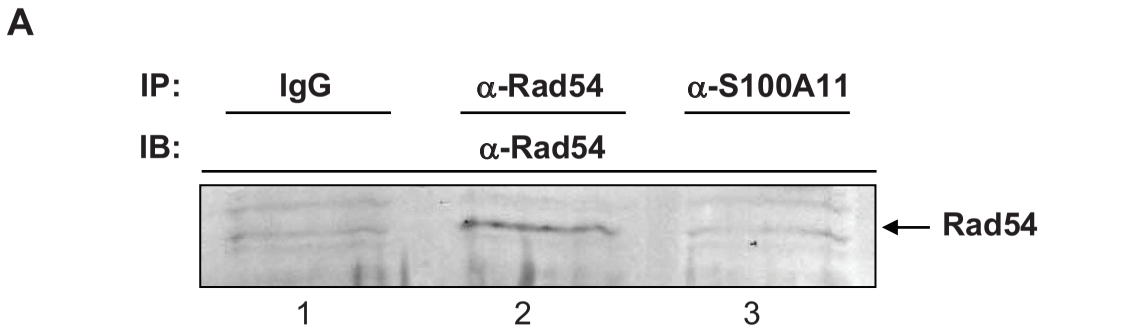

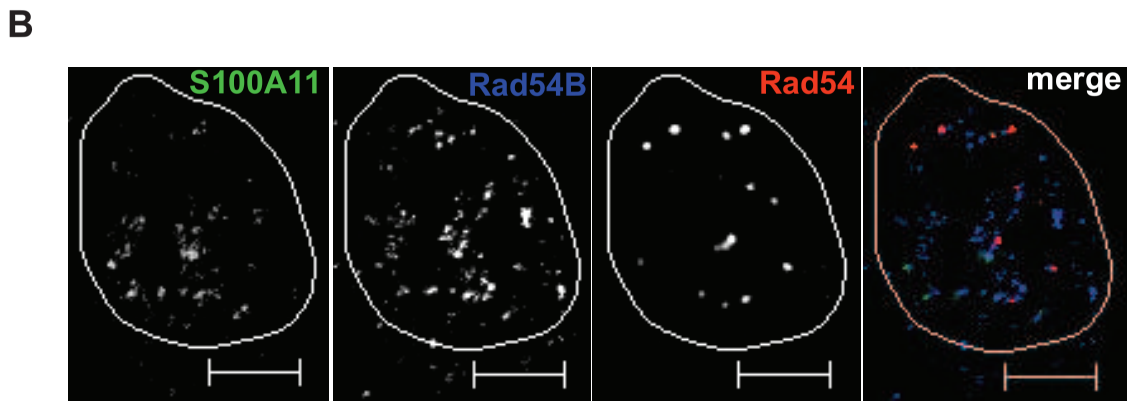

Murzik et al. **Supplemental Figure S3**

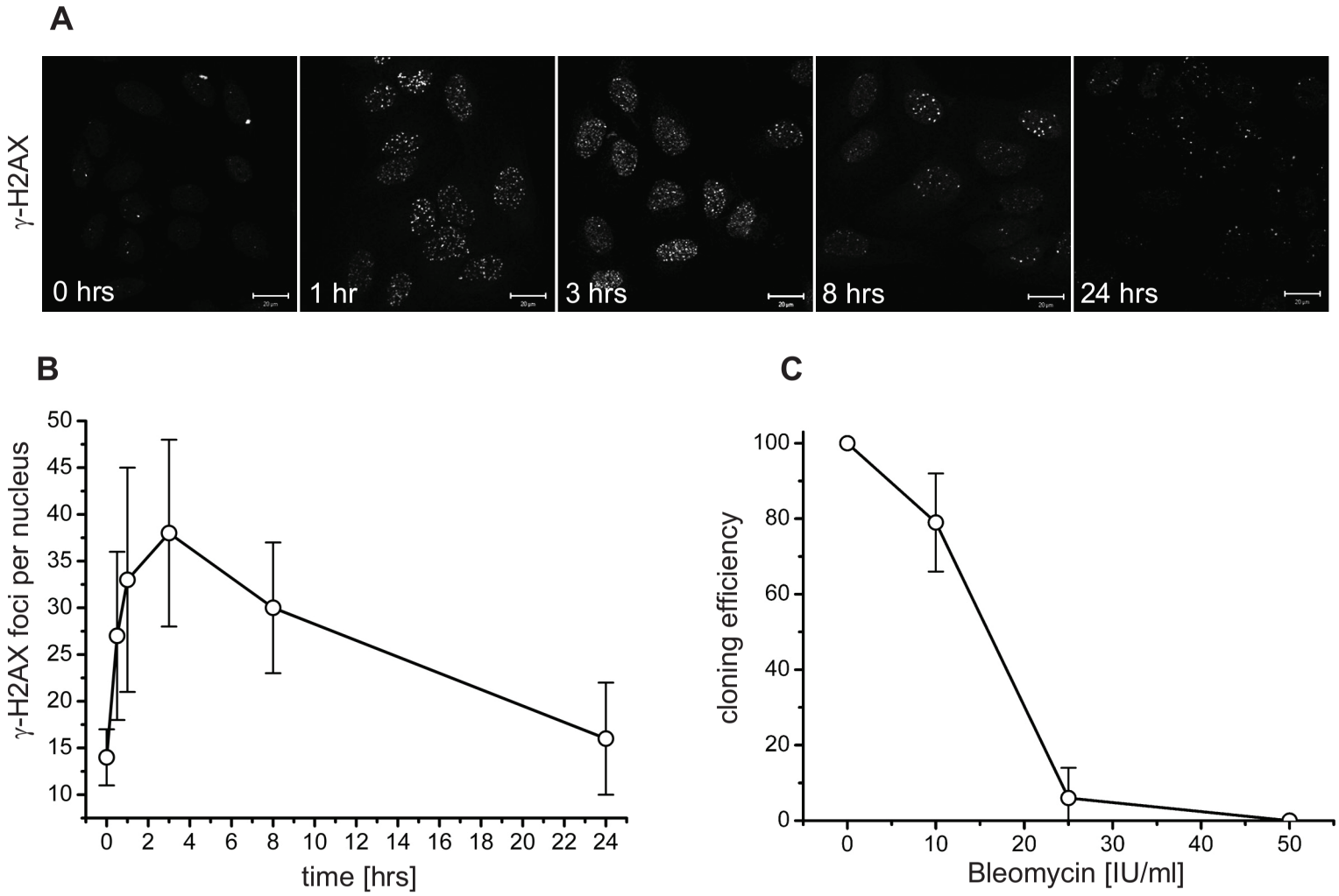

Murzik et al. **Supplemental Figure S4**

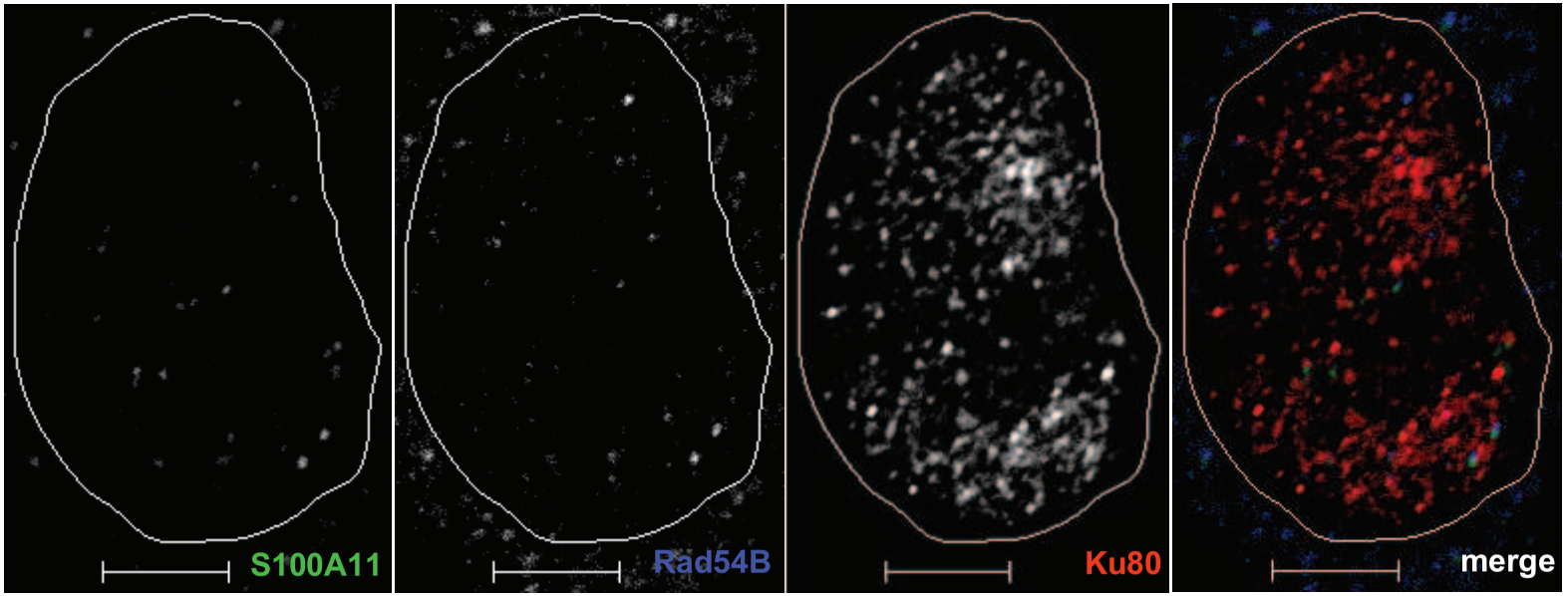

Murzik et al. **Supplemental Figure S5**

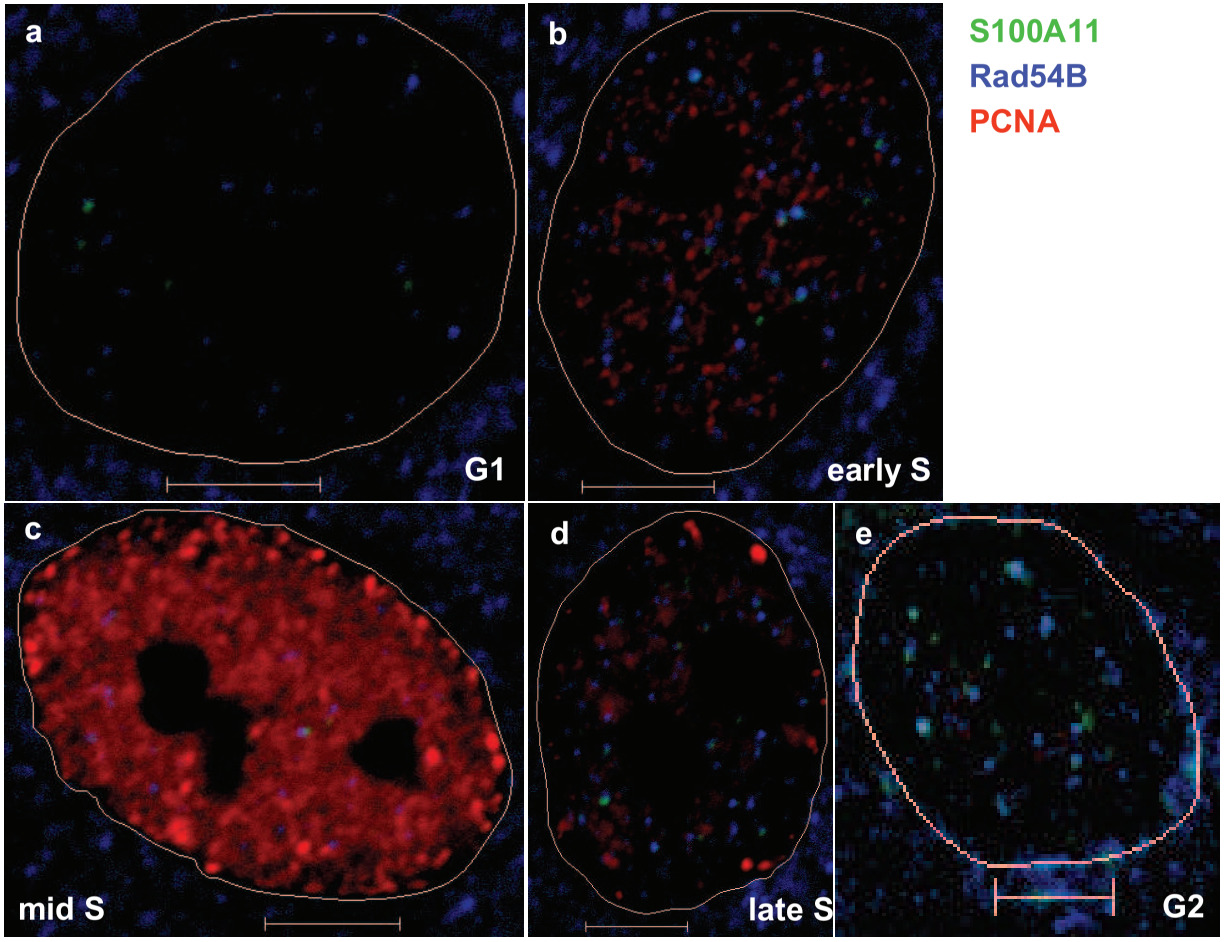

Murzik et al.

Supplemental Figure S6